THE PACIFIC MARINE HEATWAVE: MONITORING DURING A MAJOR PERTURBATION IN THE GULF OF ALASKA

GULF WATCH ALASKA LONG-TERM MONITORING PROGRAM
SYNTHESIS REPORT

Exxon Valdez Oil Spill Trustee Council Program 19120114

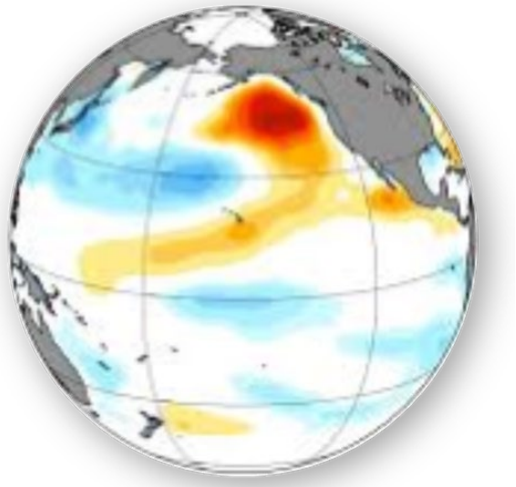

March 11, 2021

Robert M. Suryan[1], Mandy R. Lindeberg[1], and Donna Robertson Aderhold[2], editors

[1]*NOAA Alaska Fisheries Science Center, Auke Bay Laboratories, Juneau, AK*
[2]*Prince William Sound Science Center, Cordova, AK*

With contributions from: M. Arimitsu, S. Baird, S. Batten, M. A. Bishop, J. Bodkin, R. Brenner, R. Campbell, H. Coletti, D. Cushing, S. Danielson, T. Dean, D. Esler, T. Gelatt, K. Gorman, S. Hatch, S. Haught, T. Hennon, K. Holderied, D. Hondolero, R. Hopcroft, K. Iken, D. Irons, D. Kimmel, B. Konar, K. Kuletz, B. Laurel, M. R. Lindeberg, J. Maniscalco, C. Marsteller, C. Matkin, C. McKinstry, D. McGowan, D. Monson, J. Moran, D. Olsen, W. S. Pegau, J. Piatt, L. Rogers, A. Schaefer, S. Schoen, J. Straley, R. M. Suryan, K. Sweeney, M. Szymkowiak, V. von Biela, T. Weingartner, B. Weitzman, S. Zador

Cover image: Sea surface temperature anomaly, winter (January, February, and March) 2014.
Emanuele Di Lorenzo, Giovanni Liguori & Nate Mantua.

THE PACIFIC MARINE HEATWAVE: MONITORING DURING A MAJOR PERTURBATION IN THE GULF OF ALASKA

GULF WATCH ALASKA LONG-TERM MONITORING PROGRAM
SYNTHESIS REPORT

Exxon Valdez Oil Spill Trustee Council Program 19120114

March 11, 2021

Robert M. Suryan[1], Mandy R. Lindeberg[1], and Donna Robertson Aderhold[2], editors

[1]*NOAA Alaska Fisheries Science Center, Auke Bay Laboratories, Juneau, AK*
[2]*Prince William Sound Science Center, Cordova, AK*

With contributions from: M. Arimitsu, S. Baird, S. Batten, M. A. Bishop, J. Bodkin, R. Brenner, R. Campbell, H. Coletti, D. Cushing, S. Danielson, T. Dean, D. Esler, T. Gelatt, K. Gorman, S. Hatch, S. Haught, T. Hennon, K. Holderied, D. Hondolero, R. Hopcroft, K. Iken, D. Irons, D. Kimmel, B. Konar, K. Kuletz, B. Laurel, M. R. Lindeberg, J. Maniscalco, C. Marsteller, C. Matkin, C. McKinstry, D. McGowan, D. Monson, J. Moran, D. Olsen, W. S. Pegau, J. Piatt, L. Rogers, A. Schaefer, S. Schoen, J. Straley, R. M. Suryan, K. Sweeney, M. Szymkowiak, V. von Biela, T. Weingartner, B. Weitzman, S. Zador

Citation:

Suryan, R. M., M. R. Lindeberg, and D. R. Aderhold. 2021. The Pacific Marine Heatwave: Monitoring During a Major Perturbation in the Gulf of Alaska. Long-Term Monitoring Program (Gulf Watch Alaska) Synthesis Report, (*Exxon Valdez* Oil Spill Trustee Council Program 19120114). *Exxon Valdez* Oil Spill Trustee Council, Anchorage, Alaska.

The Pacific Marine Heatwave:
Monitoring During a Major Perturbation in the Gulf of Alaska

Exxon Valdez Oil Spill Trustee Council Program 19120114
Gulf Watch Alaska Synthesis Report

Preface: The purpose of this synthesis report from the long-term monitoring program, Gulf Watch Alaska, is to fulfill a deliverable asked for by the *Exxon Valdez* Oil Spill Trustee Council (EVOSTC) in their 2017-21 request for proposals (EVOSTC 2015). The Gulf Watch Alaska program management team is expected to present a draft synthesis report to the EVOSTC for review in the third year of the current 5-year cycle (December 2019) followed by a synthesis workshop (February 2020) and finalized report. Before Gulf Watch Alaska drafted this report, EVOSTC staff approved the general outline and major content of this synthesis product. A synthesis report is an important integrative product for a long-term monitoring program like Gulf Watch Alaska and allows for a pause to gain a better understanding of the Gulf of Alaska ecosystem and how resources are responding to processes driving change over time. Recently, the Gulf of Alaska has been experiencing an unprecedented Pacific marine heatwave, which offered an obvious choice for our report theme. Around this theme, the major content of our report includes an executive summary followed by four draft synthesis manuscripts destined for publication in peer reviewed journals. Each of these manuscripts utilize numerous time series datasets to evaluate effects of the Pacific marine heatwave on marine resources of the northern Gulf of Alaska. These manuscripts synthesize data from across Gulf Watch Alaska's ecosystem components, other EVOSTC programs (e.g., Herring Research and Monitoring), and even outside collaborators (e.g., NOAA Alaska Fisheries Science Center) to acquire comprehensive assessments. Through these four synthesis manuscripts a clearer picture emerges on what the physical patterns and biological responses have been to this major marine heatwave event.

Study History: In 2010 the *Exxon Valdez* Oil Spill Trustee Council issued an invitation for proposals for a long-term monitoring program (EVOSTC 2010a). The intent was to establish an ecosystem level monitoring program lasting for twenty-years that would track the recovery of resources since the spill and assess how factors other than oil may inhibit full recovery. The subsequent Gulf Watch Alaska proposal (McCammon et al. 2011) was funded by the EVOSTC and the program was initiated in 2012 (EVOSTC: #12120114 to #16120114-A, -B, -C, -D, -E, -F, -G, -H, -J, -K, -L, -M, -N, -O, -P, -Q, -R, -S). A program lead and management team provided oversight to multiple projects with principal investigators organized under three ecosystem components: 1) Environmental Drivers, 2) Pelagic Ecosystem, and 3) Nearshore Ecosystem including lingering designed as an integrated approach to monitoring. Many of the long-term monitoring projects incorporated into Gulf Watch Alaska were previously funded by the EVOSTC, with some originating before the spill in 1989 and representing more than 30-year time series. During 2012-16, required deliverables to the EVOSTC (Work Plans and Annual Reports) were completed annually for all projects including a program level synthesis report in year three, 2014 (McCammon et al. 2017). In 2015, the EVOSTC solicited proposals for a second five-year cycle of monitoring (EVOSTC 2015) and based on the success of the first five-year period, the Gulf Watch Alaska proposal (Lindeberg et al. 2016) was approved for funding to continue long-term monitoring for fiscal years 2017-21 (EVOSTC: #17120114 to #19120114-A,

-B, -C, -E, -F, -G, -J, -K, -M, -N, -O, -P) with similar deliverables, including this synthesis report in 2019.

Abstract: Gulf Watch Alaska is an interdisciplinary marine ecosystem monitoring program designed to inform restoration needs and activities for *Exxon Valdez* oil spill injured resources within the context of long-term environmental variability. One of the most significant, contemporary environmental events in the Gulf of Alaska (GOA) was the 2014-2016 northeast Pacific marine heatwave (PMH), which occurred soon after Gulf Watch Alaska began. This science synthesis report highlights major findings from Gulf Watch Alaska during the first 8 years of long-term ecosystem monitoring and the ecosystem-level impacts of the PMH. The report is structured around four manuscripts produced with the Herring Research and Monitoring Program and other collaborators. These manuscripts collectively use over 200 physical and biological time series to describe the development of the PMH and biological responses. Analyses of ocean temperature data showed that correlation length scales generally degraded considerably beyond 100 km, but that the PMH heatwave signal was so strong that surface waters (0-50 m) from the intertidal zone to the outer continental shelf warmed contemporaneously with offshore waters. Heating mechanisms and timing, however, differed for surface and near-bottom waters. The highly anomalous warming of the PMH affected rocky intertidal habitats across the northern GOA such that community structure that formerly appeared to vary independently within each region, showed remarkably similar responses across regions during and after the PMH. Likewise, in the pelagic prey and predator food web, the PMH coincided with the collapse of multiple forage fish populations, which disrupted energy flow to higher vertebrate predators and caused major reductions in abundance and productivity. Not all responses however were negative but were nonetheless together sufficiently strong to produce a GOA ecosystem community structure post-PMH that was different then years prior. Looking forward, we propose to build upon these data synthesis efforts while we continue to improve and expand the products that we provide to stakeholders. Developing a more complete understanding of the ecosystem effects of climate variability and other perturbations is critical to reducing uncertainty that can hinder marine resource recovery designations and economic development in the GOA.

Acknowledgements: This document is a summary of works contributed by numerous scientists with funding leveraged from both non-governmental and governmental entities to provide staff time and equipment. We wish to thank all of our partners for assistance and the Gulf Watch Alaska program scientists and staff for their thoughtful contributions and reviews of this report. We thank the *Exxon Valdez* Oil Spill Trustee Council-funded Data Management program, particularly Carol Janzen, Stacey Buckelew, Chris Turner, and Will Koeppen, for their invaluable support with data management and publication. Our sister program, Herring Research and Monitoring, led by W. Scott Pegau, supports data collection, program coordination, and synthesis. We also express our appreciation to the program Science Review Panel members: Hal Batchelder, Rich Brenner, Ron Heintz, Terrie Klinger, and Stanley 'Jeep' Rice, for their review and guidance in the development of this report. The Gulf Watch Alaska program thanks the *Exxon Valdez* Oil Spill Trustee Council for funding the long-term monitoring program. These findings and conclusions presented by the author(s) are their own and do not necessarily reflect the views or position of the *Exxon Valdez* Oil Spill Trustee Council.

TABLE OF CONTENTS

EXECUTIVE SUMMARY 1

BACKGROUND 1
PRODUCTS 1
FINDINGS 2
EVOS injured resources 2
Environmental variability and the Gulf of Alaska ecosystem 5
Overview of physical patterns and biological responses 6
FUTURE DIRECTIONS 10
LITERATURE CITED 11

CHAPTER 1 A STUDY OF MARINE TEMPERATURE VARIATIONS IN THE NORTHERN GULF OF ALASKA ACROSS YEARS OF MARINE HEATWAVES AND COLD SPELLS 1-1

INTRODUCTION 1-2
OCEANOGRAPHIC SETTING 1-3
Climate setting 1-5
Objectives 1-6
DATA AND METHODS 1-7
Intertidal dataloggers 1-8
Marine weather station, tide gauge and buoy data 1-11
Shipboard CTD data 1-12
Oceanographic mooring data 1-12
Gridded SST data compilations 1-13
Atmospheric reanalysis 1-13
Meteorological station data 1-14
Climate indices 1-14
Analysis 1-14
RESULTS 1-16
Climate-scale trends and patterns 1-16
Fidelity of remotely sensed SST data 1-22
Horizontal and vertical scales of variability 1-23
Variability across the coastal realm 1-29
Case study: Temperatures across the northern Gulf of Alaska 1-35
CONCLUSIONS AND SUMMARY 1-39
ACKNOWLEDGEMENTS 1-41
REFERENCES 1-42
APPENDIX 1-48

CHAPTER 2 CHANGES IN ROCKY INTERTIDAL COMMUNITY STRUCTURE DURING A MARINE HEATWAVE IN THE NORTHERN GULF OF ALASKA 2-1

INTRODUCTION 2-2
METHODS 2-4
Study design *2-4*
Statistical Analyses *2-6*
RESULTS 2-6
DISCUSSION 2-16
Summary *2-19*
ACKNOWLEDGMENTS 2-20
REFERENCES 2-20

CHAPTER 3 REDUCED QUALITY AND SYNCHRONOUS COLLAPSE OF FORAGE SPECIES DISRUPTS TROPHIC TRANSFER DURING A PROLONGED MARINE HEATWAVE 3-1

INTRODUCTION 3-2
METHODS 3-3
Study Area *3-3*
Seabird diets *3-4*
Forage fish survey indices *3-5*
Spawning capelin age-length *3-6*
Sand lance total energy *3-6*
Herring growth and energy *3-6*
Zooplankton indices *3-7*
Marine predators *3-8*
RESULTS 3-8
Forage fish trends in seabird diets *3-8*
Forage fish trends in survey indices *3-10*
Forage fish age, length, energy content, and growth *3-12*
Zooplankton indices *3-17*
Marine predators *3-21*
DISCUSSION 3-23
Truncation of age and size structure in forage fish *3-24*
Decreased quality of forage fish *3-24*
Lower biomass and diversity of euphausiids oppose copepod trends *3-25*
Changes in distribution, mass mortality, reduced breeding success, and malnutrition in predators *3-25*
CONCLUSION 3-26
ACKNOWLEDGEMENTS 3-27
REFERENCES 3-27

CHAPTER 4 ECOSYSTEM RESPONSE TO A PROLONGED MARINE HEATWAVE IN THE GULF OF ALASKA 4-1

INTRODUCTION 4-2
METHODS 4-3
Data Treatment and Statistical Analyses *4-5*
Sample Collection and Processing *4-6*
RESULTS 4-10
Dynamic factor analysis *4-10*
Community analysis *4-18*
Longer time series perspective *4-19*
DISCUSSION 4-21
Biological community response during the PMH *4-21*
Human dimension *4-22*
Signals of recovery? *4-23*
Future Gulf of Alaska *4-23*
ACKNOWLEDGEMENTS 4-24
REFERENCES 4-24
APPENDIX 4-34

LIST OF TABLES

Table 1-1. Indices of climate variability in the Pacific region. Table headings include index name, abbreviation, and source. 1-11
Table 1-2. Correlation (r) between temperature records at the GAK1 and Kachemak Bay National Estuarine Research Reserve System Wide Monitoring Program moorings, and the PDO, NPGO, PNA, MEI, NPI, PMM, and VMI climate indices, and the principal components shown in Figure 1-7. Correlations shown only for $p < 0.05$. Correlations are based on the maximum temporal overlap of each record's monthly anomaly over the period 1990-2019. See Table 1-1 for climate index abbreviation definitions. 1-21
Table 2-1. PERMANOVA table of results testing biological community structure, by tidal stratum, before and after the Pacific marine heatwave, and among regions. Top: Mid-stratum. Bottom: Low-stratum. Bold font denotes significance. 2-10
Table 2-2. PERMANOVA pairwise tests for similarity in rocky intertidal community structure before and after the Pacific marine heatwave at Mid- and Low-tidal strata, by region. Bold font denotes significance. 2-11
Table 2-3. PERMANOVA pairwise tests for similarity between regions before and after the Pacific marine heatwave at Mid- and Low-tidal strata. Bold font denotes significant differences between regions. 2-11
Table 2-4. SIMPER table of results determining the contribution of each taxa to observed variation in community structure before and during/after the Pacific marine heatwave (PMH) at Mid- and Low-tidal strata. Average dissimilarity (Av. Diss.) describes how

dissimilar the communities (and the important taxon individually) are at mid- and low-strata across regions before and during/after the PMH. Percent change (% Δ) shows the proportional change in the fourth root transformed, mean percent cover for each taxon before and after the PMH. The amount of variation explained by each taxon (% Cont.) sums to at least 70% explained variation for each stratum. Gray cells indicate taxa that were only important in one stratum. 2-15
Table 4-1. Numbers and types of biological time series (n = 113 total) used to assess response to a marine heatwave in the Gulf of Alaska. Sources of time series include 74 from the Exxon Valdez Oil Spill Trustee Council's Gulf Watch Alaska, 23 from National Oceanic and Atmospheric Administration Alaska Fisheries Science Center, 10 from Alaska Department of Fish and Game, 2 from the U.S. Fish and Wildlife Service, 2 from the Alaska SeaLife Center, and 2 from the Exxon Valdez Oil Spill Trustee Council's Herring Research and Monitoring program. See Table A1 for more details on time series metrics. 4-5
Table 4-2. Model results from dynamic factor analysis of 113 biological time series spanning 2010-2018 and encompassing the 2014-2016 northeast Pacific marine heatwave. The top five ranking models are shown based on ΔAICc. A total of nine models were run that included three different variance structures for the R matrix and three possible trends for each variance structure..... 4-10
Table 4-3. Summary of trends based on factor loadings from dynamic factor analysis by taxa and metric of 113 biological time series. Time series are described as having a positive, negative, or neutral response coincident with the 2014-2016 Pacific marine heatwave. Each time series was identified as having a negative, positive, or neutral trend when factor loadings were > 0.20, < -0.20, or > -0.20 and < 0.20, respectively. The signs of factor loadings are opposite of time series trend because factor loadings describe how a given time series relates to the common trend, which was a negative during the Pacific marine heatwave (Figure 4-3). See Table A1 for factor loadings of individual time series. 4-12

LIST OF FIGURES

Figure ES-1. Abundance of pigeon guillemots during summer in Prince William Sound. Photo: Commons.Wikimedia.org. 3
Figure ES-2. Long-term trend in abundance of resident (AB) and transient (AT1) killer whales that frequent Prince William Sound. The vertical line indicates the timing of the Exxon Valdez oil spill. Photo: Craig Matkin, North Gulf Oceanic Society. Note: values from the most recent few years assume a static population even though not all individuals were observed. It is too soon to confirm possible mortalities. 4
Figure ES-3. Trends in Pacific herring and herring dependent predators in Prince William Sound. Herring spawn (miles-day milt; grey line) from Exxon Valdez Oil Spill Trustee Council Herring Research and Monitoring program, black-legged kittiwake (Rissa tridactyla)

nesting abundance (blue line) from Exxon Valdez Oil Spill Trustee Council Pigeon Guillemot Restoration Research project, and abundance of individual humpback whales (red line) from Gulf Watch Alaska. Abundances are standardized to a mean of zero and standard deviation of one. Pacific herring and Humpback whale photos by NOAA: Mark Carls and John Moran respectively. Black-legged kittiwake photo from Commons.Wikimedia.org. 5
Figure ES-4. Sea surface temperatures in the Gulf of Alaska and Bering Sea showing that 5 (Gulf of Alaska) to 6 (Bering Sea) of the warmest 10 years over the past 119 years occurred after the onset of the marine heatwave in 2014 (Source: University of Alaska Fairbanks, Alaska Center for Climate Assessment and Policy (ACCAP)). 6
Figure ES-5. Monthly ocean temperature anomalies 2008-2017 from various depths (m) at ocean station PAPA in the northeast Pacific (50°N 145°W), Sitka, Alaska, Kachemak Bay (SWMP), and outside Resurrection Bay near Seward (GAK1). 7
Figure ES-6. Alexandrium spp. cell abundance (log_{10} scale) in lower Cook Inlet and Kachemak Bay, 2012-2018. Paralytic shellfish poisoning toxins are likely to be detected in shellfish tissues for cell abundances above 500 cells/liter (red dashed line). Photo by NOAA: Brian Bill. 8
Figure ES-7. Humpback whales in Prince William Sound showing a robust whale with large blubber layer (top) and malnourished whale showing (arrows from left to right) a sharp, less rounded spine, right scapula visible under skin, and appearance of rough skin from parasites and lesions (bottom). Photos by NOAA: John Moran. 9
Figure ES-8. Trends in sablefish juvenile growth index (bars; fish collected by seabirds nesting at Middleton Island (Gulf Watch Alaska data), recruitment (blue line) and age 2+ biomass (green line; National Oceanic and Atmospheric Administration stock assessment, Hanselman et al. 2018). Picture inset of juvenile sablefish consuming juvenile herring in Prince William Sound during the September 2019 GWA Integrated Predator-Prey cruise. Photo by NOAA: John Moran. 10
Figure 1-1. Ocean circulation, land topography, and ocean bathymetry in the Gulf of Alaska. . 1-3
Figure 1-2. Station location maps showing the GAK1 and Kachemak Bay National Estuarine Research Reserve System Wide Monitoring Program (SWMP) moorings (cyan circles), buoys and land stations (orange triangles), tide gauge stations (black stars), weather stations (blue plus symbols), intertidal HOBO data loggers (yellow squares), and conductivity-temperature-depth stations (red circles). See Table A1 for station coordinates, data temporal coverage and site characteristics. Place abbreviations include: RB = Resurrection Bay; GB = Glacier Bay; HE = Hinchinbrook Entrance; MS = Montague Strait. Bathymetric contours are drawn at 180 and 1,000 m depths. Station abbreviations are described in the text. 1-9
Figure 1-3. Typical installation of a HOBO temperature logger in the intertidal zone inside a PVC pipe and bolted to the substrate. 1-10

Figure 1-4. Three-year example of sea surface temperature (SST) at GAK1 decomposed into different periods of variability. a) Raw SST at GAK1 (T_{RAW}) and the climatological average SST for each day of year (T_{DC}). T_{DC} is low pass filtered with a cutoff period of 60 days. b) The daily anomaly (T_{RAW} -T_{DC}) low-pass filtered with 30-day cutoff period (T'_{LP}). c) The daily anomaly high-pass filtered with a 30 day cutoff period (T'_{HP}). The entire record (over which T_{DC}, T'_{LP}, and T'_{HP} are calculated) spans January 1, 2007 to May 1, 2018. 1-15
Figure 1-5. Upper panel: Extended Reconstructed Sea Surface Temperature (ERSST) annual anomalies for the Gulf of Alaska averaged over 156° W to 230° W and 56° N to 62° N. Lower panel: GAK1 annual averages of all depth-layer monthly anomalies averaged across the full 0-250 m water column. Both records are shown relative to their averages between 1970 and 2019. 1-17
Figure 1-6. North Pacific (left) and Gulf of Alaska (right) patterns of sea surface temperature (SST) variation based on empirical orthogonal function analysis of 1900-2019 Extended Reconstructed SST monthly anomaly records (left) and 1981-2019 Optimum Interpolation SST daily anomaly records (right). Anomaly time series at all grid points are detrended and normalized to unity variance and zero mean. From top to bottom, the rows represent modes 1, 2, and 3, respectively. The fraction of total variance contained in each mode is shown in the upper right-hand corner of each plot. 1-19
Figure 1-7. Times series (red bars) for the six modal patterns shown in Figure 1-6, along with the best-correlated time series of known climate patterns (see also Table 1-1). From top to bottom in the left column, the black lines show PDO, MEI, and VMI time series, respectively. From top to bottom in the right column the black lines show the PDO, VMI, and NPGO time series. Black time series have been smoothed with a 6-month moving average filter. Daily optimum interpolation sea surface temperature time series have been smoothed with a 31-day moving average filter. See Table 1-1 for climate index abbreviation definitions. 1-20
Figure 1-8. Correlation of the optimum interpolation daily sea surface temperature anomaly relative to reference points (blue circles) at Sitka (upper left), western Prince William Sound (upper right), GAK1 (lower left) and System Wide Monitoring Program (lower right). The continental slope is denoted with a thick black contour at the 1,000 m depth level. 1-21
Figure 1-9. The relation between GAK1 conductivity-temperature-depth surface (0 m) data and the optimum interpolation sea surface temperature (OISST) (blue) and group for high resolution sea surface temperature (GHRSST) (red) satellite-based records for all 506 GAK1 casts taken within the OISST period of record and for 119 GAK1 casts in the GHRSST 2007-2017 record. 1-23
Figure 1-10. Fraction of the daily thermal anomaly explained by the group for high resolution sea surface temperature (GHRSST) data (top). Differenced fraction of daily thermal anomaly explained the GHRSST and the optimum interpolation sea surface temperature (OISST)

datasets, showing that while both datasets capture a similar level of the total variance, the GHRSST dataset is a generally a more accurate data source. OISST results are shown only for grid points that lie within 30 km of an in situ observation (bottom)..... 1-25
Figure 1-11. a) Cross-correlation coefficient as a function of distance for all stations used in analysis (locations shown in inset map). Correlations between stations pairs are computed where the records have at least 1.5 overlapping years of data over the period from January 1, 2007 to May 1, 2018. Orange, blue, and purple correspond to T_{DA}, T'_{LP}, and T'_{HP}, respectively. Darker lines show bin averages. b) Same as (a), but for Automated Surface Observing System meteorological stations south of 61.5ºN. See the Data and Methods section for abbreviation definitions. 1-26
Figure 1-12. Correlation between temperature anomalies at the surface and temperature anomalies at standard depths (0, 10, 20, 30, 50, 75, 100, 150, 200, 250, 300, 400, 500, and 550 m) for winter (left) and summer (right) season as resolved by CTDs taken at stations GLBA20 (black), KIP2 (magenta), GAK1 (red), and KBAY6 (blue). Symbols o, Δ, x, and + show the location of the 10, 50, 150, and 500 m depth levels, respectively. The seafloor depth of each station is noted at the bottom of the right-hand panel. Correlations are computed for the corresponding period of record for each site: 49, 25, 22, and 7 years for the GAK1, GLBA20, KIP2, and KBAY6 stations, respectively. ... 1-27
Figure 1-13. Correlation of temperature anomalies across the Seward Line transect (stations GAK1 to GAK13) relative to the surface temperature at station GAK1. Left-hand panel shows correlations that characterize the annual cycle; the right-hand panel shows correlation of monthly anomalies. White regions depict the shelf seafloor. Seward Line stations are each separated by ~10 nmi (18.5 km). Correlations computed for 76 Seward Line occupations between 1997 and 2018. 1-28
Figure 1-14. Temperature records with the annual cycle removed (T_{RAW}-T_{DC}) at GAK1 (black line) and all other stations (gray lines) for six sub-regions during year 2016. The mean annual cycle is computed by using (sometimes incomplete) data records spanning January 1, 2007 to May 1, 2008. Inset maps show stations used for each region (in color, identical to Figure 1-2). The yellow star shows the location of GAK1. 1-29
Figure 1-15. Long-term mean and 95% confidence intervals for the temperature measured at the nearshore HOBO sites and select coastal stations. Means have been adjusted to account for varying length time series at each site relative to the 1970-2019 GAK1 reference (yellow circle, marked by the horizontal line). Red, cyan, blue, and green symbols denote HOBO sites in Katmai, Kachemak Bay (Kachemak), Kenai Fjords (Kenai) and Prince William Sound (PWS), respectively. Grey symbols denote coastal National Oceanic and Atmospheric Administration buoys. PWS is further divided (from left to right) into three areas: western, northern, and eastern. 1-30
Figure 1-16. Top: Taylor diagram representation of correlation analysis between sea surface temperature at GAK1 and all other stations in the Gulf of Alaska (azimuthal coordinate), as well as their normalized standard deviations (radial coordinate from origin) and their

root mean square difference (RMSD, radial coordinate from the GAK1 reference point). Colors distinguish the three temporal bands. Standard deviations of temperature anomalies for all stations are normalized by the standard deviation at GAK1. The RMSD and σ are both unitless. Bottom: Same as top but partitioned into winter (left, October 1st to April 30th) and summer (right, May 1st to September 30th), with analyses representing the period of station record overlap with that at GAK1 1-32
Figure 1-17. Same as Figure 1-16, but partitioning data regionally. The reference station used for each region is the station within that cluster best correlated with GAK1. Variance here is normalized to each regional reference station. 1-33
Figure 1-18. Seasonal water temperature anomalies relative to the 1970-2019 GAK1 time series for intertidal HOBOs and nearshore NOAA buoys for Katmai (upper left), Kachemak Bay (upper right), Kenai Fjords (lower left) and Prince William Sound (PWS) (lower right). For reference, dashed vertical lines denote May 1, 2014 and January 1, 2017 on each plot. 1-34
Figure 1-19. a) Monthly sea surface temperature (SST) anomaly (monthly average removed) for the Sandpoint tide gauge station. Anomalies are calculated between January 1, 2007 and January 1, 2018. b) Heat flux terms (W/m^2) computed from the tide gauge station, an Automated Surface Observing System weather station 2.3 km away, and Reanalysis-2. Downward shortwave radiation (Q_{SW}) is computed from 6-hour averages of clear-sky Reanalysis-2. The combined longwave (Q_{LW}) and backscatter (Q_{BS}) flux term is derived from both tide gauge SST and weather station data, as are the sensible (Q_{SE}) and latent (Q_{LA}) terms. c) Heat flux of the ocean (Q_{OC}) assuming the changes in SST are uniform over the upper 15 m and the sum (Q_{SUM}) of the terms in panel (b). The inset map shows the location of the Sand Point station (yellow star). 1-36
Figure 1-20. Annual averages of the anomaly of Q_{SUM} (annual cycle from 2007 to 2017 removed) for all sites with oceanographic and Automated Surface Observing System weather stations in close proximity (inset map). Error bars show the standard deviation of the anomaly divided by the square root of degrees of freedom. We assume 90 degrees of freedom in each yearly average since the decorrelation time scale for ocean and atmospheric signals is several days. 1-37
Figure 1-21. Reanalysis-2 estimates of the annual mean net surface heat flux anomaly (W/m^2) for 2010 to 2015 from the over the NE Pacific. 1-37
Figure 1-22. Monthly temperature anomalies at ocean station PAPA (from the Optimum Interpolation Sea Surface Temperature record), the Sitka tide gauge station, System Wide Monitoring Program (SWMP) mooring and GAK1 over 2008-2017. Anomalies are all referenced to the same 2008-2019 baseline. 1-39
Figure 2-1. Map of study area showing Gulf Watch Alaska nearshore rocky intertidal sites, as described in Konar et al. 2016, monitored annually 2012-2019 in each region, Western Prince William Sound (green diamonds), Kenai Fjords National Park (NP) (blue

triangles), Kachemak Bay (purple circles), and Katmai NP (red squares). Dark gray shaded land demarks National Park (NP) boundaries..... 2-4
Figure 2-2. Intertidal sea water temperature monthly anomaly plots for each of the four regions from 2012-2019 recorded at 0.5 m tidal stratum at each monitoring site by a HOBO v2 temperature logger. Anomalies are based on the annual monthly mean from all sites within region minus the total monthly mean from all years for that region. Positive anomalies (red) depict warmer than average and negative anomalies (blue) depict cooler that average temperatures. The dashed gray line shows the onset of the Pacific marine heatwave in May 2014. 2-8
Figure 2-3. nMDS of Bray Curtis similarities of rocky intertidal community structure by region: Western Prince William Sound (green diamonds), Kenai Fjords (blue triangles), Kachemak Bay (purple circles) and Katmai National Park (red squares), and by tidal stratum: low (solid symbols) and mid (open/dashed symbols) across all years (2012-2019) as denoted by the arrow vector connecting each point. Each point represents the mean similarity for each region-stratum-year sample combination. 2-9
Figure 2-4. Mean community similarity across all regions before (light gray, 2012-2014) and during/after (dark gray, 2015-2019) the Pacific marine heatwave, between mid- and low-tidal strata. 2-10
Figure 2-5. nMDS plots of similarity in rocky intertidal community structure among regions: Western Prince William Sound (green diamonds), Kenai Fjords (blue triangles), Kachemak Bay (purple circles), and Katmai National Park (red squares), between the mid (upper panel) and low (lower panel) intertidal. Trajectories are through time, before-Pacific marine heatwave (2012-2014, closed symbols) and during/after-Pacific marine heatwave (2015-2019, open symbols) periods, as depicted by the trajectory arrow by region. 2-12
Figure 2-6. Heat map of mean percent cover for taxa determined important drivers of rocky intertidal community structure for mid- and low-tidal strata, by SIMPER analysis. Cell color scale (0 to 6) shows relative mean percent cover data of fourth root transformed percent cover data, averaged among regions, through time from 2012 to 2019. Light blue and white cells indicate low to no cover, red to black indicate moderate to high cover. Symbols denote taxa as macroalga (solid circle), invertebrate (asterisk), or open space (open square). 2-13
Figure 2-7. Means (±SE) plots for taxa that contribute 70% of the observed variability in rocky intertidal community structure at 1.5 m (orange line) and 0.5 m (blue line) tidal strata through time, from 2012 to 2019, across all regions. The dashed gray line indicates the onset of the Pacific marine heatwave..... 2-14
Figure 3-1. Generalized life history strategies, indicating the monthly timing of spawning, larvae and early juvenile stages for three key forage fish species in the North Pacific as summarized from data in Doyle et al. (2019). 3-3

Figure 3-2. Map of the Northern Gulf of Alaska study area, including sampling locations for a subset of Gulf Watch Alaska long-term monitoring program (all circles; integrated predator prey survey [IPP], black line; continuous plankton recorder [CPR], blue line). Capelin survey extents by the National Oceanic and Atmospheric Administration-Alaska Fishery Science Center include the central Gulf of Alaska (CGOA, gold polygon) and the Gulf of Alaska (blue polygon, inset). Seafloor depth reaches over 4,500 m with lighter shading representing shallower depths, the 500 m isobath is denoted by a dashed-blue line..... 3-5
Figure 3-3. Standardized frequency anomalies for capelin and sand lance in diving and surface-feeding seabirds at Middleton Island. Frequencies were standardized to a mean of 0 and standard deviation of 1..... 3-9
Figure 3-4. Sand lance catch per unit effort (CPUE, number of fish/number of diet samples) by year and size group in tufted puffin and rhinoceros auklet chick diets at Middleton Island during June-August. Size group 0, 1, and 2 generally corresponds with age-0 fish (mean length range among years: 68-91 mm), age-1+ fish (mean length range among years: 111-130), and age-2+ fish (mean length range among years: 127-181), respectively..... 3-10
Figure 3-5. Indices of capelin relative abundance based on the log catch-per-unit-effort (CPUE, kg km^{-2}) from bottom trawl, pelagic trawl, and acoustic-trawl surveys conducted in the Gulf of Alaska (left panels) and central Gulf of Alaska (Central GOA) shelf near Kodiak Island (right panels). CPUEs are shown relative to the long-term mean CPUE for each index. Years in which surveys were not conducted (black 'x'), data were not available (blue 'x'), or capelin acoustic densities were too low to estimate abundance (red 'x') are indicated on x-axis (McGowan et al. 2020)..... 3-11
Figure 3-6. Prince William Sound (PWS) spawning herring abundance indices over time, including aerial surveys of milt (points) and the PWS Science Center Acoustic Index (color). Grey circles and lines indicate years in which no acoustic surveys were conducted..... 3-12
Figure 3-7. Length and age histogram from spawning male capelin at Port Etches, Prince William Sound during July 2013 and 2016. Dashed line indicates the mean length in each year..... 3-13
Figure 3-8. Interannual variability of whole fish energy for age-1 sand lance within Prince William Sound. Points represent the values of outliers, and the dotted line represents the mean value across years..... 3-14
Figure 3-9. Interannual variability of Prince William Sound herring age-3 (increment 4) growth from scale increment width measurements..... 3-15
Figure 3-10. Prince William Sound Pacific herring standardized weight anomaly by year and age (vertical panels, age in years labels to the right). Average weights were standardized across years to a mean of 0 and standard deviation of 1. Points are colored by the proportion of each age class in the population, and sized relative to the coefficient of variation of weights by age and year..... 3-16

Figure 3-11. Mean (± 95% confidence intervals) for a) whole body energy density (kJ/g), b) fork length (mm, middle), and c) total energy (kJ, bottom) of age-0 herring sampled in November (light bars) and the following March (dark bars) in Prince William Sound between 2007 and 2016. 3-17
Figure 3-12. Mean (standard deviation) biomass of euphausiids by year (x-axis), region (columns), season (rows), and species (color) sampled by multinet or bongo nets (505 µ mesh) along the Seward Line and Prince William Sound (PWS). 3-18
Figure 3-13. Interannual variability in the acoustic macrozooplankton index (NASC, nautical areas scattering coefficient, nmi^{-2}) in Prince William Sound humpback whale foraging aggregation areas. Data were collected during the September Integrated Predator Prey surveys in 2017-2019 and compared to a pre-heatwave pilot study in 2014. 3-18
Figure 3-14. Mean (standard deviation) biomass of copepods by year, region (columns), season (rows), and species (color) sampled by multinet or bongo nets (505 µ mesh) along the Seward Line and Prince William Sound (PWS). 3-19
Figure 3-15. Mean abundance of small and large copepods by season (spring = March-May, summer = June-August, fall = September-November) from continuous plankton recorder samples collected on the northern Gulf of Alaska shelf. A loess smoother identifies the general trend (blue line) and standard error (grey polygon) over time. Coefficients of variation (CV) in abundance among months for each season and year are indicated by the color of points, with darker shades indicating lower CVs. 3-20
Figure 3-16. Prince William Sound monthly zooplankton abundance anomalies for 2009-2018. Three categories are presented, the entire community, warm water copepods, and cold-water copepods. Red bars indicate positive anomalies and blue bars indicate negative anomalies. All data were $\log_{10}(n+1)$ transformed to stabilize variance, hence an anomaly of ±1 indicates an order of magnitude change. 3-21
Figure 3-17. Standardized murre density (color, standardized to a mean of 0 and standard deviation of 1 for data collected in 2006-2019) by year, season, and region (Prince William Sound [PWS]). Light grey indicates no data, and dark grey indicates zero density in every survey. 3-22
Figure 3-18. Humpback whale encounter rates (left) and crude index of birth rate (right) during fall surveys in Prince William Sound. The regression between crude index of birth rate by year (solid line) was weighted by the encounter rate ($R2 = 0.50$, $p = 0.03$). The grey circle for 2019 is provisional. 3-23
Figure 4-1. Anomalies (°C) of upper (0-50m) and lower (200-250 m) water column temperatures at the GAK1 oceanographic station in the Gulf of Alaska (for location, see Figure 4-2). The multi-year heatwave that began in 2014 was the most persistent in the 48-year time series and it extended throughout the water column of the continental shelf. 4-3
Figure 4-2. Sampling locations in the northern Gulf of Alaska. The division for references to eastern and western study area is the continuous plankton recorder transect into Cook Inlet. The black contours within the Seward Line marine bird survey area differentiate

inner continental shelf (shore to 50 km from shore), middle shelf (50 km from shore to shelf-slope break, defined using 1,000 m isobath) and oceanic (seaward of the 1,000 m isobath) domains (Sousa et al. 2016). The 1,000 m isobath is also used to distinguish shelf vs. oceanic zooplankton samples from the continuous plankton recorder. Marine bird (black-legged kittiwake, rhinoceros auklet) foraging routes provided by Shannon Whelan, McGill University..... 4-4
Figure 4-3. The common trend from the best model fit (lowest AICc; Table 4-2) identified from dynamic factor analysis of 113 biological time series including abundance (e.g., biomass) and performance (e.g., reproductive success) metrics. Grey shading represents the 2014-2016 northeast Pacific marine heatwave..... 4-11
Figure 4-4. Mainly negative trends in algal and sea star (upper and middle panels) and mainly positive trends in mussel abundance (lower panel) at four regions across the northern Gulf of Alaska. Points are annual values, middle solid line is model fit to data, and shaded area is 95% confidence interval of model fit. Values are z-score standardizations so the y-axes are unitless..... 4-13
Figure 4-5. Negative trends in abundance of juvenile capelin from surface feeding (kittiwake) and diving (auklet) marine bird diets in the eastern portion of the northern Gulf of Alaska and herring abundance and growth in Prince William Sound (PWS; upper panel). Positive trends in abundance of larval and juvenile Pacific sand lance from western and eastern study areas, respectively, and negative trend in whole body energy content of sand lance in PWS (lower panel). Points are annual values, middle solid line is model fit to data, and shaded area is 95% confidence interval of model fit. Values are z-score standardizations so the y-axes are unitless..... 4-14
Figure 4-6. Negative trends in the abundance of kittiwake nests in Prince William Sound (PWS), kittiwake reproductive success in PWS and Middleton Island (MI), and Steller sea lion pup counts on rookeries throughout the northern Gulf of Alaska (GOA; upper panel). Negative trends (with one exception) in abundance of Steller sea lion non-pups at haul-out sites and rookeries from throughout the northern GOA and humpback and killer whale abundance indices in and adjacent to PWS (lower panel). Points are annual values, middle solid line is model fit to data, and shaded area is 95% confidence interval of model fit. Values are z-score standardizations so the y-axes are unitless. 4-15
Figure 4-7. Standardized abundance of warm water (upper panel) and cool water (lower panel) associated copepod species from continuous plankton recorder (CPR) over oceanic and shelf waters and inside waters of Kachemak Bay and Prince William Sound (PWS). Points are annual values, middle solid line is model fit to data, and shaded area is 95% confidence interval of model fit. Values are z-score standardizations so the y-axes are unitless. 4-16
Figure 4-8. Contrasting negative (upper panel) and positive (lower panel) trends in various salmon and groundfish metrics during and after the 2014-2016 Pacific marine heatwave. Points are annual values, middle solid line is model fit to data, and shaded area is 95%

confidence interval of model fit. Values are z-score standardizations so the y-axes are unitless. 4-17
Figure 4-9. Marine bird abundance at sea exhibited primarily short-term, annual changes in Prince William Sound (PWS) and the Gulf of Alaska (GOA), including inshore shifts in distribution for common murres (primarily piscivores, upper panel) and northern fulmars (omnivores, lower panel). Only fork-tailed storm-petrels (primarily zooplanktivore) showed a persistent change in distribution (lower panel). Points are annual values, middle solid line is model fit to data, and shaded area is 95% confidence interval of model fit. Values are z-score standardizations so the y-axes are unitless. 4-18
Figure 4-10. Cluster and community (nMDS) analyses of all biological time series combined prior to and during (strongest from 2014-2016) a multi-year marine heatwave in the Gulf of Alaska. In the cluster analysis (left) solid lines indicate significantly (similarity profile routine) different year groupings. In the nMDS (right) the different colors represent significantly (analysis of similarities) different year groupings. 4-19
Figure 4-11. Long-term trends in water column temperature at the GAK1 station (top), the abundance of warm water associated copepod species in the Gulf of Alaska (GOA; 2nd from top), herring and herring dependent predators in Prince William Sound (3rd from top), capelin and sand lance availability to marine birds and reproductive success of kittiwakes foraging from Middleton Island (2nd from bottom), and sablefish abundance of recruits, age-2 biomass (Hanselman et al. 2018), and juvenile growth (bottom). Values are z-score standardizations so the y-axes are unitless. 4-20

This page intentionally left blank.

EXECUTIVE SUMMARY

BACKGROUND

The *Exxon Valdez* Oil Spill (EVOS) Trustee Council (EVOSTC) initiated funding for the Gulf Watch Alaska (GWA) long-term monitoring program in 2012. Gulf Watch Alaska addresses the goals and priorities of the 1994 EVOS Restoration Plan (EVOSTC 1994) and the 2010 Injured Resources and Services Update (EVOSTC 2010b). Those documents highlighted the need for a sustained and interdisciplinary monitoring system to inform restoration needs and activities for injured resources (McCammon et al. 2011). Now in year eight, GWA continues to fulfill these original objectives, in addition to providing context for ecosystem recovery from the EVOS relative to other sources of natural and anthropogenic variation (Lindeberg et al. 2016). Gulf Watch Alaska has matured into a highly collaborative program that enhances the value of EVOSTC funding by leveraging efforts with other monitoring and research programs in the Gulf of Alaska (GOA). These include both EVOSTC programs and projects, and those from state and federal agencies, the North Pacific Research Board, the Alaska Ocean Observing System, and the National Science Foundation. Gulf Watch Alaska has three components that monitor key ecosystem features of the EVOS-affected area in the northern GOA: 1) Environmental Drivers (physical and biological oceanography), 2) Pelagic Ecosystem (forage fish and predator food web), and 3) Nearshore Ecosystem (intertidal species food web). Within the three GWA components, there are 11 field sampling projects, ten of which started before GWA was formed in 2012 and several legacy datasets that started during or before the 1989 EVOS. Gulf Watch Alaska includes more than 25 principal investigators whose expertise and knowledge of GOA ecosystems and the spill-affected region is widely respected. Gulf Watch Alaska investigators identified five primary objectives in their current 5-year work plan:

1. Sustain and build upon existing time series in the EVOS-affected regions of the GOA.
2. Provide scientific data, data products and outreach to management agencies and a wide variety of users.
3. Develop science synthesis products to assist management actions, inform the public, and guide monitoring priorities for the next 15 years.
4. Continue to build on collaborations between the GWA and Herring Research and Monitoring programs, as well as other Trustee program focus areas, including the data management program, lingering oil, and potential cross-program publishing groups.
5. Leverage partnerships with outside agencies and groups to integrate data and expand capacity through collaborative efforts.

PRODUCTS

Over the past eight years, GWA investigators have archived more than 45 time series datasets that are publicly available online in DataONE (dataone.org) through 2016, or through the AOOS Gulf of Alaska data portal, where they are updated annually (portal.aoos.org; both thanks to the EVOSTC Data Management Program). Program scientists have published more than 90 papers in peer reviewed journals, including a special issue of Deep-Sea Research II titled “Spatial and Temporal Ecological Variability in the Northern Gulf of Alaska: What Have We Learned Since the *Exxon Valdez* Oil Spill?” Gulf Watch Alaska investigators also have given over 360

presentations at meetings, professional conferences, and public events. Gulf Watch Alaska participants also have contributed to community outreach activities, including several visits to EVOS-affected communities for two-way exchanges of knowledge. Additional outreach and engagement efforts included contributions each year to the Delta Sound Connection (newspaper with 10,000 copies printed and distributed annually), more than 25 media releases (interviews, radio shows, web stories, documentaries, podcasts, and YouTube videos) produced in collaboration with agency outreach efforts during the last three years, and finally, maintaining current content on the GWA webpage (GulfWatchAlaska.org).

An area of expanded focus for GWA during the current 5-year period is contributions to ecosystem-based fisheries management in the GOA. In 2019, GWA contributed 23 time series indicators from all three GWA components to the annual National Oceanic and Atmospheric Administration (NOAA) Ecosystem Status Report (Zador and Yasumiishi 2018), a three-fold increase in contributions from the start of this 5-year funding period. The Ecosystem Status Report is prepared annually by NOAA to inform the North Pacific Fishery Management Council about the current state of the ecosystem and the potential implications to commercial fish stocks. Gulf Watch Alaska is also contributing to new developments within the North Pacific Fisheries Management Council process, including Ecosystem and Socioeconomic Profiles that will quantitatively integrate relevant ecosystem indicator time series into fisheries stock assessment models.

We continue to identify individual time series and metrics that are relevant to other Trustee agencies at the state and federal level, in addition to meeting EVOSTC monitoring and research objectives. For example, GWA's sampling also contributes to the National Park Service's Southwest Alaska Network Inventory and Monitoring Program and management of Katmai and Kenai Fjords National Parks. The U.S. Fish and Wildlife Service has used GWA studies to assist in species status assessments for listing under the Endangered Species Act, and to address migratory bird management issues. Sea otter and humpback whale data collected by GWA investigators are used by U.S. Fish and Wildlife Service, US Geological Survey and NOAA Fisheries Protected Resources and Marine Mammal divisions for informing mandates under the Marine Mammal Protection Act (e.g. stock assessments, de-listing, critical habitat, and stranding network). Alaska Departments of Fish and Game and Environmental Conservation utilize GWA information for stock assessments of Pacific herring (*Clupea pallasii*) in Prince William Sound and to address water quality issues (e.g., harmful algal blooms, paralytic shellfish poisoning, and ocean acidification) that potentially affect shellfish aquaculture and harvest management. Gulf Watch Alaska time series are also widely used throughout the scientific community. For example, data from the GAK1 oceanographic sampling station have been used in more than 90 publications, with the annual rate increasing at three publications per year.

FINDINGS

EVOS INJURED RESOURCES

Since the EVOS, many injured resources have recovered, but some have not, or their status is unknown (Esler et al. 2018). The GWA program follows the EVOSTC definitions of recovery for injured resources from the spill. These definitions vary by species, but generally require a

return to conditions that would have been present had the spill not occurred and no further exposure to lingering hydrocarbons from the spill. The GWA program monitors many recovering or recently recovered species but here we highlight three key species monitored by GWA that have not recovered from the spill.

Pigeon guillemots

The abundance of pigeon guillemots (*Cepphus columba)* during summer throughout Prince William Sound remains well below pre-spill levels (Figure ES-1). Low abundance is likely due to chronic lack of lipid rich schooling forage fishes, which is consistent with long-term studies of marine birds and other wildlife in Prince William Sound (Cushing et al. 2018, Esler et al. 2018) and given that pigeon guillemots stopped showing indications of residual oil ingestion over 15 years ago (Golet et al. 2002). Seven other bird species in the Sound, primarily forage fish consumers, have declined while only three have increased over the 30-years since the EVOS (Cushing et al. 2018). Several species appear to be at a new "baseline" similar to that observed for the pigeon guillemot.

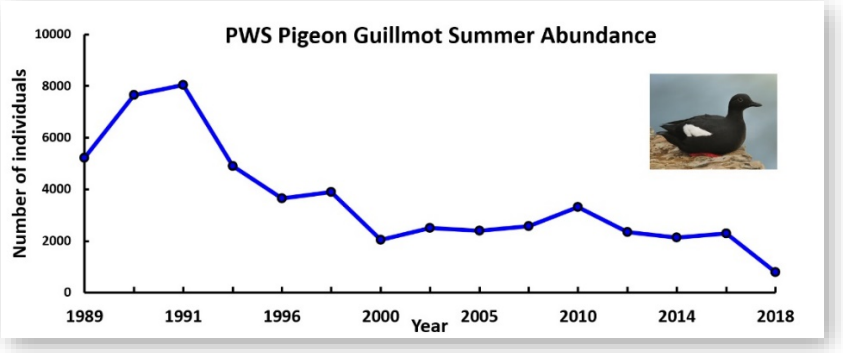

Figure ES-1. Abundance of pigeon guillemots during summer in Prince William Sound. Photo: Commons.Wikimedia.org.

Killer whales

The AT1 pod of killer whales (*Orcinus orca*) is unlikely to recover from the EVOS given that no reproductive females are left in the pod and the AB pod has had limited growth over 30-years post-spill (Figure ES-2). Furthermore, few calves and not all AB pod individuals have been observed in recent years, making current population estimates uncertain and suggesting birth rates may have decreased and mortality rates increased over the last few years.

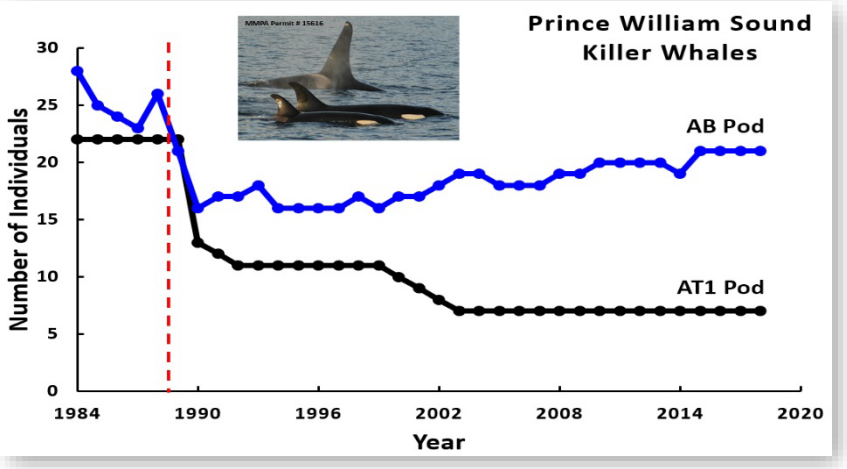

Figure ES-2. Long-term trend in abundance of resident (AB) and transient (AT1) killer whales that frequent Prince William Sound. The vertical line indicates the timing of the Exxon Valdez oil spill. Photo: Craig Matkin, North Gulf Oceanic Society. Note: values from the most recent few years assume a static population even though not all individuals were observed. It is too soon to confirm possible mortalities.

Pacific herring

The Herring Research and Monitoring program has shown that the herring population continues to decline in Prince William Sound, with a recent step change in 2016-2019. We also observed parallel declines in some herring-specialist predators in the Sound (Figure ES-3). These predators do switch to other non-herring prey when herring are not available, but apparently at a cost of lower reproductive success and abundance (Suryan et al. 2006, Moran et al. 2018).

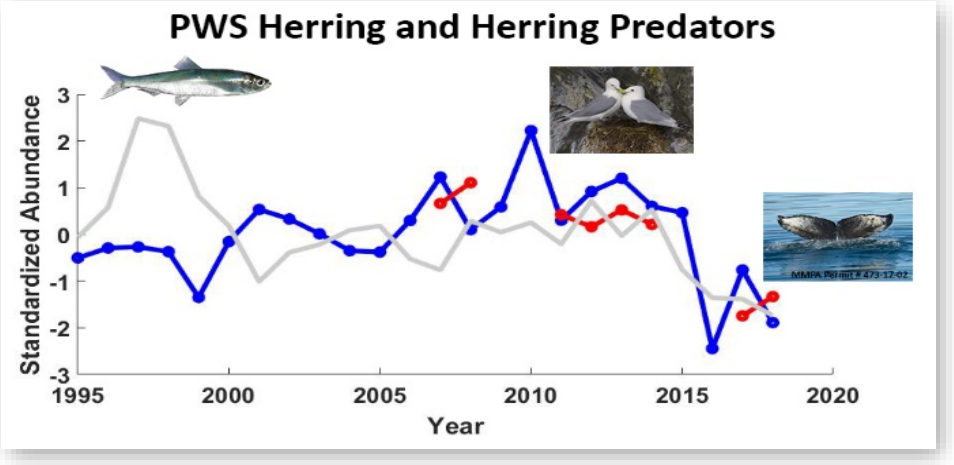

Figure ES-3. Trends in Pacific herring and herring dependent predators in Prince William Sound. Herring spawn (miles-day milt; grey line) from Exxon Valdez Oil Spill Trustee Council Herring Research and Monitoring program, black-legged kittiwake (Rissa tridactyla) nesting abundance (blue line) from Exxon Valdez Oil Spill Trustee Council Pigeon Guillemot Restoration Research project, and abundance of individual humpback whales (red line) from Gulf Watch Alaska. Abundances are standardized to a mean of zero and standard deviation of one. Pacific herring and Humpback whale photos by NOAA: Mark Carls and John Moran respectively. Black-legged kittiwake photo from Commons.Wikimedia.org.

Environmental variability and the Gulf of Alaska ecosystem

One of the most significant, contemporary ecosystem perturbations in the GOA, the Northeast Pacific marine heatwave (PMH), occurred during 2014-2016. Gulf Watch Alaska was fortuitously positioned to document this event and the ecosystem effects. The PMH was first identified as "The Blob" of anomalously warm water in the northeast Pacific during fall/winter of 2013. The warming continued in the GOA during 2014 and intensified as a strong El Nino developed and continued into 2016 (DiLorenzo and Mantua 2016). The PMH was especially anomalous in duration and spatial extent (Hobday et al. 2018). By 2016, effects of the PMH included unusual occurrence of warm water associated species not common to Alaska (Sutherland et al. 2018), whale and seabird mortality events (Savage 2017, Piatt et al. accepted), changes in the distribution and abundance of some groundfish stocks (Barbeaux et al. 2018, Yang et al. 2019), effects on fishery revenue (Fissel et al. 2019), and difficulties for whale watching tour operators to locate whales. Although there was a heatwave hiatus (as indicated by surface waters) in 2017 through fall 2018, the heatwave began to re-intensify and persisted through at least summer 2019. This prolonged heatwave is affecting most of Alaska, including the Bering Sea and Arctic Ocean, with the warmest summer temperatures (Figure ES-4) and most ice-free days on record. Given that the drivers of global marine heatwaves indicate their frequency will increase (Oliver et al. 2018, Holbrook et al. 2019), the 2014-2016 PMH in the GOA and its impact on marine resources is a particularly important event to capture and describe.

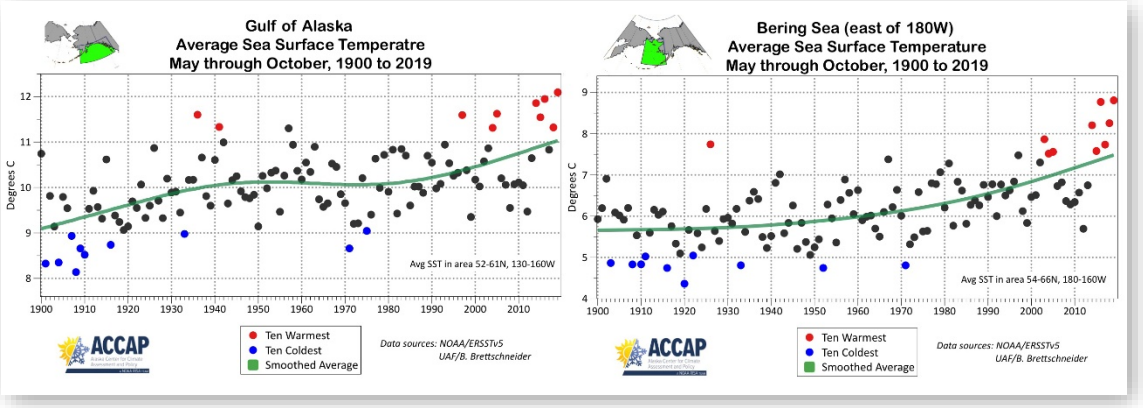

Figure ES-4. Sea surface temperatures in the Gulf of Alaska and Bering Sea showing that 5 (Gulf of Alaska) to 6 (Bering Sea) of the warmest 10 years over the past 119 years occurred after the onset of the marine heatwave in 2014 (Source: University of Alaska Fairbanks, Alaska Center for Climate Assessment and Policy (ACCAP)).

We have, therefore, structured this science synthesis report around four draft manuscripts (Chapters 1-4) that evaluate effects of the PMH on marine resources of the northern GOA. Chapter 1 used 37 time series from two GWA components and more than 30 other buoy, weather station, and satellite datasets to describe the dominant patterns, concordance, and timing of water temperatures from across the GWA study area and adjacent regions, ranging from the intertidal zone to offshore oceanic and surface to seafloor. Chapter 2 used 81 taxonomic metrics and 17 focal time series from one GWA component to describe how rocky intertidal communities from Prince William Sound to the Alaska Peninsula responded to the PMH. Chapter 3 used 31 time series from all three GWA components and the Herring Research and Monitoring program to describe constraints on forage fish condition and abundance during the PMH. Chapter 4 used 113 time series from all three GWA components, Herring Research and Monitoring program, NOAA Fisheries, and other collaborators to describe how the GOA ecosystem overall responded to the PMH and what taxa tended to show negative, neutral, or positive responses. Below, we highlight a few of the cross-component results from GWA synthesis efforts.

Overview of Physical Patterns and Biological Responses

There were multiple features that made the 2014-2016 GOA heatwave unique for the Northeast Pacific: (1) warm anomalies persisted for 2 years through all seasons, including winter - Chapter 1; (2) warm anomalies penetrated deep waters, including the entire water column over the continental shelf - Chapter 1; (3) warm anomalies were present in all areas, including intertidal zones - Chapter 1 & Chapter 2; Figure ES-5; and (4) the large spatial extent of the PMH included the coasts of Alaska, Canada, and the U.S. west coast - Chapter 1.

There was a statistically significant positive trend in bottom water salinity (becoming saltier) with the addition of the PMH years, as identified by the nearly 50-year temperature time series from GAK1. This, along with a significant negative trend in upper water column salinity (becoming fresher), increases stratification of the water column, which can hinder water column mixing that is important to replenish nutrients in the photic zone for phytoplankton growth. Freshening of surface water was noted in Kachemak Bay during record low precipitation in summer 2019, indicating that glacial ice melt is, in part, maintaining this trend. We also documented record warm upper water column temperatures in Kachemak Bay and Prince William Sound during summer 2019.

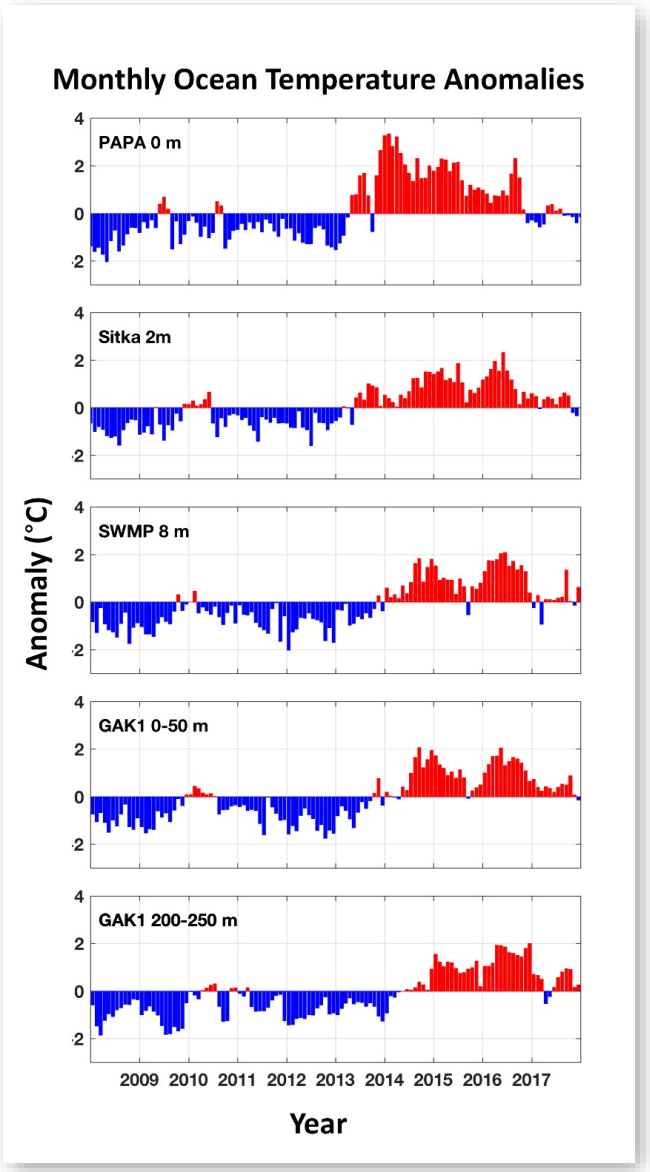

Figure ES-5. Monthly ocean temperature anomalies 2008-2017 from various depths (m) at ocean station PAPA in the northeast Pacific (50°N 145°W), Sitka, Alaska, Kachemak Bay (SWMP), and outside Resurrection Bay near Seward (GAK1).

Anomalously warm temperatures during the PMH led to several biological responses. Harmful algal blooms were detected in Kachemak Bay (Figure ES-6) and elsewhere in the GOA and other regions of Alaska. Neurotoxins associated with harmful algal blooms were also found in seabirds and forage species during and after the PMH in Prince William Sound and Lower Cook Inlet (Van Hemert et al. in review). Warm water associated copepod species showed increased abundance in all areas (Chapter 4) and their peak abundance was a month or more later during and post PMH, suggesting reduced consumption by zooplankton predators or increased productivity of zooplankton. Multiple lines of evidence provide some support for the reduced consumption of zooplankton hypothesis, especially given that forage fish populations were reduced during and after the PMH (Chapter 3).

Despite some recent increases in the biomass of large copepods during spring (Chapter 3), there has been a secular, long-term decline (1997-2019) in copepod size during fall cruises along the Seward Line.

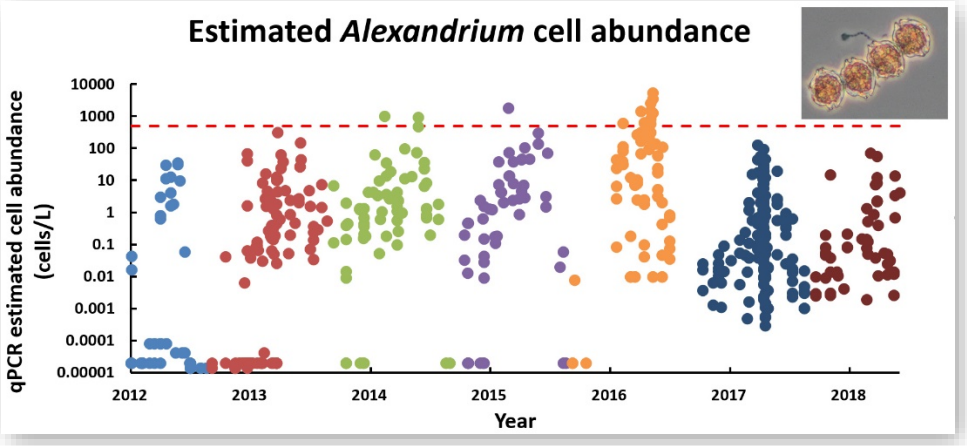

Figure ES-6. Alexandrium *spp. cell abundance (log$_{10}$ scale) in lower Cook Inlet and Kachemak Bay, 2012-2018. Paralytic shellfish poisoning toxins are likely to be detected in shellfish tissues for cell abundances above 500 cells/liter (red dashed line). Photo by NOAA: Brian Bill.*

Overall, biological responses to the PMH were evident from lower to upper trophic levels. Even intertidal organisms that tend to be resilient due to routine exposure to extreme air and water temperatures showed changes in community structure coincident with the onset of the PMH and persisting through 2019, with little indication of return to pre-heatwave conditions (Chapter 2 & Chapter 4). Likewise, abundance of key forage fishes and their marine bird and mammal predators changed (primarily declined) during the PMH and many still have not returned to pre-heatwave levels (Chapter 3 & Chapter 4). Reproductive success of many seabirds (Chapter 3 & Chapter 4), humpback whales (*Megaptera novaeangliae*; Straley et al. in prep) and killer whales declined. Furthermore, some predators showed clear signs of malnutrition, including lack of muscle mass in seabirds (Arimitsu et al. 2019) and blubber in humpback whales, thereby making skeletal features visible under their skin, as well as external parasite infestations (Figure ES-7). In over 40 years of humpback whale studies in the GOA, researchers had not observed such low apparent birth rates and malnourishment.

Figure ES-7. Humpback whales in Prince William Sound showing a robust whale with large blubber layer (top) and malnourished whale showing (arrows from left to right) a sharp, less rounded spine, right scapula visible under skin, and appearance of rough skin from parasites and lesions (bottom). Photos by NOAA: John Moran.

Several unusual mortality events occurred in the GOA during the PMH and ranged from sea stars (Konar et al. 2019; Chapter 4), to seabirds (Piatt et al. accepted, Chapter 3), and marine mammals (Savage 2017, 2019).

Through all this, there were some positives, too. For example: the abundance and distribution of large Pacific blue mussels (*Mytilus trossulus*; an important prey item in the nearshore ecosystem) increased; some marine birds exhibited distributional shifts, but no detectable changes in density; sea otter (*Enhydra lutris*) abundance did not change (although changes in diet reflect shifts in prey abundance) and juvenile sablefish (A*noplopona fimbria*) growth rates increased during the PMH (Figure ES-8; Chapter 4).

Preliminary results from 2019 offer minor encouragement regarding return of the GOA ecosystem to pre-PMH conditions. As noted above, warm water anomalies were prevalent through summer 2019. Fortunately, fall 2019 weather systems are helping to dissipate some of the heat in the upper water column. Regardless, biological indicators suggest heatwave-like conditions persist throughout the GWA study area in 2019, including increased abundance of warm water zooplankton species (after a decline in 2018) and metrics ranging from rockweed (*Fucus distichus)* and sea stars to capelin (*Mallotus villosus*) and whales collectively showed minor progress toward return to pre-PMH levels. Increased prey was observed in some areas like Prince William Sound and Lower Cook Inlet, however, there appears to be an inshore flux of typically offshore predators and thereby potentially increasing top-down effects on inshore prey populations. For example, the September 2019 GWA Integrated Predator-Prey cruise in Prince William Sound documented fin whales (*Balaenoptera physalus*), shearwaters (*Ardenna* spp.), and common murres (*Uria aalge*) inside or at entrances of Prince William Sound, and groundfish

such as sablefish (*Anoplopoma fimbria*) that have responded positively during the PMH, foraging on juvenile herring and krill (Figure ES-8). Gulf Watch Alaska investigators recorded similar observations of offshore predators feeding inshore in 2014, before major biological effects of the PMH were detected.

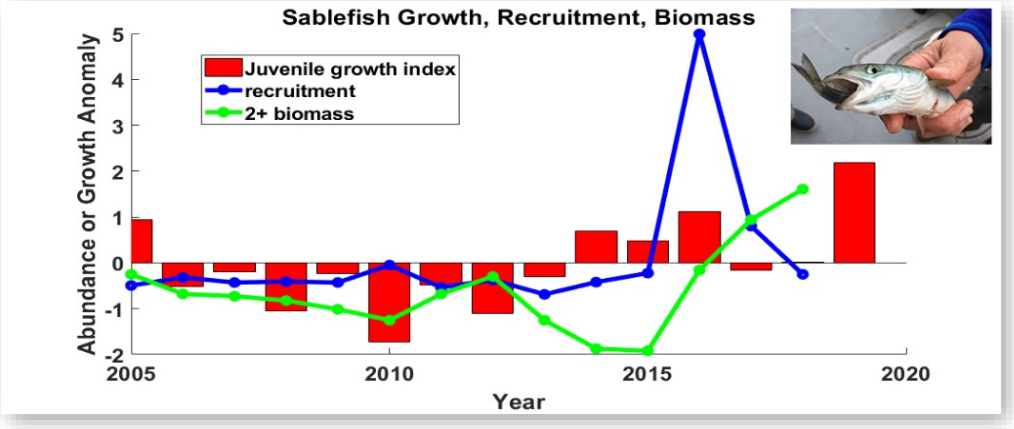

Figure ES-8. Trends in sablefish juvenile growth index (bars; fish collected by seabirds nesting at Middleton Island (Gulf Watch Alaska data), recruitment (blue line) and age 2+ biomass (green line; National Oceanic and Atmospheric Administration stock assessment, Hanselman et al. 2018). Picture inset of juvenile sablefish consuming juvenile herring in Prince William Sound during the September 2019 GWA Integrated Predator-Prey cruise. Photo by NOAA: John Moran.

In summary, the development of a large-scale marine heatwave and coincided, prolonged biological responses across multiple food webs, including commercially, culturally and ecologically important species, was well documented by GWA. The GOA community from 2014-2018 as described by our metrics appears to be different as a whole from previous years (Chapter 4) and it remains unclear if and when the GOA ecosystem might return to a pre-PMH state.

Future Directions

Gulf Watch Alaska investigators and stakeholders see the value in maintaining the existing structure and sampling regime of this long-term monitoring program (GWA program Objective 1). As the above summary and following synthesis chapters portray, the existing GWA data streams provide an understanding of the annual state of the ecosystem and potential limitations to recovery of resources in the EVOS-affected area (Objectives 2 & 3). Additionally, with our many collaborators we are poised to help understand mechanisms of change that can be used to model ecosystem response to future climate scenarios and their impact on resources throughout the GOA (Objectives 4 & 5). Therefore, we are not recommending changes to field sampling and data collection for the next 5-year funding cycle (FY22-26). Instead, we are proposing to build upon the data synthesis efforts presented in this report while we continue to improve the current products that we provide to stakeholders and develop additional products

that benefit a full range of stakeholders (Objectives 1-5). We recommend remaining adaptive as a program to address changing GOA conditions and resource management needs. Alaska is currently experiencing unexpectedly rapid environmental change with broad-scale effects on marine-dependent businesses and industries. The progressive vision in establishing GWA to inform management decisions regarding the recovery of EVOS-injured resources has the potential to be equally valuable to state, federal, and tribal interests in further developing the blue economy in the GOA. Developing a more complete understanding of the ecosystem effects of climate variability and other perturbations, anthropogenic or otherwise, are critical to reducing uncertainty that can hinder marine resource recovery designations and economic development.

LITERATURE CITED

Arimitsu, M., S. Schoen, J. Piatt, C. Marsteller, B. Heflin, and G. Drew. 2019. Status of forage fish and seabirds in Lower Cook Inlet during 2018. Annual report. USGS Alaska Science Center. Anchorage, AK.

Barbeaux, S., K. Aydin, B. Fissel, K. K. Holsman, B. Laurel, W. A. Palsson, K. Shotwell, Q. Yang, and S. Zador. 2018. Assessment of the Pacific cod stock in the Gulf of Alaska. National Marine Fisheries Service, Alaska Fisheries Science Center.

Bond, N. A., M. F. Cronin, H. Freeland, and N. Mantua. 2015. Causes and impacts of the 2014 warm anomaly in the NE Pacific. Geophysical Research Letters 42:3414-3420.

Cushing, D. A., D. D. Roby, and D. B. Irons. 2018. Patterns of distribution, abundance, and change over time in a subarctic marine bird community. Deep Sea Research Part II: Topical Studies in Oceanography 147:148-163.

Esler, D., B. E. Ballachey, C. Matkin, D. Cushing, R. Kaler, J. Bodkin, D. Monson, G. Esslinger, and K. Kloecker. 2018. Timelines and mechanisms of wildlife population recovery following the *Exxon Valdez* oil spill. Deep Sea Research Part II: Topical Studies in Oceanography 147:36-42.

EVOSTC (*Exxon Valdez* Oil Spill Trustee Council). 1994. *Exxon Valdez* Oil Spill Restoration Plan. *Exxon Valdez* Oil Spill Trustee Council, Anchorage, AK.

_____. 2010a. *Exxon Valdez* Oil Spill Trustee Council: Invitation for Proposals Federal Fiscal Years 2012-16. *Exxon Valdez* Oil Spill Trustee Council, Anchorage, Alaska.

_____. 2010b. *Exxon Valdez* Oil Spill Restoration Plan: 2010 Update Injured Resources and Services. *Exxon Valdez* Oil Spill Trustee Council, Anchorage, AK.

_____. 2015. *Exxon Valdez* Oil Spill Trustee Council: Invitation for Proposals Federal Fiscal Years 2017-21. *Exxon Valdez* Oil Spill Trustee Council, Anchorage, Alaska.

Di Lorenzo, E., and N. Mantua. 2016. Multi-year persistence of the 2014/15 North Pacific marine heatwave. Nature Clim. Change 6:1042-1047.

Fissel, B., M. Dalton, B. Garber-Yonts, A. C. Haynie, S. Kasperski, J. Lee, D. Lew, A. Lavoie, C. Seung, K. Sparks, M. Szymkowiak, and S. Wise. 2019. Stock assessment and fishery evaluation report for the groundfish fisheries of the Gulf of Alaska and Bering Sea/Aleutian Islands area: Economic status of the groundfish fisheries off Alaska, 2017.

Alaska Fisheries Science Center, National Marine Fisheries Service, National Oceanic and Atmospheric Administration.

Golet, G. H., P. E. Seiser, A. D. McGuire, D. D. Roby, J. B. Fischer, K. J. Kuletz, D. B. Irons, T. A. Dean, S. C. Jewett, and S. H. Newman. 2002. Long-term direct and indirect effects of the *Exxon Valdez* oil spill on pigeon guillemots in Prince William Sound, Alaska. Marine Ecology Progress Series 241:287-304.

Hanselman, D. H., C. J. Rodveller, K. H. Fenske, S. K. Shotwell, K. B. Echave, P. W. Malecha, and C. R. Lunsford. 2018. Assessment of the Sablefish stock in Alaska. NOAA Alaska Fisheries Science Center, Seattle, WA. https://www.afsc.noaa.gov/REFM/Docs/2018/BSAI/BSAIsablefish.pdf

Hobday, A., E. Oliver, A. Sen Gupta, J. Benthuysen, M. Burrows, M. Donat, N. Holbrook, P. Moore, M. Thomsen, T. Wernberg, and D. Smale. 2018. Categorizing and Naming Marine Heatwaves. Oceanography 31. https://doi.org/10.5670/oceanog.2018.205

Holbrook, N. J., H. A. Scannell, A. Sen Gupta, J. A. Benthuysen, M. Feng, E. C. J. Oliver, L. V. Alexander, M. T. Burrows, M. G. Donat, A. J. Hobday, P. J. Moore, S. E. Perkins-Kirkpatrick, D. A. Smale, S. C. Straub, and T. Wernberg. 2019. A global assessment of marine heatwaves and their drivers. Nature Communications 10:2624.

Konar, B., T. J. Mitchell, K. Iken, H. Coletti, T. Dean, D. Esler, M. Lindeberg, B. Pister, and B. Weitzman. 2019. Wasting disease and static environmental variables drive sea star assemblages in the Northern Gulf of Alaska. Journal of Experimental Marine Biology and Ecology 520:151209.

Lindeberg, M. R. 2016. Gulf Watch Alaska Program: Long-Term Monitoring of Marine Conditions and Injured Resources. FY17-21 Proposal to the *Exxon Valdez* Oil Spill Trustee Council. 57 p. http://www.evostc.state.ak.us/Store/ScienceSynthesisReports/LTM_Program_Proposal.pdf

McCammon, M., K. Hoffman, K. Holderied. D. R. Aderhold, and T. H. Neher. 2017. Long-term monitoring of marine conditions and injured resources and services. *Exxon Valdez* Oil Spill Restoration Project Final Report (Restoration Project 16120114), Alaska Ocean Observing System, Anchorage, Alaska.

McCammon, M., K. Holderied, and N. Bird. 2011. Long-term monitoring of marine conditions and injured resources and services. Proposal to *Exxon Valdez* Oil Spill Trustee Council. 879 p. http://www.evostc.state.ak.us/Store/Proposal_Documents/2196.pdf.

Moran, J. R., R. A. Heintz, J. M. Straley, and J. J. Vollenweider. 2018. Regional variation in the intensity of humpback whale predation on Pacific herring in the Gulf of Alaska. Deep Sea Research Part II: Topical Studies in Oceanography 147:187-195.

Oliver, E. C. J., M. G. Donat, M. T. Burrows, P. J. Moore, D. A. Smale, L. V. Alexander, J. A. Benthuysen, M. Feng, A. Sen Gupta, A. J. Hobday, N. J. Holbrook, S. E. Perkins-Kirkpatrick, H. A. Scannell, S. C. Straub, and T. Wernberg. 2018. Longer and more frequent marine heatwaves over the past century. Nature Communications 9:1324.

Piatt, J. F., J. K. Parrish, H. M. Renner, S. K. Schoen, T. Jones, M. L. Arimitsu, K. J. Kuletz, B. Bodenstein, M. García-Reyes, R. S. Duerr, R. M. Corcoran, R. Kaler, G. McChesney, R. Golightly, H. Coletti, R. M. Suryan, H. Burgess, J. Lindsey, K. Lindquist, P. Warzybok, J. Jahnke, J. Roletto, and W. J. Sydeman. Accepted. Extreme mortality and reproductive failure of common murres resulting from the northeast Pacific marine heatwave of 2014-2016. PLoS ONE.

Savage, K. 2017. Alaska and British Columbia large whale unusual mortality event summary report. Protected Resources Division, National Marine Fisheries Service, Alaska Region, Juneau, Alaska 99802.

_____. 2019. 2018 Alaska Region marine mammal stranding summary. Protected Resources Division, National Marine Fisheries Service, Alaska Region, Juneau, Alaska 99802.

Straley, J., J. Moran, C. Gabriele, J. Neilson, R. Suryan. In prep. Local collapse of a humpback whale population during a marine heatwave. Unpubl. manuscript.

Suryan, R. M., D. B. Irons, E. D. Brown, P. G. R. Jodice, and D. D. Roby. 2006. Site-specific effects on productivity of an upper trophic-level marine predator: Bottom-up, top-down, and mismatch effects on reproduction in a colonial seabird. Progress in Oceanography 68:303-328.

Sutherland, K. R., H. L. Sorensen, O. N. Blondheim, R. D. Brodeur, and A. W. E. Galloway. 2018. Range expansion of tropical pyrosomes in the northeast Pacific Ocean. Ecology 99:2397-2399.

VanHemert, C., S. K. Schoen, R. W. Litaker, M. M. Smith, W. C. Holland, M. L. Arimitsu, J. F. Piatt, D. R. Hardison, and J. M. Pearce. In Review. Assessment of algal toxins in Alaska seabirds associated with a large-scale Common Murre mortality event. Harmful Algae.

Yang, Q., E. D. Cokelet, P. J. Stabeno, L. Li, A. B. Hollowed, W. A. Palsson, N. A. Bond, and S. J. Barbeaux. 2019. How “The Blob” affected groundfish distributions in the Gulf of Alaska. Fisheries Oceanography 28:434-453.

Zador, S., and E. Yasumiishi. 2018. Ecosystem Status Report 2018 - Gulf of Alaska. NOAA Alaska Fisheries Science Center, Seattle, WA, https://access.afsc.noaa.gov/reem/ecoweb/Index.php

This page intentionally left blank.

CHAPTER 1 A STUDY OF MARINE TEMPERATURE VARIATIONS IN THE NORTHERN GULF OF ALASKA ACROSS YEARS OF MARINE HEATWAVES AND COLD SPELLS

Seth L. Danielson[1], Tyler D. Hennon[1], Daniel H. Monson[2], Rob M. Suryan[3], Rob W. Campbell[4], Steven J. Baird[5], Kristine Holderied[6] and Thomas J. Weingartner[1]

[1]*College of Fisheries and Ocean Sciences, University of Alaska Fairbanks, Fairbanks, AK 99775*
[2]*US Geological Survey, Alaska Science Center, Anchorage, AK 99508*
[3]*Alaska Fisheries Science Center, National Oceanographic and Atmospheric Administration, Juneau, AK 99801*
[4]*Prince William Sound Science Center, Cordova, AK 99574*
[5]*Kachemak Bay Research Reserve, Alaska Center for Conservation Science, University of Alaska Anchorage, Homer, AK 99603*
[6]*Kasitsna Bay Laboratory, National Centers for Coastal Ocean Science, National Oceanic and Atmospheric Administration, Homer AK, 99603*

Abstract

We use over 100 *in situ* and remotely sensed temperature datasets to investigate thermal variability within and across the intertidal nearshore, coastal and offshore waters of the northern Gulf of Alaska. For the years 1970 through 2019 we document a warming trend of 0.24±0.10 °C per decade for the coastal northern shelf (0-250 m depth average) and a Gulf-wide sea surface temperature (SST) trend of 0.25±0.11 °C per decade. The Gulf-wide SST trend in the last half-century is more than twice that of the 0.11±0.003 °C warming rate computed for 1900-2019. Decorrelation length scales vary regionally and correlation of synoptic scale fluctuations (less than one month) between two stations rapidly degrades with increasing station distance, accounting for less than 10% of the covariance for separations exceeding 100 km. In contrast, stations separated by as much as 500 km retain 50% of their covariance in common for seasonal and sub-seasonal fluctuations. While satellite-based measures often capture most of the daily SST anomaly in coastal and offshore waters, a significant portion of the variance (30-40%) can remain unresolved, even exceeding 75% in the nearshore realm. Similarly, the North Pacific and Gulf of Alaska leading modes of SST variability leave large fractions (25-50%) of the sub-seasonal thermal variance unresolved. These evaluations show the importance of *in situ* temperature records for studies that seek to understand mechanistic responses of marine organisms to habitat variability at biologically important time and space scales. We find that near-bottom temperature anomalies on the outer shelf vary inversely with surface temperatures and with near-bottom salinity, suggesting that thermal anomalies are also linked with nutrient flux anomalies. A case study of the recent Pacific marine heatwave and transition out of preceding cool years shows that the northern Gulf of Alaska surface temperatures (0-50 m) were elevated from 2014 to 2019 relative to the long-term record. Coastal temperatures warmed contemporaneously with offshore waters through the 2013 calendar year. In contrast, deep inner shelf waters (200-250 m) exhibited delayed warming relative to the surface and relative to deep waters offshore at the same depth. While offshore surface waters cooled from early 2014 into

early 2016, the shelf continued to warm over this time as the effects of local air-sea and advective heat fluxes continued to permeate across the northern Gulf. These results highlight the importance of different heating mechanisms for surface and near-bottom waters across the northern Gulf of Alaska.

INTRODUCTION

Gulf of Alaska (Figure 1-1) marine waters provide and regulate myriad socioeconomic and ecosystem services, including culturally and economically important fisheries harvests, tourism, shipping, habitat for seabirds and marine mammals, and the translation and transformation of physical and biogeochemical constituents of the marine carbon pump (Mundy 2005). The functioning and structure of these services have evolved into their present state under the influence of the regional bathymetry, surrounding landforms, and the physical drivers that maintain the system within the characteristic bounds of the sub-Arctic North Pacific climate. Climate change is driving this system beyond previously observed limits (Litzow et al. 2020), with spatially broad and temporally extended temperature anomalies such as the North Pacific marine heatwave of 2014-2016 (Bond et al. 2015, Walsh et al. 2018). This paper focuses on the Gulf of Alaska between the Aleutian Islands and Southeast (SE) Alaska, assessing thermal variability across synoptic (1-30 days), seasonal, and inter-annual time scales and across intertidal nearshore, coastal, and offshore waters. We use more than 100 *in situ* and remotely sensed temperature datasets to quantify local, regional, and basin-scale variability and to better understand the manifestation extended intervals of cold and warmth, and consequences of a changing climate.

Since the 1989 *Exxon Valdez* oil spill, monitoring of the Gulf of Alaska marine environment and the recovery of injured resources have been important components of the post-spill responses, which also include habitat protection and restoration efforts (Weiner et al. 1997, Peterson et al. 2003). Marine environmental and ecosystem monitoring has continued uninterrupted over this time through a succession of research programs since the oil spill (Rice and Peterson 2018) and much of the *in situ* data used in the present analysis derives from these efforts. Presently, a consortium of federal agencies and academic partners carry out this monitoring under the frameworks of the Gulf Watch Alaska program (Aderhold et al. 2018), the National Science Foundation's Long-Term Ecological Research program (Gosz et al. 2010) in the Northern Gulf of Alaska, and other efforts. Together, these ongoing studies document environmental conditions, biological communities, and population dynamics in the intertidal zone, in coastal waters, and in offshore waters across the northern Gulf of Alaska, including Prince William Sound (PWS) and Cook Inlet.

The value of the time series datasets increases with passing time because analyses of longer records can better separate natural scales and causes of variability from variations that are triggered by discrete disturbances such as the *Exxon Valdez* oil spill or shifts in climate (e.g., Agler et al. 1999, Lance et al. 2001). Only with the extended, multi-decade datasets such as those being collected by Gulf Watch Alaska and partner programs are we beginning to well appreciate some of the complex and interconnected relationships between climate, marine resource variations and management actions. These advances now permit such data to meaningfully

inform an ecosystem approach to fisheries management (Zador et al. 2017); the North Pacific Fishery Management Council uses these data to help guide decisions on fisher catch limits.

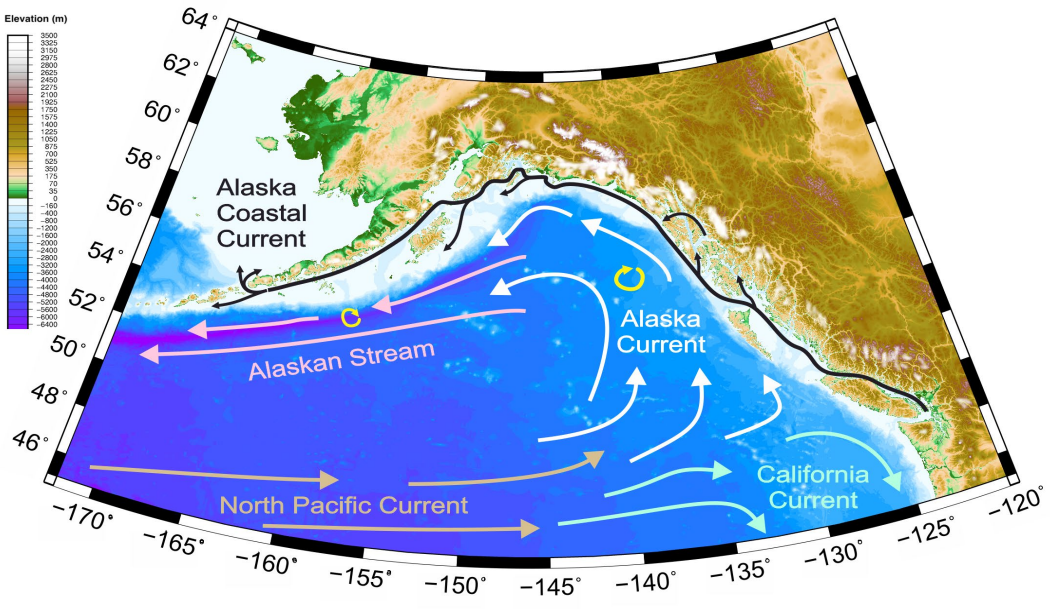

Figure 1-1. Ocean circulation, land topography, and ocean bathymetry in the Gulf of Alaska.

OCEANOGRAPHIC SETTING

The bathymetric variations and basin geometry (Figures 1-1 and 1-2) exert defining control on the Gulf of Alaska's flow field, which is important for the lateral advection of heat (Janout et al. 2013), freshwater (Royer 1982), and biota (Weingartner et al. 2002). The geomorphology includes island archipelagos, glacially carved fjord systems and subsea relict moraines and canyons, all of which impact oceanic communication between offshore and coastal waters. The continental shelf is often <100 km wide in the eastern Gulf of Alaska, so coastal freshwater sources and deep basin currents are not distantly separated. Hence, cross-slope flows that induce dispersal of iron-rich coastal waters into the basin require smaller lateral extent scales than over the broader (>200 km wide) northern Gulf continental shelf (Ladd et al. 2016). The coastline is punctuated by numerous bays, fjords and islands but also long stretches of unbroken coastline that lack any protected estuary at all. The steep mountainsides that rim the Gulf of Alaska route freshwater runoff into the nearshore zone, and this low salinity water feeds currents that advectively connect the inner continental shelves (Royer 1982, Stabeno et al. 2004, Weingartner et al. 2005, Stabeno et al. 2016).

The shelves are heavily corrugated, with multiple banks and shoals that extend to within 150 m of the surface, and troughs and canyons that extend to depths of 200-300 m from the shelf break shoreward. Many of the canyons are dynamically wide, inducing a cyclonic circulation, in which for north-south oriented canyons slope waters flow inshore on their eastern sides and shelf waters flow offshore on their western flanks, thereby facilitating shelf-slope exchanges of heat, salt, nutrients and organisms (Kämpf 2007).

PWS is a complex embayment rimmed by many fjords in the northern Gulf (Figure 1-2) and is connected to the open shelf waters through the relatively deep (~300 m) Hinchinbrook Entrance and the shallower (~150 m) Montague Strait. It receives a massive coastal runoff (~4.6 x 10^3 m^3 s^{-1}) that is more than twice the Copper River discharge (~1.8 x 10^3 m^3 s^{-1}), which is the single largest river outflow in the region (Simmons 1994). This runoff forces an outflow of highly stratified and low salinity near-surface waters through Montague Strait and the other western PWS passages. These are balanced by a net inflow through Hinchinbrook Entrance (Royer et al. 1990, Niebauer et al. 1994).

Cook Inlet is a long estuary, extending over 350 km in length, and hosts one of the largest tidal ranges in the world, with an average range of 5.5 m and maximum range of 8.5 m in the lower Inlet and Kachemak Bay. Freshwater inputs to Cook Inlet from glacial and non-glacial streams couple with inflows of shelf waters at depth, especially in southeast Cook Inlet at Kennedy Entrance. Together, these produce highly stratified conditions in both lower Cook Inlet and Kachemak Bay from May to October. The strong tidal currents in Cook Inlet continually exert mixing influence on the water column so many shallower regions exhibit no stratification at all.

Coastal freshwater runoff is supplied to the Gulf of Alaska by Aleutian Low storms (Royer 1982). Seasonal variability in freshwater discharge is driven by inputs from snowpack and glacial melt in late spring and summer months and from rain during fall storms (Hill et al. 2015). Seasonality of coastal freshwater discharges and the wind field together determine the character of the along-shelf circulation field, especially that of Alaska Coastal Current, a swift and narrow (~10 – 30 km) baroclinic flow associated with cross-shelf salinity gradients and downwelling-favorable winds (Muench et al. 1978, Royer 1982, Stabeno et al. 2004, Weingartner et al. 2005, Dobbins et al. 2009, Williams et al. 2010). The Alaska Coastal Current is important to the along-shelf connectivity of coastal habitats (Mundy 2005), the along- and across-shelf dispersal of freshwater (Weingartner et al. 2005) and iron (Wu et al. 200x), and the advection of heat (Janout et al. 2010).

The cyclonic wind stress associated with Aleutian Low storms forces downwelling over the shelf (Royer and Emery 1987) and upwelling within the subarctic gyre in the Gulf of Alaska (Muench et al. 1978, Wilson and Overland 1987, Macklin et al. 1990, Ladd et al. 2016). The gyre system includes the relatively sluggish and broad Alaska Current that flows along the Gulf's eastern boundary and the narrower and swifter Alaskan Stream that flows along the western boundary (Figure 1-1). These currents advect heat from lower latitudes along the continental slope. Shelf-basin exchange occurs along the slope in association with canyons, eddies and wind-driven flows (Okkonen et al. 2003, Ladd et al. 2005, Janout et al. 2009, Ladd et al. 2016). The storm systems carry relatively moist and warm marine air into the coastal mountain range, resulting in precipitation in the form of rain or snow. Precipitation rates for some drainage basins are estimated at up to 8 m yr^{-1} in coastal Gulf of Alaska (Beamer et al. 2016), with 2-4 m yr^{-1} common at most sites. For the Gulf of Alaska drainage basin as a whole, approximately 750 km^3 yr^{-1} of runoff is delivered into the coastal zone (Royer 1982, Hill et al. 2015, Beamer et al. 2016), with the vast majority of the discharge likely occurring between April and October.

The coastal freshwater runoff and surface heat fluxes from the atmosphere into the ocean represent positive oceanic buoyancy inputs that stratify the water column, while ocean-to-

atmosphere heat fluxes and mixing by winds and currents exert work to break down the stratification. Strong wind-induced mixing through fall months redistributes heat downward into the water column; the mixing is assisted by thermal convection fueled by rapid surface heat losses in late fall, winter and early spring (Janout et al. 2010).

Tidal amplitudes in the northern Gulf of Alaska are large, particularly with semidiurnal tides that are resonant with the dimensions of the Cook Inlet embayment (Muench et al. 1978, Isaji and Spaulding 1987, Foreman et al. 2000, Oey et al. 2007). Tidal currents dominate the near-bottom mixing environment through frictional interactions with the seafloor. In nearshore waters, the balance of tidal stirring versus buoyancy inputs likely defines the basic character of the near-shore stratification fields and locations of density fronts.

Water column stratification impacts the distribution of near-surface sensible heat and depends on an intricate balance of buoyancy inputs and destratifying effects of mixing (Janout et al. 2010). These develop over storm cycles and seasons as a function of the volume and timing of freshwater runoff from the coast, cloud cover, advection, and mixing. The summer Gulf of Alaska water column is typically characterized by strong near-surface stratification (~ 20 m), and surface properties are strongly influenced by surface heat fluxes and freshening (by precipitation and snowmelt runoff). While wind and surface heat fluxes strongly impact the vertical layering, lateral advection also contributes to the heat and haline balances and water column structure. For example, as the Gulf of Alaska wind stress declines from winter into summer, shelf-break waters upwell onto the shelf (Weingartner et al. 2005), influencing the characteristics and structure of near-bottom and mid-depth waters in a fashion that is only indirectly related to wind and freshwater fluctuations at the surface.

CLIMATE SETTING

The Gulf of Alaska is subject to hemispheric-scale modes of climate variability, including the Pacific Decadal Oscillation (PDO; Mantua et al. 1997), the North Pacific Gyre Oscillation (NPGO; Di Lorenzo et al. 2008), and the El Niño Southern Oscillation (ENSO; Cane and Zebiak 1985). Atmospheric teleconnections can reinforce and transmit the influence of climate signals across broad latitudinal and longitudinal extents (e.g., Chiang and Vimont 2004) with time scales corresponding to the structure, length scales, and propagation characteristics of the oceanic and atmospheric processes and interactions. Examples of such processes include planetary (Rossby) waves and the Quasi-Biannual Oscillation, which exert influence on the Gulf of Alaska through the jet stream and Aleutian Low storm tracks. El Niño conditions typically return on a 2 to 5-year repeat pattern, while PDO and NPGO are generally described as decadal-scale variations. Characteristic time scales of such fluctuations span multiple years, but they induce atmospheric-oceanic communications at much shorter time scales via their coupling with and response to individual weather systems.

A Pacific marine heatwave (PMH) developed in the northeast (NE) Pacific during late 2013 (Bond et al. 2015) because of a persistent atmospheric high-pressure ridge that inhibited winter storm mixing in the region (Swain 2015). Spatially nonuniform warming continued through 2014 and intensified as strong El Niño conditions developed in 2015-2016 (Di Lorenzo and Mantua 2016). Mixed layer heat budget analyses identified resulting anomalies in atmospheric and

oceanic processes and conditions that together caused the anomalously warm sea surface temperatures (SSTs) to persist for multiple years (Schmeisser et al. 2019), although over-winter mixed layer re-emergence mechanisms also may have played a role (Alexander et al. 1999). The PMH was, indeed, particularly unusual in duration and magnitude, persisting through all seasons for two years (Hobday et al. 2018), with massively large positive temperature anomalies, and unusual warming down to 300 m depth in the basin and over the entire shelf water column (Jackson et al. 2018). Climate models predict marine heatwaves will increase in frequency and magnitude (Joh and Di Lorenzo 2017, Oliver et al. 2018), so it is especially important to understand how these events manifest across the Gulf of Alaska and how they impact biological communities. Amongst other effects, warm conditions associated with the timing and strength of North Pacific modes of climate variability have been linked to year-class strength of commercial fish stocks (Hollowed et al. 2001) and warming associated with ecosystem regime shifts (Anderson and Piatt 1999).

OBJECTIVES

We sought an improved understanding of intertidal, coastal, and offshore co-variability of temperatures and, where possible, factors that help determine their linkages. We assessed the nature of coastal Gulf of Alaska thermal co-variability across space and time and the fidelity of satellite-based observations in the nearshore domain (see Box 1) using a variety of *in situ* observations from benthic dataloggers in the intertidal zone, tide gauges, coastal and offshore data buoys, oceanographic moorings, oceanographic research vessels, and satellite-based blended products.

In situ SST datasets that are not incorporated into any corrections of satellite-based SST products (the Gulf Watch Alaska program has collected a number of these) provide valuable independent data for assessing the utility of satellite-based observations in our regions of interest. The Gulf of Alaska is commonly subject to dense cloud cover, so satellite-based thermal-infrared measurements are not reliably available. Cloud-penetrating technologies such as the passive microwave sensors are useful but are limited to select satellites. Blended multi-satellite SST products are available on a daily basis at a variety of spatial resolutions (e.g., 1, 25, and 200 km) but it is not clear how accurately these products represent the very near-shore region (especially in the North Pacific) because of potential interference of the satellite signals at the land-water interface, and because the interpolated products rely on methods primarily tuned to the offshore waters. Bernardello et al. (2016) suggest that satellite-derived MODIS SST provide a reliable measure of nearshore surface water temperatures in the low-latitude Mediterranean Sea, but this result may not hold in a high-latitude freshwater dominated system like the North Pacific. Local variations in upwelling, sea breezes, forest fire smoke, fog, extensive tidal flats, and variations in optical properties due to varying sediment loads all carry potential to drive temperature differences at small spatial scales and locally influence the overall accuracy of satellite SST data in the Gulf of Alaska.

Box 1. Distinguishing NE Pacific nearshore coastal, shelf, outer shelf and offshore realms.

- **Coastal waters** are those within the riverine coastal domain (Carmack et al. 2015), which lies over the inner portion of the continental shelf and is strongly under the influence of terrestrial freshwater discharge. For the northern Gulf of Alaska, the Alaska Coastal Current front defines the coastal domain mid-shelf boundary, commonly found 25-35 km of the coast in non-summer months (Weingartner et al. 2005).
- **Nearshore waters**, a subset of coastal waters lying immediately adjacent to land, include the intertidal zone and subtidal waters where the proximity of these sites to land alters the character of the water column chemistry, biological communities, and physical dynamics relative to their properties in the coastal shelf waters. From a physical perspective, the nearshore zone is often an energetically active environment under the influence of surface waves and swell, where the effects of sunlight illumination can reach the seafloor, where the relative importance of cross-shelf wind forcing often dominates over along-shelf winds, where along-shore tidal currents strongly dominate over cross-shelf tidal currents, and is a region in which the surface and seafloor boundary layers tend to overlap (Fewings et al. 2008). Hence, the nearshore zone primarily occupies the realm in which bottom depths are less than 30 m, but a variety of site characteristics determine its actual local extent.
- **Shelf waters** lie beyond the nearshore zone but inshore of the continental shelf break.
- **Outer shelf waters** lie between coastal waters and the shelf break.
- **Offshore or oceanic waters** lie beyond the shelf break over the deep basin.

This paper is organized as follows: The Data and Methods section provides an overview of the data, data handling, and analytical techniques. The Results section begins with an overview of thermal variations from observational records spanning 120 years. We assess the fidelity of the satellite data in reproducing *in situ* records. Thermal variations, expressed as anomalies, are compared to large-scale climate modes of variability. We also investigate (on local and regional scales) the seasonal and synoptic co-variability of temperature anomalies across the regions of interest. A case study of the 2014-2016 PMH provides insight to its manifestation in the northern Gulf of Alaska. The Conclusions and Summary section provides a synthesis of the results.

DATA AND METHODS

Ocean temperature data were assembled from moored buoys, ship-based water column conductivity-temperature-depth (CTD) instruments, and data loggers fixed within the intertidal zone (Figure 1-2). The datasets, their sources, their handling and our approach to analyses are described below. Site locations and characteristics for time series data in analyses are given in Appendix Table A1.

Different SST measurement techniques necessarily impart cross-platform differences in this parameter's measurement. For example, satellites that measure the surface radiative heat report the "skin temperature" associated with the thin molecular layer at the very surface, while ship-based CTD data are typically averaged into 1 m thick layers. CTD dimensions and mixing associated with a vessel's propellers may only allow a CTD profile to resolve the surface temperature as a blended average of the uppermost few meters of the water column. Sensors affixed to the seafloor in the nearshore environment (even within a meter of the surface) constantly change depth relative to the sea surface due to waves, storm surges, and tidal fluctuations. A buoy floating at the surface will often have an SST sensor maintained at a fixed depth (typically 1 m) below the surface. For our purposes, we consider each of these measurement types to provide comparable SST data. Cross-platform differences are important to appreciate insofar as they likely contribute to modest degradations of coherence relative to SST measured in the same way between any two locations.

INTERTIDAL DATALOGGERS

We deployed HOBO water temperature loggers (Onset Computer Corporation, Bourne, MA, USA) at 28 intertidal sites distributed among six focal areas in the northern Gulf of Alaska: eastern PWS (EPWS), northern PWS (NPWS), western PWS (WPWS), Kenai Fjords National Park (KEFJ), Kachemak Bay (KBAY) and Katmai National Park and Preserve (KATM; Figure 1-2 and Appendix Table A1). HOBO sensors are capable of measuring temperatures to ± 0.2° C. They were placed inside a short length of 1.5" diameter white PVC pipe that was securely bolted to a boulder or bedrock using stainless steel bolts and bolt anchors placed in holes drilled into the rock surface with a cordless hammer drill (Figure 1-3).

We placed temperature loggers at 0.5 m mean lower low water (MLLW) tidal elevation by observing the water level at the site when the tide was predicted to be at 0.5 m, based on the nearest tide station's predicted tide chart (Tides and Currents software, NOBELTEC, Beaverton, OR, USA). Each logger was deployed for 1 year except for loggers in EPWS and NPWS, which were left in place for 2 years at their initial deployment. We retrieved and replaced the loggers annually thereafter, maintaining the original mounting location. We programmed the loggers to record temperature at 20-, 30- or 60-minute intervals. The length of each time-series varies by site and most sites have data gaps due to sensor malfunction, loss, or break in deployment (Table 1-1).

Prior to 2014, loggers were not checked for calibration errors before deployment, but all data were corrected post-deployment by aligning temperature records from one deployment to the next to remove sensor drift. Several calibration errors were discovered with this process and from 2015 on, each temperature logger went through a calibration soak pre- and post-deployment at three temperature levels (0, 10 and 20 °C) using a high accuracy thermometer in a circulating water bath. Any identified post-deployment calibration errors were applied as a constant offset to the entire temperature record from that deployment. Any temperature logger that did not meet the ± 0.2 °C recording accuracy threshold at any one of the three temperature levels in the pre-deployment soaks were removed from the instrument pool.

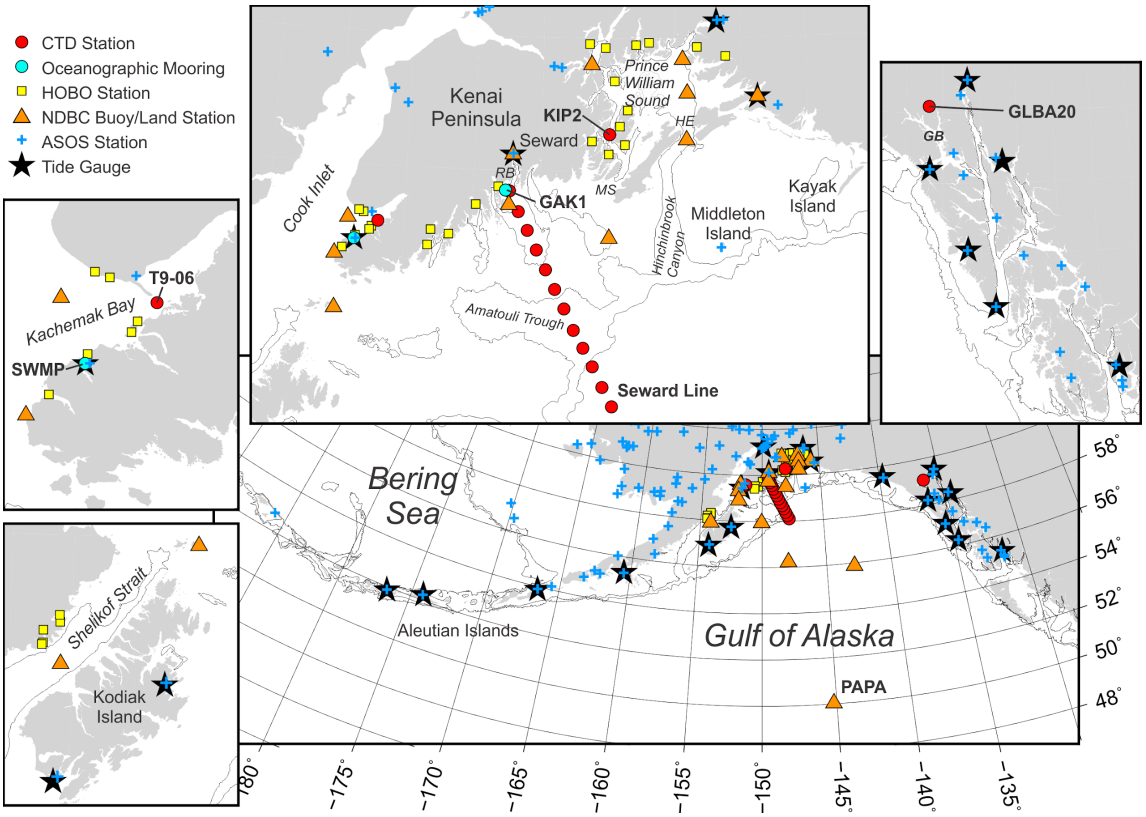

Figure 1-2. Station location maps showing the GAK1 and Kachemak Bay National Estuarine Research Reserve System Wide Monitoring Program (SWMP) moorings (cyan circles), buoys and land stations (orange triangles), tide gauge stations (black stars), weather stations (blue plus symbols), intertidal HOBO data loggers (yellow squares), and conductivity-temperature-depth stations (red circles). See Table A1 for station coordinates, data temporal coverage and site characteristics. Place abbreviations include: RB = Resurrection Bay; GB = Glacier Bay; HE = Hinchinbrook Entrance; MS = Montague Strait. Bathymetric contours are drawn at 180 and 1,000 m depths. Station abbreviations are described in the text.

Figure 1-3. Typical installation of a HOBO temperature logger in the intertidal zone inside a PVC pipe and bolted to the substrate.

Because the HOBO temperature loggers are placed within the intertidal zone, they alternate between being submerged and being exposed to air under the influence of sea level changes (typically twice per day with the dominant semi-diurnal tide, although storm surges and river freshets also impact sea level). Hence, the HOBOs record the water temperature fluctuations that include the influence of near-surface thermal stratification rising and falling past the sensor. Loggers were assumed to be submerged when the predicted tide level from the nearest tide station was ≥ 1.5 m above MLLW; other data (~ 30%) were discarded. We determined the fraction of time each logger was submerged each day (Appendix Table A1) and explored different methods to estimate daily averages from these incomplete records, ranging from averaging over only submerged measurements to averages that include interpolations (linear or spline) over gaps when the HOBOs were not submerged. These different techniques yielded little quantitative difference in analysis, implying that the magnitude of the distorted signal is small relative to the magnitude of thermal fluctuations of primary interest. Ultimately, daily averages reported here are computed from only the submerged measurements, which is the simplest approach.

Table 1-1. Indices of climate variability in the Pacific region. Table headings include index name, abbreviation, and source.

Index Name	Abbreviation	Source
Pacific Decadal Oscillation	PDO	http://jisao.washington.edu/pdo/PDO.latest
North Pacific Gyre Oscillation	NPGO	http://www.o3d.org/npgo/npgo.php
Multivariate ENSO (El Niño Southern Oscillation) Index version 2	MEI	https://www.esrl.noaa.gov/psd/enso/mei
Pacific North American Index	PNA	https://www.cpc.ncep.noaa.gov/data/teledoc/pna.shtml
Pacific Meridional Mode	PMM	https://www.esrl.noaa.gov/psd/data/timeseries/monthly/PMM/
North Pacific Index	NPI	https://climatedataguide.ucar.edu/climate-data/north-pacific-np-index-trenberth-and-hurrell-monthly-and-winter
Victoria Mode Index	VMI	Computed with the Extended Reconstructed Sea Surface Temperature grid following Ding et al. (2015)

MARINE WEATHER STATION, TIDE GAUGE AND BUOY DATA

The National Oceanic and Atmospheric Administration's (NOAA's) National Data Buoy Center (https://www.ndbc.noaa.gov/) maintains an extensive archive and real-time data repository of marine fixed stations and drifting buoys. We downloaded records from 16 land-based stations and moored buoys spanning both coastal and offshore realms (Appendix Table A1). Of the 16 stations, 2 are located on the Alaskan mainland, 5 are within 10 km of shore, 5 are 10-50 km from shore, 3 are 150-500 km from shore and one (Ocean Station PAPA) is 1090 km from shore (Appendix Table A1). The NOAA Center for Operational Oceanographic Products and Services operates coastal tide gauge stations as the National Water Level Observation Network, and many stations also have sensors that measure near-surface water temperature. Sensor elevation is typically fixed relative to the seafloor, with a range of 1.7 to 4.4 m below MLLW (Appendix Table A1). Temperature data from 18 tide gauge stations were obtained from the Center for Operational Oceanographic Products website (https://tidesandcurrents.noaa.gov/). Following screening for data quality, water and air temperature time series data were compiled from the original 6-, 30- or 60-minute observation intervals into daily averages. NOAA specifies estimated accuracy for tide gauge water temperature data to be ±0.2 °C, with ±0.1 °C resolution, and that buoy SST data are accurate to better than ±1.0 °C, with ±0.1 °C resolution (https://www.ndbc.noaa.gov/rsa.shtml).

SHIPBOARD CTD DATA

A CTD profile time series has been maintained on a quasi-monthly basis since December 1970 at oceanographic station GAK1, which is located at the mouth of Resurrection Bay near Seward, AK in 273 m of water (Figure 1-2) at 59.845 °N, 149.4667 °W. GAK1 is the innermost station of the Seward Line hydrographic transect, which stretches from the coast to the foot of the northern Gulf of Alaska continental slope. The Seward Line has been occupied 92 times from 1974 to 2018 and we use these data to examine the co-variability of temperature through the water column and across the shelf.

Since 1993, CTD monitoring has been accomplished 4-9 times per year in the marine waters of Glacier Bay National Park and Preserve (GLBA) using SeaBird Electronics (SBE; Seattle, WA, USA) 19 CTD profilers. Data from monitoring station GLBA20 provides a record of temperature and salinity variations close to meltwater discharges from a tidewater glacier.

Routine monthly oceanographic profiles have been conducted at 10 stations along a cross-bay transect in Kachemak Bay from 2012 to present with SBE19 CTD profilers. For this paper, we use water column temperature data from the mid-bay station KBAY6 (designated T09-06 on Figure 1-2) from the 78 monthly surveys conducted from 2012 to 2018.

Typical accuracy of SeaBird CTD temperature sensor data are better than ±0.01 °C, and precision is better than ±0.001 °C. CTDs used for the GAK1 profiles have varied over the years; since the 1990s all GAK1, GLBA, and Kachemak Bay CTD data have been collected using SeaBird Inc. SBE9, SBE19, and SBE25 model dataloggers that are annually calibrated by the manufacturer.

OCEANOGRAPHIC MOORING DATA

SBE37 CTD dataloggers are calibrated annually at the manufacturer's calibration facility. Datalogger clocks are checked for drift (typically less than 120 seconds over 1 year) and time stamps are corrected by using a time-linear drift model. We combine the GAK1 CTD and mooring data into two time series: an aggregate monthly mean vertical profile time series spanning the entire 1970-2019 GAK1 period of record, and a daily profile time series spanning only the 2000-2019 period of GAK1 mooring deployments. SBE sensor temperature data accuracy and resolution are better than ±0.01 °C. GAK1 data are available through the Alaska Ocean Observing System Gulf of Alaska data portal (https://portal.aoos.org/gulf-of-alaska).

CTD dataloggers have also been deployed on a mooring continuously near the Seldovia ferry dock in Kachemak Bay since August 2001, at 59.44097 °N, 151.72089 °W, as part of Kachemak Bay National Estuarine Research Reserve's System Wide Monitoring Program (SWMP). Instrumentation consists of either a 6600-series or EXO-2 YSI sonde with temperature probes having 0.2 °C accuracy, and a variety of ancillary sensors. The logger is deployed 1 m above the seafloor at a depth of ~8 m. Instruments are swapped, cleaned, and calibrated monthly. Temperature probes are checked against a Davis Instruments National Institute of Standards and Technology-standard probe and replaced if measurements differ by greater than ±0.2 °C. Data are uploaded to the NOAA National Estuarine Research Reserve System Central Data Management Office monthly, where they go through automated and manual quality

assurance/quality control procedures. Data, metadata, data handling procedures, and other information are available at the Central Data Management Office website (https://cdmo.baruch.sc.edu).

GRIDDED SST DATA COMPILATIONS

The Group for High Resolution Sea Surface Temperature (GHRSST) Level 4 sea surface temperature analysis is a high-resolution (daily, 0.01 degree spatial grid) surface temperature analysis that uses data from multiple satellites (Chin et al. 2017). To assess the fidelity of the GHRSST record in reproducing the observed *in situ* temperature variations, we extract data from GHRSST at the grid points closest to the fixed intertidal datalogger and station used herein. GHRSST data are maintained and provided by the Jet Propulsion Laboratory's Physical Oceanography Distributed Active Archive Center at https://podaac.jpl.nasa.gov/dataset/MUR-JPL-L4-GLOB-v4.1.

The NOAA Earth System Research Lab compiles a blended medium-resolution (1981-present daily time step, 1/4 degree) SST dataset from available Advanced Very High Resolution Radiometer satellite, ship, and buoy data into the Optimum Interpolation SST (OISST) dataset (Reynolds et al. 2007). We downloaded 1981-2018 OISST version 2 dataset spanning the Gulf of Alaska from the NOAA Physical Sciences Division (https://www.ncdc.noaa.gov/oisst) and use this dataset to show the spatial coherence of SST variations across the Gulf and to fill gaps of select *in situ* datasets (described below in the Fidelity of remotely sensed SST data section).

The NOAA also compiles a blended low-resolution long-term (1854 to present monthly time step, 2 degree) SST from available ship, satellite and buoy data (Huang et al. 2017) as the Extended Reconstructed SST (ERSST) dataset. To provide a long time perspective to Gulf of Alaska SST fluctuations, we downloaded the ASCII ERSST version 5 global dataset from the National Centers for Environmental Information website (https://www.ncdc.noaa.gov/data-access/marineocean-data/extended-reconstructed-sea-surface-temperature-ersst-v5).

ATMOSPHERIC REANALYSIS

We obtain monthly mean surface heat flux estimates from the NOAA Earth System Research Laboratory Physical Sciences Division, National Centers for Environmental Prediction-Department of Energy, Atmospheric Model Intercomparison Project-II Reanalysis (Reanalysis-2) (http://www.cpc.ncep.noaa.gov/products/wesley/reanalysis2/) for 2010-2015. The Reanalysis-2 model is computed on a coarse 208 km global grid, but this resolution, similar to the ERSST resolution, is sufficient to reveal broad-scale ocean-atmosphere heat exchange patterns across the North Pacific. Downloaded model parameters include the downward (Q_{DSW}) and upward (Q_{USW}) shortwave radiation heat flux, the downward (Q_{DLW}) and upward (Q_{ULW}) longwave radiation heat flux, the sensible heat flux (Q_{SE}), and the latent heat flux (Q_{LA}). The individual surface heat flux terms are combined to form the net surface heat flux $Q_{NET} = Q_{DLW} + Q_{DSW} - Q_{ULW} - Q_{USW} - Q_{SE} - Q_{LA}$, using the convention that positive heat flux represents a gain of heat by the ocean from the atmosphere. Although Reanalysis-2 model heat fluxes have known biases in the NE Pacific (Ladd and Bond 2002), by evaluating monthly anomalies relative to the annual climatology we are able to assess relative changes in the heat flux forcing and the anomalies should be relatively insensitive to any residual bias.

METEOROLOGICAL STATION DATA

The Iowa Environmental Mesonet at Iowa State University maintains an archive of Automated Surface Observing System (ASOS) meteorological data (https://mesonet.agron.iastate.edu/ASOS/), including records from 185 Alaskan land-based stations. We downloaded air temperature, dew point temperature, relative humidity, wind speed and direction, sea level pressure, and sky cover data covering 1 January 2000 to 15 October 2019 for all Alaska region stations. Sky cover octants were converted into fractional cloudiness using the following conversions: clear = 0/8 = 0; few = 1/8 = 0.125; scattered = 2.5/8 = 0.3125; broken = 6/8 = 0.75; overcast = 8/8 = 1. Obscured sky cover records (e.g., by smoke, snow, etc.) were excluded. Data were examined for quality and obvious outliers; stuck sensor readings and other errors were eliminated.

The ASOS weather data are used to compare atmospheric and oceanic thermal variability and to estimate bulk surface heat fluxes at representative coastal and offshore sites.

The longwave loss (Q_{LW}) from the ocean is estimated using daily averages of SST from the oceanographic station, assuming blackbody radiation ($Q_{LW} = \varepsilon\sigma T^4$ where the emissivity $\varepsilon = 0.98$ and the Stefan-Boltzman constant $\sigma = 5.7 \times 10^{-8}$ J s^{-1} m^2 K^{-1}). The downwelling longwave radiation is backscatter (Q_{BS}) reflected into the ocean from the cloud cover (CC) with modified emissivity $\varepsilon=0.78(1+0.22CC^{2.75})$ and air temperature. Estimates of Q_{LA} use the relative humidity, latent heat of evaporation, and wind speed from the weather station and assume 100% saturation at the surface of the ocean. Q_{SE} is derived from wind speed and the difference between SST and air temperature at the weather station. Q_{SW} estimates are based on 6-hour averages of clear-sky downward radiation from the Reanalysis-2 and an assumed ocean albedo of 0.2. The total surface heat flux estimate Q_{SUM} using the bulk formulae is the combination of the shortwave, longwave, sensible, and latent terms.

CLIMATE INDICES

Time series of large-scale climate patterns (Table 1-1) are used to help diagnose the source of local Gulf of Alaska SST fluctuations.

ANALYSIS

We define synoptic-scale variability to be fluctuations for periods spanning 1 to 30 days. Seasonal to interannual (low-frequency) variability occurs at time scales longer than 30 days; analyses of the low-frequency signals are often best accomplished by using daily or monthly anomalies in which the annual climatology is removed.

Working with daily mean temperature data, monthly anomaly time series are computed by subtracting the climatological monthly mean from each monthly average to create an anomaly that retains units of °C. The time span used for creating the anomalies varies by available dataset length and analysis application; the baseline time span can make a difference in anomaly zero offset level and magnitude if the record length is short (i.e., < 10 years in length) or does not well represent the associated climatology. Daily and seasonal anomalies are constructed in a parallel fashion but using a daily/seasonal climatological mean and standard deviation rather than the monthly climatology. Some operations require normalized anomalies, for which each individual

monthly anomaly is divided by the standard deviation for the corresponding set of monthly means, resulting in a record having zero mean and unity variance. Some analyses require normalization of a record relative to a reference station; such instances are noted where they occur.

Some analyses are based on frequency band evaluations that separately consider three components of variation: the annual cycle based on smoothed climatological day-of-year average (T_{DC}); synoptic-scale fluctuations of less than 30 days are formed by high-pass filtering the daily anomalies (T'_{HP}), where daily anomalies are computed by subtracting T_{DC} from the raw temperature record; the remaining low frequency variations encompass both seasonal and interannual variability and are formed by low-pass filtering the daily anomalies (T'_{LP}). To ensure minimal filter-induced distortion, the frequency separation is based on a 6th order phase-preserving band-pass Butterworth filter applied to the daily averaged records. An example of the signal decomposition is shown for three years of the record at oceanographic station GAK1 (Figure 1-4), which demonstrates that the seasonal anomalies (T'_{LP}) capture multi-month deviations away from the annual climatology (T_{DA}).

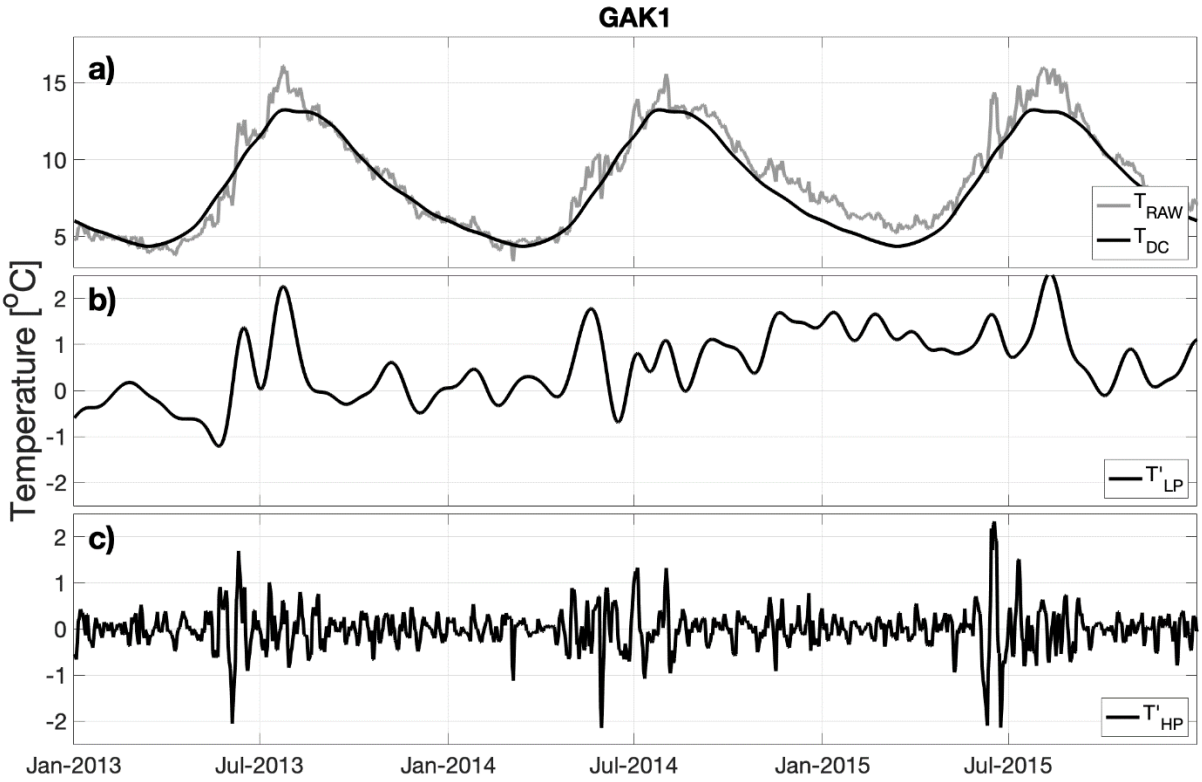

Figure 1-4. Three-year example of sea surface temperature (SST) at GAK1 decomposed into different periods of variability. a) Raw SST at GAK1 (T_{RAW}) and the climatological average SST for each day of year (T_{DC}). T_{DC} is low pass filtered with a cutoff period of 60 days. b) The daily anomaly (T_{RAW} -T_{DC}) low-pass filtered with 30-day cutoff period (T'_{LP}). c) The daily anomaly high-pass filtered with a 30 day cutoff period (T'_{HP}). The entire record (over which T_{DC}, T'_{LP}, and T'_{HP} are calculated) spans January 1, 2007 to May 1, 2018.

To assess the statistical strength and significance of covariation, we compute the standard deviation (σ), root-mean-square-difference (RMSD), Spearman's cross-correlation (r) and p-value parameters. Statistical significance throughout is ascribed for $p < 0.05$. Detrending operations are linear and based on a least-squares fit. The first zero crossing of the autocorrelation function provides a measure of the decorrelation time scale for both oceanographic and atmospheric time series. Empirical orthogonal function (EOF) analysis is used to identify linked spatial and temporal patterns of variability. We compute an EOF decomposition of the gridded ERSST and OISST datasets by using standard normalized (unity variance and zero mean) and detrended monthly anomalies. Stepwise multivariate regressions incrementally assess available predictor time series to identify best fit relations for a given response time series. We use the stepwise approach for assessing the role of large-scale climate patterns in directly corresponding to local temperature fluctuations.

Taylor diagrams provide a compact means to display the results of multiple variance analyses, combining the inter-dependent parameters σ, RMSD, and r into a single graphic having a separate axis for each of the three parameters (Taylor 2001). In each plot, the variations of a time series at one point is shown at the reference dataset origin. For normalized anomalies the reference lies at $\sigma = 1$, RMSD = 0, and r = 1. Variance analysis results plotted on a Taylor diagram depict the data relative to the reference, with strongly similar data falling close to the reference origin and weakly related data located far from the origin.

RESULTS

In this section we first examine thermal fluctuations across the Gulf and across the entire North Pacific. Next, we examine the fidelity of satellite records in reproducing coastal *in situ* temperature readings and then assess the covariability of temperature laterally, with depth, across and between the Gulf of Alaska sub-regional domains that include Katmai, Kachemak Bay, Kenai Fjords, PWS, SE Alaska, and the Aleutians. Finally, we provide a case study of the recent Gulf of Alaska marine heatwave to demonstrate the tightly coupled synchrony of large-scale thermal events across the entire Gulf, as well as the importance of local dynamics in controlling the response at individual sites.

CLIMATE-SCALE TRENDS AND PATTERNS

For the period of GAK1 and ERSST record overlap (1970-2019), these two time series show event-scale correspondence in the relative magnitude and sign of periods where strong temperature anomalies occur, showing that the Gulf-wide average surface temperature during strong events generally varies in phase with the depth-mean temperatures on the inner shelf (Figure 1-5). Cooler-than-average years are found from 1901-1933, 1946-1952, 1964-1976, and 2007-2013.

The Gulf-wide SST record of annual anomalies since the start of the 20th century exhibits a linear warming trend ($p < 0.001$) of 0.11 ± 0.003 °C per decade from 1900 to 2019 (Figure 1-5). The trend explains 26% of the total annually averaged SST variance over this time period. For 1970-2019 we find a warming trend of 0.24 ± 0.10 °C per decade for the coastal northern shelf at oceanographic station GAK1 (0-250 m depth average) and an indistinguishable Gulf-wide SST

trend of 0.25±0.11 °C per decade. Statistics for the 1970-2019 analysis are based on ~400 degrees of freedom (DOF) for GAK1 and 600 DOF for the SST, assuming each month's anomaly to represent an independent measurement.

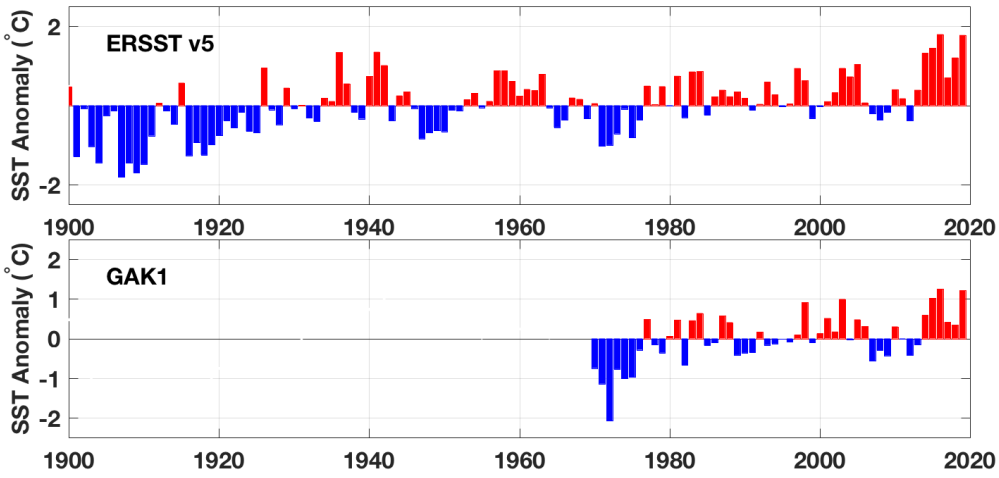

Figure 1-5. Upper panel: Extended Reconstructed Sea Surface Temperature (ERSST) annual anomalies for the Gulf of Alaska averaged over 156° W to 230° W and 56° N to 62° N. Lower panel: GAK1 annual averages of all depth-layer monthly anomalies averaged across the full 0-250 m water column. Both records are shown relative to their averages between 1970 and 2019.

A climate shift in 1976 impacted much of the North Pacific (Litzow and Mueter 2014) and was associated with far-reaching biological and economic consequences as this warming played an important role in the restructuring of the Gulf of Alaska marine ecosystem and its fisheries (Anderson and Piatt 1999). Debate persists over appropriate terminology and designation of climate and ecological regime shifts (Overland et al. 2008) but regardless of the definition, we find that of the 44 years since 1976, 33 have been warmer than the period of record mean in the ERSST record, suggesting that most of the last half-century has been in a fundamentally different thermal state than for the 20th century preceding 1976. For example, the Gulf-wide average SST since the start of the recent PMH (2014-2019) has been 1.37 °C above the long-term mean and 2.25 °C warmer than the first decade of the 1900s.

Basin-scale signals emerge from the leading modes of SST variation using EOF analysis of the ERSST and OISST datasets (left and right columns of Figures 1-6 and 1-7, respectively). The loading functions exhibit only modest magnitudes in the northern Gulf of Alaska, raising the question of their importance to local conditions in the Alaskan coastal zone where the coarsely gridded SST records are not expected to accurately represent small-scale spatial variations (e.g., the ERSST 2 degree grid vastly exceeds a typical 10 km coastal baroclinic Rossby radius of deformation). Unsurprisingly, the EOF time series for the selected analysis regions (Figure 1-7) relate closely to well-known patterns of climate variability. The PDO (Mantua et al. 1997), multivariate ENSO index version 2 (MEI; Wolter and Timlin 2011), and Victoria Mode Index

(VMI; Ding et al. 2015) indices (left hand column of Figures 1-6 and 1-7 and Table 1-1) emerge from the ERSST monthly records. For the daily time series confined to the Gulf of Alaska (right hand column of Figures 1-6 and 1-7), the first three OISST EOF modes are significantly correlated to the PDO, VMI, and NPGO (Di Lorenzo et al. 2008) time series (Table 1-2).

The relation between the large-scale climate modes and the coastal Gulf of Alaska is further diagnosed by using simple correlation between surface layer (0-50 m average) temperature fluctuations at GAK1 and each record (Table 1-2). We also calculate a stepwise multiple regression between the GAK1 record and the leading modes of variability. The univariate regressions show that the leading mode of variability (PDO or EOF1 of the OISST) captures ~ 50% of the GAK1 thermal anomaly. We note that coastal warming from 2012 through 2014 (discussed in detail below in the Case Study section) is captured in the time series of the PDO, ENSO, and VMI time series. In particular, the VMI signal stands out with a record maximum in 2014.

The stepwise multivariate regression captures ~ 65% of the total variance. The leading covariates that are included in the best stepwise models include the EOF1 and EOF3 of the OISST record, the PDO and the MEI with a 6-month lag. At the Seldovia tide gauge station, the stepwise model only accounts for about 50% of the total variance, suggesting that thermal variability in the Cook Inlet nearshore zone is even less closely linked to the large-scale thermal fluctuations than those at GAK1.

We next assess the zero-lag correlation of surface temperature daily anomalies across the Gulf, which exhibit both cross-shore and along-shore spatial structure (Figure 1-8). For the reference locations shown in Figure 1-8, GAK1 is found to be the most representative of the northern shelf, with the $r = 0.7$ contour (which accounts for ~ 50% of the variance) extending from east of Kayak Island to nearly Kodiak Island. The grid point at Sitka is well correlated only to a narrow band of grid points that stretches along the SE shelf, suggesting that this region is characterized by relatively small spatial scales of variability. Similarly, SST variations within PWS appear to be primarily confined to the Sound, as are the variations in lower Cook Inlet.

The regression analysis of Figure 1-8 suggests that temporal thermal anomalies in the Gulf of Alaska exhibit spatial characteristics that can be ascribed to the influence of the generally counter-clockwise ocean circulation field in both coastal and slope region waters (Figure 1-1). For example, the correlation at GAK1 in the upper right panel of Figure 1-8 is near $r = 0.6$, which extends SW from PWS. The $r = 0.5$ contour extends over 100 km downstream along the coast to the southwest of GAK1, suggesting that temperature variations at GAK1 are more representative of those in the waters passing by the Kenai Peninsula than they are of the variations in the waters that are located a similar distance to the east of PWS. Correlation contours over the central Gulf of Alaska are aligned primarily zonally and near the SE Alaska archipelago they intersect the continental slope at approximately a right angle, while in the region of the swift Alaskan Stream in the west the correlation contours are more aligned along the shelf break. The correlation contours for the reference point in PWS show some connectivity downstream along the Kenai Peninsula coast, but the correlation magnitudes here are only modest ($r < 0.6$).

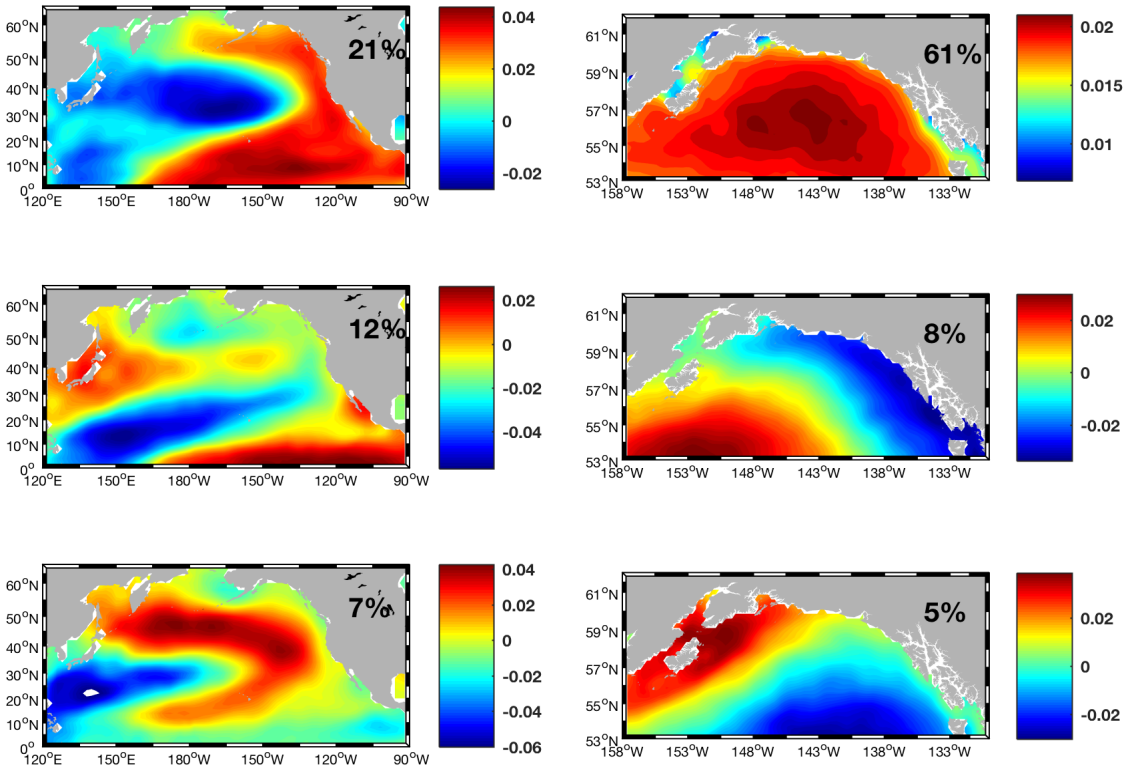

Figure 1-6. North Pacific (left) and Gulf of Alaska (right) patterns of sea surface temperature (SST) variation based on empirical orthogonal function analysis of 1900-2019 Extended Reconstructed SST monthly anomaly records (left) and 1981-2019 Optimum Interpolation SST daily anomaly records (right). Anomaly time series at all grid points are detrended and normalized to unity variance and zero mean. From top to bottom, the rows represent modes 1, 2, and 3, respectively. The fraction of total variance contained in each mode is shown in the upper right-hand corner of each plot.

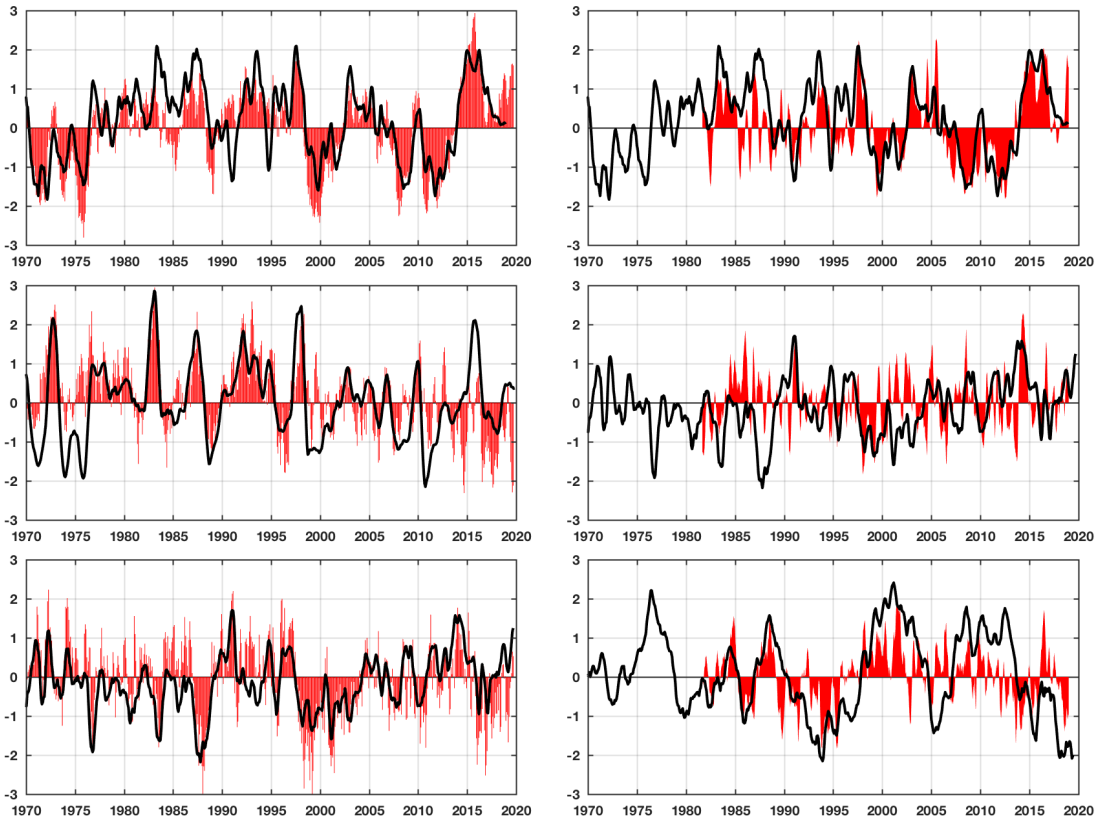

Figure 1-7. Times series (red bars) for the six modal patterns shown in Figure 1-6, along with the best-correlated time series of known climate patterns (see also Table 1-1). From top to bottom in the left column, the black lines show PDO, MEI, and VMI time series, respectively. From top to bottom in the right column the black lines show the PDO, VMI, and NPGO time series. Black time series have been smoothed with a 6-month moving average filter. Daily optimum interpolation sea surface temperature time series have been smoothed with a 31-day moving average filter. See Table 1-1 for climate index abbreviation definitions.

Table 1-2. Correlation (r) between temperature records at the GAK1 and Kachemak Bay National Estuarine Research Reserve System Wide Monitoring Program moorings, and the PDO, NPGO, PNA, MEI, NPI, PMM, and VMI climate indices, and the principal components shown in Figure 1-7. Correlations shown only for $p < 0.05$. Correlations are based on the maximum temporal overlap of each record's monthly anomaly over the period 1990-2019. See Table 1-1 for climate index abbreviation definitions.

	PDO														
PDO	1	NPGO													
NPGO	0.19	1	PNA												
PNA	0.43	0.15	1	MEI											
MEI	0.5	0.27	0.29	1	NP										
NP			0.36		1	PMM									
PMM	0.25	0.5				1	VM								
VM	0.42	0.37	0.37	0.19		0.2	1	ERSST EOF1							
ERSST EOF1	0.66	0.49	0.27	0.76		0.49	0.09	1	ERSST EOF2						
ERSST EOF2				0.35	0.12	0.29	0.19		1	ERSST EOF3					
ERSST EOF3	0.18	0.37	0.31	0.14		0.29	0.73			1	OISST EOF1				
OISST EOF1	0.69	0.32	0.22	0.41	0.15	0.2		0.62			1	OISST EOF2			
OISST EOF2				0.11		0.13	0.23		0.11	0.21		1	OISST EOF3		
OISSTEOF3		0.44	0.11	0.12		0.28	0.34	0.27		0.35			1	GAK1	
GAK1	0.7	0.28	0.23	0.36		0.42	0.15	0.55	0.21	0.19	0.76		0.17	1	Seldovia
Seldovia	0.59	0.41	0.21	0.35	0.19	0.43		0.52			0.7			0.78	1

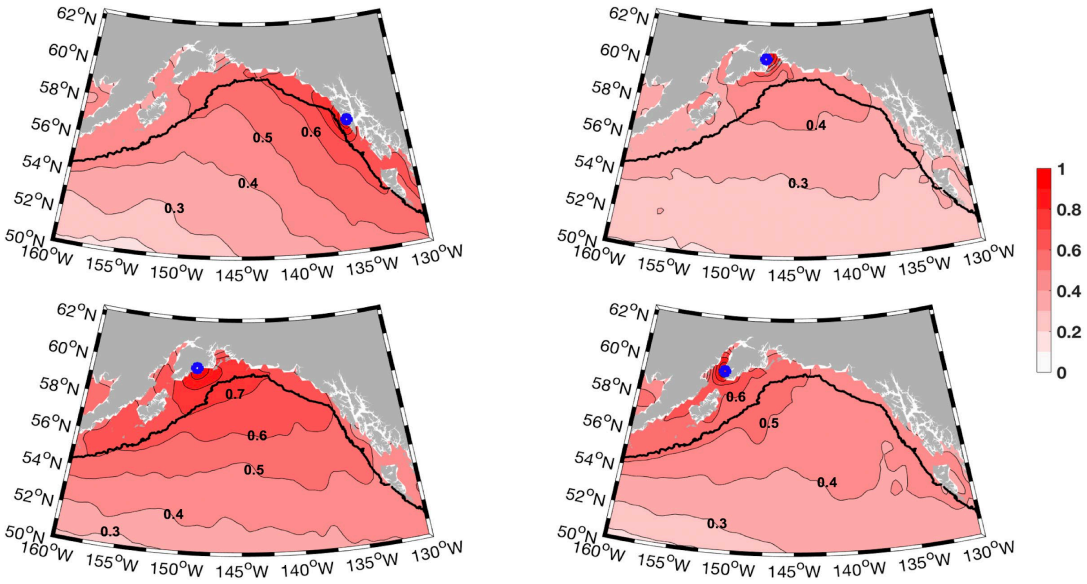

Figure 1-8. Correlation of the optimum interpolation daily sea surface temperature anomaly relative to reference points (blue circles) at Sitka (upper left), western Prince William Sound (upper right), GAK1 (lower left) and System Wide Monitoring Program (lower right). The continental slope is denoted with a thick black contour at the 1,000 m depth level.

Even with the relatively coarse quarter-degree grid resolution of the OISST compilation, the correlation contours of Figure 1-8 show differences in coastal vs. offshore thermal regimes. This can be seen, for example, in anomalies connected to the coast of SE Alaska and extending to the

northern coast past Kayak island, and with the decline of correlation over the basin relative to the GAK1 reference point. Similarly, relative to GAK1 the correlations degrade in north PWS and in upper Cook Inlet. The OISST product does not extend into the narrow passages of SE Alaska or PWS, so to better understand the conditions in these locations we turn to other *in situ* data sources below.

The above analyses raise the question of how well satellite products capture *in situ* temperature fluctuations, and whether the satellite data are equally reliable in the nearshore, coastal, and offshore realms. In the next section, we assess the OISST and GHRSST products relative to direct SST observations in order to place this broad-scale analyses described above into a more complete context.

FIDELITY OF REMOTELY SENSED SST DATA

The monthly GAK1 profile time series is based in part on mooring data and so lacks data between the surface and the uppermost mooring sensor in months with no ship-based CTD profiles. To extend the GAK1 temperature data across this gap, we generated a hybrid *in situ* and remotely sensed dataset compilation by using the daily OISST time series from the grid point closest to the GAK1 site. The OISST dataset is corrected by using a variety of buoy and ship-based surface measurements but not hydrographic profile data so comparisons against measurements made at GAK1 are not biased by assimilation.

Comparing surface temperatures from GAK1 CTD profiles and the OISST data from the closest grid point on the day of observation, we find an overall (annual cycle included) cross-correlation of $r = 0.98$, $p < 0.001$, and a RMSD of 0.61 °C (Figure 1-9). The *in situ* standard deviation (3.5 °C) is somewhat larger than that of the gridded product (3.1 °C). Correlation of 0 m depth CTD daily anomalies with OISST daily anomalies shows that the OISST dataset accounts for nearly 60% of the *in situ* daily variance ($r = 0.77$, $p < 0.001$). Corresponding analyses for the GHRSST dataset show $r = 0.99$, $p < 0.001$, and RMSD=0.39 for the raw data and almost 70% of the daily anomaly variance ($r = 0.83$, $p = 0$). For context, individual ship-based measurements of SST are known to often have a bias of a few tenths of a degree and RMSD errors on the order of 1 °C (Reynolds et al. 2007). Hence, the satellite SST data capture the annual cycle of local conditions with appreciable accuracy and they reproduce the majority of the synoptic-scale variability; however, a large fraction (30-40%) of the daily anomaly variance remains unresolved by the satellite data, with typical random errors of about ± 0.5 °C.

Comparing the OISST and GHRSST daily anomalies to those at the HOBO deployment sites, tide gauge and buoy stations, we find that the relation is strongest for the offshore stations (Figure 1-10). Weak correlations ($r < 0.4$) exist across all the SE Alaska stations, around the perimeter of PWS and along the Aleutian Islands. Often, these stations with low correlations are in relatively protected embayments that do not have a strong or direct connection to the shelf circulation, and they also exist in regions of very high precipitation rates and cloud cover. Because of its smaller observation footprint, the GHRSST measurements capture a higher fraction (5-25%) of the *in situ* variability at some sites, but at many of the stations the OISST and GHRSST datasets are in very close agreement, with differences within ± 5%. Turbidity affects

water surface emissivity (Wei et al. 2017) and shortwave absorption (Kara et al. 2002). Consequently, remotely sensed SST measurements are less accurate in turbid coastal waters.

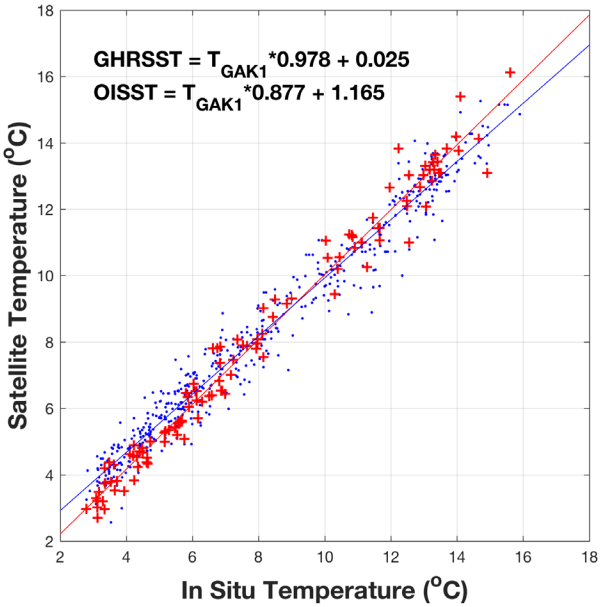

Figure 1-9. The relation between GAK1 conductivity-temperature-depth surface (0 m) data and the optimum interpolation sea surface temperature (OISST) (blue) and group for high resolution sea surface temperature (GHRSST) (red) satellite-based records for all 506 GAK1 casts taken within the OISST period of record and for 119 GAK1 casts in the GHRSST 2007-2017 record.

In summary, we find the higher spatial resolution GHRSST data superior to the lower resolution OISST data in representing nearshore surface temperatures, but even GHRSST data fail to capture the majority of the daily anomaly at some sites, particularly in the nearshore zone. Hence, the satellite products are not necessarily useful for applications requiring a detailed understanding of synoptic scale temperature fluctuations.

HORIZONTAL AND VERTICAL SCALES OF VARIABILITY

Using all available SST data and surface air temperature station data south of 61.5 °N, we separately assess the oceanographic and atmospheric decorrelation length scales for temperature anomalies at synoptic (T'_{HP}) and seasonal-to-interannual time scales (T'_{LP}), as well as the annual signal of raw temperature (T_{DA}) (Figure 1-11). Methods identical to those used for the oceanographic data are used to calculate T'_{HP}, T'_{LP} and T_{DA} for the atmospheric data. For T'_{HP}, the atmosphere retains a higher level of covariability over length scales up to approximately 750 km. Both the ocean and the atmosphere exhibit very strong covariability T_{DA}. The correlation for T'_{LP} drops to $r \leq 0.5$ (25% of the variance) for station separations > ~ 1000 km for both the ocean and the atmosphere.

The four ocean station pairs with a separation distance 1-10 km have a synoptic-scale correlation of $\sim 0.75 < r < 0.85$. Nearly all ocean stations separated by 10-30 km have a correlation

coefficient of $r < 0.5$ (eleven of the station pairs in this range show $0.5 < r < 0.8$). These results show that the day-to-day variability of ocean station pairs separated by only a few tens of km is extremely large. We note that the typical horizontal length scale for stratified geophysical flows, the baroclinic Rossby radius of deformation, is generally less than 10 km in high latitude coastal regions (Chelton et al. 1998).

The cross-correlation of air temperatures for T'_{LP} and T'_{HP} exhibit negative correlations for length scales > 2000 km, a separation distance that only occurs for stations near the outer edges of our domain. We interpret this behavior as being associated with the horizontal length scale of large atmospheric storm systems, which are associated with pole-ward blowing winds on their eastern flank and equator-ward blowing winds on their western flank.

Hence, cyclones that lie within the bounds of our station range exert a differential advective influence on station air temperatures. When a low-pressure system advects warm southern air masses into the eastern Gulf of Alaska, it also advects cooler high latitude air into the western Gulf of Alaska and along the Aleutian Islands. Interestingly, this character is observed for both the synoptic and seasonal frequency bands, while the ocean seasonal correlations are not significantly different than zero.

We next assess the correlation of monthly temperature anomalies for surface and subsurface variations at four distantly separated CTD profile stations: KBAY 6 in lower Cook Inlet, station GAK1 in the coastal waters of the outer Kenai Peninsula, station KIP2 in western PWS, and station GLBA-20 in Glacier Bay.

The results (Figure 1-12) generally exhibit higher correlations in the winter months, except for the deep (150-550 m depth) waters of KIP2. The correlation patterns during winter are consistent with our expectation of deeper winter mixed layers, decreased seasonal stratification and deeper wind-induced mixing at this time of year. Summer stratification decouples the upper and lower water column and thus degrades the surface-to-depth correlation at this time of year. Both KIP2 and GAK1 show correlation minima near 50 m depth and maxima near 150 m depth in summer, suggestive of a system with at least three functionally distinct layers. The upper layer warms in concert with surface heating, the middle of the water column may adjust relative to interior Ekman return flows and the lower layer warms due to the deep inflow associated with the summer relaxation of downwelling winds (Weingartner et al. 2005). However, mechanistic links between the surface and near-bottom temperature covariation are not fully clear. The shallowest of the four sites, KBAY6, shows the strongest correlations through the entire water column in both seasons, a characteristic consistent with the strong tidal currents of Cook Inlet.

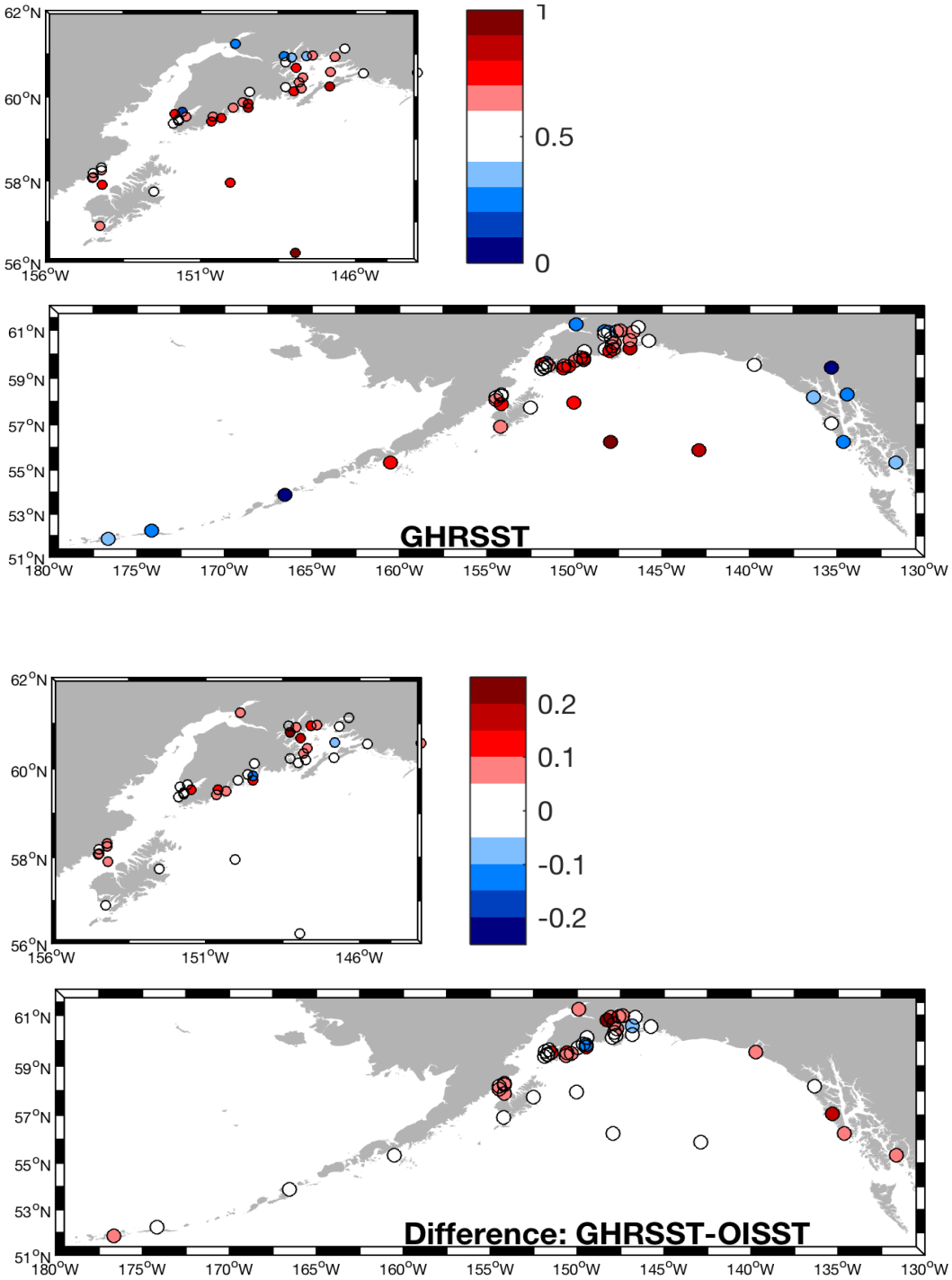

Figure 1-10. Fraction of the daily thermal anomaly explained by the group for high resolution sea surface temperature (GHRSST) data (top). Differenced fraction of daily thermal anomaly explained the GHRSST and the optimum interpolation sea surface temperature (OISST) datasets, showing that while both datasets capture a similar level of the total variance, the GHRSST dataset is a generally a more accurate data source. OISST results are shown only for grid points that lie within 30 km of an in situ observation (bottom).

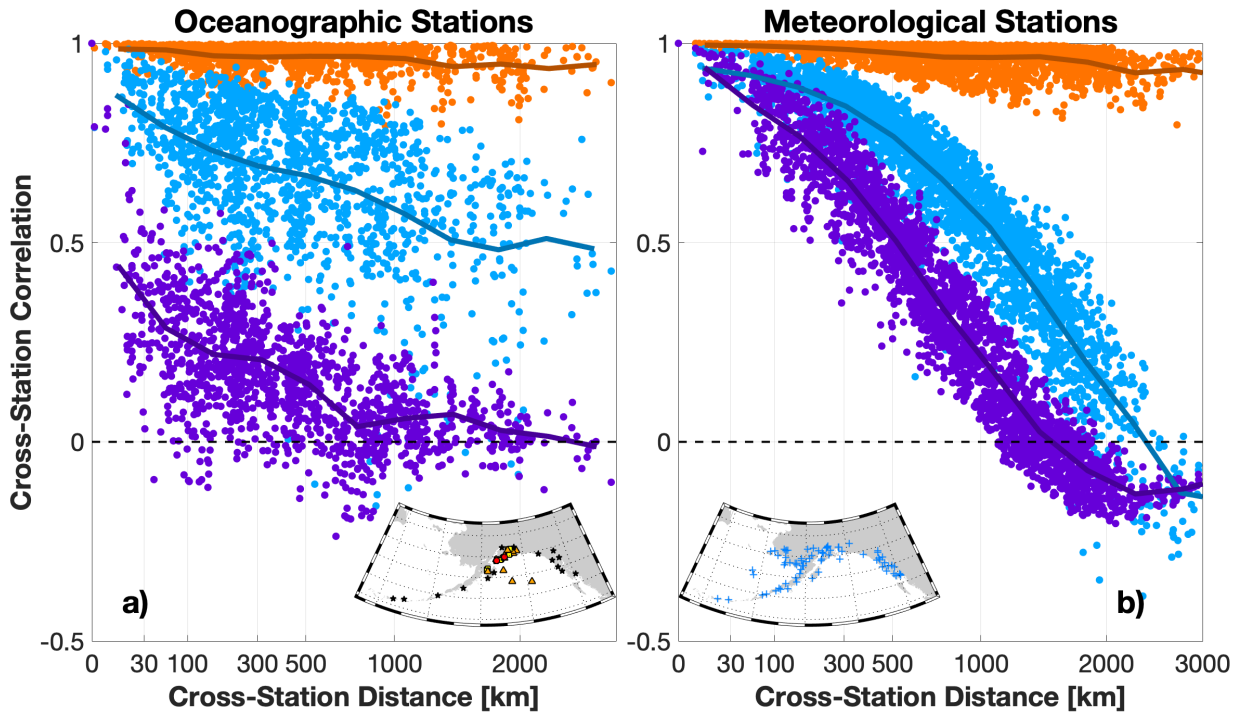

Figure 1-11. a) Cross-correlation coefficient as a function of distance for all stations used in analysis (locations shown in inset map). Correlations between stations pairs are computed where the records have at least 1.5 overlapping years of data over the period from January 1, 2007 to May 1, 2018. Orange, blue, and purple correspond to T_{DA}, T'_{LP}, and T'_{HP}, respectively. Darker lines show bin averages. b) Same as (a), but for Automated Surface Observing System meteorological stations south of 61.5°N. See the Data and Methods section for abbreviation definitions.

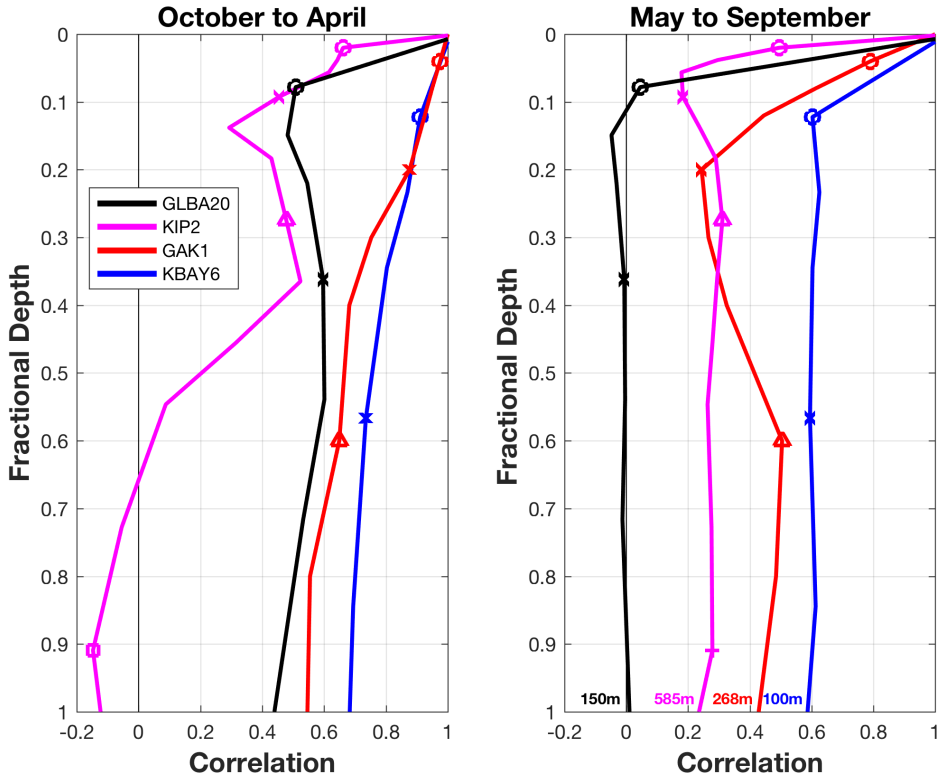

Figure 1-12. Correlation between temperature anomalies at the surface and temperature anomalies at standard depths (0, 10, 20, 30, 50, 75, 100, 150, 200, 250, 300, 400, 500, and 550 m) for winter (left) and summer (right) season as resolved by CTDs taken at stations GLBA20 (black), KIP2 (magenta), GAK1 (red), and KBAY6 (blue). Symbols o, Δ, x, and + show the location of the 10, 50, 150, and 500 m depth levels, respectively. The seafloor depth of each station is noted at the bottom of the right-hand panel. Correlations are computed for the corresponding period of record for each site: 49, 25, 22, and 7 years for the GAK1, GLBA20, KIP2, and KBAY6 stations, respectively.

KIP2 and GLBA20 are located in sheltered estuaries under the influence of strongly stratified water columns. In both seasons these stations show strong declines in correlation between the surface and 10 m depth. At GLBA20, this very shallow stratified layer is also associated with cool thermal anomalies that covary in phase with fresh haline anomalies in summer and fall months (not shown). More typically, warm anomalies (which correspond to greater rates of snow and glacier ice melt) are associated with fresh haline anomalies in the coastal zone. Our interpretation is that the close proximity of GLBA20 and KIP2 stations to glaciers allows the CTD data from these stations to exhibit the influence of sensible heat directly associated with glacier meltwater.

To show the nature of the covariability of surface and subsurface variations across the northern shelf, we examine the Seward Line CTD data from stations GAK1 through GAK13. We compute correlations across all depths and all stations of the Seward Line relative to the surface

measurement at GAK1 (Figure 1-13, left panel). We repeat the correlation analysis using monthly anomalies for both the CTD data at all stations and at the GAK1 reference (Figure 1-13, right panel).

In both analyses, we find strong correlations at the surface between the coast and the continental slope, although the surface anomaly correlation noticeably weakens beyond the shelf break (station GAK9) where the Seward Line extends into the swift Alaskan Stream over the slope. The correlations show a strongly layered structure, with larger values extending farther into the water column at stations closer to the coast. An anomaly correlation minimum observed between about 50 and 75 m depth near GAK1 shoals farther offshore to approximately 30 to 40 m depth, following the offshore shoaling of isopycnals (not shown). Below the correlation minimum, a local maximum suggests some indirect connectivity between the surface and depth.

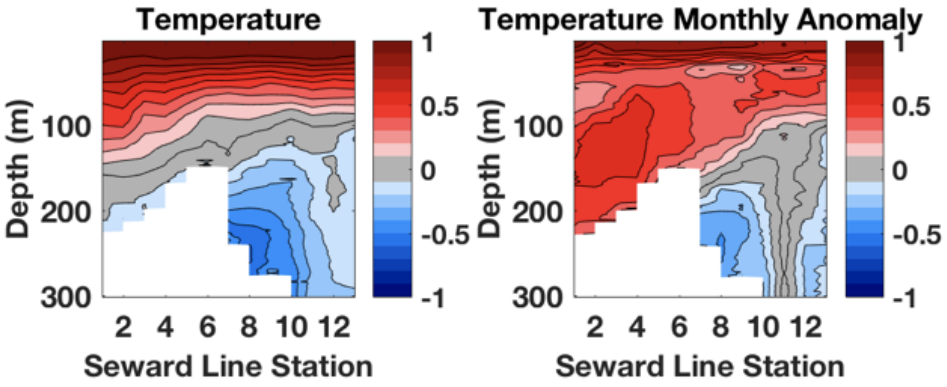

Figure 1-13. Correlation of temperature anomalies across the Seward Line transect (stations GAK1 to GAK13) relative to the surface temperature at station GAK1. Left-hand panel shows correlations that characterize the annual cycle; the right-hand panel shows correlation of monthly anomalies. White regions depict the shelf seafloor. Seward Line stations are each separated by ~10 nmi (18.5 km). Correlations computed for 76 Seward Line occupations between 1997 and 2018.

The spatial structure of the negative correlations shown in Figure 1-13 relate to the structure and behavior of the shelf-break front, which typically intersects the outer shelf seafloor between 200 and 300 m depth (Okkonen et al. 2003, Weingartner et al. 2005). The negative correlations found over the outer shelf shows that surface and seafloor temperatures tend to fluctuate out of phase with each other, both seasonally and at monthly time scales. At 250 m depth at the shelf break, temperature and salinity have a significant inverse correlation ($r = -0.54$, $p < 0.001$, $N = 92$). Additionally, because of a positive correlation between nutrients and salinity (Childers et al. 2005), the panels of (Figure 1-13) suggest that the negative temperature anomalies depicted at the seafloor near the shelf break are also associated with positive nutrient concentration anomalies. The portion of the shelf located between stations GAK6 and GAK9 spans the eastern flank of Amatouli Trough (Figure 1-2), indicating that near-bottom westward along-isobath flows at these stations are primarily directed toward the inner shelf and therefore represent an onshelf-flux of nutrients.

The above results, based on both remotely sensed and *in situ* data, show that thermal covariation degrades with increasing distance both laterally and with depth through the water column. However, all six of our primary focal sub-regions (Katmai, offshore Gulf, Kachemak Bay, Kenai Peninsula, PWS, and SE Alaska) also exhibit a considerable degree of synoptic scale covariability (Figure 1-14).

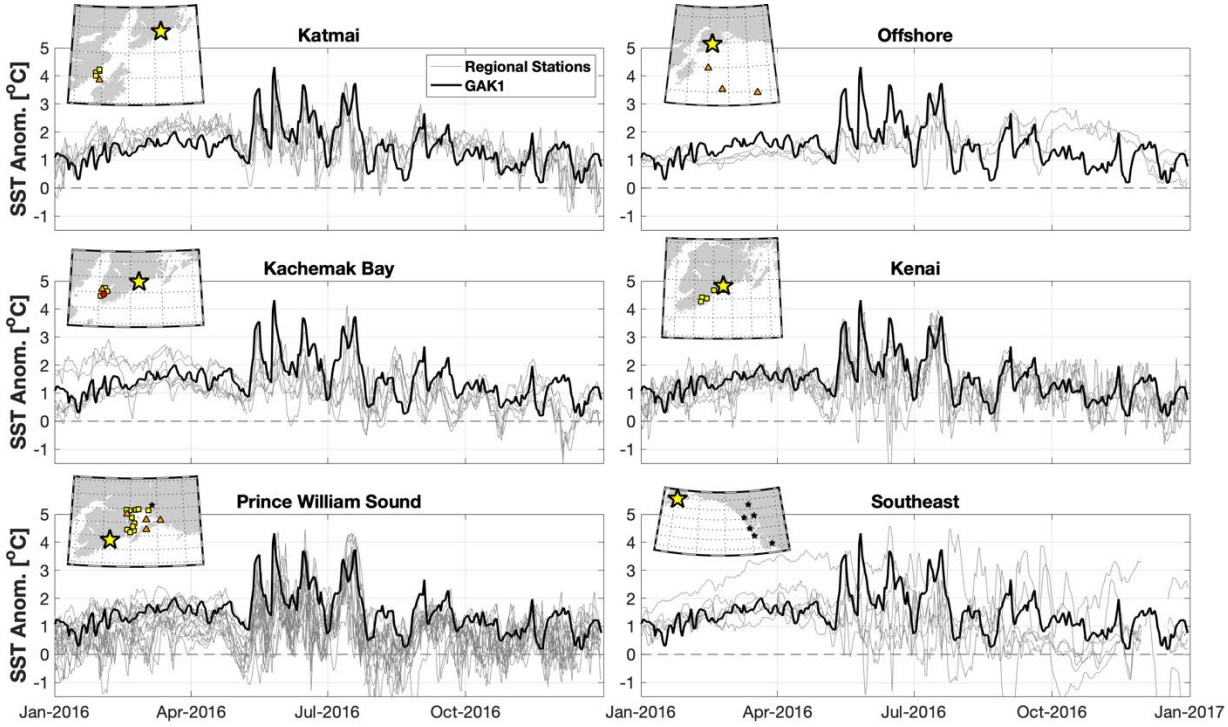

Figure 1-14. Temperature records with the annual cycle removed (T_{RAW}-T_{DC}) at GAK1 (black line) and all other stations (gray lines) for six sub-regions during year 2016. The mean annual cycle is computed by using (sometimes incomplete) data records spanning January 1, 2007 to May 1, 2008. Inset maps show stations used for each region (in color, identical to Figure 1-2). The yellow star shows the location of GAK1.

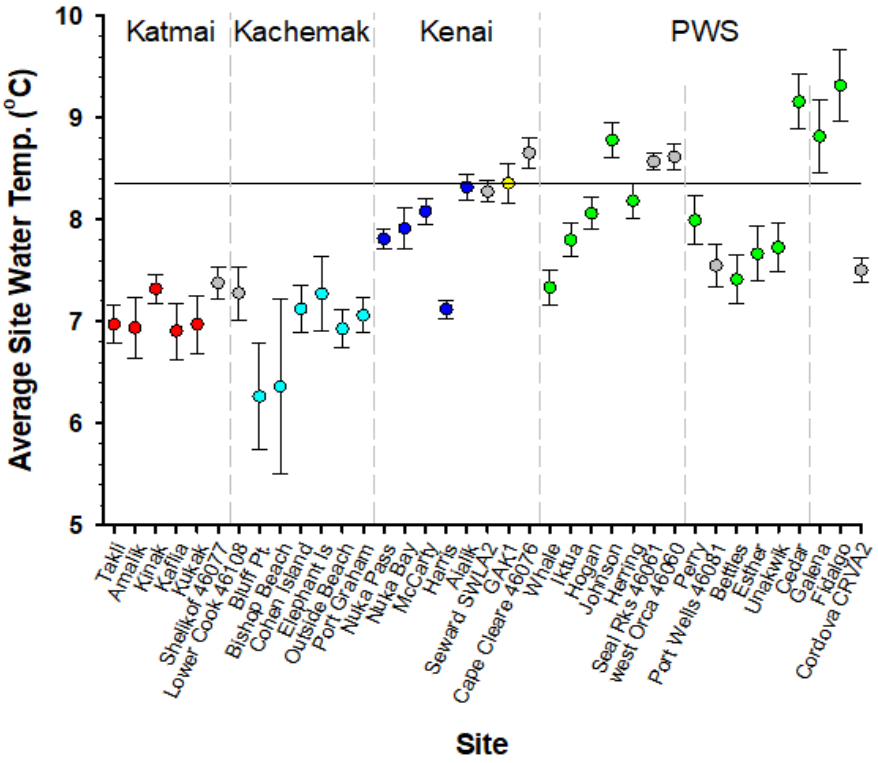

Figure 1-15. Long-term mean and 95% confidence intervals for the temperature measured at the nearshore HOBO sites and select coastal stations. Means have been adjusted to account for varying length time series at each site relative to the 1970-2019 GAK1 reference (yellow circle, marked by the horizontal line). Red, cyan, blue, and green symbols denote HOBO sites in Katmai, Kachemak Bay (Kachemak), Kenai Fjords (Kenai) and Prince William Sound (PWS), respectively. Grey symbols denote coastal National Oceanic and Atmospheric Administration buoys. PWS is further divided (from left to right) into three areas: western, northern, and eastern.

GAK1, centrally located relative to the HOBO and buoy stations, is well correlated with the daily SST anomaly across relatively large distances (Figure 1-8) and provides a nearly 5-decade record that is suitable as a baseline reference for the shorter time series. Corrected for varying time series durations that unequally cover years, we find that GAK1 is warmer than most of the intertidal locations where the HOBO dataloggers were sited (Figure 1-15). This characteristic likely reflects the closer connectivity of GAK1 to the shelf circulation, where waters are advected along-shore from warmer sites to the south, and the nature of nearshore sites, which are subject to strong heat losses. Notable exceptions are associated with stations in PWS that are all located in protected or semi-protected bays that are generally upstream of and far from tidewater glaciers. In contrast, the coldest sites tend to be nearer to tidewater glacier influences and/or downstream of Cook Inlet outflows. In particular, the Harris Bay site in Kenai Fjords and the Whale Bay, Bettles, Esther, and Unakwik sites in PWS have the closest proximity to tidewater glaciers in their respective regions. Relative to Cook Inlet, the Bluff Point and Bishop Beach sites (see Appendix Table A1 for precise site locations) are located near the western edge of

Kachemak Bay and are most directly connected to the lower Cook Inlet through flow while all the Katmai sites are located downstream of Cook Inlet. We also note that Janout et al. (2013) show enhanced rates of surface heat losses in the western Gulf of Alaska from Cook Inlet to Unimak pass, relative to the northern and eastern portions of the shelf.

Notable extrema of both summer and winter found in the GAK1 record exhibit similar but not identical signals within the other records (Figure 1-14). Many of the large peaks that stand out in Figure 1-14 are separated by about two weeks, suggesting possible influence of the fortnightly tide, although the fact that the fluctuations are not precisely regular on this time scale means that additional processes such as wind-induced forcing may also play a significant role. Instances of both positive and negative phase lags relative to GAK1 can be found in each of the panels in Figure 1-14, suggesting the likely possibility that multiple forcing mechanisms and heat distribution processes exert asynchronous and variable magnitude control over local thermal variations.

The typical decorrelation time scale ($\tau 0$), calculated using the first zero crossing of a record's autocorrelation function, is 9-13 days in winter and 8–11 days in summer. Longer time scales occur offshore and at coastal sites (Katmai, GAK1) where along-shore advection is important. The more protected sites (Kachemak Bay) tend to have shorter decorrelation time scales, suggesting stronger local influences on temperature. The decorrelation time scale results are also consistent with our expectation that nearshore realms have relatively large lateral gradients, while offshore regions are associated with weaker lateral gradients. The fact that all estimates of $\tau 0$ fall within the timescale of the fortnightly spring-neap cycle suggests the potential for the effects of tide-induced mixing in helping to set the important time scales of variability.

Selecting GAK1 as a reference site, analysis of variance shows that T_{DA} (annual cycle), T'_{LP} (temperature anomaly low-pass filtered at 30 days) and T'_{HP} (temperature anomaly high-pass filtered at 30 days) each exhibit distinctive character, with less pronounced but still evident variations between subregions (Figure 1-16 top). The annual cycle at all sites is well captured by T_{DA} (orange symbols in all sections of Figures 1-16 and 1-17), with most stations showing $r > 0.95$ relative to GAK1, with the weakest correlations found in SE Alaska, along the Aleutian Islands, and in upper Cook Inlet (Anchorage). The scatter of T'_{LP} evenly about $\sigma = 1$ shows that the GAK1 variance magnitude is typical of the mean of the other stations. The RMSD of the data (concentric circles about GAK1) shows that the typical magnitude of error for T_{DA} is small, often $RMSD < 0.4$.

T'_{LP} (blue symbols in Figure 1-16 top) is less well correlated than T_{DA}, typically $0.2 < r < 0.6$ but still the relations remain statistically significant ($p < 0.05$) for the most part. Moreover, GAK1 shows little bias relative to the other stations. T'_{HP} (purple symbols in Figure 1-16 top) are only weakly correlated to those at GAK1, indicating that day-to-day temperature fluctuations do not covary amongst sites. In both T'_{LP} and T'_{HP}, regional differences can be detected in Figures 1-16 and 1-17, with the tendency for closely spaced stations to exhibit similar behavior to each other.

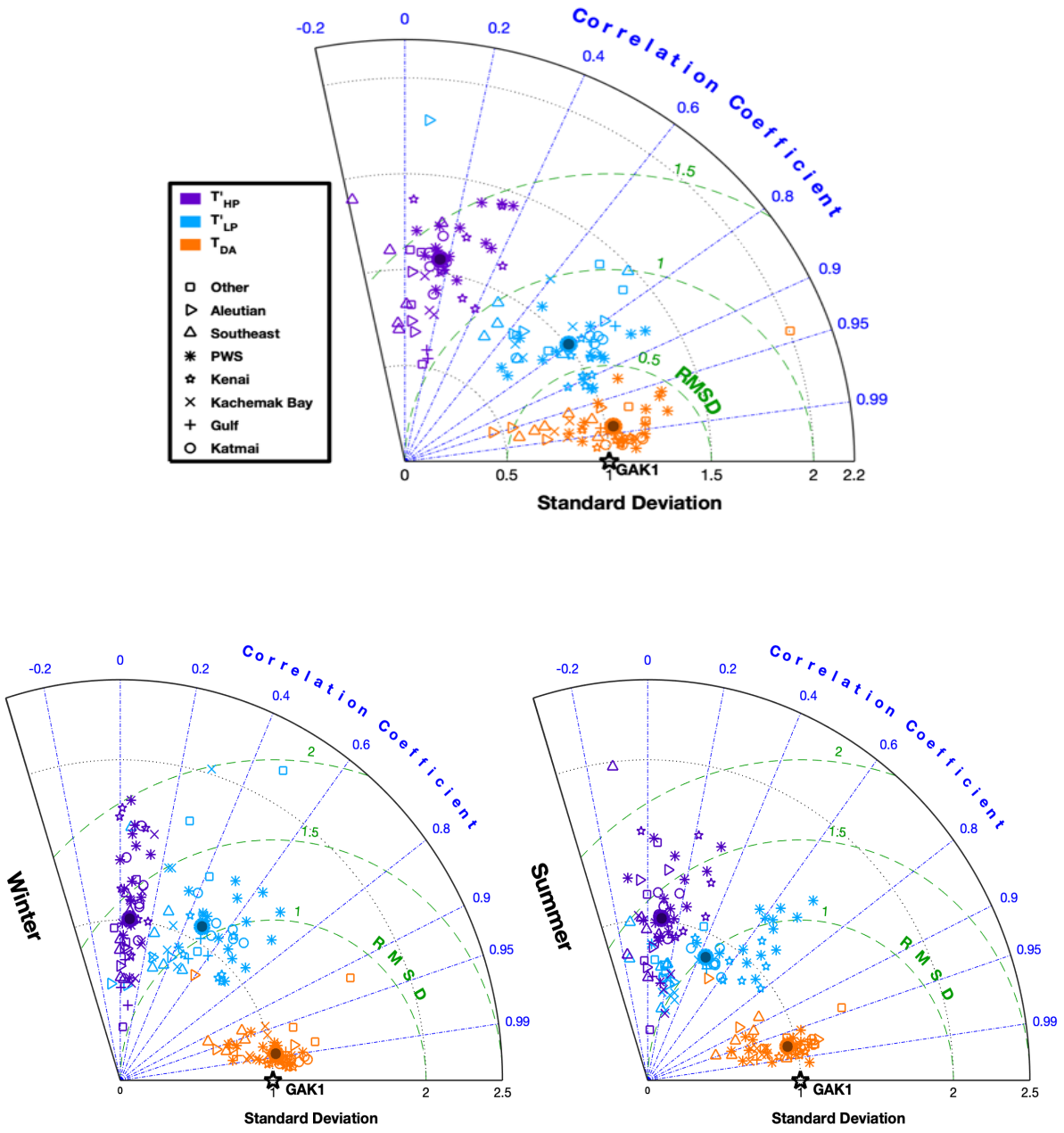

Figure 1-16. Top: Taylor diagram representation of correlation analysis between sea surface temperature at GAK1 and all other stations in the Gulf of Alaska (azimuthal coordinate), as well as their normalized standard deviations (radial coordinate from origin) and their root mean square difference (RMSD, radial coordinate from the GAK1 reference point). Colors distinguish the three temporal bands. Standard deviations of temperature anomalies for all stations are normalized by the standard deviation at GAK1. The RMSD and σ are both unitless. Bottom: Same as top but partitioned into winter (left, October 1st to April 30th) and summer (right, May 1st to September 30th), with analyses representing the period of station record overlap with that at GAK1.

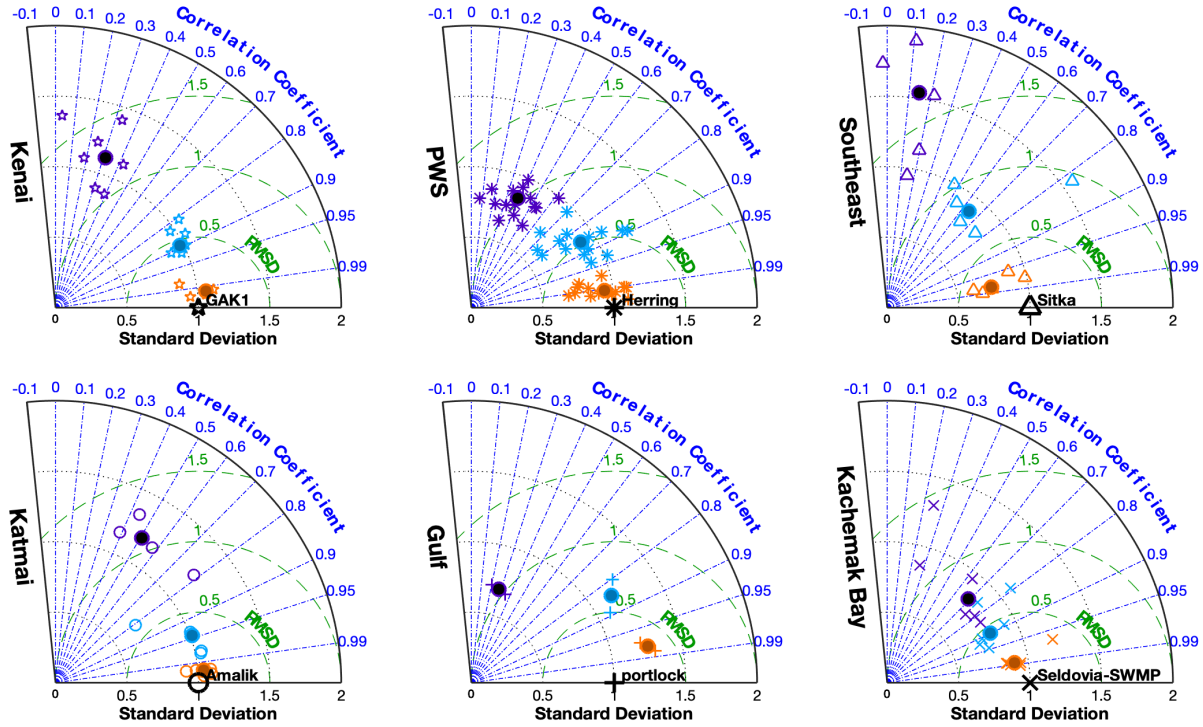

Figure 1-17. Same as Figure 1-16, but partitioning data regionally. The reference station used for each region is the station within that cluster best correlated with GAK1. Variance here is normalized to each regional reference station.

To assess the covariability of temperature between sites within each of the focal sub-domains, we selected regional reference stations (choosing the station best correlated with GAK1 from within each domain) and repeat the above analyses (Figure 1-17). We find that stations within most of the domains each exhibit stronger covariation to the local reference than to the GAK1 reference. Most show $r \geq 0.99$, $r > 0.8$ and $r > 0.3$ for T_{DA}, T'_{LP} and T'_{HP}, respectively. The SE Alaska domain is notably less well correlated with $r \sim 0.98$, 0.6 and 0.1 for the three frequency bands, respectively, although stations here are much more spatially dispersed and geographically isolated than within the other domains (see Figure 1-2).

Nearly all intertidal and coastal SST time series within and across the various northern Gulf of Alaska regions depict a coherent pattern of seasonal to interannual variability (Figure 1-18), with most prominent peaks and troughs coincident at these time scales. Results of variance analysis of the seasonal anomalies shown in Figure 1-18 would thus lie between the blue and orange markers in Figures 1-11 and 1-16.

Figures 1-5 and 1-18 depict two distinct temperature regimes for the 2006 to 2019 time period: a cool interval from 2006-2013 and a warm interval from 2014-2019. The seasonal anomalies in Figure 1-18 show that the transition to the PMH began after the cool interval minimum in 2012. Nearly all sites showed warming through calendar year 2013 with large (3-4 °C) positive

temperature anomalies recorded across the region. The positive temperature anomalies are associated with the PMH experienced across the entire NE Pacific during this time (e.g., Jackson et al. 2018). While the seasonal anomaly patterns tightly covary in time, the amplitude of the signal is typically larger than that at GAK1, reflecting the larger impact of air-sea heat fluxes in very shallow waters relative to deeper surface mixed layers found beyond the nearshore zone.

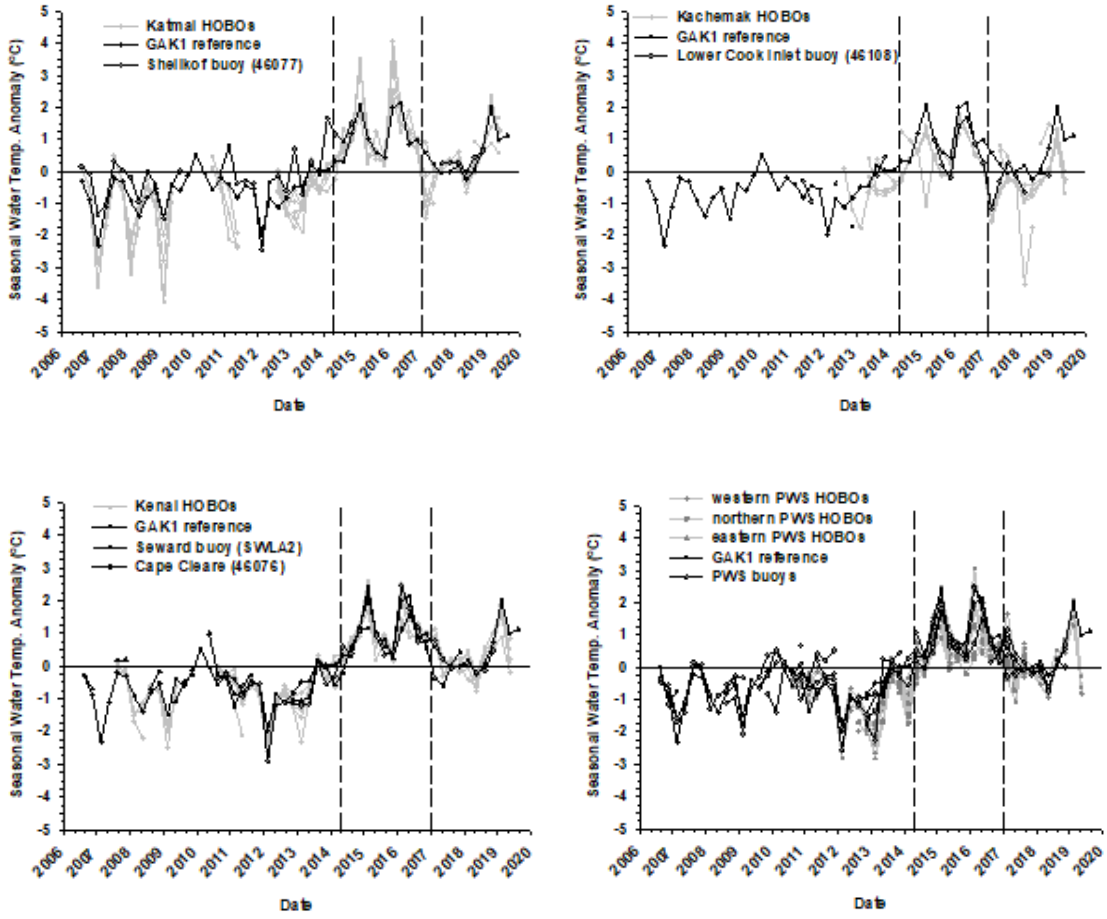

Figure 1-18. Seasonal water temperature anomalies relative to the 1970-2019 GAK1 time series for intertidal HOBOs and nearshore NOAA buoys for Katmai (upper left), Kachemak Bay (upper right), Kenai Fjords (lower left) and Prince William Sound (PWS) (lower right). For reference, dashed vertical lines denote May 1, 2014 and January 1, 2017 on each plot.

In summary, we have shown that spatial variability of surface temperature fluctuations varies greatly at synoptic time scales, even between sites that are separated by fewer than 10 km. In contrast, over seasonal and interannual time scales temperature anomalies are well correlated for station separations of many hundreds of kilometers. Hence, monitoring of individual bays is important if it is critical to differentiate their day-to-day local variations of heat. On the other hand, very few monitoring stations are required to well document seasonal and longer period anomalies, which tend to manifest broadly across the regional basin scale (e.g., 100-1000 km)

with a high degree of temporal synchrony. The above insights of temporal and spatial structure in the temperature fluctuations provides a foundation for us to next undertake a case study of the warm and cool temperature anomalies depicted in Figure 1-18.

CASE STUDY: TEMPERATURES ACROSS THE NORTHERN GULF OF ALASKA

We seek a better understanding of the manifestation of the PMH and subsequent warm anomalies (Figure 1-18) and their relation to conditions in the central Gulf of Alaska where the first signs of the PMH were identified. The central Gulf of Alaska was known to be undergoing a highly unusual warming event in the upper 100 m of the water column as the 2013 winter passed into 2014 (Freeland 2014). By the end of 2015 this surface heat had penetrated across the upper 300 m of the offshore water column, where it persisted with positive heat content anomalies into 2018 (Jackson et al. 2018, Ross et al. 2019). At station GAK1 on the northern shelf, a multi-year cool interval persisted below 100 m depth throughout 2013 although surface anomalies turned positive. However, by early 2015 the entire water column (250 m) showed large positive anomalies at GAK1. This was followed by a cooling interval through late summer 2015 although temperatures still remained above normal. A strong El Niño event contributed to even warmer conditions in 2016 (Gentemann et al. 2017). Below, we examine additional aspects of the temporal synchrony of the preceding cool phase, the warming transition that led to positive thermal anomalies, and the surface heat fluxes that drove these anomalies.

There are eleven oceanographic stations that also have a nearly co-located ASOS weather station in our data compilation. These are nearly evenly distributed around rim of the Gulf of Alaska from Adak Island in the Aleutians to Port Alexander in SE Alaska. Observed quantities at these stations include air temperature, relative humidity, wind speed, and cloud cover. Coupled with the measurements of SST, these records provide sufficient information to compute bulk surface heat flux terms as described above in the Gridded SST data compilations section. We neglect consideration of advective and diffusive terms, as it is not possible to compute these without measurements of velocity or temperature gradients. Estimating the net surface heat flux (Q_{SUM}) is nevertheless valuable as it allows us to assess the importance of local surface forcing relative to observed changes in near-surface ocean temperature. To provide a rough sense of the change in upper ocean heat content (Q_{OC}), we assume that changes in near-surface temperature are uniform over the upper 15 m.

We find that the annual cycle of Q_{OC} and Q_{SUM} are reasonably similar in both magnitude and phase (Figure 1-19). Frequently Q_{SUM} has a negative offset relative to Q_{OC}, potentially implying a supply of heat from diffusive or advective processes.

The monthly anomalies of Q_{OC} and Q_{SUM} are significantly correlated (95% confidence) for six of the eleven stations used for heat flux analysis, though none have correlation coefficients greater than 0.5. This suggests that the terms in Q_{SUM} have only a modest degree of influence on local conditions across the Gulf of Alaska and that other drivers dominate. Stations close to the Alaska Coastal Current may be heavily influenced by the advective terms, whereas diffusive terms may be of first order importance at stations near regions of strong tidal mixing (e.g., the Aleutians). The assumption that temperature changes are uniform over the upper 15 m is clearly an

oversimplification, since mixed layer depths vary seasonal and spatially, and thus are a factor contributing to the low correlations between the anomalies of Q_{OC} and Q_{SUM}.

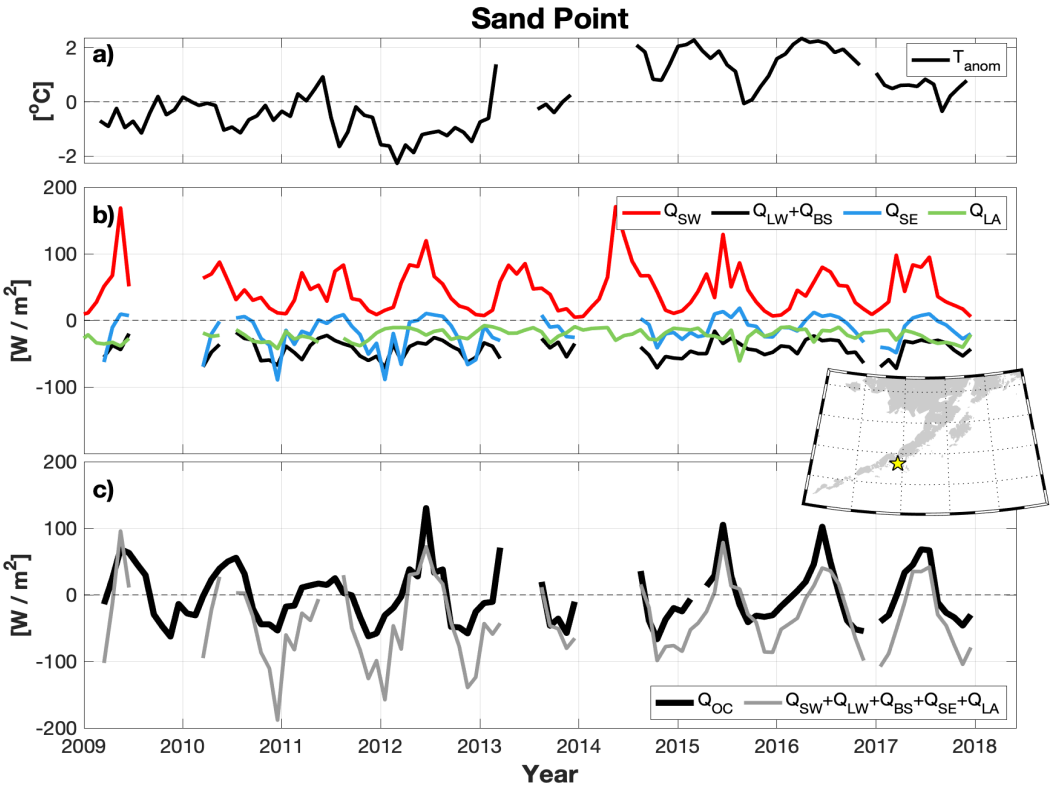

Figure 1-19. a) Monthly sea surface temperature (SST) anomaly (monthly average removed) for the Sandpoint tide gauge station. Anomalies are calculated between January 1, 2007 and January 1, 2018. b) Heat flux terms (W/m^2) computed from the tide gauge station, an Automated Surface Observing System weather station 2.3 km away, and Reanalysis-2. Downward shortwave radiation (Q_{SW}) is computed from 6-hour averages of clear-sky Reanalysis-2. The combined longwave (Q_{LW}) and backscatter (Q_{BS}) flux term is derived from both tide gauge SST and weather station data, as are the sensible (Q_{SE}) and latent (Q_{LA}) terms. c) Heat flux of the ocean (Q_{OC}) assuming the changes in SST are uniform over the upper 15 m and the sum (Q_{SUM}) of the terms in panel (b). The inset map shows the location of the Sand Point station (yellow star).

To assess the temporal patterns of surface heat fluxes (Q_{SUM}) across the whole domain of the Gulf of Alaska, we use the estimates at the eleven stations to compute the total annual heat flux anomaly (annual cycle removed) for each year (Figure 1-20). Strong warming occurred in 2009, 2013, and 2014, while 2008, 2011, and 2017 exhibit significant cooling. We note that these results are in close agreement with the year-to-year changes of heat content suggested by Figures 1-5, 1-14, 1-21, and 1-22. The surface forcings that triggered the 2006-2013 cool phase were associated with anomalies in coastal runoff, winter cooling, stratification, and winds associated with an eastward-shifted Aleutian Low relative warmer years (Janout et al. 2010).

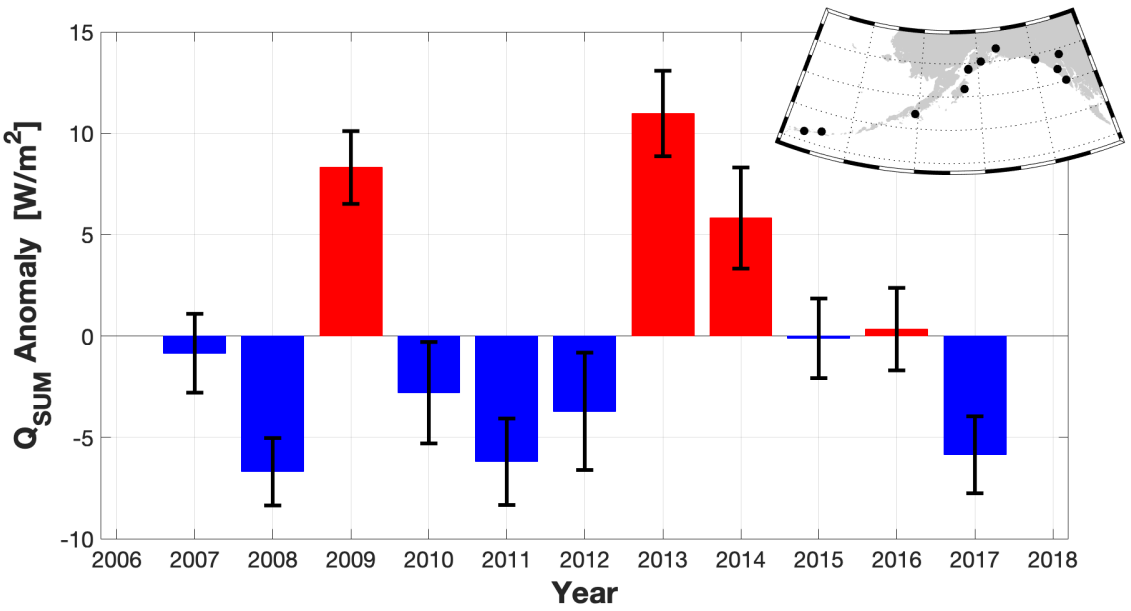

Figure 1-20. Annual averages of the anomaly of Q_{SUM} (annual cycle from 2007 to 2017 removed) for all sites with oceanographic and Automated Surface Observing System weather stations in close proximity (inset map). Error bars show the standard deviation of the anomaly divided by the square root of degrees of freedom. We assume 90 degrees of freedom in each yearly average since the decorrelation time scale for ocean and atmospheric signals is several days.

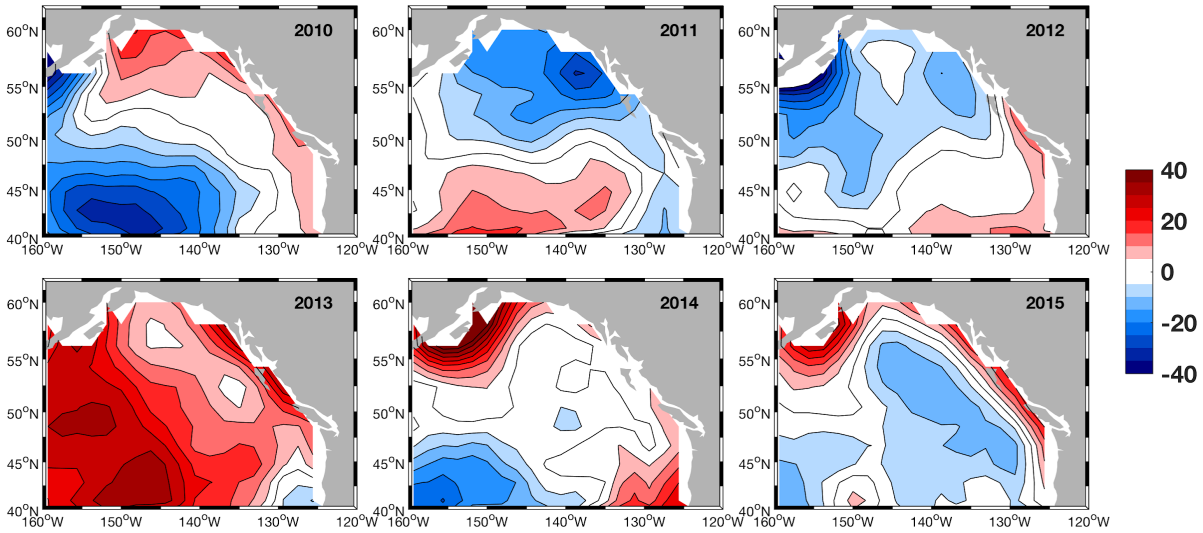

Figure 1-21. Reanalysis-2 estimates of the annual mean net surface heat flux anomaly (W/m^2) for 2010 to 2015 from the over the NE Pacific.

We can assess the importance of the estimated (Figure 1-20) 2013 heat flux anomaly (~11 W m^{-2}) relative to the observed magnitude of warming. The change in water column temperature (ΔT) over one year (Δt) can be estimated as $\Delta T = Q_{SUM}\Delta t/\rho C_P H$ where CP ~ 4000 J °C-1 kg^{-1} is the heat capacity of seawater, $\rho = 1025$ kg m^{-3}, and H = 15 m. We find $\Delta T = 5.6$ °C, which is much larger than the temperature increase seen at any nearshore or coastal station in 2013, so the heat must have been mixed much deeper than the upper 15 m. For a typical shelf depth of 200 m in the Gulf of Alaska, the warming implied by this heating rate is 0.42 degrees. This estimate is smaller than most temperature changes during our time period of interest (see Figures 1-18 and 1-21), meaning that a substantial amount of the heat gained over the shelf and in the nearshore realm must have been advected there from regions to the south and/or offshore.

The above results are also roughly congruent in timing, magnitude and sign with Reanalysis-2 estimates of heat flux in the northern Gulf of Alaska (Figure 1-21). Except for 2009, between 2006 and 2012 the northern Gulf of Alaska experienced weak to moderate cooling before the strong warming in 2013 triggered the onset of the PMH that became obvious in 2014. Early in this cool phase, the temperature decline was associated with strong ocean-to-atmosphere heat loss in November 2006 and March 2007 and below-average runoff in fall (Janout et al. 2010). Together, winter surface heat fluxes and salinity stratification can explain over 80% of thermal variations below 100 m depth at station GAK1 (Janout et al. 2010). We further note that the Reanalysis-2 distribution of surface heat fluxes also suggest that warming is mostly confined to the northern shelf in 2014 and 2015, but with a larger magnitude in 2014. This signal stands in contrast to the near zero or negative heat flux anomalies found offshore in these two years. Hence, while the central Gulf of Alaska upper water column was being forced back towards mean conditions in 2014 and 2015 (but still remaining warmer than usual), the shelf regions did not experience anomalously negative heat fluxes until 2017 (Figure 1-20).

How did the spatial and temporal variations in surface heat fluxes manifest in the temperature records? Figure 1-22 shows that while all of the stations warmed in 2013, the surface temperature at Ocean Station PAPA (near the geographic center of the “blob” feature (Bond et al. 2015) increased much more rapidly than at any of the Alaskan coastal stations. Furthermore, while the signal at PAPA peaked in early 2014, the warming over the shelf continued until mid-late 2014 at the surface.

Temperatures near the seafloor at GAK1 commonly lag temperature signals observed in the upper water column and this was also true for the PMH signal. Near-bottom temperatures abruptly warmed in January 2015 and remained elevated by nearly 1 °C above normal until early spring 2016 when they further increased to near 2 °C above normal. Warming associated with the 2015 El Niño further increased temperatures in the northern Gulf of Alaska in 2016, and water column average temperatures remained above normal throughout 2017, 2018, and 2019 (Figure 1-5).

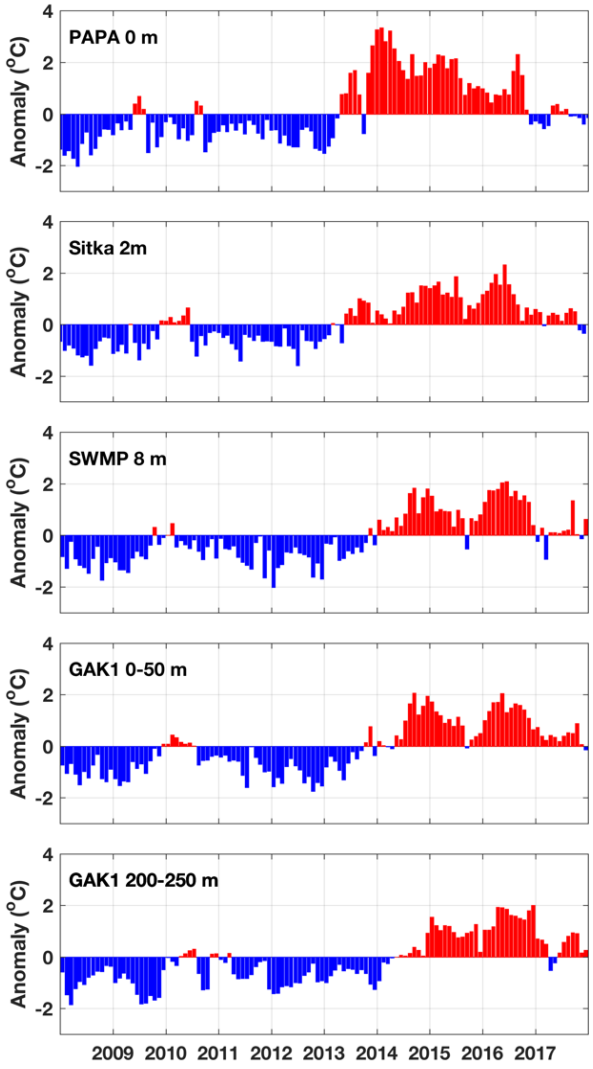

Figure 1-22. Monthly temperature anomalies at ocean station PAPA (from the Optimum Interpolation Sea Surface Temperature record), the Sitka tide gauge station, System Wide Monitoring Program (SWMP) mooring and GAK1 over 2008-2017. Anomalies are all referenced to the same 2008-2019 baseline.

Conclusions and Summary

This combined analysis of anchored, buoy, moored, ship-based, and remotely sensed data from the northern Gulf of Alaska provides new insights to the nature of spatial and temporal thermal variations in the nearshore and coastal zones. We find that Gulf of Alaska surface nearshore, coastal and offshore thermal anomalies tend to exhibit synchrony at seasonal time scales but subsurface anomalies over the shelf exhibit lagged responses that depend on advection. Surface temperature correlation patterns vary regionally as a function of local shelf and coastline geomorphology and the locally important oceanic processes. Synoptic scale coastal thermal variability manifests with short (< 10 day and < 10 km) decorrelation time and space scales. In

the vertical direction, highly stratified water columns under the proximal influence of snow and glacier melt runoff exhibit positive temperature vs. salinity anomaly relations, while more commonly fresh anomalies are associated with elevated temperatures.

While satellites are valuable especially for capturing seasonal and longer temperature variations, their accuracy in the Gulf of Alaska degrades in nearshore and coastal realms and in these locations the relative importance of *in situ* measurements expands. Biological productivity is often high in many nearshore and coastal regions, so ecosystem studies that seek to mechanistically link environmental conditions to abundance, biomass and community composition may not be able to rely solely on satellite measures of temperature. Similarly, the covariability of temperature fluctuations degrades rapidly with depth, thus measures of SST alone may be insufficient to fully characterize the nearshore thermal environment.

Our CTD data analysis shows that near-bottom temperature anomalies over the outer shelf exhibit a negative correlation with surface thermal anomalies and near-bottom salinity anomalies. As salinity and nitrate exhibit a positive relation in the Gulf of Alaska (Childers et al. 2005), the inverse correlation of thermal and haline anomalies suggests that positive surface temperature anomalies are associated with elevated nutrient anomalies at depth. These signals manifest at the upwelling-favorable side of Amatouli Trough where flows near the seafloor will generally be directed onto the shelf. This linkage deserves closer investigation because if the relation is due to coupling by the ocean current field it would provide a means by which we may be able to use the long record of surface temperature data as a proxy for cross-shelf nutrient flux anomalies.

Oceanic conditions, particularly temperatures, play both top-down and bottom-up roles in the control of offshore, coastal, and intertidal biological communities. For example, the development of stratification (due to both heat- and freshwater-sourced buoyancy) in spring allows phytoplankton productivity to maintain sufficiently elevated levels, which results in a bloom that marks the start of the annual cycle of carbon fixation and the trophic cascade of biomass through secondary producers and upper tropic levels (Gargett 1997, Strom et al. 2016). In the intertidal zone, species such as the Pacific blue mussel (*Mytilus trossulus*), are abundant consumers with growth characteristics tightly coupled to their habitat temperature. Before the onset of the recent PMH, intertidal invertebrate and algal community structure and dynamics appeared to vary independently among observations in our focal blocks (PWS, Kenai Fjords, Kachemak Bay, and Katmai), suggesting that intertidal community structure is largely driven by local dynamic drivers (Konar et al. 2016). As shown above, temperatures did not become anomalously high in the nearshore zone until mid to late summer 2014 and, correspondingly, the intertidal community structure showed no change in early summer of 2014 (Weitzman et al., this report Chapter 2). However, by the summer of 2015, intertidal macroalgae biomass declined (primarily *Fucus distchus*), which increased the amount of open space available for settlement of intertidal organisms. This, in turn, led to a successional sequence that moved community composition towards a more similar structure across all blocks through time (Weitzman et al., this report Chapter 2). For example, barnacle cover increased in 2016, followed by an increase in mussel cover by 2017, and finally, a slow return of *Fucus* by 2018 and 2019 as temperatures declined from the heights of 2015 and 2016 (Weitzman et al., this report Chapter 2). This sequence of events represented a shift in the intertidal communities across the Gulf of Alaska from one

dominated by macroalgae to one dominated by filter-feeding invertebrates. The synchrony of these changes aligned with the timing of the PMH effects, suggesting that large-scale oceanographic and atmospheric forcing can override local drivers to regionally influence patterns of intertidal community structure (Weitzman et al., this report Chapter 2).

Our results suggest potential tradeoffs between the effort of monitoring and the benefits of data returns across multiple spatial and temporal scales. While not all reference sites are as representative of the greater shelf as all others, all stations do relatively well at capturing the large-scale seasonal and sub-seasonal signals that dominate interannual variability. At seasonal, annual and interannual time scales, only a few broadly distributed monitoring stations capture thermal variability that similarly manifests across the region as a whole. However, knowing thermal variations at time intervals of less than one month at even relatively closely spaced stations requires closely spaced dataloggers.

While temperature is a key parameter that helps regulate biological activity, other factors that we have not considered in great detail also play defining roles. Clearly, a comprehensive understanding of thermal variations is incomplete without additional consideration of the advective environment, the diffusive environment, stratification, and, especially, salinity. Because stratification and hence many advective features are controlled by salinity rather than temperature in subarctic seas such as the Gulf of Alaska, detangling the influence of thermal variability on the physical system and the ecosystem can only be done with additional consideration of the haline environment. For example, warming trends and associated longer, rainier winters will also increase the onset of springtime stratification on the inner shelf (Weingartner et al. 2005). Such local physical processes in the Gulf of Alaska can also have far reaching effects, as the Alaska Coastal Current may be an important freshwater source for the Bering Sea shelf and Arctic Ocean (Aagaard et al. 2006). Similarly, the influence of ocean flows around the biologically productive banks near Kodiak Island and along the continental slope are also likely important contributors to the character of the thermal field relations depicted in Figure 1-8. This analysis provides a foundation upon which these other necessary studies can be conducted in the future.

ACKNOWLEDGEMENTS

The authors thank the many students, researchers, and volunteers for assisting with intertidal surveys over the years; the Kachemak Bay National Estuarine Research Reserve staff who have assisted with our System Wide Monitoring Program; University of Alaska Seward Marine Center Staff David Leech and Peter Shipton for carrying out the GAK1 field program; and the scientific team of the Gulf Watch Alaska long-term monitoring program for their expertise and resources in support of this publication. System Wide Monitoring Program data collection is supported financially by National Estuarine Research Reserve System operations with funding from NOAA to the Alaska Center for Conservation Science at the University of Alaska Anchorage, with technical and data management support provided by the National Estuarine Research Reserve System Central Data Management Office. We also thank the full scientific team of the Gulf Watch Alaska long-term monitoring program for their expertise and resources in support of this publication. The research described in this paper was in part, supported by the *Exxon Valdez* Oil Spill Trustee Council. However, the findings and conclusions presented by the authors are their

own and do not necessarily reflect the views or position of the Trustee Council. Any use of trade, firm, or product names is for descriptive purposes only and does not imply endorsement by the U.S. Government. This manuscript has been approved for publication consistent with U.S. Geological Survey Fundamental Science Practices (http://pubs.usgs.gov/circ/1367/). This research was supported by the *Exxon Valdez* Oil Spill Trustee Council and National Science Foundation grants.

REFERENCES

Aagaard, K., T.J. Weingartner, S.L. Danielson, R.A. Woodgate, G.C. Johnson, and T.E. Whitledge. 2006. Some controls on flow and salinity in Bering Strait. Geophysical Research Letters 33.

Aderhold, D.G. R., K. Holderied, M.R. Lindeberg, and W.S. Pegau. 2018. Spatial and temporal ecological variability in the northern Gulf of Alaska: What have we learned since the *Exxon Valdez* oil spill? Deep-Sea Research Part Ii-Topical Studies in Oceanography 147:3-8.

Agler, B.A., S.J. Kendall, D.B. Irons, and S.P. Klosiewski. 1999. Declines in marine bird populations in Prince William Sound, Alaska coincident with a climatic regime shift. Waterbirds 22:98-103.

Alexander, M.A., C. Deser, and M.S. Timlin. 1999. The reemergence of SST anomalies in the North Pacific Ocean. Journal of Climate 12:2419-2433.

Anderson, P.J., and J.F. Piatt. 1999. Community reorganization in the Gulf of Alaska following ocean climate regime shift. Marine Ecology Progress Series 189:117-123.

Beamer, J.P., D.F. Hill, A. Arendt, and G.E. Liston. 2016. High-resolution modeling of coastal freshwater discharge and glacier mass balance in the Gulf of Alaska watershed. Water Resources Research 52:3888-3909.

Bernardello, R., E. Serrano, R. Coma, M. Ribes, and N. Bahamon. 2016. A comparison of remote-sensing SST and *in situ* seawater temperature in near-shore habitats in the western Mediterranean Sea. Marine Ecology Progress Series 559:21-34.

Bond, N.A., M.F. Cronin, H. Freeland, and N. Mantua. 2015. Causes and impacts of the 2014 warm anomaly in the NE Pacific. Geophysical Research Letters 42:3414-3420.

Cane, M.A., and S.E. Zebiak. 1985. A Theory for El-Nino and the Southern Oscillation. Science 228:1085-1087.

Chelton, D.B., R.A. DeSzoeke, M.G. Schlax, K. El Naggar, and N. Siwertz. 1998. Geographical variability of the first baroclinic Rossby radius of deformation. Journal of Physical Oceanography 28:433-460.

Chiang, J.C.H., and D.J. Vimont. 2004. Analogous Pacific and Atlantic Meridional Modes of Tropical Atmosphere–Ocean Variability. Journal of Climate 17:4143-4158.

Childers, A.R., T.E. Whitledge, and D.A. Stockwell. 2005. Seasonal and interannual variability in the distribution of nutrients and chlorophyll a across the Gulf of Alaska shelf: 1998-2000. Deep-Sea Research Part Ii-Topical Studies in Oceanography 52:193-216.

Chin, T.M., J. Vazquez-Cuervo, and E.M. Armstrong. 2017. A multi-scale high-resolution analysis of global sea surface temperature. Remote Sensing of Environment 200:154-169.

Di Lorenzo, E., and N. Mantua. 2016. Multi-year persistence of the 2014/15 North Pacific marine heatwave. Nature Clim. Change 6:1042-1047.

Di Lorenzo, E., N. Schneider, K.M. Cobb, P.J.S. Franks, K. Chhak, A.J. Miller, J.C. McWilliams, S.J. Bograd, H. Arango, E. Curchitser, T.M. Powell, and P. Riviere. 2008. North Pacific Gyre Oscillation links ocean climate and ecosystem change. Geophysical Research Letters 35.

Ding, R., J. Li, Y.-h. Tseng, C. Sun, and Y. Guo. 2015. The Victoria mode in the North Pacific linking extratropical sea level pressure variations to ENSO. Journal of Geophysical Research: Atmospheres 120:27-45.

Dobbins, E.L., A.J. Hermann, P. Stabeno, N.A. Bond, and R.C. Steed. 2009. Modeled transport of freshwater from a line-source in the coastal Gulf of Alaska. Deep Sea Research Part II: Topical Studies in Oceanography 56:2409-2426.

Foreman, M.G.G., W.R. Crawford, J.Y. Cherniawsky, R.F. Henry, and M.R. Tarbotton. 2000. A high-resolution assimilating tidal model for the northeast Pacific Ocean. Journal of Geophysical Research-Oceans 105:28629-28651.

Freeland, H. 2014. Something odd in the Gulf of Alaska, February 2014. CMOS Bulletin SCMO 42.

Gargett, A.E. 1997. The optimal stability 'window': a mechanism underlying decadal fluctuations in North Pacific salmon stocks? Fisheries Oceanography 6:109-117.

Gentemann, C.L., M.R. Fewings, and M. Garcia-Reyes. 2017. Satellite sea surface temperatures along the West Coast of the United States during the 2014-2016 northeast Pacific marine heat wave. Geophysical Research Letters 44:312-319.

Gosz, J.R., R.B. Waide, and J.J. Magnuson. 2010. Twenty-eight years of the US-LTER program: experience, results, and research questions. Pages 59-74 in Long-term ecological research. Springer.

Hill, D.F., N. Bruhis, S.E. Calos, A. Arendt, and J. Beamer. 2015. Spatial and temporal variability of freshwater discharge into the Gulf of Alaska. Journal of Geophysical Research-Oceans 120:634-646.

Hobday, A., E. Oliver, A. Sen Gupta, J. Benthuysen, M. Burrows, M. Donat, N. Holbrook, P. Moore, M. Thomsen, T. Wernberg, and D. Smale. 2018. Categorizing and Naming Marine Heatwaves. Oceanography 31.

Hollowed, A.B., S.R. Hare, and W.S. Wooster. 2001. Pacific Basin climate variability and patterns of Northeast Pacific marine fish production. Progress in Oceanography 49:257-282.

Huang, B., P.W. Thorne, V.F. Banzon, T. Boyer, G. Chepurin, J.H. Lawrimore, M.J. Menne, T.M. Smith, R.S. Vose, and H.-M. Zhang. 2017. Extended reconstructed sea surface

temperature, version 5 (ERSSTv5): Upgrades, validations, and intercomparisons. Journal of Climate 30:8179-8205.

Isaji, T., and M.L. Spaulding. 1987. A numerical-model of the M2 and K1 tide in the northwestern Gulf of Alaska. Journal of Physical Oceanography 17:698-704.

Jackson, J.M., G.C. Johnson, H.V. Dosser, and T. Ross. 2018. Warming From Recent Marine Heatwave Lingers in Deep British Columbia Fjord. Geophysical Research Letters 45:9757-9764.

Janout, M.A., T.J. Weingartner, S.R. Okkonen, T.E. Whitledge, and D.L. Musgrave. 2009. Some characteristics of Yakutat Eddies propagating along the continental slope of the northern Gulf of Alaska. Deep-Sea Research Part Ii-Topical Studies in Oceanography 56:2444-2459.

Janout, M.A., T.J. Weingartner, T.C. Royer, and S.L. Danielson. 2010. On the nature of winter cooling and the recent temperature shift on the northern Gulf of Alaska shelf. Journal of Geophysical Research-Oceans 115.

Janout, M.A., T.J. Weingartner, and P.J. Stabeno. 2013. Air-sea and oceanic heat flux contributions to the heat budget of the northern Gulf of Alaska shelf. Journal of Geophysical Research-Oceans 118:1807-1820.

Joh, Y., and E. Di Lorenzo. 2017. Increasing coupling between NPGO and PDO leads to prolonged marine heatwaves in the northeast Pacific. Geophysical Research Letters 44:11,663-611,671.

Kämpf, J. 2007. On the magnitude of upwelling fluxes in shelf-break canyons. Continental Shelf Research 27:2211-2223.

Kara, A.B., H.E. Hurlburt, P.A. Rochford, and J.J. O'Brien. 2004. The impact of water turbidity on interannual sea surface temperature simulations in a layered global ocean model. Journal of physical oceanography 34:345-359.

Konar, B., K. Iken, H. Coletti, D. Monson, and B. Weitzman. 2016. Influence of static habitat attributes on local and regional rocky intertidal community structure. Estuaries and Coasts 39:1735-1745.

Ladd, C., and N.A. Bond. 2002. Evaluation of the NCEP/NCAR reanalysis in the NE Pacific and the Bering Sea. Journal of Geophysical Research: Oceans 107:22-21-22-29.

Ladd, C., W. Cheng, and S. Salo. 2016. Gap winds and their effects on regional oceanography Part II: Kodiak Island, Alaska. Deep-Sea Research Part Ii-Topical Studies in Oceanography 132:54-67.

Ladd, C., N.B. Kachel, C.W. Mordy, and P.J. Stabeno. 2005. Observations from a Yakutat eddy in the northern Gulf of Alaska. Journal of Geophysical Research-Oceans 110.

Lance, B.K., D.B. Irons, S.J. Kendall, and L.L. McDonald. 2001. An evaluation of marine bird population trends following the *Exxon Valdez* oil spill, Prince William Sound, Alaska. Marine pollution bulletin 42:298-309.

Litzow, M.A., and F.J. Mueter. 2014. Assessing the ecological importance of climate regime shifts: An approach from the North Pacific Ocean. Progress in Oceanography 120:110-119.

Macklin, S.A., N.A. Bond, and J.P. Walker. 1990. Structure of a low-level jet over lower Cook Inlet, Alaska. Monthly Weather Review 118:2568-2578.

Mantua, N.J., S.R. Hare, Y. Zhang, J.M. Wallace, and R.C. Francis. 1997. A Pacific interdecadal climate oscillation with impacts on salmon production. Bulletin of the American Meteorological Society 78:1069-1080.

Muench, R.D., H.O. Mofjeld, and R.L. Charnell. 1978. Oceanographic conditions in lower cook inlet: spring and summer 1973. Journal of Geophysical Research: Oceans 83:5090-5098.

Mundy, P.R. 2005. The Gulf of Alaska: biology and oceanography. Alaska Sea Grant College Program.

Niebauer, H.J., T.C. Royer, and T.J. Weingartner. 1994. Circulation of Prince William Sound, Alaska. Journal of Geophysical Research-Oceans 99:14113-14126.

Oey, L.Y., T. Ezer, C.M. Hu, and F.E. Muller-Karger. 2007. Baroclinic tidal flows and inundation processes in Cook Inlet, Alaska: numerical modeling and satellite observations. Ocean Dynamics 57:205-221.

Okkonen, S.R., T.J. Weingartner, S.L. Danielson, D.L. Musgrave, and G.M. Schmidt. 2003. Satellite and hydrographic observations of eddy-induced shelf-slope exchange in the northwestern Gulf of Alaska. Journal of Geophysical Research-Oceans 108.

Oliver, E.C.J., M.G. Donat, M.T. Burrows, P.J. Moore, D.A. Smale, L.V. Alexander, J.A. Benthuysen, M. Feng, A. Sen Gupta, A.J. Hobday, N.J. Holbrook, S.E. Perkins-Kirkpatrick, H.A. Scannell, S.C. Straub, and T. Wernberg. 2018. Longer and more frequent marine heatwaves over the past century. Nature Communications 9:1324.

Overland, J., S. Rodionov, S. Minobe, and N. Bond. 2008. North Pacific regime shifts: Definitions, issues and recent transitions. Progress in Oceanography 77:92-102.

Peterson, C.H., S.D. Rice, J.W. Short, D. Esler, J.L. Bodkin, B.E. Ballachey, and D.B. Irons. 2003. Long-term ecosystem response to the *Exxon Valdez* oil spill. Science 302:2082-2086.

Reynolds, R.W., T.M. Smith, C. Liu, D.B. Chelton, K.S. Casey, and M.G. Schlax. 2007. Daily high-resolution-blended analyses for sea surface temperature. Journal of Climate 20:5473-5496.

Rice, S., and C. Peterson. 2018. Foreword: The evolution from species-specific damage assessment to ecosystem centric studies over the multi-decade period following the *Exxon Valdez* oil spill. Deep-Sea Research Part Ii-Topical Studies in Oceanography 147:1-2.

Ross, T., J. Fisher, N. Bond, M. Galbraith, and F. Whitney. 2019. The Northeast Pacific: Current status and recent trends. PICES Press 27:36-39.

Royer, T.C. 1982. Coastal fresh water discharge in the northeast Pacific. Journal of Geophysical Research: Oceans 87:2017-2021.

Royer, T.C., and W.J. Emery. 1987. Circulation in the Gulf of Alaska, 1981. Deep-Sea Research Part a-Oceanographic Research Papers 34:1361-1377.

Royer, T.C., J.A. Vermersch, T.J. Weingartner, H.J. Niebauer, and R.D. Muench. 1990. Ocean Circulation Influencing the *Exxon Valdez* Oil Spill. Oceanography 3:3-10.

Schmeisser, L., N.A. Bond, S.A. Siedlecki, and T.P. Ackerman. 2019. The Role of Clouds and Surface Heat Fluxes in the Maintenance of the 2013–2016 Northeast Pacific Marine Heatwave. Journal of Geophysical Research: Atmospheres 124:10772-10783.

Stabeno, P.J., S. Bell, W. Cheng, S. Danielson, N.B. Kachel, and C.W. Mordy. 2016. Long-term observations of Alaska Coastal Current in the northern Gulf of Alaska. Deep-Sea Research Part Ii-Topical Studies in Oceanography 132:24-40.

Stabeno, P.J., N.A. Bond, A.J. Hermann, N.B. Kachel, C.W. Mordy, and J.E. Overland. 2004. Meteorology and oceanography of the Northern Gulf of Alaska. Continental Shelf Research 24:859-897.

Strom, S.L., K.A. Fredrickson, and K.J. Bright. 2016. Spring phytoplankton in the eastern coastal Gulf of Alaska: Photosynthesis and production during high and low bloom years. Deep-Sea Research Part Ii-Topical Studies in Oceanography 132:107-121.

Swain, D.L. 2015. A tale of two California droughts: Lessons amidst record warmth and dryness in a region of complex physical and human geography. Geophysical Research Letters 42:9999-9910,9003.

Taylor, K.E. 2001. Summarizing multiple aspects of model performance in a single diagram. Journal of Geophysical Research: Atmospheres 106:7183-7192.

Walsh, J.E., R.L. Thoman, U.S. Bhatt, P.A. Bieniek, B. Brettschneider, M. Brubaker, S. Danielson, R. Lader, F. Fetterer, and K. Holderied. 2018. The high latitude marine heat wave of 2016 and its impacts on Alaska. Bulletin of the American Meteorological Society 99:S39-S43.

Wei, J., D. Wang, F. Gong, X. He, and Y. Bai. 2017. The Influence of Increasing Water Turbidity on Sea Surface Emissivity. IEEE Transactions on Geoscience and Remote Sensing 55:3501-3515 doi: 10.1109/TGRS.2017.2675623.

Weiner, A., C. Berg, T. Gerlach, J. Grunblatt, K. Holbrook, and M. Kuwada. 1997. The *Exxon Valdez* oil spill: Habitat protection as a restoration strategy. Restoration Ecology 5:44-55.

Weingartner, T.J., K. Coyle, B. Finney, R. Hopcroft, T. Whitledge, R. Brodeur, M Dagg, E. Farley, D. Haidvogel, and T. Royer. 2002. The northeast Pacific GLOBEC program: coastal Gulf of Alaska. Oceanography 15:48-63.

Weingartner, T.J., S.L. Danielson, and T.C. Royer. 2005. Freshwater variability and predictability in the Alaska Coastal Current. Deep Sea Research Part II: Topical Studies in Oceanography 52:169-191.

Weitzman, B., B. Konar, K. Iken, H. Coletti, D. Monson, R. Suryan, T. Dean, D. Hondolero, and M. Lindeberg. Chapter 2, this report. Changes in rocky intertidal community structure during a marine heatwave in the northern Gulf of Alaska. In The Pacific Marine Heatwave: monitoring during a major perturbation in the Gulf of Alaska. Gulf Watch Alaska Long-Term Monitoring Program (#19120114) Synthesis Report to the *Exxon Valdez* Oil Spill Trustee Council.

Williams, W.J., T.J. Weingartner, and A.J. Hermann. 2010. Idealized Two-Dimensional Modeling of a Coastal Buoyancy Front, or River Plume, under Downwelling-Favorable Wind Forcing with Application to the Alaska Coastal Current. Journal of Physical Oceanography 40:279-294.

Wilson, J.G., and J.E. Overland. 1987. Meteorology. Pages 31 – 56 in D. W. Hood, andS. T. Zimmerman, editors. The Gulf of Alaska: Physical Environment and Biological Resources. U.S. Department of Commerce, Washington D.C.

Wolter, K., and M.S. Timlin. 2011. El Niño/Southern Oscillation behaviour since 1871 as diagnosed in an extended multivariate ENSO index (MEI.ext). International Journal of Climatology 31:1074-1087.

Zador, S.G., K.K. Holsman, K.Y. Aydin, and S.K. Gaichas. 2017. Ecosystem considerations in Alaska: the value of qualitative assessments. Ices Journal of Marine Science 74:421-430.

Table A1. Site locations and characteristics for time series data used in analyses including Station Name, Latitude, Longitude, station type (CTD, surface buoy, HOBO, fixed station on land, tide gauge station), depth and altitude of data, water depth and general site characteristics. MLLW = Mean Lower Low Water tidal reference.

Station Name	Latitude (°N)	Longitude (°W)	Type	Ocean Temp. Depth (m)	In/out %	Air Temp. Height (m)	Dist. from Shore (km)	Bottom Depth (m)	Characteristics
GAK1	59.845	-149.467	CTD	0-262; 20, 30, 60, 100, 150, 200, 250	100/0	N/A	3	273	Coastal exposed
GLBA12	59.033	-137.018	CTD	0-143	100/0	N/A	1	150	Tidewater glacier
KIP2	60.278	-147.987	CTD	0-585	100/0	N/A	2	585	Coastal protected
SWMP - Seldovia	59.441	-151.721	CTD	1 & 8	100/0	N/A	0	8	Nearshore
Cape Cleare (46076)	59.502	-147.990	Buoy	1	100/0	4	30	195	Gulf of Alaska nearshore
Central Gulf of Alaska (46085)	55.883	-142.882	Buoy	1	100/0	4	463	3721	Gulf of Alaska offshore
Lower Cook Inlet (46108)	59.597	-151.829	Buoy	0.5	100/0	N/A	10.7	32.9	Inlet
Ocean Station PAPA (46246)	50.033	-145.200	Buoy	0.5	100/0	N/A	1090	4252	Gulf of Alaska offshore
Portlock Bank (46080)	57.947	-150.042	Buoy	1	100/0	4	153	255	Gulf of Alaska offshore

Station Name	Latitude (°N)	Longitude (°W)	Type	Ocean Temp. Depth (m)	In/out %	Air Temp. Height (m)	Dist. from Shore (km)	Bottom Depth (m)	Characteristics
Seal Rocks (46061)	60.238	-146.833	Buoy	0.6	100/0	4	7.1	222	Strait
Shelikof Strait (46077)	57.902	-154.176	Buoy	0.6	100/0	4	21.8	200	Strait
West Orca Bay (46060)	60.587	-146.819	Buoy	0.6	100/0	4	14.2	445	Mid Sound
Western Gulf of Alaska (46001)	56.232	-147.949	Buoy	1	100/0	4	380	4054	Gulf of Alaska offshore
Western Prince William Sound (46081)	60.799	-148.263	Buoy	0.6	100/0	4	4.1	424	Fjord (mid)
Aialik Bay	59.877	-149.633	HOBO	0.5 MLLW	59 / 18	0	0	0	Fjord (mid), inside bay
Amalik Bay	58.079	-154.466	HOBO	0.5 MLLW	69 / 16	0	0	0	Bay (mouth)
Bettles Bay	60.955	-148.299	HOBO	0.5 MLLW	64 / 18	0	0	0	Fjord (mouth), inside bay
Bishop's Beach	59.643	-151.602	HOBO	0.5 MLLW	74 / 11	0	0	0	North Kachemak
Bluff Point	59.657	-151.671	HOBO	0.5 MLLW	74 / 11	0	0	0	North Kachemak
Cedar Bay	60.966	-147.395	HOBO	0.5 MLLW	64 / 11	0	0	0	Bay (head)
Cohen Island	59.539	-151.477	HOBO	0.5 MLLW	74 / 20	0	0	0	South Kachemak

Station Name	Latitude (°N)	Longitude (°W)	Type	Ocean Temp. Depth (m)	In/out %	Air Temp. Height (m)	Dist. from Shore (km)	Bottom Depth (m)	Characteristics
Elephant Island	59.514	-151.506	HOBO	0.5 MLLW	74 / 14	0	0	0	South Kachemak (passage)
Esther Passage	60.926	-148.059	HOBO	0.5 MLLW	64 / 15	0	0	0	Fjord (mouth), inside passage
Galena Bay	60.933	-146.665	HOBO	0.5 MLLW	63 / 17	0	0	0	Bay (mid), inside shallow bite
Harris Bay	59.738	-149.958	HOBO	0.5 MLLW	60 / 18	0	0	0	Fjord (behind sill)
Herring Bay	60.460	-147.718	HOBO	0.5 MLLW	64 / 15	0	0	0	Bay (mid)
Hogan Bay	60.202	-147.760	HOBO	0.5 MLLW	63 / 20	0	0	0	Bay (head), inside bite, shaded
Iktua Bay	60.130	-147.998	HOBO	0.5 MLLW	63 / 16	0	0	0	Passage
Johnson Bay	60.340	-147.835	HOBO	0.5 MLLW	65 / 17	0	0	0	Bay (mid)
Kaflia Bay	58.257	-154.198	HOBO	0.5 MLLW	65 / 17	0	0	0	Bay (head)
Kinak Bay	58.187	-154.466	HOBO	0.5 MLLW	69 / 16	0	0	0	Bay (head)
Kukak Bay	58.317	-154.207	HOBO	0.5 MLLW	65 / 17	0	0	0	Bay (mouth)

Station Name	Latitude (°N)	Longitude (°W)	Type	Ocean Temp. Depth (m)	In/out %	Air Temp. Height (m)	Dist. from Shore (km)	Bottom Depth (m)	Characteristics
McCarty Fjord	59.509	-150.342	HOBO	0.5 MLLW	62 / 14	0	0	0	Fjord (mouth), inside bay
Nuka Bay	59.537	-150.607	HOBO	0.5 MLLW	62 / 15	0	0	0	Fjord (mid), in passage
Nuka Passage	59.421	-150.647	HOBO	0.5 MLLW	63 / 14	0	0	0	Passage (mouth)
Outside Beach	59.464	-151.709	HOBO	0.5 MLLW	74 / 14	0	0	0	South Kachemak
Perry Island	60.677	-147.917	HOBO	0.5 MLLW	64 / 20	0	0	0	Island
Port Fidalgo	60.863	-146.230	HOBO	0.5 MLLW	63 / 15	0	0	0	Bay (mid), inside passage
Port Graham	59.370	-151.889	HOBO	0.5 MLLW	73 / 18	0	0	0	South Kachemak, behind reef
Takli Island	58.064	-154.484	HOBO	0.5 MLLW	69 / 15	0	0	0	Bay (mouth), inside shallow passage
Unakwik Inlet	60.949	-147.594	HOBO	0.5 MLLW	63 / 18	0	0	0	Fjord (mouth)
Whale Bay	60.227	-148.251	HOBO	0.5 MLLW	64 / 17	0	0	0	Bay (mid)
Bligh Reef (BLIA2)	60.839	-146.884	Land	N/A	N/A	21.3	3.6	0	Nearshore Reef

Station Name	Latitude (°N)	Longitude (°W)	Type	Ocean Temp. Depth (m)	In/out %	Air Temp. Height (m)	Dist. from Shore (km)	Bottom Depth (m)	Characteristics
Cordova Alaska (CRVA2)	60.558	-145.752	Land	-3.0 MLLW	100/0	7.8	0	4.6	Inlet
East Amatuli Island (AMAA2)	58.915	-151.952	Land	N/A	N/A	49.9	33.3	33.2	Island
Flat Island (FILA2)	59.322	-151.995	Land	N/A	N/A	33.6	1.7	17.9	Island
Pilot Rock (PILA2)	59.742	-149.470	Land	N/A	N/A	30.4	2.5	24	Nearshore Rock
Seward Alaska (SWLA2)	60.120	-149.427	Land	-2.7 MLLW	100/0	N/A	0	4.7	Fjord (head)
PAPA	50.000	-145.000	OISST	0	100/0	N/A	900	4230	Offshore
Adak	51.862	-176.635	Tide Gauge	-1.4 MLLW	100/0	N/A	0	N/A	Bay
Alitak	56.897	-154.248	Tide Gauge	-2.3 MLLW	100/0	N/A	0	N/A	Inlet
Anchorage	61.238	-149.890	Tide Gauge	N/A	100/0	N/A	0	N/A	Inlet
Atka	52.232	-174.173	Tide Gauge	-1.7 MLLW	100/0	N/A	0	N/A	Bay
Cordova	60.558	-145.755	Tide Gauge	-3.1 MLLW	100/0	N/A	0	N/A	Inlet
Elfin Cove	58.195	-136.347	Tide Gauge	-2.1 MLLW	100/0	N/A	0	N/A	Inlet

Station Name	Latitude (°N)	Longitude (°W)	Type	Ocean Temp. Depth (m)	In/out %	Air Temp. Height (m)	Dist. from Shore (km)	Bottom Depth (m)	Characteristics
Juneau	58.299	-134.411	Tide Gauge	-4.0 MLLW	100/0	N/A	0	N/A	Inlet
Ketchikan	55.333	-131.625	Tide Gauge	-3.2 MLLW	100/0	N/A	0	N/A	Inlet
Kodiak	57.730	-152.514	Tide Gauge	-2.8 MLLW	100/0	N/A	0	N/A	Inlet
Port Alexander	56.247	-134.648	Tide Gauge	-2.0 MLLW	100/0	N/A	0	N/A	Inlet
Sand Point	55.332	-160.504	Tide Gauge	-2.4 MLLW	100/0	N/A	0	N/A	Inlet
Seldovia	59.441	-151.720	Tide Gauge	-3.0 MLLW	100/0	N/A	0	N/A	Bay
Seward	60.120	-149.427	Tide Gauge	-2.7 MLLW	100/0	N/A	0	N/A	Fjord
Sitka	57.052	-135.342	Tide Gauge	-2.2 MLLW	100/0	N/A	0	N/A	Inlet
Skagway	59.451	-135.328	Tide Gauge	-3.2 MLLW	100/0	N/A	0	N/A	Fjord
Unalaska	53.880	-166.537	Tide Gauge	-4.4 MLLW	100/0	N/A	0	N/A	Bay
Valdez	61.124	-146.363	Tide Gauge	-2.2 MLLW	100/0	N/A	0	N/A	Fjord

Station Name	Latitude (°N)	Longitude (°W)	Type	Ocean Temp. Depth (m)	In/out %	Air Temp. Height (m)	Dist. from Shore (km)	Bottom Depth (m)	Characteristics
Yakutat	59.549	-139.733	Tide Gauge	-2.6 MLLW	100/0	N/A	0	N/A	Bay

Table A2. Site locations and start date (Year-Month) of sea surface temperature records.

Station Name	Latitude (°N)	Longitude (°W)	Start Date (year-month)
GAK1	59.845	-149.467	1970-Dec
GLBA12	59.033	-137.018	1993-Jul
KIP2	60.278	-147.987	1998-Apr
SWMP - Seldovia	59.441	-151.721	2001-Sep
Cape Cleare (46076)	59.502	-147.99	2007-May
Central Gulf of Alaska (46085)	55.883	-142.882	2007-May
Lower Cook Inlet (46108)	59.597	-151.829	2011-May
Ocean Station PAPA (46246)	50.033	-145.2	2002-Aug
Portlock Bank (46080)	57.947	-150.042	2002-Aug
Seal Rocks (46061)	60.238	-146.833	1995-May
Shelikof Strait (46077)	57.902	-154.176	2005-Oct
West Orca Bay (46060)	60.587	-146.819	1995-May
Western Gulf of Alaska (46001)	56.232	-147.949	1972-Sep
Western Prince William Sound (46081)	60.799	-148.263	2003-Sep
Aialik Bay	59.877	-149.633	2008-Jun
Amalik Bay	58.079	-154.466	2007-Jun
Bettles Bay	60.955	-148.299	2013-Jun
Bishop's Beach	59.643	-151.602	2014-Apr
Bluff Point	59.657	-151.671	2012-Jun
Cedar Bay	60.966	-147.395	2012-Jun
Cohen Island	59.539	-151.477	2013-May
Elephant Island	59.514	-151.506	2017-Apr
Esther Passage	60.926	-148.059	2018-Jun
Galena Bay	60.933	-146.665	2012-Jul
Harris Bay	59.738	-149.958	2007-Jun
Herring Bay	60.46	-147.718	2010-May
Hogan Bay	60.202	-147.76	2010-May
Iktua Bay	60.13	-147.998	2010-May
Johnson Bay	60.34	-147.835	2010-May
Kaflia Bay	58.257	-154.198	2007-Jul
Kinak Bay	58.187	-154.466	2006-Jun
Kukak Bay	58.317	-154.207	2008-Jul
McCarty Fjord	59.509	-150.342	2007-Jun
Nuka Bay	59.537	-150.607	2010-Jun

Station Name	Latitude (°N)	Longitude (°W)	Start Date (year-month)
Nuka Passage	59.421	-150.647	2007-Jun
Outside Beach	59.464	-151.709	2013-May
Perry Island	60.677	-147.917	2012-Jun
Port Fidalgo	60.863	-146.23	2013-May
Port Graham	59.37	-151.889	2006-Jun
Takli Island	58.064	-154.484	2013-Jun
Unakwik Inlet	60.949	-147.594	2010-May
Whale Bay	60.227	-148.251	1991-Jul
Bligh Reef (BLIA2)	60.839	-146.884	1995-May
Cordova Alaska (CRVA2)	60.558	-145.752	2010-Jul
East Amatuli Island (AMAA2)	58.915	-151.952	2010-Jul
Flat Island (FILA2)	59.322	-151.995	2003-May
Pilot Rock (PILA2)	59.742	-149.47	1999-Dec
Seward Alaska (SWLA2)	60.12	-149.427	2010-Jul
PAPA	50	-145	1981-Sep
Adak	51.862	-176.635	1991-Jul
Alitak	56.897	-154.248	2006-Jul
Anchorage	61.238	-149.89	1995-Jul
Atka	52.232	-174.173	2007-May
Cordova	60.558	-145.755	1994-Jun
Elfin Cove	58.195	-136.347	2005-Oct
Juneau	58.299	-134.411	1995-Dec
Ketchikan	55.333	-131.625	1995-Jan
Kodiak	57.73	-152.514	1994-Jun
Port Alexander	56.247	-134.648	2009-Sep
Sand Point	55.332	-160.504	1995-Jul
Seldovia	59.441	-151.72	1995-Mar
Seward	60.12	-149.427	1995-Dec
Sitka	57.052	-135.342	1996-May
Skagway	59.451	-135.328	2006-Apr
Unalaska	53.88	-166.537	1995-Dec
Valdez	61.124	-146.363	2009-May
Yakutat	59.549	-139.733	1994-Jun

CHAPTER 2 CHANGES IN ROCKY INTERTIDAL COMMUNITY STRUCTURE DURING A MARINE HEATWAVE IN THE NORTHERN GULF OF ALASKA

Ben Weitzman[1, 2], Brenda Konar[2], Katrin Iken[2], Heather Coletti[3], Daniel Monson[4], Robert M. Suryan[5], Thomas Dean[6], Dominic Hondolero[1], and Mandy R. Lindeberg[5]

[1]*NOAA, National Ocean Service, National Centers for Coastal Ocean Sciences, Kasitsna Bay Laboratory, 95 Sterling Hwy, Suite 2, Homer, AK 99603, USA*
[2]*University of Alaska Fairbanks, College of Fisheries and Ocean Sciences, PO Box 757220, Fairbanks, AK 99709, USA*
[3]*National Park Service, Inventory & Monitoring Program, Southwest Alaska Network, 4175 Geist Rd, Fairbanks, AK 99709, USA*
[4]*U.S. Geological Survey, Alaska Science Center, 4210 University Drive, Anchorage, AK 99508, USA*
[5]*NOAA, National Marine Fisheries Service, Alaska Fisheries Science Center, Auke Bay Laboratories, 17109 Pt. Lena Loop Rd., Juneau, AK 99801 USA*
[6]*Coastal Resource Associates, 5190 El Arbol Dr, Carlsbad, CA 92008, USA*

Abstract

Marine heatwaves are global phenomena that can have major impacts on the structure and function of coastal ecosystems. In May 2014, the Pacific marine heatwave (PMH), or "Blob", was evident in intertidal waters of the northern Gulf of Alaska and persisted for multiple years. While a response was documented in offshore ecosystems to the effects of warmer waters, it remained unclear, if and how, rocky intertidal ecosystems in the northern Gulf of Alaska would respond to the PMH. The seaweeds and invertebrates that inhabit rocky intertidal systems are important to coastal human communities for food and recreation, while simultaneously supporting a growing coastal tourism industry. Given that current climate change projections suggest increased frequency and duration of marine heatwaves, monitoring intertidal habitats can inform resource managers and users about future variation in intertidal resources and identify potential mechanisms driving change. We examined sessile community structure at 21 rocky intertidal sites, part of the Gulf Watch Alaska long-term monitoring program, across four regions spanning 1,200 km of coastline: Western Prince William Sound, Kenai Fjords National Park, Kachemak Bay, and Katmai National Park and Preserve. Sites were monitored annually from 2012 to 2019 at two tidal strata, 0.5 m and 1.5 m. Before-PMH (2012-2014) community structure was clearly different among regions and between strata and appeared to vary independently within each region. During/after-PMH (2015-2019), similarities in community structure increased across regions due to a Gulf-wide decline in macroalgal cover, driven mostly by a decline in the rockweed *Fucus distichus* and fleshy red algae in 2015, followed by an increase in barnacle cover in 2016, and an increase in mussel cover in 2017 that expanded into the lower tidal stratum. Gulf-wide changes in rocky intertidal habitats from macroalgae- to invertebrate-dominated were concurrent with changing environmental conditions during the PMH and persisted for several years following dissipation of the heatwave event in 2017. Strong, large-scale oceanographic events, like the PMH, may override local drivers to similarly influence patterns of intertidal community structure despite regional differences.

INTRODUCTION

The ocean's climate varies naturally over a range of temporal and spatial scales, from seasonal cycles to interannual or interdecadal patterns, such as the El Niño-Southern Oscillation (ENSO) or the Pacific Decadal Oscillation (PDO) to longer-term cycles termed "regime shifts" (Anderson and Piatt 1999, Beaugrand 2004, Litzow 2006, Litzow and Mueter 2014). These naturally occurring cycles overlay the anthropogenic trend of increasing temperature (and associated physical and chemical changes) resulting from climatic forcing mediated primarily by greenhouse gas emissions (Gleckler et al. 2012). Marine biological systems respond to these changes in a multitude of ways with the outcomes ultimately culminating in either an increase or decrease in population abundance or distribution (Fields et al. 1993, Kordas et al. 2011). Expansions of population distribution or increases in population numbers may be some of the positive outcomes and can include many fish (Murawski 1993) and coral species (Baird et al. 2012). Negative outcomes can include reductions in phytoplankton production (Barber and Chavez 1983) and associated decreases in forage fish, sea birds, and piscivorous fishes (Piatt et. al. 1999, Piatt et al. 2020). In nearshore systems, a reduction in canopy forming kelps as well as the grazers of these kelps is a common result of warming (Tegner and Dayton 1987, Edwards 2004).

Determining how various marine communities respond to a warmer ocean's climate is further complicated when extreme events occur. Marine heatwaves are one type of extreme event, defined as prolonged anomalously warm water events that are distinct in their duration, intensity, and spatial extent (Hobday et al. 2016). Marine heatwaves are occurring on a global scale (DiLorenzo and Mantua 2016, Couch et al. 2017, Oliver et al. 2017, Benthuysen et al. 2020) and are impacting many different types of habitats (Le Nohaïc et al. 2017, Arias-Ortiz et al. 2018) and organisms (Short et al. 2015, Jones et al. 2018). The severity, coupled with the temporal and spatial extent of marine heatwaves, likely dictates a species' response. Over the past century, there has been an increase in marine heatwave frequency and intensity (Frölicher et al. 2018). From 1925 to 2016, global average marine heatwave frequency and duration increased by 34% and 17%, respectively, resulting in a 54% increase in annual marine heatwave days globally (Oliver et al. 2018).

In the Northeast Pacific, an extreme marine heatwave occurred from 2014 through 2016. This Pacific marine heatwave (PMH), initially identified as the North Pacific "Blob", was first observed in offshore waters in January 2014 and had encroached on coastal regions in the spring of that year (Bond et al. 2015) with ocean water temperatures peaking in 2016 exacerbated by an El Niño (Walsh et al. 2018). During 2016, sea surface temperatures (SST) in the Gulf of Alaska (GOA) were among the highest on record, and coastal areas of Alaska had their warmest winter-spring on record (Walsh et al. 2018). Reports of impacts in the pelagic zone from the 2014-2017 PMH indicate similar biological responses to previous warming events at lower trophic levels, including a shift in phytoplankton species composition (Batten et al. 2018, Peña et al. 2019), a reduction in phytoplankton production (Gomez-Ocampa et al. 2018), and increases in harmful algal species (Vandersea et al. 2018). These effects also were evident in higher trophic levels with observations of poleward shifts in the distribution for migratory fish species and reductions in forage fish abundance and nutritional composition (von Biela et al. 2019), along with

redistribution and die-offs of sea birds (especially common murres [*Uria aalge*]) (Walsh et al. 2018, Piatt et al. 2020).

Rocky intertidal habitats naturally experience a wide range of physical conditions and are notably resistant to these varying conditions and resilient to changes in community structure that may sometimes result. At low tide, these habitats are exposed to the air, which may desiccate organisms, while they also may be experiencing extreme heat or freezing temperatures (Carroll and Highsmith 1996). While immersed, organisms may experience fluctuations in salinity, temperature, and wave forcing. The specific physical attributes that may structure a particular intertidal habitat will vary depending on the location and its associated local environmental conditions (Cruz-Motta et al. 2010, Konar et al. 2016). On smaller spatial scales, zonation patterns along the tidal elevation gradient are common (Underwood 1985, Hawkins et al. 1992, Bertness et al. 2006) and may be more obvious than regional differences (Konar et al. 2009). Understanding drivers of intertidal habitats is a continuing effort (Hacker et al. 2019, Lara et al. 2019). Extreme events, such as marine heatwaves, provide unique opportunities to study how highly variable intertidal habitats respond to large-scale perturbations.

Assessing the effects of extreme warming events like marine heatwaves is especially compelling in rocky intertidal systems. The mostly sessile nature of the dominant organisms in rocky intertidal habitats does not allow them to move to thermal refugia as may be possible for open water organisms. Furthermore, although rocky intertidal organisms are likely pre-adapted to extreme environmental fluctuation (Wethey et al. 2011, Vinagre et al. 2016), documenting responses to warming is not new (e.g., Harley 2008) and some extreme responses in rocky intertidal taxa have been specifically attributed to recent marine heatwave events. For example, a marine heatwave along Australia and New Zealand coasts resulted in the loss of the local low intertidal bull kelp *Durvillea* spp. and replacement by the invasive kelp *Undaria pinnatifida* (Thomsen et al. 2019). During the recent Mediterranean heatwave, the presence of the invasive mussel *Xenostrobus secures* increased the survival of the native mussel *Mytilus galloprovincialis*, indicating complex physical and ecological interactions (Olabarria et al. 2016). Strong increases in the recruitment of limpets and barnacles as well as unprecedented numbers of species moving northwards were observed along the northern California coast during the PMH (Sanford et al. 2019). The recent sea star wasting disease outbreak from Mexico to Alaska coincided with the PMH, although causal relationships are uncertain (Harvell et al. 2019, Konar et al. 2019). Here, we examined information from an existing program to monitor intertidal habitats and associated sessile seaweed and invertebrate taxa across the northern GOA, to assess the response of rocky intertidal habitats prior to, during, and after the recent PMH. We tested for changes in community structure, described by benthic percent cover of sessile taxa, concurrent with the PMH and which species groups may be particularly responsive to such warming events. In addition, we tested whether responses were similar across 21 sites among four different regions of the northern GOA.

METHODS

STUDY DESIGN

We collected rocky intertidal habitat data from four regions in the northern GOA, spanning approximately 1,200 km of coastline, annually in the summer from 2012 to 2019. Starting in 2012, two independent monitoring programs in the northern GOA (Rigby et al. 2007, Dean et al. 2014), were combined and expanded into the Gulf Watch Alaska monitoring network (https://gulfwatchalaska.org/monitoring/nearshore-ecosystems, Coletti et al. 2018). Regions include Western Prince William Sound, Kenai Fjords National Park, Kachemak Bay, and Katmai National Park and Preserve (Figure 2-1). Within each region, we monitored five rocky intertidal sites except for Kachemak Bay, where six sites were monitored. All sites were initially chosen based on the presence of hard substrate, exposure (relatively protected from high wave exposure), slope (not vertical), and extent (at least 100 m continuous rocky habitat), but do range in geographic location from small embayments and fjords along the outer coast to more estuarine influenced coves in protected inland waters. Further descriptions of these regions and sites can be found in Konar et al. (2016).

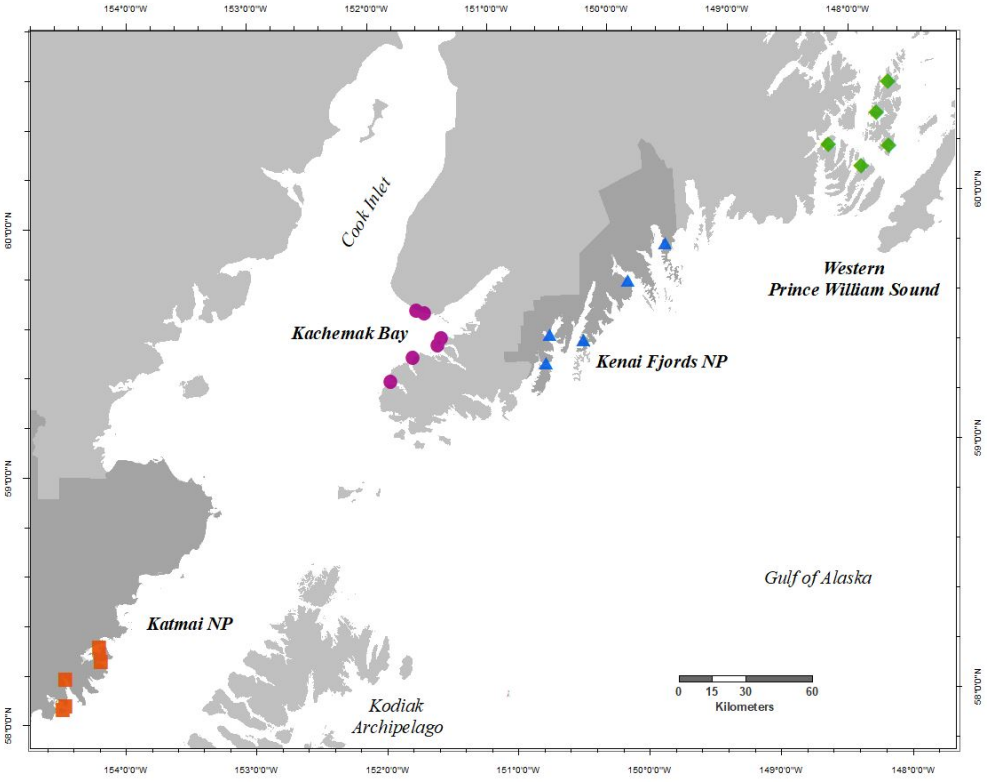

Figure 2-1. Map of study area showing Gulf Watch Alaska nearshore rocky intertidal sites, as described in Konar et al. 2016, monitored annually 2012-2019 in each region, Western Prince William Sound (green diamonds), Kenai Fjords National Park (NP) (blue triangles), Kachemak Bay (purple circles), and Katmai NP (red squares). Dark gray shaded land demarks National Park (NP) boundaries.

In summary, we estimated percent cover of sessile marine invertebrates and macroalgae, identified in the field to the lowest feasible taxonomic level (as low as species but sometimes phylum), in quadrats along a single permanently fixed 50-m transect at 0.5 m and 1.5 m tidal strata, relative and parallel to 0.0 mean lower low water. We quantified percent cover from quadrats using one of two ways to maintain consistency through time with the prior long-term monitoring programs. At all sites except for those in Kachemak Bay, percent cover was determined within twelve 0.25 m^2 quadrats in each stratum, which were systematically placed along the transects based on a random start point uniquely selected each year. We determined the occurrence, by layer (from surface to substrate), of macroalgae and sessile invertebrates within quadrats at 25 systematically placed points. Percent cover was calculated based on the proportion of layers and points occupied by each taxon, including a minimum percent (1%) for all species present within a quadrat, but not encountered in the 25 points (Dean and Bodkin 2011). In Kachemak Bay, percent cover of the overstory kelp layer (i.e., primarily species of *Alaria, Hedophyllum, Laminaria,* and *Saccharina*), if present, and all other sessile invertebrates and algae were visually estimated from 10 randomly placed 1.0 m^2 quadrats (Rigby et al. 2007). Within each data stream, all layers were then combined, and the proportion of each taxon was determined for each quadrat to create a standardized percent cover for each replicate sample. Consistent observers were used when feasible across regions to minimize observer bias in sampling. Additionally, Konar et al. (2016) conducted a methods comparison to ensure data comparability among sampling methods.

At all sites, water and air (when exposed at low tide) temperature were monitored with HOBO V2 temperature loggers (Onset Computer Corporation, Bourne, MA, USA) during the study period. HOBO sensors are capable of measuring temperatures to ± 0.2° C. They were placed inside a short length of perforated (to allow water flow around the sensor) 2.54 cm diameter grey PVC pipe that was securely bolted to a boulder or bedrock. We attempted to place the temperature loggers as close as possible to the 0.5 m mean lower low water tidal elevation, (the low tidal stratum in this study), by observing the water level at the site when the tide was predicted to be at 0.5 m, based on the nearest tide station's predicted tide chart (Tides and Currents software, NOBELTEC, Beaverton, OR, USA). Each logger was deployed for one year at their initial deployment. Loggers were retrieved and replaced annually thereafter, maintaining the original mounting location. Loggers were programmed to record temperature at 20-, 30- or 60-minute intervals.

Prior to 2014, loggers were not checked for calibration errors before deployment, but all data were checked post-deployment by aligning temperature records from one deployment to the next. That is, the temperature record on the day a logger was retrieved was matched against the temperature record for the same day by the logger that replaced it. Several calibration errors were discovered with this process and from 2015 on, each temperature logger went through a calibration soak pre- and post-deployment using three temperature targets (0°, 10° and 20° C) using a high accuracy thermometer in a circulating water bath. Any post-deployment calibration errors that were found were applied to the entire temperature record from that deployment. Any temperature logger that did not meet the ± 0.2° C recording accuracy threshold at any one of the three temperature targets in pre-deployment soaks were subsequently removed from the instrument pool.

The HOBO temperature loggers were placed within the intertidal zone, where they alternate between being submerged and being exposed to air under the influence of sea level changes (typically twice per day with the dominant semi-diurnal tide, although storm surges and river freshets also impact sea level). Data are assumed to be submerged water temperatures when the predicted tide level from the nearest tide station was ≥ 1.5 m; records from below this tide height (i.e., logger was exposed to air) were discarded. From the resulting data, we plotted monthly water temperature averages and anomalies (relative to mean across all years of study) for each of the four regions. The length of each temperature time-series varied by site and most sites had some data gaps due to sensor malfunction, loss, or break in deployment.

Statistical Analyses

Percent cover data were analyzed using PRIMER v7 and PERMANOVA+ (PRIMER-e ltd, Quest Research Limited; Anderson et al. 2008, Clarke et al. 2014, Clarke and Gorley 2015). To examine changes in intertidal community structure among regions before and during/after the PMH, percent cover data from mid- and low-tidal strata were analyzed independently from 2012-2019, based on prior work that showed significant differences among tidal strata (Konar et al. 2009). Categorical designations for time periods before (2012-2014) and during/after (2015-2019) the PMH were defined by Northeast Pacific and GOA-wide analyses (Di Lorenzo and Mantua 2016, Hobday et al. 2018, Cornwall 2019) and intertidal water temperatures recorded at our sites (Danielson et al. 2020, this report Chapter 1). We designated 2012-2014 as pre-PMH because our focus is on the response of the intertidal community, which we expected to show a 1-year lag. Given that our summer sampling coincided with the start of the PMH in 2014, we did not expect there to be a detectable response from the intertidal community in that same year. The standardized percent cover data from all regions were used so that the total percent cover from each sample fell between 0 and 1. Data were fourth-root transformed ($\sqrt{(\sqrt{(x + 0.01)})}$; a dummy variable of 0.01 was added to account for zeros), and a Bray-Curtis similarity matrix was constructed for both tidal strata. A similarity percentage analysis (SIMPER) was performed to determine which taxa contributed to at least 70% of observed variation in each region-PMH grouping for both elevations. Similarity in community structure before and during/after the PMH among regions was calculated with the SIMPER routine. A 3-factor permutational multivariate ANOVA (PERMANOVA; McArdle and Anderson 2001) design was constructed with PMH and region as fixed factors and site nested within region as a random factor for 9,999 permutations of variables to determine differences in community structure. Pairwise tests were performed to test for significant differences in community structure before and during/after the PMH by region and differences between regions before and during/after the PMH. Visualizations of community structure were made for tidal strata separately by calculating centroid values for each block-year group and ordinating them in a non-metric multi-dimensional scaling (nMDS) plot. Means plots were used to visually determine PMH-related trends in taxa deemed important by SIMPER analysis. Statistical significance was determined by using $\alpha = 0.05$.

Results

The PMH was evident in intertidal water temperature records by May 2014 with temperatures cooling in early 2017, but winter months remained warm and temperatures continued warming again by late 2018 through summer 2019 (Figure 2-2). The mean monthly changes in

temperature were observed synchronously across all regions. Although exposure to extreme warm air could also affect intertidal organisms (Helmuth et al. 2010), the maximum air temperatures and cumulative number of hours our sites were exposed to unusually high air temperatures was similar through time in all areas (U.S. Geological Survey unpublished data).

Rocky intertidal community structure across the study sites in the northern GOA differed by region, stratum, and trajectory of their change in community structure (Figure 2-3). Regional differences diminished during/after the PMH as the structure of communities across regions became more similar. Sites were also more similar at the mid-tidal stratum than at the low-stratum (Figure 2-4) before and during/after the PMH. While increases in similarity were observed after the onset of the PMH, rocky intertidal community structure still varied significantly before and during/after the PMH for each of the tidal strata and among regions (Table 2-1).

Changes in community similarity before and during/after the PMH in the Katmai region were consistent in pattern but of slightly less statistical significance at the mid ($p=0.057$) and low ($p = 0.055$) sampling zones, while the other three regions showed consistent and significant change ($p \leq 0.02$) between before and during/after the PMH (Table 2-2). There were slightly fewer significantly different between-region pairings in the during/after-PMH period than before the PMH (7 versus 10; Table 2-3).

Before the PMH, Kachemak Bay was the most dissimilar among the regions for the mid-stratum and both Kachemak Bay and Western Prince William Sound for the low-stratum (Figure 2-5). Regional patterns of variability began to converge at both tidal strata and through time in the during/after-PMH period, with sites being the most similar in 2019 (Figure 2-5). At the mid-stratum, Kachemak Bay showed the greatest variability through time; while, at the low-stratum, Kenai Fjords and Western Prince William Sound showed the greatest variability through time (Figure 2-5). Differences in the full community composition through time revealed that not all taxa showed clear and consistent changes coincident with the PMH (Figure 2-6). There were some clear winners and losers after the PMH. For example, there was an overall increase in the mussel *Mytilus trossulus*, barnacles (i.e., *Balanus glandula*, *Semibalanus* spp., *Chthamalus dali*), bare substrate, and some perennial species of algae such as the red *Odonthalia/Neorhodomela* spp., but a precipitous decrease in brown algae, *Fucus distichus*, and red algae (*Devaleraea/Palmaria* spp.) (Figure 2-7). Overall, a SIMPER analysis revealed that 17 of 81 taxa (or taxonomical groupings), including bare substrate (open space), could explain most of the observed differences in community structure between pre- and during/after PMH periods, at both strata (Table 2-4). In both strata, most foliose macroalgae declined in cover during/after PMH, while bare substrate and sessile macroinvertebrates increased in cover and an increase in encrusting coralline algae was observed in the low-stratum (Table 2-4).

Changes in the percent cover for each SIMPER-defined important taxon by tidal stratum demonstrated that strata often showed similar trends (Figure 2-7). Specifically, bare substrate and taxa such as barnacles, *Mytilus,* and *Fucus* all varied similarly in both strata. Other seasonal or annual algal species such as the kelp *Alaria marginata,* the red alga *Cryptosiphonia woodii,* and the green algal complex *Cladophora/Chaetomorpha* spp. were more variable over time in the low- than the mid-intertidal zone (primarily because these species only occur, or are at least

much more prevalent, in the low intertidal zone). Other species such as the red alga *Gloiopeltis furcata* and the *Boreophyllum*/*Pyropia*/*Wildemania* spp. complex (species of laver) were more variable in the mid compared to the low for similar reasons (Table 2-4).

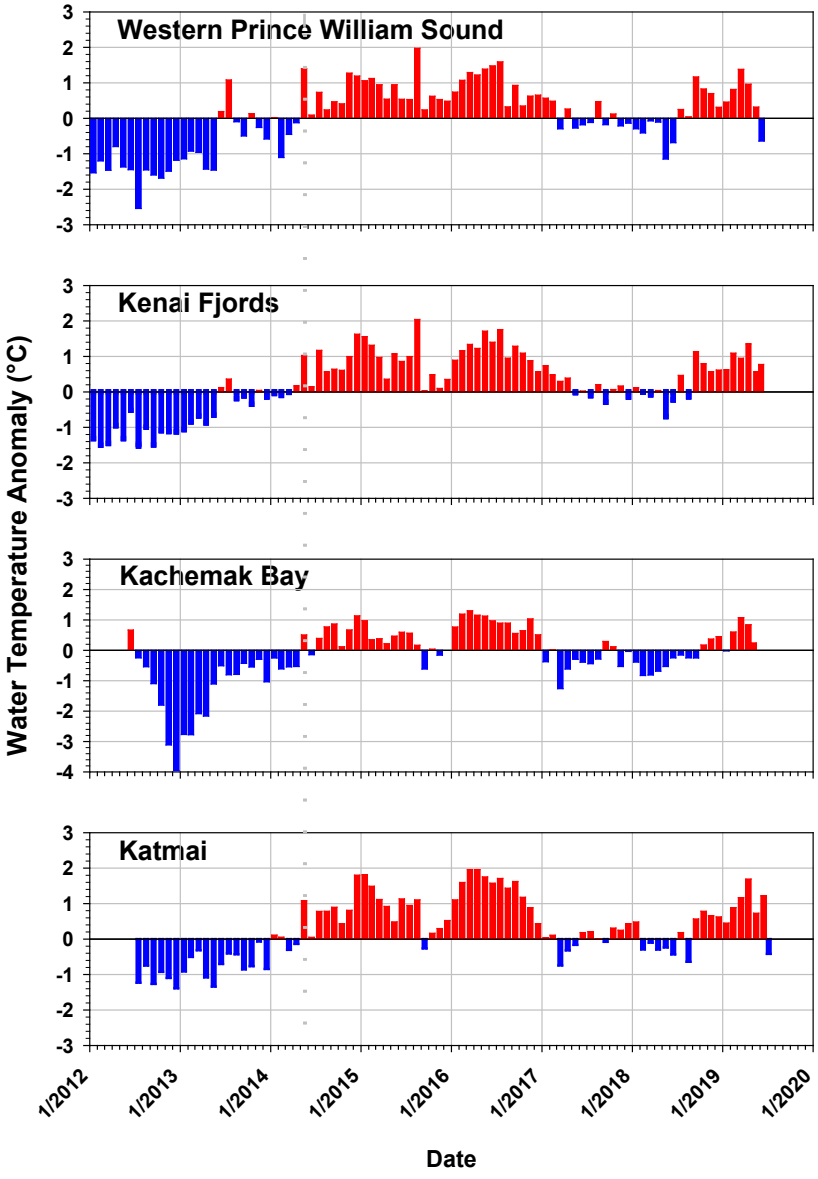

Figure 2-2. Intertidal sea water temperature monthly anomaly plots for each of the four regions from 2012-2019 recorded at 0.5 m tidal stratum at each monitoring site by a HOBO v2 temperature logger. Anomalies are based on the annual monthly mean from all sites within region minus the total monthly mean from all years for that region. Positive anomalies (red) depict warmer than average and negative anomalies (blue) depict cooler that average temperatures. The dashed gray line shows the onset of the Pacific marine heatwave in May 2014.

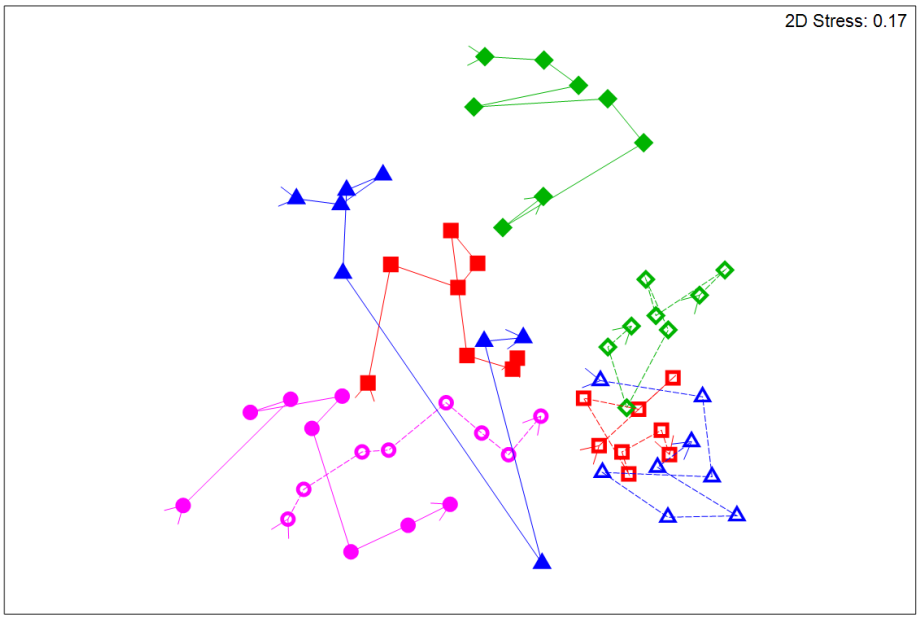

Figure 2-3. nMDS of Bray Curtis similarities of rocky intertidal community structure by region: Western Prince William Sound (green diamonds), Kenai Fjords (blue triangles), Kachemak Bay (purple circles) and Katmai National Park (red squares), and by tidal stratum: low (solid symbols) and mid (open/dashed symbols) across all years (2012-2019) as denoted by the arrow vector connecting each point. Each point represents the mean similarity for each region-stratum-year sample combination.

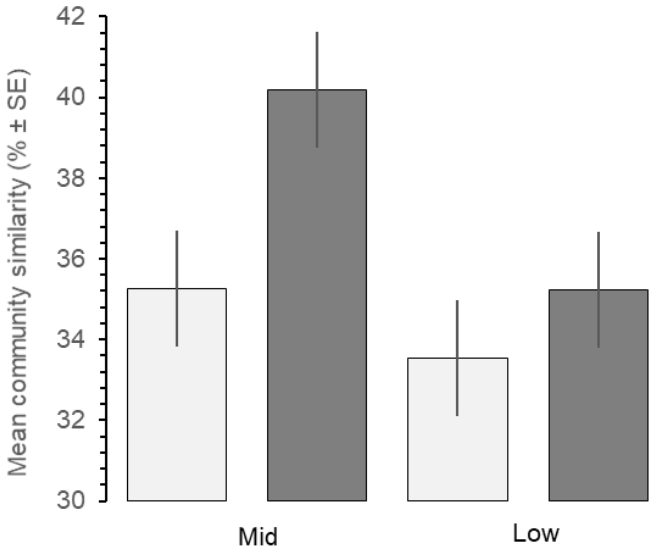

Figure 2-4. Mean community similarity across all regions before (light gray, 2012-2014) and during/after (dark gray, 2015-2019) the Pacific marine heatwave, between mid- and low-tidal strata.

Table 2-1. PERMANOVA table of results testing biological community structure, by tidal stratum, before and after the Pacific marine heatwave, and among regions. Top: Mid-stratum. Bottom: Low-stratum. Bold font denotes significance.

Mid Source	**df**	**SS**	**MS**	**Pseudo-*F***	***P(perm)***
PMH	1	42376	42376	**8.869**	**0.001**
Region	3	4.18E+05	1.39E+05	**4.2446**	**0.001**
Site(Region)	17	5.62E+05	33056	**35.336**	**0.001**
PMHxRegion	3	41008	13669	**2.841**	**0.001**
PMHxSite(Region)	17	82303	4841.4	**5.1752**	**0.001**
Residual	1856	1.74E+06	935.49		
Total	1897	2.95E+06			
Low Source	**df**	**SS**	**MS**	**Pseudo-*F***	***P(perm)***
PMH	1	75762	75762	**15.816**	**0.001**
Region	3	4.82E+05	1.61E+05	**3.2166**	**0.001**
Site(Region)	17	8.54E05	50246	**51.808**	**0.001**
PMHxRegion	3	43374	14458	**2.9859**	**0.002**
PMHxSite(Region)	17	82664	4862.6	**5.0137**	**0.001**
Residual	1829	1.77E+06	969.86		
Total	1870	3.40E+06			

Table 2-2. PERMANOVA pairwise tests for similarity in rocky intertidal community structure before and after the Pacific marine heatwave at Mid- and Low-tidal strata, by region. Bold font denotes significance.

	Mid		Low	
Region	**t**	**P*(perm)***	**t**	**P*(perm)***
Katmai	1.575	0.057	2.019	0.055
Kachemak Bay	**2.325**	**0.010**	**2.349**	**0.005**
Kenai Fjords	**2.536**	**0.017**	**2.960**	**0.010**
Western PWS	**2.157**	**0.017**	**2.498**	**0.007**

Table 2-3. PERMANOVA pairwise tests for similarity between regions before and after the Pacific marine heatwave at Mid- and Low-tidal strata. Bold font denotes significant differences between regions.

Mid	**Before**		**After**	
Between Groups	**t**	**P*(perm)***	**t**	**P*(perm)***
Kachemak Bay, Katmai	**1.537**	**0.045**	**1.796**	**0.004**
Kachemak Bay, Kenai Fjords	**2.449**	**0.004**	**1.767**	**0.009**
Kachemak Bay, Western PWS	**2.316**	**0.006**	**2.266**	**0.012**
Katmai, Kenai Fjords	1.532	0.081	1.020	0.378
Katmai, Western PWS	**1.598**	**0.049**	1.385	0.099
Kenai Fjords, Western PWS	**1.732**	**0.046**	1.387	0.115

Low	**Before**		**After**	
Between Groups	**t**	**P*(perm)***	**t**	**P*(perm)***
Kachemak Bay, Katmai	**2.932**	**0.003**	**1.967**	**0.002**
Kachemak Bay, Kenai Fjords	**2.594**	**0.002**	**2.232**	**0.005**
Kachemak Bay, Western PWS	**3.230**	**0.002**	**1.986**	**0.028**
Katmai, Kenai Fjords	1.162	0.233	1.114	0.274
Katmai, Western PWS	**1.939**	**0.017**	1.511	0.089
Kenai Fjords, Western PWS	**1.957**	**0.019**	**1.998**	**0.019**

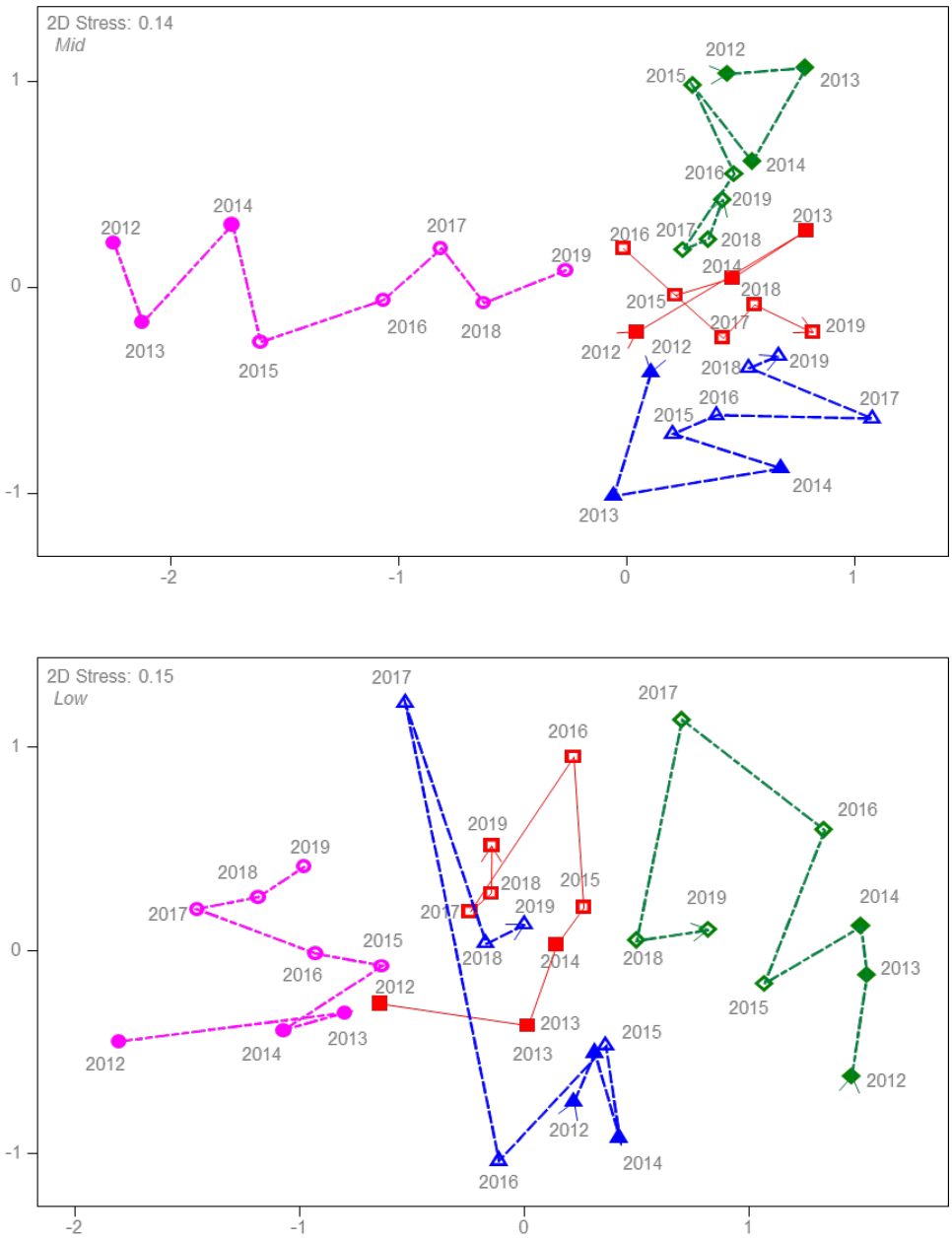

Figure 2-5. nMDS plots of similarity in rocky intertidal community structure among regions: Western Prince William Sound (green diamonds), Kenai Fjords (blue triangles), Kachemak Bay (purple circles), and Katmai National Park (red squares), between the mid (upper panel) and low (lower panel) intertidal. Trajectories are through time, before-Pacific marine heatwave (2012-2014, closed symbols) and during/after-Pacific marine heatwave (2015-2019, open symbols) periods, as depicted by the trajectory arrow by region.

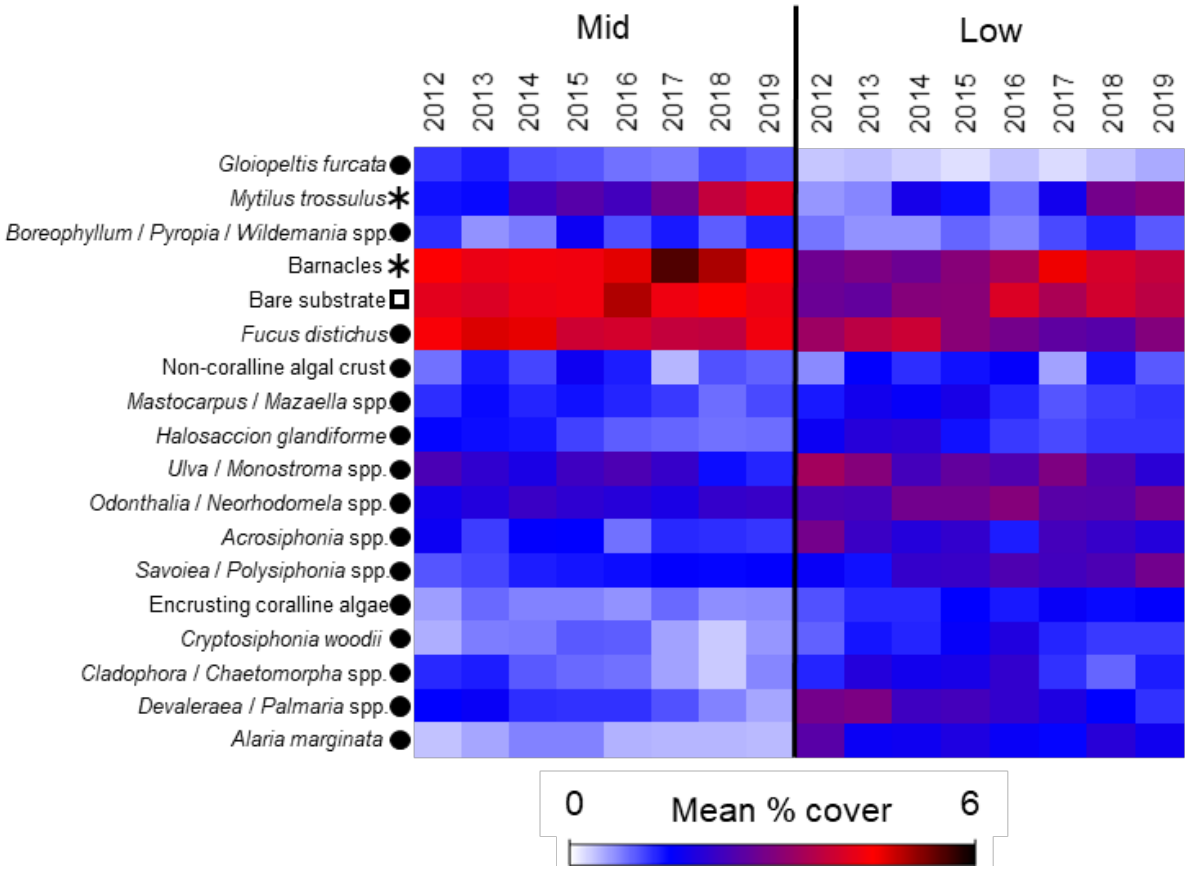

Figure 2-6. Heat map of mean percent cover for taxa determined important drivers of rocky intertidal community structure for mid- and low-tidal strata, by SIMPER analysis. Cell color scale (0 to 6) shows relative mean percent cover data of fourth root transformed percent cover data, averaged among regions, through time from 2012 to 2019. Light blue and white cells indicate low to no cover, red to black indicate moderate to high cover. Symbols denote taxa as macroalga (solid circle), invertebrate (asterisk), or open space (open square).

Figure 2-7. Means (±1SE) plots for taxa that contribute 70% of the observed variability in rocky intertidal community structure at 1.5 m (orange line) and 0.5 m (blue line) tidal strata through time, from 2012 to 2019, across all regions. The dashed gray line indicates the onset of the Pacific marine heatwave.

Table 2-4. SIMPER table of results determining the contribution of each taxa to observed variation in community structure before and during/after the Pacific marine heatwave (PMH) at Mid- and Low-tidal strata. Average dissimilarity (Av. Diss.) describes how dissimilar the communities (and the important taxon individually) are at mid- and low-strata across regions before and during/after the PMH. Percent change (% Δ) shows the proportional change in the fourth root transformed, mean percent cover for each taxon before and after the PMH. The amount of variation explained by each taxon (% Cont.) sums to at least 70% explained variation for each stratum. Gray cells indicate taxa that were only important in one stratum.

	Mid						**Low**					
	Mean Cover (fourth root trans.)			*Av. Diss. = 50.08*			*Mean Cover (fourth root trans.)*			*Av. Diss. = 55.06*		
Taxa	**Before**	**After**	**% Δ**	**Av. Diss**	**Diss/ SD**	**% Cont.**	**Before**	**After**	**% Δ**	**Av. Diss**	**Diss/ SD**	**% Cont.**
Acrosiphonia spp.	0.60	0.49	-11%	2.52	0.96	4.95	1.03	0.86	-17%	2.66	1.08	4.84
Alaria marginata							0.69	0.53	-16%	2.19	0.79	3.97
Bare substrate	1.54	1.72	18%	3.68	1.06	7.23	1.05	1.41	36%	2.91	1.10	5.29
Barnacles	1.78	1.98	20%	2.92	1.02	5.74	1.02	1.48	46%	3.49	1.21	6.34
Boreophyllum / Pyropia / Wildemania spp.	0.34	0.48	14%	2.03	0.75	4.00						
Cladophora / Chaetomorpha spp.							0.53	0.46	-7%	1.87	0.70	3.40
Cryptosiphonia woodii							0.50	0.57	7%	2.03	0.90	3.68
Devaleraea / Palmaria spp.	0.50	0.33	-17%	1.72	0.64	3.38	1.09	0.73	-36%	2.88	1.12	5.23
Encrusting coralline algae							0.46	0.56	10%	1.99	0.87	3.62
Fucus distichus	1.88	1.70	-18%	3.07	0.99	6.03	1.53	1.21	-32%	2.86	1.11	5.20
Gloiopeltis furcata	0.46	0.36	-10%	2.15	0.80	4.22						
Halosaccion glandiforme	0.52	0.33	-19%	2.08	0.83	4.09	0.81	0.48	-33%	2.40	1.08	4.36
Mastocarpus / Mazaella spp.	0.45	0.35	-10%	2.10	0.78	4012	0.71	0.52	-19%	2.17	1.01	3.94
Mytilus trossulus	0.60	1.11	51%	3.88	1.06	7.63	0.36	0.67	31%	2.41	0.85	4.38
Non-coralline algal crust	0.45	0.37	-8%	2.15	0.81	4.22	0.71	0.52	-19%	2.17	1.01	3.94
Odonthalia / Neorhodomela spp.	0.68	0.75	7%	3.13	1.02	6.14	1.02	1.18	16%	2.86	1.11	5.19
Savoiea / Polysiphonia spp.	0.41	0.60	19%	2.44	0.91	6.22	0.74	1.06	32%	2.71	1.10	4.92
Ulva / Monostroma spp.	0.87	0.82	-5%	3.17	1.09	6.22	1.39	1.19	-20%	2.59	1.06	4.70

DISCUSSION

Changes from generally colder to warmer water anomalies were coincident with major changes in intertidal community structure by the summer of 2015, followed by a progression of key taxa that continued into 2019. We observed that any effects of the PMH on intertidal community structure lagged the onset of the PMH event by at least a year; however, this observation may have been an artefact of the timing of our sampling in early to mid-summer, causing any effects of the PMH that may have occurred later in the summer or fall of 2014 to remain undetected until the following year. Despite the timing artefacts, there was an obvious change in rocky intertidal community structure, coincident with the PMH, driven by defoliation and the resulting increase in open space, setting in motion a progression of community change and reorganization that shaped patterns at rocky intertidal habitats for several years following the PMH. Previous studies documenting perturbations in the northern GOA have seen similar successional responses in following years (Highsmith et al. 1996, Highsmith et al. 2001, Lindstrom et al. 1999, Klinger and Fukuyama 2011). The shift in rocky intertidal habitats from predominately seaweed to mussel represents a change in resources available to nearshore consumers, like sea otters, black oystercatchers, and humans. The extent of a shift towards a mussel dominated intertidal habitat at some sites was likely exacerbated by the loss of sea stars due to sea star wasting syndrome (Hewson et al. 2019), which was also correlated with the timing of the PMH event (Konar et al. 2019).

Prior to the PMH, local drivers were important in maintaining the differences among rocky intertidal sites in the northern GOA, but the relative strength of local effects dissipated during and after the PMH. This suggests that local and regional drivers all influence community structure, likely through processes such as regional environmental drivers or biotic interactions such as disturbance, predation, or competition (Harley 2006, Cruz-Motta et al. 2010). Rocky intertidal systems can be hierarchically shaped by processes from system-wide, regional, to local scales (Martins et al. 2008, Menge et al. 2015). Environmental conditions often separate rocky intertidal communities on regional or system-wide scales, if those conditions are sufficiently different (Blanchette et al. 2008, Martins et al. 2008, Merder et al. 2018). Site level drivers such as wave exposure can also be important drivers of rocky intertidal community structure (McQuaid and Branch 1984) and when acting on organisms that have experienced heat stress or desiccation, can have even stronger effects (Haring et al. 2002). The pre-PMH dissimilarity among our study regions has been reported previously, but static environmental conditions such as slope, substrate composition, exposure, distance to glaciers and freshwater, only played a minor role in driving differences in community composition, suggesting that dynamic environmental conditions such as temperature, salinity, nutrient availability and dissolved oxygen are probably important local-scale drivers of community structure (Konar et al. 2016). Despite the increased similarity during/after the PMH, block level variation was still evident and especially so between Kachemak Bay and each of the other blocks; the differences likely attributed to different physical drivers, like a larger tidal range or geographic location within Cook Inlet. The geographic location and arrangement of each block sets up differences in the degree of freshwater water discharge into the system and subsequently influences how the Alaska Coastal Current flows through, mixes, and connects each block from east to west. In addition to the physical drivers defining differences among blocks, biological drivers such as

competition, predation, and supply may be influential on rocky intertidal community composition in these regions. For example, there was a marked decline in sea star abundance in nearshore waters that was observed coincident with the onset of the PMH, and likely due to sea star wasting disease (Konar et al. 2019). The decline in sea stars, and especially those species known to be effective predators of mussels (*Pisaster ochraceus* and *Evasterias troschelii*), was coincident with a subsequent increased mussel abundance (Coletti et al. 2018). During/after the PMH, increased similarity of the rocky intertidal community structure among the study regions suggests that strong, large-scale oceanographic events like the PMH may override local drivers to homogenize community structure across regions. Whether the changes were the direct result of high temperatures or were due to other associated physical or biological changes, such as changing freshwater inputs or the loss of sea star predation, is unclear.

After the onset of the PMH in the northern GOA, differences in community structure response were evident between the mid- and low-tidal strata, probably due to the inherent significant differences in intertidal community structure at these strata (Konar et al. 2009). The mid-stratum community structure became more similar across regions and time than the low-stratum, potentially due to the smaller species pool at the mid-stratum than at the low, where kelps and other fleshy macroalgae were more abundant. The changes among particular species at the mid-stratum may be a result of these species at this stratum being adapted to the high environmental variability typical of mid intertidal communities. Whereas the community at the low-stratum experiences less variability and is not as resilient to temperature disturbances as communities higher in the tidal zone (Somero 2002). A large number of taxa did not show any obvious or directional responses to the PMH while a few species showed strong responses. Strongest responses were detected in those taxa that dominate overall percent cover in the system, their high abundance emphasizing the effect. Other less-abundant taxa certainly also responded to environmental perturbations but while their relative change may have been high, their absolute impact on community composition was limited.

Fucus distichus declined concurrent with the onset of the PMH. *Fucus* cover varied by about 30% compared to the mean over a 12-year study period at a different study site in Kachemak Bay (Klinger and Fukuyama 2011) and similarly at sites in Prince William Sound over a 9-year study period (Driskell et al. 2001). This indicates that *Fucus* cover varies naturally based on life-history cycles over longer time frames in this GOA system. However, against this background of natural variation, strong disturbances have elicited synchronous responses in *Fucus* in the northern GOA before, both to experimental manipulation (Klinger and Fukuyama 2011) and to oil contamination from the *Exxon Valdez* oil spill in 1989 (Highsmith et al. 1996, Van Tomelen et al. 1997, Driskell et al. 2001). The synchrony of response in these studies scaled to the severity of the disturbance, with the most synchronous responses in direction (decrease or increase in cover) and strength coinciding with more severe, catastrophic events. Similarly, we observed a synchronous response of declining *Fucus* cover across our study regions, indicating that environmental conditions were severe enough to elicit such synchrony. While we present only correlative evidence for a relationship between changes in community structure and PMH, the scale of detectable responses suggests that changes in structure were attributable (either directly or indirectly) to increased ocean temperatures, and that the PMH was a major disturbance that caused synchronous responses across a large geographic scale. While intertidal

species naturally experience and are often adapted to temperature variation (e.g., Somero 2002), the fact that many intertidal species already live at the upper limits of their temperature tolerance might make them particularly susceptible to severe warming events such as during the PMH (Lindstrom et al. 1999, Helmuth et al. 2006, Tomanek 2010). Studies of *Fucus* have reported significant responses to changes in temperature ranging from physiological responses such as an increase in heat shock proteins (Smolina et al. 2016) and decrease in photosynthesis and growth (Graiff et al. 2015) to population-level responses through decreased post-settlement survivorship (Alestra and Schiel 2015). However, *Fucus* populations are often genotypically distinct and have high phenotypic plasticity in their stress responses, representative of low dispersal and local-scale adaptations (Wahl et al. 2011). The fact that we observed a consistent response in this species across a large spatial scale emphasizes the overwhelming strength of an environmental stressor at play, likely the PMH. The decline in *Fucus* also allowed for the increase of bare substrate (open space) that was subsequently populated by barnacles and then mussels (Figure 2-7).

Barnacle cover increased during/after the PMH in both intertidal strata following the increase in bare substrate. Barnacles are adapted to the temperature fluctuations in rocky intertidal systems and severe or irreversible physiological responses only occur at extremely high temperatures (Berger and Emlet 2007). Our study focused on the mid- and low- intertidal regions, which experienced the warmer water temperatures from the PMH but are less exposed (shorter duration) to the extreme variations in air temperature that can cause significant heat stress in higher intertidal organisms (Tomanek and Somero 1999, Somero 2002). This tolerance of the long-lived adult barnacles to warm temperatures may explain their persistence during the PMH. Post-settlement barnacles can also be tolerant of elevated temperatures (Findlay et al. 2010) but decreases in survival at high temperatures during the larval phase have also been observed (Kendall et al. 1985). If barnacle recruitment indeed declines over long periods of ocean warming, overall population declines may become evident after a lag time when populations become limited by recruitment. This could explain the drop in barnacle abundance we observed after 2017, several years after the onset of the PMH. Barnacles are the first settlers after a perturbation and set in motion the progression of *Fucus* and mussels (Highsmith et al. 2001). For example, barnacles provide the needed rugosity for *Fucus* egg settlement (Farrell 1991, Van Tamelen et al. 1997).

Another key taxon that changed after the PMH event by an increase in cover was the mussel *Mytilus trossulus*. A major *Mytilus* recruitment event was observed at the Gulf-wide scale following the PMH, potentially driven by favorable conditions during larval life stages and high post-settlement survival (Bodkin et al. 2018). Thermal tolerance of newly recruited mussels is higher in cohorts that experience higher temperatures during the dispersal phase, indicating that selection occurs during dispersal (Sorte et al. 2018). Once settled, *Mytilus* can be more sensitive to desiccation than to heat (Jenewein and Gosselin 2013). Temperature-tolerant phenotypes may have been able to disperse across regions during the PMH and occupy the open space left by the decline of *Fucus* and other species. While juvenile *Mytilus* survival is higher when associated with other species that influence microhabitat and climate such as macroalgae or other invertebrates (de Nesnera 2016, Barbier et al. 2017). *Mytilus* abundance can also be dependent on predator abundance as they are often prey for sea otters, shorebirds, sea ducks, and sea stars

(Marsh 1986, Miller and Dowd 2019). *Mytilus* abundance is currently high within the northern GOA, possibly because predator numbers of smaller mussels (e.g., sea stars) are low after recent sea star wasting impacts (Konar et al. 2019). Without these predators to control settling *Mytilus,* recruits could persist at much higher abundances at lower tidal strata where they typically would be preyed on. Furthermore, changes in water temperature can influence the role that predators play in shaping prey community structure (Sanford 1999).

The loss of *Fucus* and other foliose macroalgae (e.g., *Devaleraea*/*Palmaria* spp.) following the onset of the PMH resulted in an increase in relative and absolute abundance of primary space-occupying filter feeders, specifically *Mytilus* and barnacles. This increase is concurrent with a decrease of other typical space occupiers, such as other macroalgae (Menge and Sutherland 1987). This change not only represents a shift in taxonomic structure but also in functional structure of the community (Bremner et al. 2006, Scrosati et al. 2011). A decline in species or functional richness or shift in relative abundances can lead to an imbalance of resource uses (under- or overutilization) in the system (Naeem et al. 1994). In our case, the northern GOA rocky intertidal systems experienced a loss of macroalgal primary producers while primary consumers increased. Both mussels and barnacles are known to consume a mixture of organic matter derived from phytoplankton as well as macroalgal production in many rocky intertidal systems worldwide (Bustamante and Branch 1996, Tallis 2009), including Alaska (Duggins et al. 1989). Typically, these consumers have sufficient trophic plasticity to compensate for the decline in one of the food sources. However, multiple food subsidies to a system are considered essential elements of long-term food web stability (Huxel et al. 2002). Hence, if our observed loss of significant amounts of macroalgae were to persist over long time periods, destabilization of trophic links and community function could be expected.

SUMMARY

We observed community changes in dominant taxa after the PMH leading to increases in open space (bare substrate), which allowed for the settlement of pioneer species and possibly the restart of well-documented processes of succession in rocky intertidal communities (Sousa 1979, Farrell 1991) that continued after the PMH had dissipated. Indeed, after the initial responses at the onset of the PMH, sequential patterns in decline and increase of colonizing taxa in our study could be interpreted as a successional progression. With the noticeable nearshore onset of the PMH in spring 2014, the increase in open space was clear by the 2015 sampling, owing to the decline of many of the above-mentioned macroalgal species through the winter of 2014. Barnacles increased but that increase was most prominent starting in 2016 with a peak in cover in 2017, followed by an increase in mussel cover in 2017. Simultaneous to these sequential increases, bare substrate declined after 2016. Even *Fucus*, one of the declining species in the PMH disturbance, has recently started to show increases in cover in 2019. The recovery of *Fucus* several years following the disturbance, and subsequent increase in bare substrate, fits with observations from other studies in this region (Van Tamelen et al. 1997, Highsmith et al. 2001, Klinger and Fukuyama 2011). Recent changes in water temperature, back towards warmer conditions, may impede recovery to a pre-PMH community state if a similar disturbance response is triggered. Continued monitoring of intertidal community structure may elucidate further progression and key environmental and biotic drivers. Understanding how natural variation intertwines with patterns of community response to a disturbance is critical when

assessing the causes and drivers of trends in an ecosystem. Our findings seem to indicate that water temperature changes can trigger intertidal communities to undergo a predictable progression pattern, but that local biotic and abiotic drivers will further influence how the community responds to and recovers from disturbances.

ACKNOWLEDGMENTS

The authors thank the many students, researchers, and volunteers for assisting with intertidal surveys over the years. We also thank the scientific team of the Gulf Watch Alaska long-term monitoring program for their expertise and resources in support of this publication. Daniel Esler, John Pearce, Sarah Hile, Terri Klinger and the *Exxon Valdez* Oil Spill Trustee Council Science Panel provided critical reviews of this manuscript. The research described in this paper was in part, supported by the *Exxon Valdez* Oil Spill Trustee Council; however, the findings and conclusions presented by the authors are their own and do not necessarily reflect the views or position of the Trustee Council. Any use of trade, firm, or product names is for descriptive purposes only and does not imply endorsement by the U.S. Government. This manuscript has been approved for publication consistent with USGS Fundamental Science Practices (http://pubs.usgs.gov/circ/1367/). The authors declare that the research was conducted in the absence of any commercial or financial relationships that could be construed as a potential conflict of interest.

REFERENCES

Alestra, T., and D.R. Schiel. 2015. Impacts of local and global stressors in intertidal habitats: Influence of altered nutrient, sediment and temperature levels on the early life history of three habitat-forming macroalgae. Journal of Experimental Marine Biology and Ecology 468:29-36.

Anderson, M.J., R.N. Gorley, and K.R. Clarke. 2008. PERMANOVA+ for PRIMER: Guide to software and statistical methods. PRIMER-E ltd Plymouth, UK.

Anderson, P.J., and J.F. Piatt. 1999. Community reorganization in the Gulf of Alaska following ocean climate regime shift. Marine Ecology Progress Series 189:117e123.

Arias-Ortiz, A., O. Serrano, P. Masqué, P.S. Lavery, U. Mueller, G.A. Kendrick, M. Rozaimi, A. Esteban, J.W. Fourqurean, N. Marbà, and M.A. Mateo. 2018. A marine heatwave drives massive losses from the world's largest seagrass carbon stocks. Nature Climate Change 8:338.

Baird, A.H., B. Sommer, and J.S. Madin. 2012. Pole-ward range expansion of *Acropora* spp. along the east coast of Australia. Coral Reefs 31:1063-1063.

Barber, R.T., and F.P. Chavez. 1983. Biological consequences of El Nino. Science 222:1203-1210.

Barbier, P., T. Meziane, M. Forêt, R. Tremblay, R. Robert, and F. Olivier. 2017. Nursery function of coastal temperate benthic habitats: New insight from the bivalve recruitment perspective. Journal of Sea Research 121:11-23.

Batten, S.D., D.E. Raitsos, S. Danielson, R. Hopcroft, K. Coyle, and A. McQuatters-Gollop. 2018. Interannual variability in lower trophic levels on the Alaskan Shelf. Deep Sea Research Part II: Topical Studies in Oceanography 147:58-68.

Beaugrand, G. 2004. The North Sea regime shift: evidence, causes, mechanisms and consequences. Progress in Oceanography 60*:*245-262.

Benthuysen, J.A., E.C. Oliver, K. Chen, and T. Wernberg. 2020. Advances in Understanding Marine Heatwaves and Their Impacts. Frontiers in Marine Science 7:147.

Berger, M.S., and R.B. Emlet. 2007. Heat-shock response of the upper intertidal barnacle *Balanus glandula*: thermal stress and acclimation. The Biological Bulletin 212:232-241.

Bertness, M.D., C.M. Crain, B.R. Silliman, M.C. Bazterrica, M.V. Reyna, F. Hildago, and J.K. Farina. 2006. The community structure of Western Atlantic Patagonian rocky shores. Ecological Monographs 76:439-460.

Blanchette, C.A., C. M. Miner, P.T. Raimondi, D. Lohse, K.E. Heady, and B.R. Broitman, 2008. Biogeographical patterns of rocky intertidal communities along the Pacific coast of North America. Journal of Biogeography 35:1593-1607.

Bodkin, J.L., H.A. Coletti, B.E. Ballachey, D.H. Monson, D. Esler, and T.A. Dean. 2018. Variation in abundance of Pacific Blue Mussel (*Mytilus trossulus*) in the Northern Gulf of Alaska, 2006–2015. Deep Sea Research Part II: Topical Studies in Oceanography 147:87-97.

Bond, N.A., M.F. Cronin, H. Freeland, and N. Mantua. 2015. Causes and impacts of the 2014 warm anomaly in the NE Pacific. Geophysical Research Letters 42:3414-3420.

Bremner, J., S. Rogers, and C. Frid. 2006. Methods for describing ecological functioning of marine benthic assemblages using biological traits analysis (BTA). Ecological Indicators 6:609-622.

Bustamante, R.H., and G.M. Branch. 1996. The dependence of intertidal consumers on kelp-derived organic matter on the west coast of South Africa. Journal of Experimental Marine Biology and Ecology 196:1-28.

Carroll, M.L., and R.C. Highsmith. 1996. Role of catastrophic disturbance in mediating *Nucella-Mytilus* interactions in the Alaskan rocky intertidal. Marine Ecology Progress Series 138:125-133.

Clarke, K.R., R.N. Gorley, P.J. Somerfield, and R.M. Warwick. 2014. Change in marine communities: an approach to statistical analysis and interpretation. PRIMER-E ltd Plymouth, UK

Clarke, K.R., and R.N. Gorley. 2015. Getting started with PRIMER v7 PRIMER-E ltd Plymouth, UK

Coletti, H., J. Bodkin, T. Dean, K. Iken, B. Konar, D. Monson, D. Esler, M. Lindeberg, and R. Suryan. 2018. Intertidal Ecosystem Indicators in the Northern Gulf of Alaska. In Zador, S.G., and, Yasumiishi, E.M., 2018. Ecosystem Status Report 2018: Gulf of Alaska. Report to the North Pacific Fishery Management Council, 605 W 4th Ave, Suite 306,

Anchorage, AK 99301. https://www.fisheries.noaa.gov/resource/data/2018-status-gulf-alaska-ecosystem

Cornwall, W. 2019. A new 'Blob' menaces Pacific ecosystems. Science 365:1233-1233.

Couch, C.S., J.H. Burns, G. Liu, K. Steward, T.N. Gutlay, J. Kenyon, C.M. Eakin, and R.K. Kosaki. 2017. Mass coral bleaching due to unprecedented marine heatwave in Papahānaumokuākea Marine National Monument (Northwestern Hawaiian Islands). PLoS One 12(9), p.e0185121.

Cruz-Motta, J.J., P. Miloslavich, G. Palomo, K. Iken, B. Konar, G. Pohle, T. Trott, L. Benedetti-Cecchi, C. Herrera, A. Hernández, and A. Sardi. 2010. Patterns of spatial variation of assemblages associated with intertidal rocky shores: a global perspective. PLoS One 5(12), p.e14354.

Danielson, S.L., T.D. Hennon, D.H. Monson, R. Suryan, K. Holderied, S. Baird, R. Campbell, and T.J. Weingartner. 2020. Thermal variability and the importance of *in situ* temperature observations across the northern Gulf of Alaska. In The Pacific Marine Heatwave: monitoring during a major perturbation in the Gulf of Alaska. Gulf Watch Alaska Long-Term Monitoring Program (#19120114) Synthesis Report to the *Exxon Valdez* Oil Spill Trustee Council.

Dean, T.A., and J.L. Bodkin. 2011. SOP for sampling of intertidal invertebrates and algae on sheltered rocky shores - Version 4.6: Southwest Alaska Inventory and Monitoring Network. Natural Resource Report. NPS/SWAN/NRR—2011/397. National Park Service, Natural Resource Stewardship and Science. Fort Collins, Colorado

Dean, T.A., J.L. Bodkin, and H.A. Coletti, 2014. Protocol narrative for nearshore marine ecosystem monitoring in the Gulf of Alaska: version 1.1. Natural Resource Report NPS/SWAN/NRR – 2014/756. Fort Collins, Colorado, USA.

de Nesnera, K.L. 2016. Stress, ontogeny, and movement determine the relative importance of facilitation for juvenile mussels. Ecology 97:2199-2205.

Di Lorenzo, E., and N. Mantua. 2016. Multi-year persistence of the 2014/15 North Pacific marine heatwave. Nature Climate Change 6:1042.

Driskell, W.B., J.L. Ruesink, D.C. Lees, J.P. Houghton, and S.C. Lindstrom. 2001. Long-term signal of disturbance: *Fucus gardneri* after the *Exxon Valdez* oil spill. Ecological Applications 11:815-827.

Duggins, D.O., C.A. Simenstad, and J.A. Estes. 1989. Magnification of secondary production by kelp detritus in coastal marine ecosystems. Science 245:170-173.

Edwards, M.S. 2004. Estimating scale-dependency in disturbance impacts: El Niños and giant kelp forests in the northeast Pacific. Oecologia 138:436-447.

Farrell, T.M. 1991. Models and mechanisms of succession: An example from a rocky intertidal community. Ecological Monographs 61:95-113.

Fields, P.A., J.B. Graham, R.H. Rosenblatt, and G.N. Somero. 1993. Effects of expected global climate change on marine faunas. Trends in Ecology & Evolution 8:361-367.

Findlay, H.S., M.A. Kendall, J.I. Spicer, and S. Widdicombe. 2010. Relative influences of ocean acidification and temperature on intertidal barnacle post-larvae at the northern edge of their geographic distribution. Estuarine, Coastal and Shelf Science 86:675-682.

Frölicher, T.L., E.M. Fischer, and N. Gruber. 2018. Marine heatwaves under global warming. Nature 560:360.

Gleckler, P.J., B.D. Santer, C.M. Domingues, D.W. Pierce, T.P. Barnett, J.A. Church, K.E. Taylor, K.M. AchutaRao, T.P. Boyer, M. Ishii, and P.M. Caldwell. 2012. Human-induced global ocean warming on multidecadal timescales. Nature Climate Change 2:524.

Gomez-Ocampo, E., G. Gaxiola-Castro, R. Durazo, and E. Beier. 2018. Effects of the 2013-2016 warm anomalies on the California Current phytoplankton. Deep Sea Research Part II: Topical Studies in Oceanography 151:64-76.

Graiff, A., D. Liesner, U. Karsten, and I. Bartsch. 2015. Temperature tolerance of western Baltic Sea *Fucus vesiculosus*–growth, photosynthesis and survival. Journal of Experimental Marine Biology and Ecology 471:8-16.

Hacker, S.D., B.A. Menge, K.J. Nielsen, F. Chan, and T.C. Gouhier. 2019. Regional processes are stronger determinants of rocky intertidal community dynamics than local biotic interactions. Ecology p.e02763.

Haring, R.N., M.N. Dethier, and S.L.Williams. 2002. Desiccation facilitates wave-induced mortality of the intertidal alga *Fucus gardneri*. Marine Ecology Progress Series 232:75-82.

Harley, C.D. 2006. Effects of physical ecosystem engineering and herbivory on intertidal community structure. Marine Ecology Progress Series 317:29-39.

Harley, C.D. 2008. Tidal dynamics, topographic orientation, and temperature-mediated mass mortalities on rocky shores. Marine Ecology Progress Series 371:37-46.

Harvell, C.D., D. Montecino-Latorre, J.M. Caldwell, J.M. Burt, K. Bosley, A. Keller, S.F. Heron, A.K. Salomon, L. Lee, O. Pontier, and C. Pattengill-Semmens. 2019. Disease epidemic and a marine heat wave are associated with the continental-scale collapse of a pivotal predator (*Pycnopodia helianthoides*). Science Advances 5:7042.

Hawkins S.J., R.G. Hartnoll, J.M. Kain, and T.A. Norton. 1992. Plant-animal interactions on hard substrata in the Northeast Atlantic. In: John, D.M., S.J. Hawkins, and J.H. Price (Eds), Plant-Animal Interactions in the Marine Benthos, Systematics Association Spec Vol. 46:1-32 Clarendon Press, Oxford.

Highsmith, R.C., T.L. Rucker, M.S. Stekoll, S.M. Saupe, M.R. Lindeberg, R.N. Jenne, and W.P. Erickson. 1996. Impact of the *Exxon Valdez* Oil Spill on intertidal biota. American Fisheries Society Symposium 18:212-237.

Highsmith, R.C., S.M. Saupe, and A.L. Blanchard. 2001. Kachemak Bay experimental and monitoring studies: Recruitment, succession, and recovery in seasonally disturbed rocky-intertidal habitat. Final Report. Dept. of the Interior Minerals Management Service, Outer Continental Shelf study (OCS MMS 2001-053). Coastal Marine Institute, Univ. of AK Fairbanks.

Helmuth, B., N. Mieszkowska, P. Moore, and S.J. Hawkins. 2006. Living on the edge of two changing worlds: forecasting the responses of rocky intertidal ecosystems to climate change. Annual Review of Ecology, Evolution, and Systematics 37:373-404.

Helmuth, B., B.R. Broitman, L. Yamane, S.E. Gilman, K. Mach, K.A.S. Mislan, and M.W. Denny. 2010. Organismal climatology: analyzing environmental variability at scales relevant to physiological stress. Journal of Experimental Biology 213:995-1003.

Hobday, A.J., L.V. Alexander, S.E. Perkins, D.A. Smale, S.C. Straub, E.C. Oliver, J.A. Benthuysen, M.T. Burrows, M.G. Donat, M. Feng, and N.J. Holbrook. 2016. A hierarchical approach to defining marine heatwaves. Progress in Oceanography 141:227-238.

Hobday, A., E. Oliver, A. Sen Gupta, J. Benthuysen, M. Burrows, M. Donat, N. Holbrook, P. Moore, M. Thomsen, T. Wernberg, and D. Smale. 2018. Categorizing and naming marine heatwaves. Oceanography 31:162-173.

Huxel, G.R., K. McCann and G.A. Polis. 2002. Effects of partitioning allochthonous and autochthonous resources on food web stability. Ecological Research 17:419-432.

Jenewein, B.T., and L.A. Gosselin. 2013. Ontogenetic shift in stress tolerance thresholds of *Mytilus trossulus*: effects of desiccation and heat on juvenile mortality. Marine Ecology Progress Series 481:147-159.

Jones, T., J.K. Parrish, W.T. Peterson, E.P. Bjorkstedt, N.A. Bond, L.T. Ballance, V. Bowes, J.M. Hipfner, H.K. Burgess, J.E. Dolliver, and K. Lindquist. 2018. Massive mortality of a planktivorous seabird in response to a marine heatwave. Geophysical Research Letters 45:3193-3202.

Kendall, M.A., R.S. Bowman, P. Williamson, and J.R. Lewis. 1985. Annual variation in the recruitment of *Semibalanus balanoides* on the North Yorkshire coast 1969–1981. Journal of the Marine Biological Association of the United Kingdom 65:1009-1030.

Klinger, T., and A.K. Fukuyama. 2011. Decadal-scale dynamics and response to pulse disturbance in the intertidal rockweed *Fucus distichus* (Phaeophyceae). Marine Ecology 32:313-319.

Konar, B., K. Iken, H. Coletti, D. Monson, and B. Weitzman. 2016. Influence of static habitat attributes on local and regional rocky intertidal community structure. Estuaries and Coasts 39:1735-1745.

Konar, B., K. Iken, and M. Edwards. 2009. Depth-stratified community zonation patterns on Gulf of Alaska rocky shores. Marine Ecology 30:63-73.

Konar, B., T.J. Mitchell, K. Iken, H. Coletti, T. Dean, D. Esler, M. Lindeberg, P. Pister, and B. Weitzman. 2019. Wasting disease and static environmental variables drive sea star assemblages in the Northern Gulf of Alaska. Journal of Experimental Marine Biology and Ecology 520:151209.

Kordas, R.L., C.D. Harley, and M.I. O'Connor. 2011. Community ecology in a warming world: the influence of temperature on interspecific interactions in marine systems. Journal of Experimental Marine Biology and Ecology 400:218-226.

Lara, C., G.S. Saldías, B. Cazelles, M.M. Rivadeneira, P.A. Haye, and B.R. Broitman. 2019. Coastal biophysical processes and the biogeography of rocky intertidal species along the south-eastern Pacific. Journal of Biogeography 46:420-431.

Le Nohaïc, M., C.L. Ross, C.E. Cornwall, S. Comeau, R. Lowe, M.T. McCulloch, and V. Schoepf. 2017. Marine heatwave causes unprecedented regional mass bleaching of thermally resistant corals in northwestern Australia. Scientific Reports 7:14999.

Lindstrom, S.C., J.P. Houghton, and D.C. Lees. 1999. Intertidal macroalgal community structure in Southwestern Prince William sound, Alaska. Botanica Marina 42:265-280.

Litzow, M.A. 2006. Climate regime shifts and community reorganization in the Gulf of Alaska: How do recent shifts compare with 1976/1977? ICES Journal of Marine Science 63:1386-1396.

Litzow, M.A., and F.J. Mueter. 2014. Assessing the ecological importance of climate regime shifts: An approach from the North Pacific Ocean. Progress in Oceanography 120:110-119.

Marsh, C.P. 1986. Rocky intertidal community organization: the impact of avian predators on mussel recruitment. Ecology 67:771-786.

Martins, G.M., R.C. Thompson, S.J. Hawkins, A.I. Neto, and S.R. Jenkins. 2008. Rocky intertidal community structure in oceanic islands: scales of spatial variability. Marine Ecology Progress Series 356:15-24.

McArdle, B.H., and M.J. Anderson. 2001. Fitting multivariate models to community data: A comment on distance-based redundancy analysis. Ecology 82:290-297.

McQuaid, C.D. and G.M. Branch. 1984. Influence of sea temperature, substratum and wave exposure on rocky intertidal communities: An analysis of faunal and floral biomass. Marine Ecology Progress Series 19:145-151.

Menge, B.A., and J.P. Sutherland. 1987. Community regulation: variation in disturbance, competition, and predation in relation to environmental stress and recruitment. The American Naturalist 130:730-757.

Menge, B.A., T.C. Gouhier, S.D. Hacker, F. Chan, and K.J. Nielsen. 2015. Are meta-ecosystems organized hierarchically? A model and test in rocky intertidal habitats. Ecological Monographs 85:213-233.

Merder, J., J.A. Freund, L. Meysick, C. Simkanin, R.M. O'Riordan, and A.M. Power. 2018. East-west spatial groupings in intertidal communities, environmental drivers and key species. Journal of the Marine Biological Association of the United Kingdom 98:423-435.

Miller, L.P., and W.W. Dowd. 2019. Dynamic measurements of black oystercatcher (*Haematopus bachmani*) predation on mussels (*Mytilus californianus*). Invertebrate Biology 138:67-73.

Murawski, S.A. 1993. Climate change and marine fish distributions: Forecasting from historical analogy. Transactions of the American Fisheries Society 122:647-658.

Naeem, S., L.J. Thompson, S.P. Lawler, J.H. Lawton, and R.M. Woodfin. 1994. Declining biodiversity can alter the performance of ecosystems. Nature 368(6473):734.

Olabarria, C., I. Gestoso, F.P. Lima, E. Vázquez, L.A. Comeau, F. Gomes, R. Seabra, and J.M. Babarro. 2016. Response of two mytilids to a heatwave: the complex interplay of physiology, behaviour and ecological interactions. PloS One 11(10), p.e0164330.

Oliver, E.C., J.A. Benthuysen, N.L. Bindoff, A.J. Hobday, N.J. Holbrook, C.N. Mundy, and S.E. Perkins-Kirkpatrick. 2017. The unprecedented 2015/16 Tasman Sea marine heatwave. Nature Communications 8:16101.

Oliver, E.C., M.G. Donat, M.T. Burrows, P.J. Moore, D.A. Smale, L.V. Alexander, J.A. Benthuysen, M. Feng, A.S. Gupta, A.J. Hobday, and N.J. Holbrook. 2018. Longer and more frequent marine heatwaves over the past century. Nature Communications 9:1324.

Peña, M.A., N. Nemcek, and M. Robert. 2019. Phytoplankton responses to the 2014–2016 warming anomaly in the northeast subarctic Pacific Ocean. Limnology and Oceanography 64:515-525.

Piatt, J.F., G. Drew, T. Van Pelt, A. Abookire, A. Nielsen, M. Shultz, and A. Kitaysky. 1999. Biological effects of the 1997/1998 ENSO event in lower Cook Inlet, Alaska. Proceedings of The 1998 Symposium on The Impacts of the 1997/98 El Niño Event on the North Pacific Ocean and Its Marginal Seas. North Pacific Marine Science Organization (PICES) Scientific Report No. 10:82-86.

Piatt, J.F., J.K. Parrish, H.M. Renner, S. Schoen, T. Jones, K. Kuletz, B. Bodenstein, M. Arimitsu, M. García-Reyes, R. Duerr, R. Corcoran, R. Kaler, G. McChesney, R. Golightly, H.Coletti, R.M. Suryan, H. Burgess, J. Lindsey, K. Lindquist, P. Warzybok, J. Jahncke, J. Roletto, and W. Sydeman. 2020. Mass mortality and chronic reproductive failure of common murres during and after the 2014-2016 northeast Pacific marine heatwave. PLoS One 15(1):e0226087.

Rigby, P.R., K. Iken, and Y. Shirayama, Eds. 2007. Sampling biodiversity in coastal communities: NaGISA protocols for seagrass and macroalgal habitats. NUS Press.

Sanford, E. 1999. Regulation of keystone predation by small changes in ocean temperature. Science 283(5410):2095-2097.

Sanford, E. 2002. Water temperature, predation, and the neglected role of physiological rate effects in rocky intertidal communities. Integrative and Comparative Biology 42:881-891.

Sanford, E., J.L. Sones, M. García-Reyes, J.H. Goddard, and J.L. Largier. 2019. Widespread shifts in the coastal biota of northern California during the 2014–2016 marine heatwaves. Scientific Reports 9:4216.

Scrosati, R.A., B. van Genne, C.S. Heaven, and C.A. Watt. 2011. Species richness and diversity in different functional groups across environmental stress gradients: a model for marine rocky shores. Ecography 34:151-161.

Short, J., T. Foster, J. Falter, G.A. Kendrick, and M.T. McCulloch. 2015. Crustose coralline algal growth, calcification and mortality following a marine heatwave in Western Australia. Continental Shelf Research 106:38-44.

Smolina, I., S. Kollias, A. Jueterbock, J.A. Coyer, and G. Hoarau. 2016. Variation in thermal stress response in two populations of the brown seaweed, *Fucus distichus*, from the Arctic and subarctic intertidal. Royal Society Open Science 3:150429.

Somero, G.N. 2002. Thermal physiology and vertical zonation of intertidal animals: Optima, limits, and costs of living. Integrative and Comparative Biology 42:780-789.

Sorte, C.J., L.L. Pandori, S. Cai, and K.A. Davis. 2018. Predicting persistence in benthic marine species with complex life cycles: linking dispersal dynamics to redistribution potential and thermal tolerance limits. Marine Biology 165:20.

Sousa, W.P. 1979. Experimental investigations of disturbance and ecological succession in a rocky intertidal algal community. Ecological Monographs 49:227-254.

Tallis, H. 2009. Kelp and rivers subsidize rocky intertidal communities in the Pacific Northwest (USA). Marine Ecology Progress Series 389:85-96.

Tegner, M.J., and P.K. Dayton. 1987. El Nino effects on southern California kelp forest communities. In Advances in Ecological Research 17:243-279. Academic Press.

Thomsen, M.S., L. Mondardini, T. Alestra, S. Gerrity, L. Tait, P. South, S. Lilley, and D. Schiel. 2019. Local extinction of bull kelp (*Durvillaea* spp.) due to a marine heatwave. Frontiers in Marine Science 6:84.

Tomanek, L. 2010. Variation in the heat shock response and its implication for predicting the effect of global climate change on species' biogeographical distribution ranges and metabolic costs. Journal of Experimental Biology 213:971-979.

Tomanek, L., and G.N. Somero. 1999. Evolutionary and acclimation-induced variation in the heat-shock responses of congeneric marine snails (genus *Tegula*) from different thermal habitats: implications for limits of thermotolerance and biogeography. Journal of Experimental Biology 202:2925-2936.

Underwood, A.J. 1985. Physical factors and biological interactions: the necessity and nature of ecological experiments. In: Moore, P.G., and Seed, R. (Eds), The Ecology of Rocky Coasts. Hodder and Stoughton, London: 372-390.

Van Tamelen, P.G., M.S. Stekoll, and L. Deysher. 1997. Recovery processes of the brown alga *Fucus gardneri* following the *Exxon Valdez* oil spill: settlement and recruitment. Marine Ecology Progress Series 160:265-277.

Vandersea, M.W., S.R. Kibler, P.A. Tester, K. Holderied, D.E. Hondolero, K. Powell, S. Baird, A. Doroff, D. Dugan, and R.W. Litaker. 2018. Environmental factors influencing the distribution and abundance of *Alexandrium catenella* in Kachemak Bay and lower Cook Inlet, Alaska. Harmful Algae 77:81-92.

Vinagre C., I. Leal, V. Mendonça, D. Madeira, L. Narciso, M.S. Diniz, and A.A.V. Flores. 2016. Vulnerability to climate warming and acclimation capacity of tropical and temperate coastal organisms. Ecological Indicators 62:317-327.

von Biela, V.R., M.L. Arimitsu, J.F. Piatt, B. Heflin, S.K. Schoen, J.L. Trowbridge, and C.M. Clawson. 2019. Extreme reduction in nutritional value of a key forage fish during the Pacific marine heatwave of 2014-2016. Marine Ecology Progress Series 613:171-182.

Wahl, M., V. Jormalainen, B.K. Eriksson, J.A. Coyer, M. Molis, H. Schubert, M. Dethier, R. Karez, I. Kruse, M. Lenz, and G. Pearson. 2011. Stress ecology in *Fucus*: abiotic, biotic and genetic interactions. In Advances in Marine Biology 59:37-105. Academic Press.

Walsh, J.E., R.L. Thoman, U.S. Bhatt, P.A. Bieniek, B. Brettschneider, M. Brubaker, S. Danielson, R. Lader, F. Fetterer, K. Holderied, and K. Iken. 2018. The high latitude marine heat wave of 2016 and its impacts on Alaska. Bulletin of the American Meteorological Society 99:S39-S43.

Wethey, D.S., S.A. Woodin, T.J. Hilbish, S.J. Jones, F.P. Lima, and P.M. Brannock. 2011. Response of intertidal populations to climate: effects of extreme events versus long term change. Journal of Experimental Marine Biology and Ecology 400:132-144.

CHAPTER 3 REDUCED QUALITY AND SYNCHRONOUS COLLAPSE OF FORAGE SPECIES DISRUPTS TROPHIC TRANSFER DURING A PROLONGED MARINE HEATWAVE

Mayumi Arimitsu[1], John Piatt[2], Scott Hatch[3], Robert M. Suryan[4], Sonia Batten[5], Mary Anne Bishop[6], Rob W. Campbell[6], Heather Coletti[7], Dan Cushing[8], Kristen Gorman[5], Stormy Haught[9], Russell R. Hopcroft[10], Kathy J. Kuletz[11], Caitlin Marsteller[2], Caitlin McKinstry[5], David McGowan[12] John Moran[3], R. Scott Pegau[5], Anne Schaefer[5], Sarah Schoen[2], Jan Straley[13], and Vanessa R. von Biela[2]

[1]*U.S. Geological Survey Alaska Science Center, Juneau, Alaska*
[2]*U.S. Geological Survey Alaska Science Center, Anchorage, Alaska*
[3]*Institute for Seabird Research and Conservation, Anchorage, Alaska*
[4]*NOAA Alaska Fisheries Science Center, Auke Bay Lab, Juneau, Alaska*
[5]*Marine Biological Association, Nanaimo, BC, Canada*
[6]*Prince William Sound Science Center, Cordova, Alaska*
[7]*Southwest Alaska Inventory and Monitoring Network, National Park Service, Fairbanks, Alaska*
[8]*Pole Star Ecological Research LLC, Anchorage, Alaska*
[9]*Alaska Department of Fish & Game, Cordova, Alaska*
[10]*University of Alaska Fairbanks, College of Fisheries and Ocean Sciences, Fairbanks, Alaska*
[11]*Migratory Bird Management, U.S. Fish and Wildlife Service, Anchorage, Alaska*
[12]*University of Washington, School of Aquatic and Fisheries Sciences, Seattle, Washington*
[13]*University of Alaska Southeast, Sitka, Alaska*

Abstract

The Gulf of Alaska forage fish community includes a few key species that differ markedly in their timing of spawning, somatic growth and lipid storage, and in their migration behavior. This diversity in life history strategies facilitates resilience in marine food webs because it buffers predators against the naturally high variance in abundance of pelagic forage fish populations by decreasing the likelihood that all species will be scarce at the same time. During the prolonged North Pacific marine heatwave of 2014-2016, the availability and quality of at least three key forage species with different life history strategies were reduced simultaneously in the system. Capelin and sand lance occurrence in predator diets declined abruptly, and Prince William Sound herring spawning biomass declined to historically low levels. Biomass of euphausiids was also reduced, in part due to the loss of a cold-water species. Changes in age structure, growth, and energy content of capelin, sand lance, and herring were also associated with warming during the heatwave, but not all species responded in the same way. For example, spawning capelin grew faster and matured at a younger age but were shorter in length than usual, while sand lance in Prince William Sound experienced anomalously low growth rates and lipid storage in 2015-2016. Changes in forage fish populations had immediate impacts on predator populations in 2015-2016, when seabirds and marine mammals experienced shifts in distribution, mass mortality, and reproductive failures in the Gulf of Alaska. In contrast, copepod abundance increased on the shelf and in some coastal regions during the heatwave, suggesting that food availability was not a primary factor limiting forage fish populations at this time. The reduced

quality and collapse of multiple forage fish populations reduced the efficiency of energy transfer through the middle trophic level of pelagic food webs, disrupting energy flow to piscivorous pelagic predators and causing abrupt and extreme reductions in their numbers and productivity.

INTRODUCTION

Small pelagic schooling fishes ("forage fish") play a critical role in energy transfer from plankton to predators within marine food webs. In the Gulf of Alaska (GOA) there are three main forage fish species common in the diets of seabirds, marine mammals, and large predatory fish: Pacific capelin (*Mallotus catervarius*), Pacific herring (*Clupea pallasii*), and Pacific sand lance (*Ammodytes personatus*). Other important forage species in this region include juvenile walleye pollock (*Gadus chalcogrammus*) and euphausiids (Order: Euphausiacea). For our purposes here we consider these forage species to represent the middle trophic level in this pelagic food web.

Diversity in life history strategies within forage fish communities promotes resilience in marine food webs (Kondoh 2003, Perry et al. 2010). Important aspects of forage fish life histories include migration patterns, age at maturity, and seasonality of life stages (Figure 3-1). Capelin migrate inshore to spawn over protracted spawning periods from spring through fall (Brown 2002, Arimitsu et al. 2008). Most die after spawning. Capelin larvae overwinter, a strategy that favors transformation into their juvenile form at a large size, and development during the peak of productivity in spring (Doyle et al. 2019). It also allows for growth and lipid storage in summer/fall periods at age-1 (Figure 3-1).

Herring are also a migratory species, as juveniles are reared inshore, then move offshore prior to returning as adults primarily at age-3+ to spawn in spring. Herring spawn multiple times, their larval development occurs rapidly during spring, and transformation to their juvenile state occurs by their first summer at age-0 (Doyle et al. 2019). Growth of juveniles during summer and fall is critical to successful overwintering of herring (Heintz et al. 2013, Gorman et al. 2018).

In contrast, sand lance is a non-migratory species associated with nearshore sandy bottom habitats (Ostrand et al. 2005, Baker et al. 2018) that spawns from fall to winter months (Robards et al. 1999). Hatch timing in sand lance is mediated by temperature, with larvae undergoing rapid growth during spring (Doyle et al. 2019). Like herring, juvenile growth of sand lance occurs during summer and fall prior to their first winter at age-0.

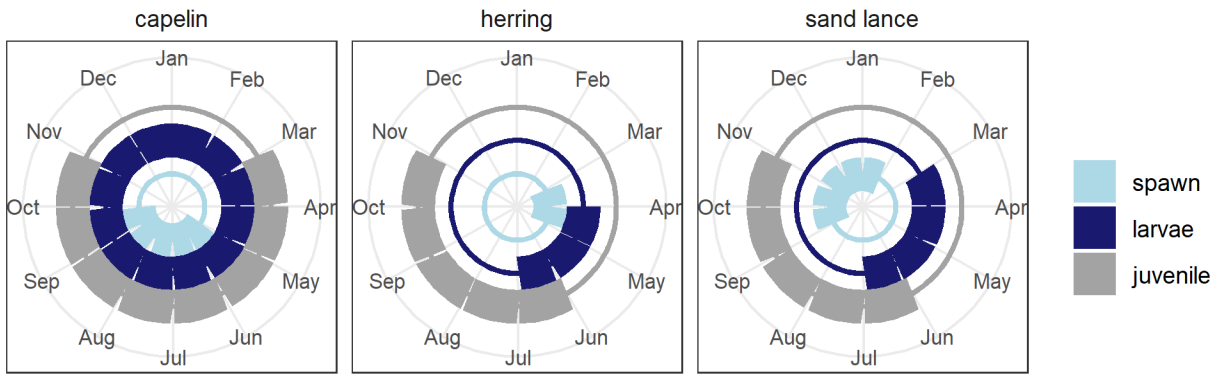

Figure 3-1. Generalized life history strategies, indicating the monthly timing of spawning, larvae and early juvenile stages for three key forage fish species in the North Pacific as summarized from data in Doyle et al. (2019).

During 2014-2016, following several years of cooler sea-surface temperatures, the North Pacific Ocean experienced an unprecedented marine heatwave that led to a major perturbation in the marine ecosystem (Walsh et al. 2018). Marine heatwaves are unusually warm water events that occur over large areas of the ocean, last long periods of time (Hobday et al. 2018), and have impacts to biodiversity, fisheries, and other ecosystem services (Smale et al. 2019, Suryan et al. Chapter 4, this report). The Pacific marine heatwave (PMH) of 2014-2016 was the longest marine heatwave documented to date (711 days), when ocean temperatures reached 2.5 °C above normal in many areas (Bond et al. 2015, Di Lorenzo and Mantua 2016). By the winter of 2015/2016 one of the strongest El Niño events of the 20th century had developed (Joh and Di Lorenzo 2017). This persistent, large-scale warm-water event impacted marine resources along the west coast of North America from California to Alaska (Barbeaux et al. 2018, Brodeur et al. 2019a, Brodeur et al. 2019b, Piatt et al. 2020, Savage 2017, Suryan et al. Chapter 4, this report).

The Gulf Watch Alaska (GWA) long-term monitoring program supports a coordinated effort to understand population status, trends and trophic interactions within the GOA marine ecosystem. Building on long-term datasets in the region, the GWA includes an integrated collection of projects designed to detect changes in environmental drivers and key ecosystem components such as zooplankton, forage fish, and marine predators. In this study, we document changes in key forage fish populations, by examining trends in abundance, and changes in age, growth, and energy content. We also examine coincident changes in lower and upper trophic level taxa that provide supporting evidence of reduced energy transfer through the middle trophic level during the PMH.

METHODS

STUDY AREA

The study area that is the focus of the GWA long-term monitoring program (http://www.gulfwatchalaska.org) includes the northern GOA, Prince William Sound (PWS), Cook Inlet, and the offshore region roughly between 144-157 ºW, and 56-61 ºN (Figure 3-2).

Circulation in the coastal and shelf regions of the northern GOA are influenced by the Alaska Coastal Current, the dominant alongshore current, as well as wind mixing and freshwater input (Weingartner et al. 2005, Stabeno et al. 2016). The dynamic oceanography, currents, and mixing characteristic of the region is partly driven by the complex bottom topography, with deep canyons extending well onto the continental shelf, and bordered by large embayments and fjords along the coast (Figure 3-2). Strong winter downwelling relaxes seasonally that enriches the nutrient supply to the shelf and promotes spring and fall bloom activity that are important in driving higher trophic level productivity (Childers et al. 2005, Waite and Mueter 2013).

SEABIRD DIETS

Seabird diet samples were collected from provisioning adults during the chick rearing period (June-August) from 1993-2018 using methods described elsewhere (Thayer et al. 2008, Hatch 2013, Schoen et al. 2018). Frequency of occurrence in diets of obligate surface feeders (black-legged kittiwakes, *Rissa tridactyla*) and divers (rhinoceros auklets, *Cerorhinca monocerata*, and tufted puffins, *Fratercula cirrhata*) provide indices of availability (frequency of occurrence in samples) for preferred species, such as sand lance and capelin.

Diving auklets and puffins deliver whole and undigested prey samples to their chicks, which allows for measurements of fish length and mass (Thompson et al. 2019). Fish length data were limited or not available from surface feeding bird samples because those samples contain regurgitated prey.

To identify changes in sand lance size from annual multi-modal length distributions, we estimated the proportion of each size class using lognormal mixture models (MacDonald and Pitcher 1979). Although the first size group, typically contained fish < 100 mm in length and corresponds to age-0 fish in summer, age-classes of the second and third size groups could not be determined from length (von Biela et al. 2019b), but are assumed to be between age-1 and age-4 (Robards et al. 1999). Capelin length data were more sparse (Thompson et al. 2019) over the timeseries and were not included in the analysis.

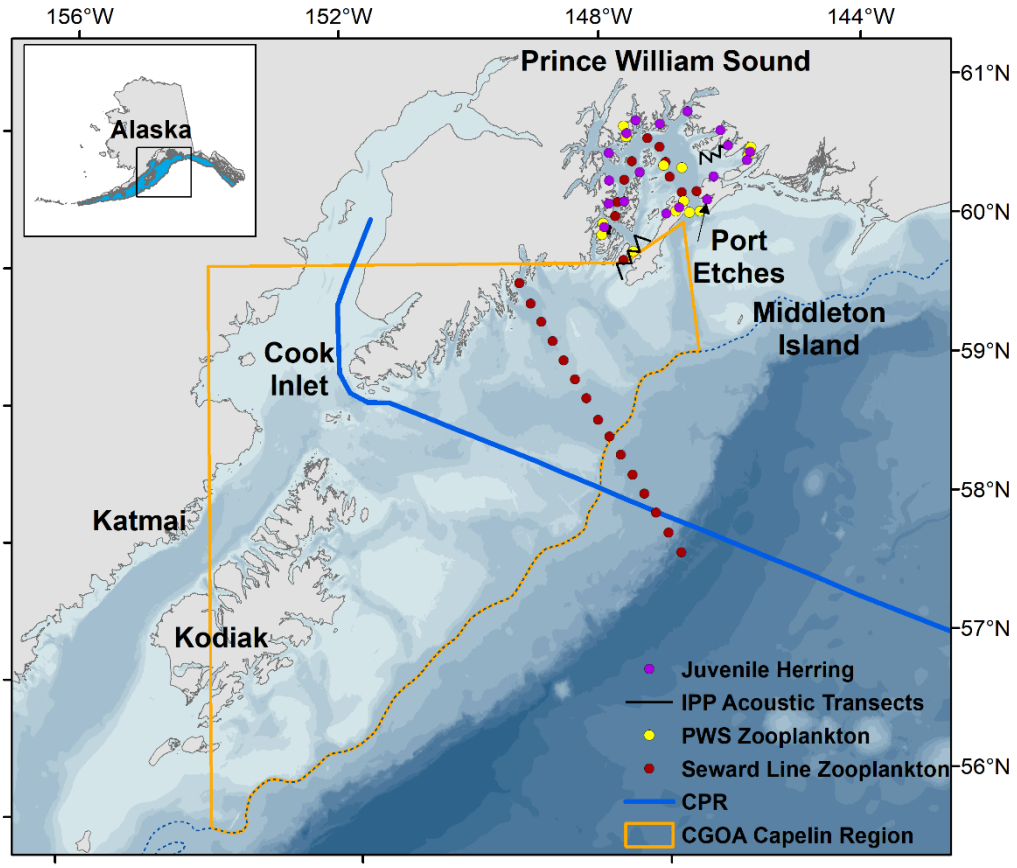

Figure 3-2. Map of the Northern Gulf of Alaska study area, including sampling locations for a subset of Gulf Watch Alaska long-term monitoring program (all circles; integrated predator prey survey [IPP], black line; continuous plankton recorder [CPR], blue line). Capelin survey extents by the National Oceanic and Atmospheric Administration-Alaska Fishery Science Center include the central Gulf of Alaska (CGOA, gold polygon) and the Gulf of Alaska (blue polygon, inset). Seafloor depth reaches over 4,500 m with lighter shading representing shallower depths, the 500 m isobath is denoted by a dashed-blue line.

Forage Fish Survey Indices

Trends in capelin relative abundance over the GOA continental shelf were examined by using annual estimates of mean densities of age-1+ capelin from three fisheries-independent surveys conducted by the National Oceanic and Atmospheric Administration Alaska Fisheries Science Center between 2000 and 2019. Indices of relative abundance based on mean catch-per-unit-effort for age-1+ capelin (>6 cm fork length) biomass (kg km^{-2}) were calculated from the summer GOA walleye pollock acoustic-trawl survey, the late-summer small-mesh midwater trawl survey (hereafter pelagic trawl survey), and the summer GOA bottom trawl survey over the GOA shelf and upper slope (<500 m depth) following McGowan et al. (2020). While these surveys were not designed to sample capelin, they collectively track years of relatively high and low capelin abundance (McGowan et al. 2020). Due to differences in each survey's domain,

indices of relative abundance were also derived for the central GOA shelf between longitudes 147 °W and 154 °W near Kodiak Island and lower Cook Inlet where coverage for all surveys overlap. The Kodiak shelf has been the core area for capelin over the GOA shelf since at least the 1980s (Mueter and Norcross 1997, Ormseth 2012).

Trends in PWS spawning herring stock are inferred from Alaska Department of Fish and Game's annual spawning surveys (miles of milt per day), and the PWS Science Center acoustic biomass index (metric tons, mt). Both of these indices provide fishery independent data for the age-structured stock assessment model (Muradian et al. 2017).

No fisheries surveys for sand lance are available in the region. We therefore rely only on seabird diets for indices of availability for this species.

SPAWNING CAPELIN AGE-LENGTH

Age-structure of spawning capelin was assessed by using otoliths of fish in spawning condition collected from Port Etches in PWS in early July. Samples were collected with a dip net in 2013 and a cast net in 2016 (Arimitsu et al. 2018). Age was assigned by counting translucent zones in sagittal otoliths. To reduce variability associated with sexual dimorphism in spawning capelin, we identified changes in the distribution of length at age (total length, mm) for male capelin in spawning condition (i.e., with an enlarged anal fin and raised lateral line) only. Energy density data for capelin were not available at the time of this report.

SAND LANCE TOTAL ENERGY

Bomb calorimetry (von Biela et al. 2019b) of individuals with age assessed from otoliths (Arimitsu et al. 2018) was used to document interannual variability in total energy of age-1 sand lance in PWS, with data updated through 2018.

HERRING GROWTH AND ENERGY

Age, sex, and length data from Pacific herring were collected from commercial fisheries and fishery independent research projects since the early 1970s as outlined in Baker et al. (1991). Briefly, the most commonly used gear types were an anchovy seine to collect pre-spawning fish and cast nets to collect spawning fish. Samples were collected periodically through the spawning season targeting a sample size of 450 fish for measurements of standard length (mm), weight (g), and sex. Maturity was determined from the gonads. Growth and age were determined from scales. For the analysis presented here, we only use the weight information from pre-spawn fish. The scales are mounted on slides, annuli counted to determine age, and archived by the Alaska Department of Fish and Game. A subset of the scales was imaged and the growth increment calculated, with a target of 180 scales from each sample year. They were evenly split between age-4, -5, and -6 and evenly split within each age class between males and females. Age and sex were not significantly related to growth (ANOVA, $p = 0.82$ and 0.69, respectively) and we pooled the data for further analysis. The scales were photographed or scanned at known magnification, and growth increments were determined in Image-Pro software as the distance between annuli. Scale growth data document long-term patterns of growth in Pacific herring from 1978-2017 (Batten et al. 2016, Moffitt 2017).

Energetics data for juvenile herring collected in PWS were also produced as part of the *Exxon Valdez* Oil Spill Trustee Council Herring Research and Monitoring program (Gorman et al. 2018). Between 2007 and 2016, early (November) and late (March) winter trawl surveys of PWS nursery bays were conducted (Figure 3-2) to collect juvenile (age-0) herring for energetics analysis using both calorimetry and stable isotope methods (Gorman et al. 2018). Whole-body energy density (kJ/g) was calculated as the carbon/nitrogen atomic ratio x 0.103 + 32.6 x dry/wet weight ratio - 2.902, and whole fish energy (kJ) was calculated as whole body energy density x net wet weight/1000.

ZOOPLANKTON INDICES

To identify coincident changes in seasonal zooplankton standing stock during the PMH we summarized trends in the mean biomass of euphausiids by species and copepods by genus from 2012-2017 along the Seward Line and associated sampling in PWS (http://research.cfos.uaf.edu/sewardline/) during spring (May) and fall (September). These samples were collected at night by using 500-µm mesh stratified nets towed from 100 m depth (Sousa et al. 2016). To identify spatial differences along the Seward Line and PWS, we summarized the station-level data by season and region: Inner Shelf region (shore to 50 km from shore), which is heavily influenced by the Alaska Coastal Current; the transitional Middle Shelf region (50 km from shore to the shelf-break, defined using the 1,000 m depth contour); and the Oceanic region (slope and basin, beyond the 1,000 m depth contour).

Additionally, the GWA fall integrated predator-prey survey in PWS includes an acoustic survey in humpback whale foraging areas that provides an acoustic index of macrozooplankton (e.g., euphausiids, amphipods, and mysids) in the water column because of their unique scattering characteristics (De Robertis et al. 2010). Acoustic surveys were conducted with a calibrated split beam dual frequency echosounder system (120-38 kHz Simrad EK60) along transects in three sub-regions in Bainbridge Passage, Montague Strait, and Port Gravina (Figure 3-2). Echosounder calibration was conducted by using a 38.1 mm tungsten carbide sphere (Foote et al. 1987, Demer et al. 2015). We classified acoustic backscatter in the water column using frequency response methods described for inshore waters (for more details see De Robertis and Ormseth 2018). Briefly, the frequency response ($\Delta S_{v_{120kHz-38\,kHz}}$) in each 5 ping by 5 m acoustic sample was computed using a minimum threshold of -80 dB. Samples in the range of 8 to 30 were classified as macrozooplankton (De Robertis et al. 2010). For each 5 m deep by 0.5 km horizontal increment along transects (150 km total) in each region and year, we computed the acoustic macrozooplankton index the log-transformed mean NASC (Nautical Area Scattering coefficient, nmi^{-2}) as a proxy for biomass. For comparison, we also included data from 2014, a pilot year when fixed transects had not been established but survey areas overlapped in Bainbridge and Montague Strait.

We also summarized trends in the abundance of small (< 2 mm adult total length) and large (> 2 mm total length) copepods from the continuous plankton recorder (Batten et al. 2018), sampling near-surface and updated through 2017. We summarized trends in the mean abundance of small and large copepods across spring (March-May), summer (June-August), and fall (September-November) using local polynomial regression fitting (loess) in R (R Core Team 2018).

Prince William Sound zooplankton anomalies were calculated from zooplankton tows (0.6 m bongo net with 202 μm mesh; 0-50m) collected at 12 stations throughout the Sound 6-9 times per year between early spring and late fall (McKinstry and Campbell 2018). These data cover a time frame before and after the PMH (fall 2009-fall 2018). Anomalies were calculated as the difference between observed monthly abundance and long-term monthly average from the duration of the GWA monitoring efforts. Two subgroups of zooplankton were defined, including warm water copepods typically found in the California Current System (Hooff and Peterson 2006, Batten and Walne 2011, Fisher et al. 2015; *Calanus pacificus*, *Clausocalanus* spp., *Corycaeus anglicus*, *Ctenocalanus* spp., *Mesocalanus tenuicornis*, and *Paracalanus parvus*), and large calanoid copepods that are common in the subarctic (*Calanus marshallae*, *Neocalanus cristatus*, *N. flemingeri*, *N. plumchrus*, and *Eucalanus bungii*).

Marine predators

We summarized changes in distribution and abundance of common murre (*Uria aalge*) and humpback whale (*Megaptera novaeangliae*) during and after the PMH. We used both published sources and data collected by the GWA program.

To identify recent changes in at-sea distribution of murres, visual surveys were conducted 2006-2019 using modified strip transect methods (Kuletz et al. 2008) in nearshore areas of Katmai National Park and Preserve in late winter (March) and summer (June-July) (Coletti and Kloecker 2017, updated through 2019), and along the Seward Line and in PWS (Figure 3-2) in spring (May), and early fall (September), and within PWS during late fall (October-November) and late winter (February-March) (Stocking et al. 2018, updated through 2019). Transects were processed into ~3-km segments to calculate densities (birds km^{-2}), averaged, and standardized to a mean of 0 and standard deviation of 1 by season and year for each of the following regions: Katmai, PWS, Inner Shelf, Middle Shelf, and Oceanic.

Interannual variability in humpback whale encounter rates (number of whales/km surveyed) were determined from fall (September) surveys in PWS from 2007-2019. A crude index of birth rate was also calculated as the proportion of calves in relation to the total number of individuals sighted.

Results

Forage fish trends in seabird diets

Frequency of capelin and sand lance in seabird diets at Middleton Island indicated reduced availability of these forage fish during and after the PMH. Following several years of increased availability between 2008-2013, the frequency of capelin abruptly declined in predator diets and had not recovered by summer 2018. Frequencies of capelin in obligate surface feeding seabirds declined more abruptly between 2013 and 2014 (from 0.88 to 0.02) than in diving seabirds (from 0.62 to 0.19) (Figure 3-3), suggesting that capelin availability may have been greater at deeper depths in 2014 and 2015. Although capelin frequencies changed abruptly after 2013, frequencies of sand lance were anomalously low for diving and surface feeding seabirds during the cooler period between 2010-2013 in addition to the PMH in 2014-2015 (Figure 3-3). From 2016-2019

sand lance frequencies in diets of divers were closer to the long-term mean, while negative anomalies persisted in diets of surface feeders.

Seabird diets also showed that the proportion of larger size classes of sand lance (>age-0) declined steeply after 2008 and remained low through 2019 (Figure 3-4). The pattern of low frequency of occurrence and high proportion of age-0 sand lance persisted through the PMH years; however, this pattern began well before the PMH. In 2016, 90% of sand lance sampled by diving seabirds (n = 1,160) were fish from the smallest size class. These data suggest several years of low availability and lower quality of sand lance to seabird predators in offshore waters.

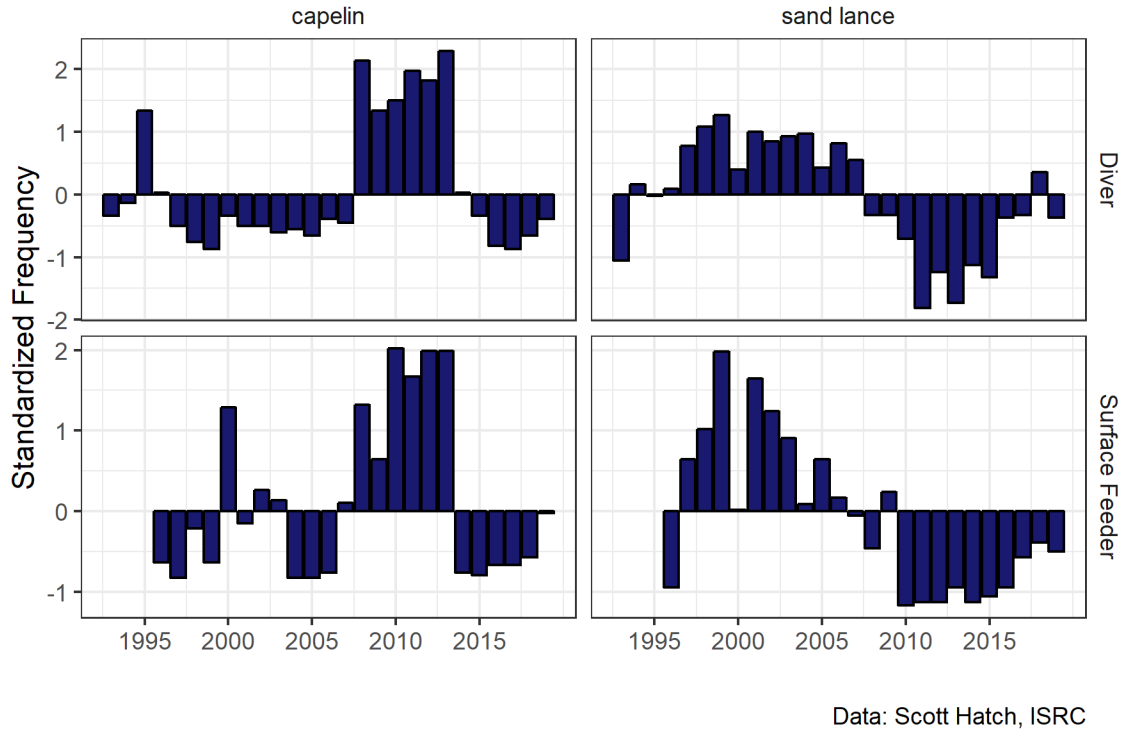

Figure 3-3. Standardized frequency anomalies for capelin and sand lance in diving and surface-feeding seabirds at Middleton Island. Frequencies were standardized to a mean of 0 and standard deviation of 1.

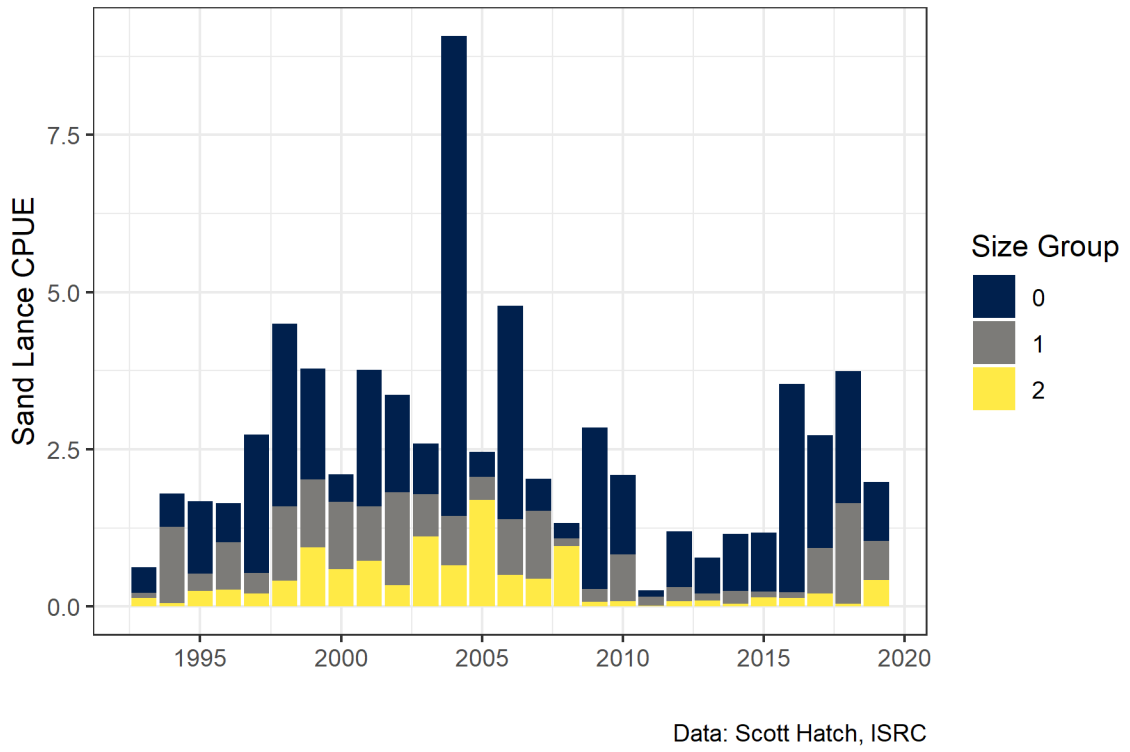

Figure 3-4. Sand lance catch per unit effort (CPUE, number of fish/number of diet samples) by year and size group in tufted puffin and rhinoceros auklet chick diets at Middleton Island during June-August. Size group 0, 1, and 2 generally corresponds with age-0 fish (mean length range among years: 68-91 mm), age-1+ fish (mean length range among years: 111-130), and age-2+ fish (mean length range among years: 127-181), respectively.

FORAGE FISH TRENDS IN SURVEY INDICES

Survey-based indices of relative abundance from the GOA shelf indicate that capelin abundance declined by at least 98% from 2013 to 2015, reaching the lowest values observed between 2000 to 2019 (Figure 3-5). Prior to the PMH, all surveys indicated that capelin were either at average or relatively high abundance levels during 2013 relative to the 20-year mean. The sharp decline of capelin densities in 2015 was the greatest 2-year change between 2000 to 2019 in both the bottom and pelagic trawl surveys, and capelin densities during the acoustic-trawl surveys were too low to calculate abundance estimates for 2015 and 2017. Low abundances during 2015 persisted though 2017, indicating that the population had effectively collapsed both across the GOA and within its core area around Kodiak. All surveys observed signs of a recovery during 2019, with the bottom trawl survey indicating that capelin had returned to average abundance levels while the other surveys indicated the population was increasing but remained below average levels.

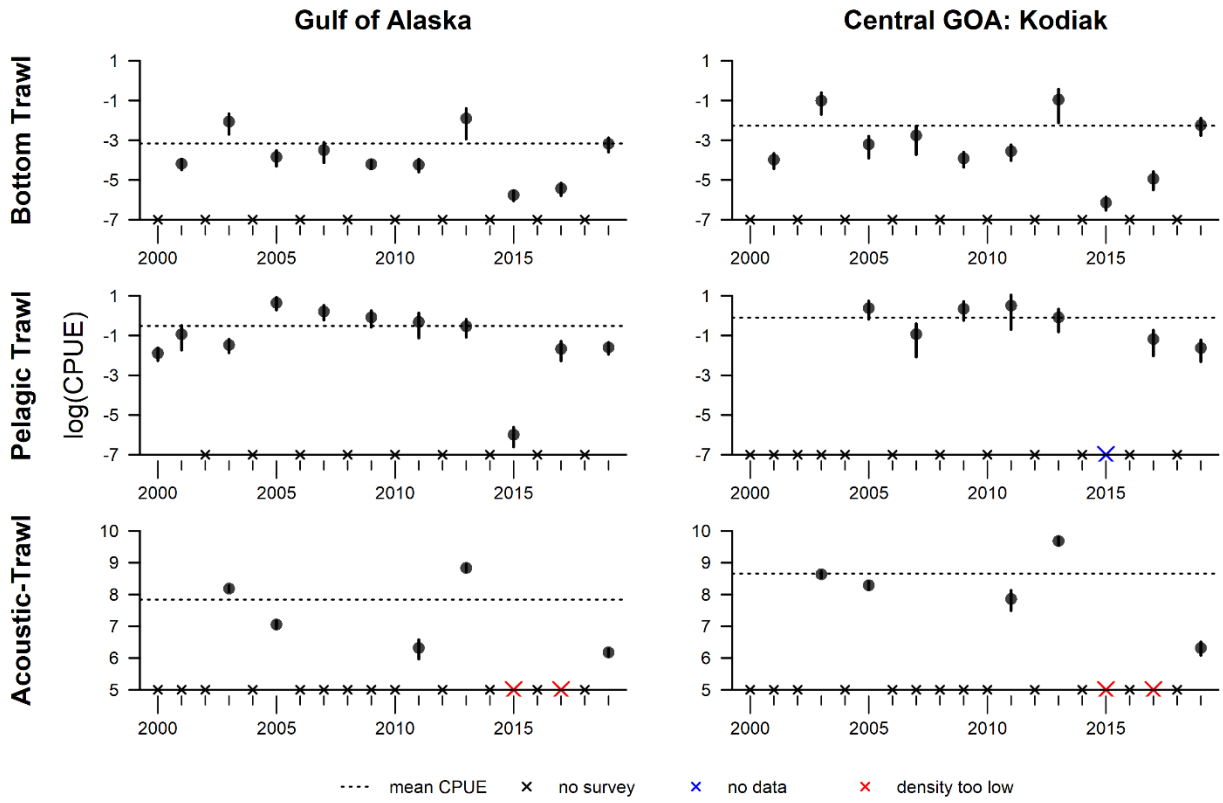

Figure 3-5. Indices of capelin relative abundance based on the log catch-per-unit-effort (CPUE, kg km^{-2}) from bottom trawl, pelagic trawl, and acoustic-trawl surveys conducted in the Gulf of Alaska (left panels) and central Gulf of Alaska (Central GOA) shelf near Kodiak Island (right panels). CPUEs are shown relative to the long-term mean CPUE for each index. Years in which surveys were not conducted (black 'x'), data were not available (blue 'x'), or capelin acoustic densities were too low to estimate abundance (red 'x') are indicated on x-axis (McGowan et al. 2020).

Prince William Sound spawning herring indices, including aerial surveys for spawning activity (miles of milt/day) and the PWS Science Center acoustic biomass estimates (mt) were at historically low levels during the PMH (Figure 3-6). Between springs of 2014 and 2015 the spawning activity index decreased by 73%.

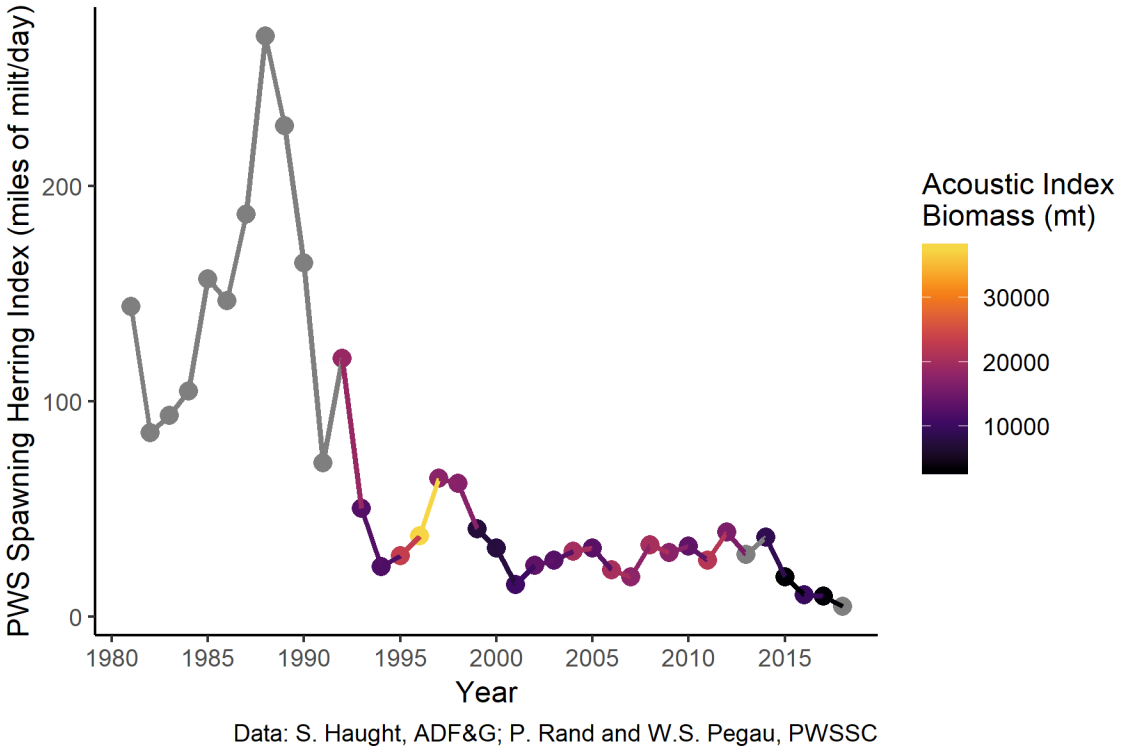

Figure 3-6. Prince William Sound (PWS) spawning herring abundance indices over time, including aerial surveys of milt (points) and the PWS Science Center Acoustic Index (color). Grey circles and lines indicate years in which no acoustic surveys were conducted.

Forage fish age, length, energy content, and growth

Spawning capelin in PWS were younger and smaller during 2016 than they were during 2013 (Figure 3-7). Distributions by age shifted from primarily age-2 fish for 2013 to primarily age-1 fish for 2016. This shift in age structure suggests high mortality during the 2014 year class, and that conditions for growth of the 2015 year class to reach length at maturity at age-1 in 2016 were favorable in at least some areas within the migratory range.

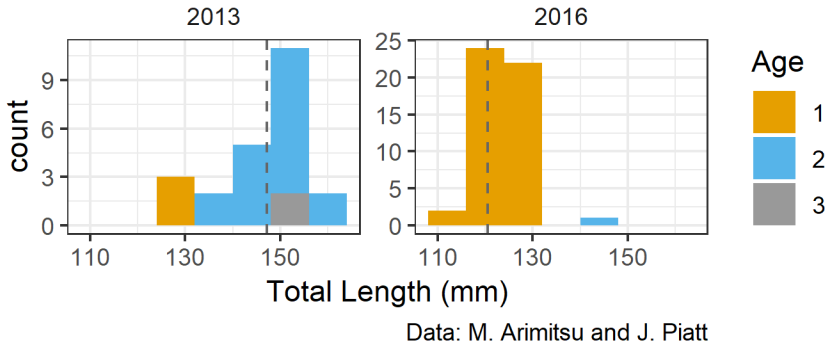

Figure 3-7. Length and age histogram from spawning male capelin at Port Etches, Prince William Sound during July 2013 and 2016. Dashed line indicates the mean length in each year.

Within PWS, the total energy of age-1 sand lance declined significantly for 2015-2016 compared to 2012-2014 (von Biela et al. 2019). No sampling occurred during 2017; however, by 2018 total energy of age-1 sand lance had returned to levels that were not significantly different from those observed during 2012 and 2013 ($ANOVA_{df:1,8;\ F = 146.7;}$ $R^2 = 0.94$, $p < 0.001$; Tukey HSD, $\alpha < 0.05$) (Figure 3-8).

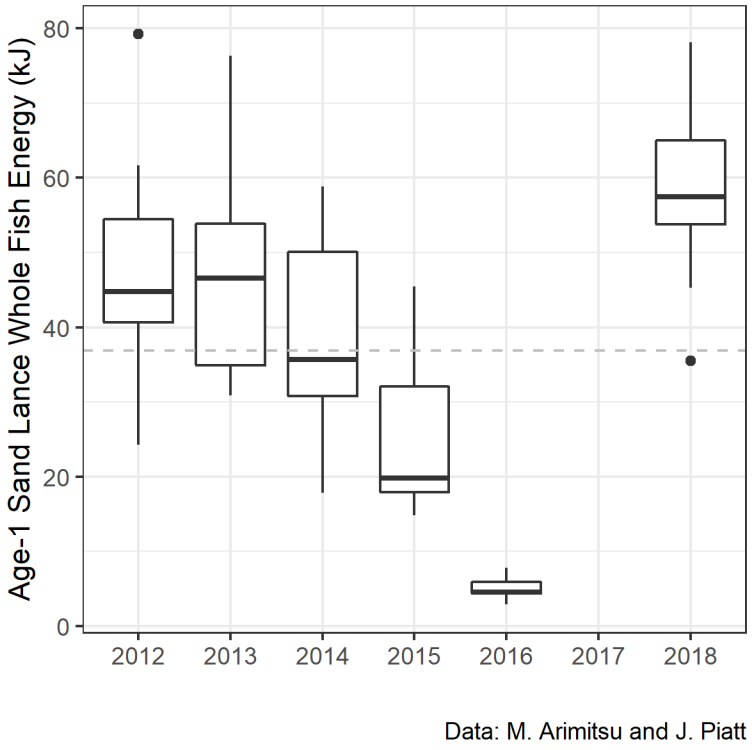

Figure 3-8. Interannual variability of whole fish energy for age-1 sand lance within Prince William Sound. Points represent the values of outliers, and the dotted line represents the mean value across years.

Pacific herring growth index anomalies showed a steady decline beginning during 2015 with the lowest values observed during 2017 (Figure 3-9). Although the growth anomalies in recent years are not unprecedented in the time-series, the low growth during 2017 indicates poor growth conditions persisted within the region after the PMH.

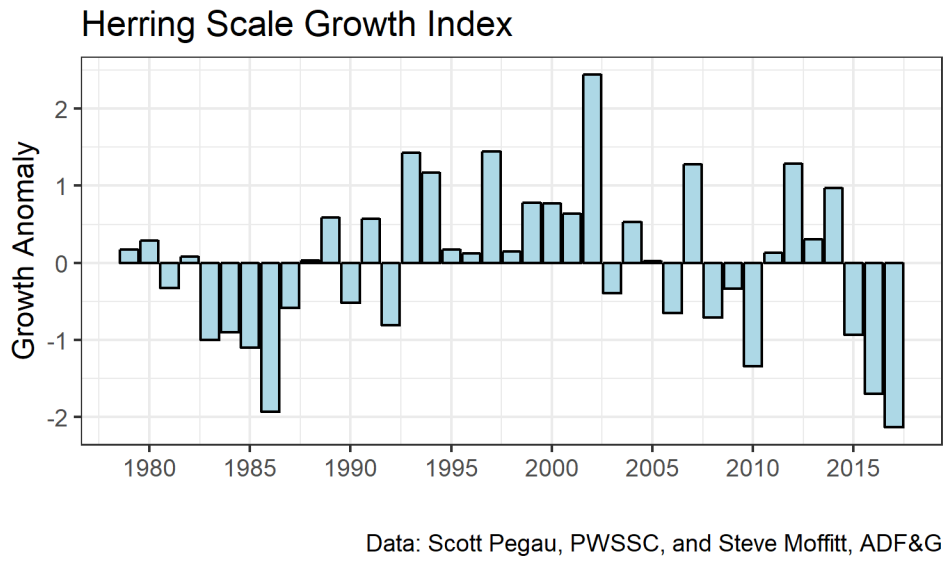

Figure 3-9. Interannual variability of Prince William Sound herring age-3 (increment 4) growth from scale increment width measurements.

The weight-at-age of PWS herring also began to decline after 2015 and reached record low values during 2017 for older fish (Figure 3-10). The decline in weight-at-age was not present for age-3 herring. The greater loss of weight-at-age in older fish is likely due to more energy being used for reproduction than in younger fish.

Consistent with the slow growth indices, whole-body energy density and total energy content in age-0 herring was diminished during fall of 2014 and more so during 2015 compared to 2013; however, it was not outside the range of variability seen during the time series (Figure 3-11). For example, fall whole body energy density was similarly low for 2010 as to 2015, and total energy was lowest during fall 2010 and 2012. However, juvenile herring size was also lowest during fall 2010 and 2012 (Figure 3-11b), which contributed to total energy content being low for these years (Figure 1-11). In contrast, during fall 2014 and 2015, age-0 herring were an average size (Figure 3-11b) but had lower energy densities (Figure 3-11a), which contributed to the reduced total energy values for these years. Fall 2010 was the most anomalous year in the time series as age-0 herring had among the lowest energy densities, smallest size and lowest total energy content (Figure 3-11a, b, c).

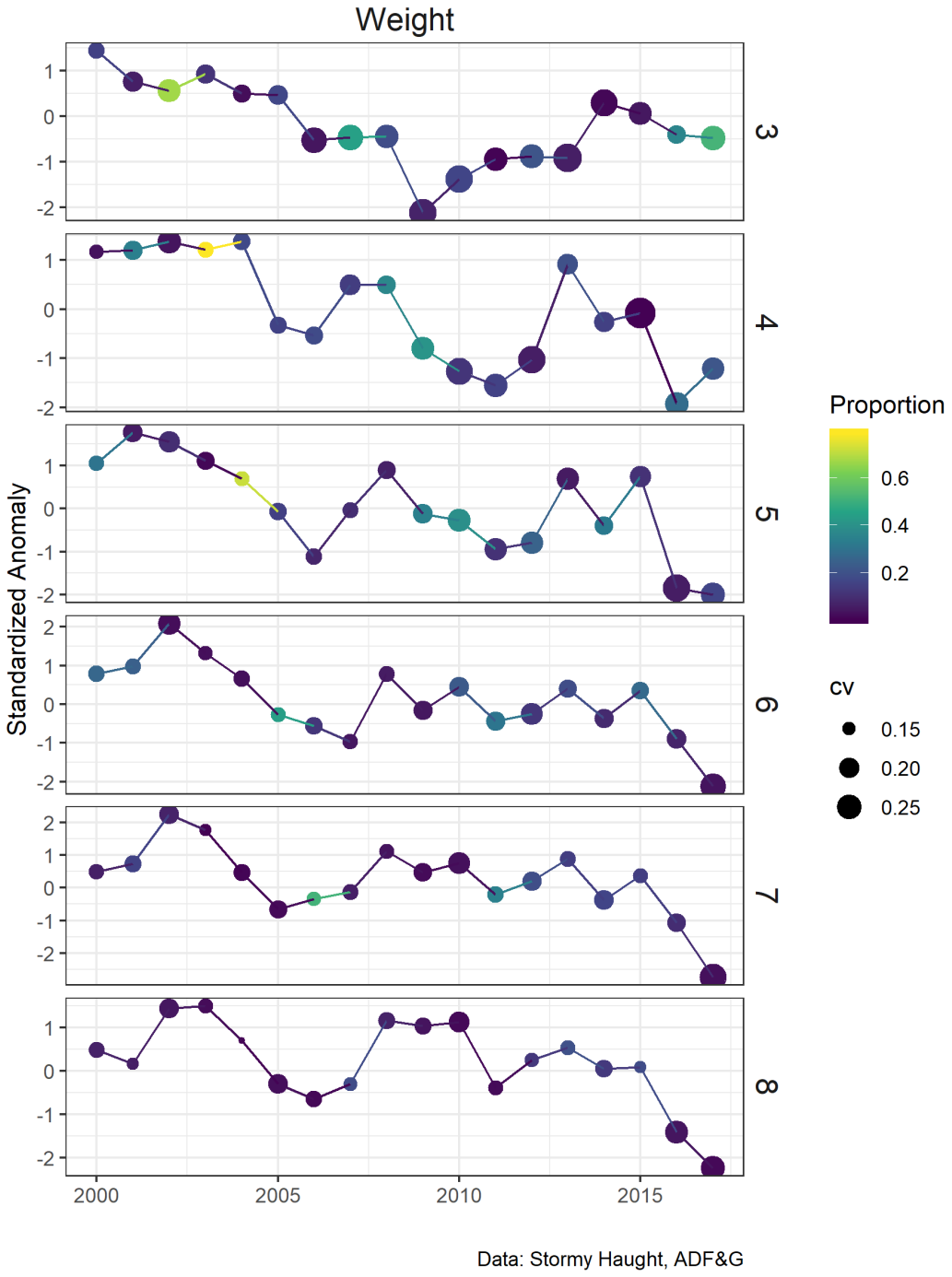

Figure 3-10. Prince William Sound Pacific herring standardized weight anomaly by year and age (vertical panels, age in years labels to the right). Average weights were standardized across years to a mean of 0 and standard deviation of 1. Points are colored by the proportion of each age class in the population, and sized relative to the coefficient of variation of weights by age and year.

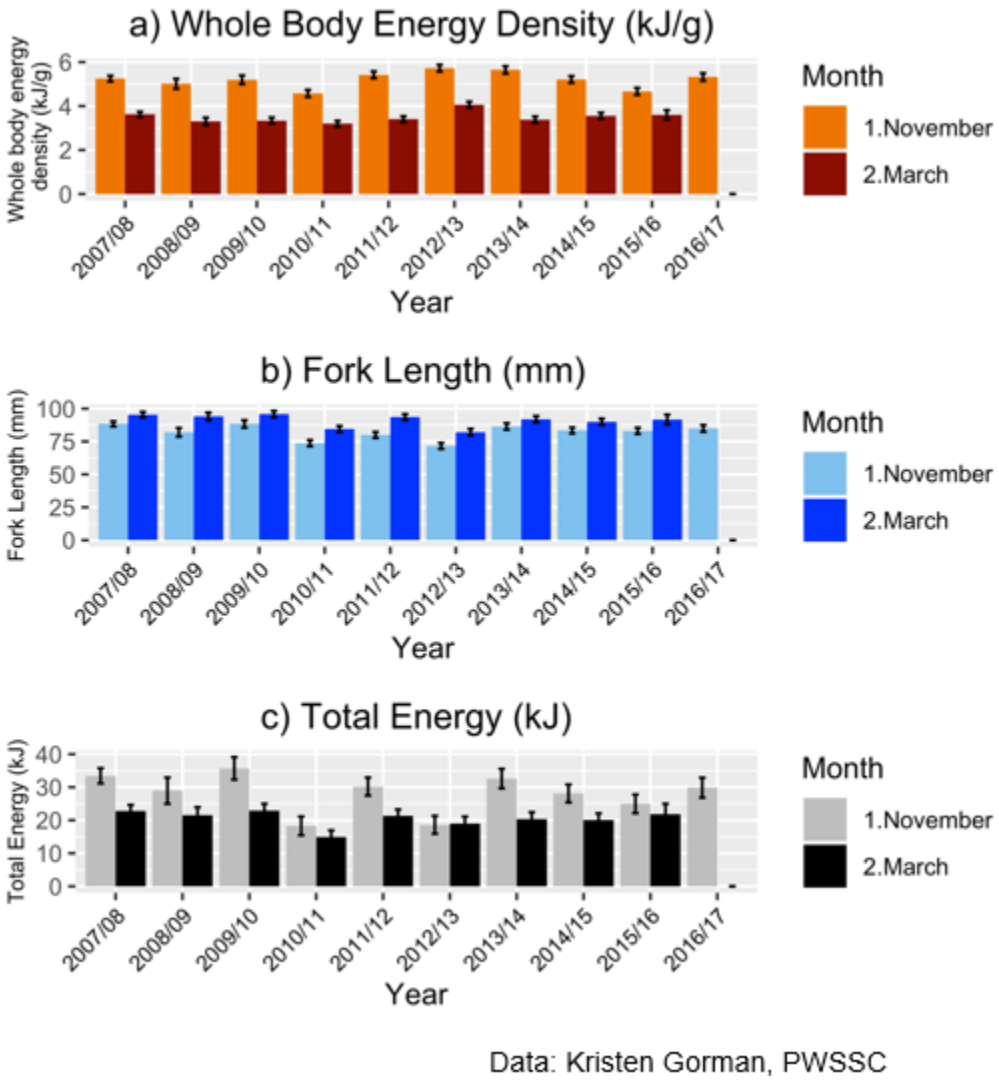

Figure 3-11. Mean (± 95% confidence intervals) for a) whole body energy density (kJ/g), b) fork length (mm, middle), and c) total energy (kJ, bottom) of age-0 herring sampled in November (light bars) and the following March (dark bars) in Prince William Sound between 2007 and 2016.

ZOOPLANKTON INDICES

In general, euphausiid biomass along the Seward Line and in PWS was dominated by *Thyanoessa inermis* and *Thysanoessa longipes* from 2012-2014 and these two species virtually disappeared during 2015 (Figure 3-12). Changes in mean biomass of euphausiids, therefore, were driven by the loss of diversity, particularly during spring.

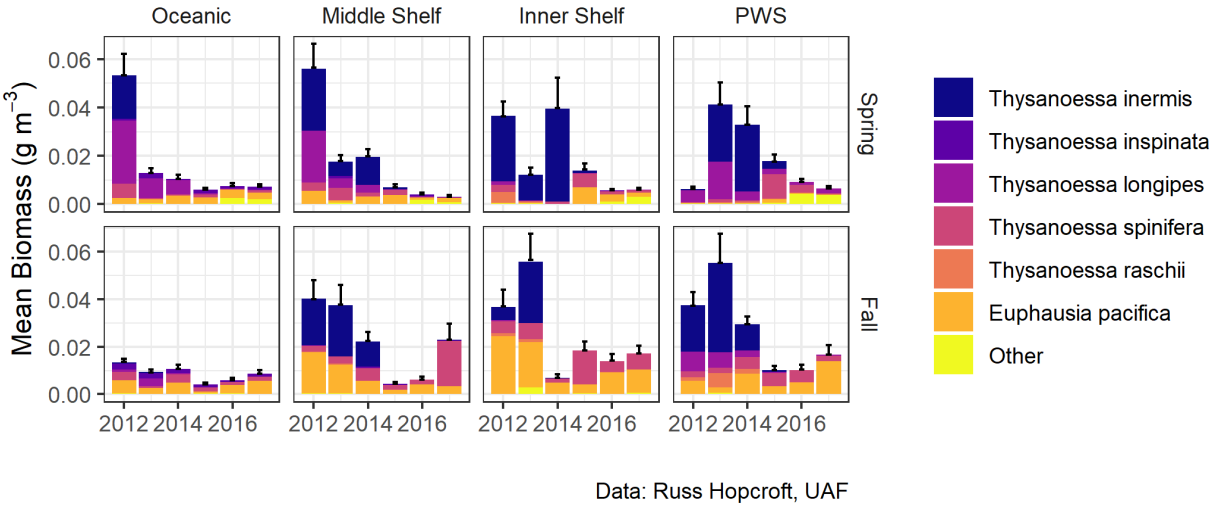

Figure 3-12. Mean (standard deviation) biomass of euphausiids by year (x-axis), region (columns), season (rows), and species (color) sampled by multinet or bongo nets (505 μ mesh) along the Seward Line and Prince William Sound (PWS).

Additionally, variability in the acoustic macrozooplankton index in PWS indicate that the macrozooplankton densities declined in key regions with foraging predator aggregations after 2014 (Figure 3-13).

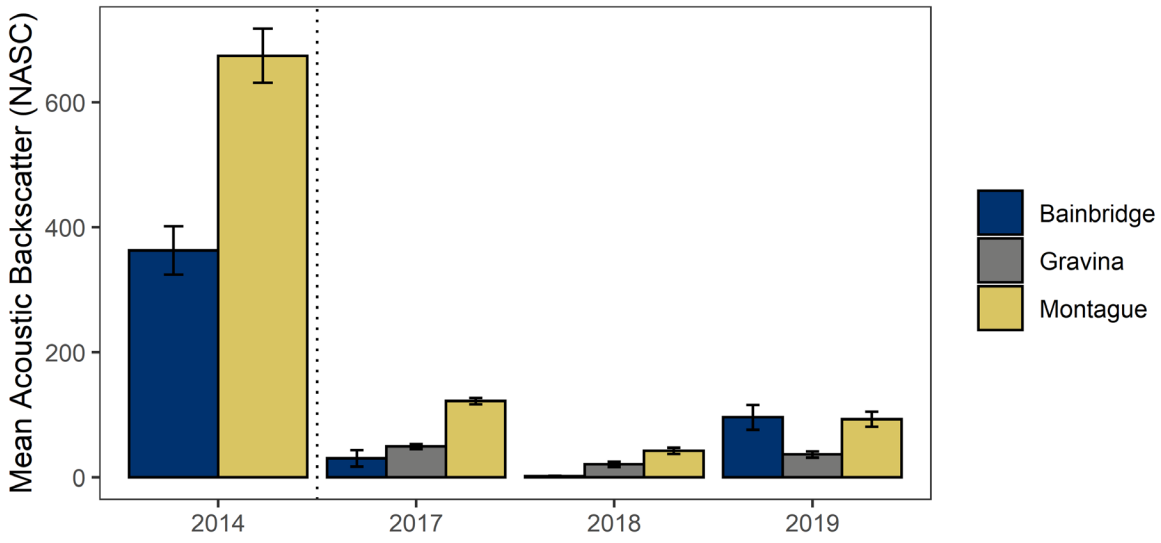

Figure 3-13. Interannual variability in the acoustic macrozooplankton index (NASC, nautical areas scattering coefficient, nmi^{-2}) in Prince William Sound humpback whale foraging aggregation areas. Data were collected during the September Integrated Predator Prey surveys in 2017-2019 and compared to a pre-heatwave pilot study in 2014.

In contrast to the data on euphausiids and macrozooplankton in these regions, the plots of copepod mean biomass over time along the Seward Line (Figure 3-14) indicates a pattern of generally increasing *Neocalanus* spp. (i.e., large copepod species) biomass trends from 2012 to 2017, during the spring, while there was no discernable trend in copepod biomass along the shelf during fall. Spring data from open areas of the PWS embayment show that biomass of *Neocalanus* spp. was greater in 2012 than in more recent years, and that species composition within PWS differs from that on the shelf (as we would expect). The pattern of increasing spring biomass along the shelf during the PMH was at least in part driven by accelerated temperature-dependent development that resulted in population dominated by their final feeding stage rather than larger population sizes during the PMH. Furthermore, observations suggest these animals were less lipid-rich than what is typical for these stages.

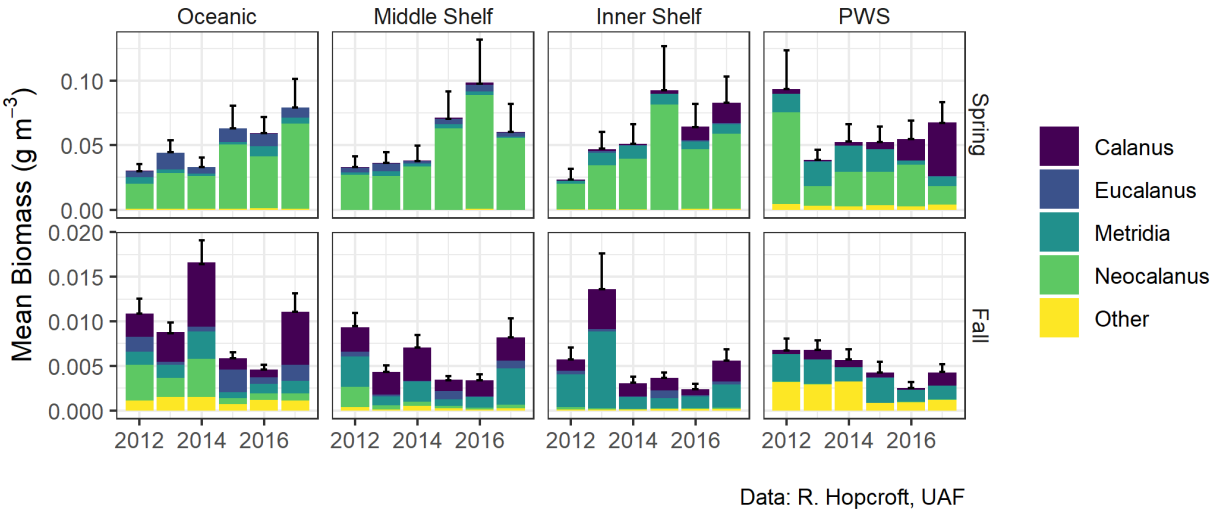

Figure 3-14. Mean (standard deviation) biomass of copepods by year, region (columns), season (rows), and species (color) sampled by multinet or bongo nets (505 µ mesh) along the Seward Line and Prince William Sound (PWS).

Continuous plankton recorder data from shelf regions in the northern GOA show that small copepod abundance began to increase during summer of 2014, and that large copepods during spring and small copepods during fall were also trending higher by 2016 (Figure 3-15).

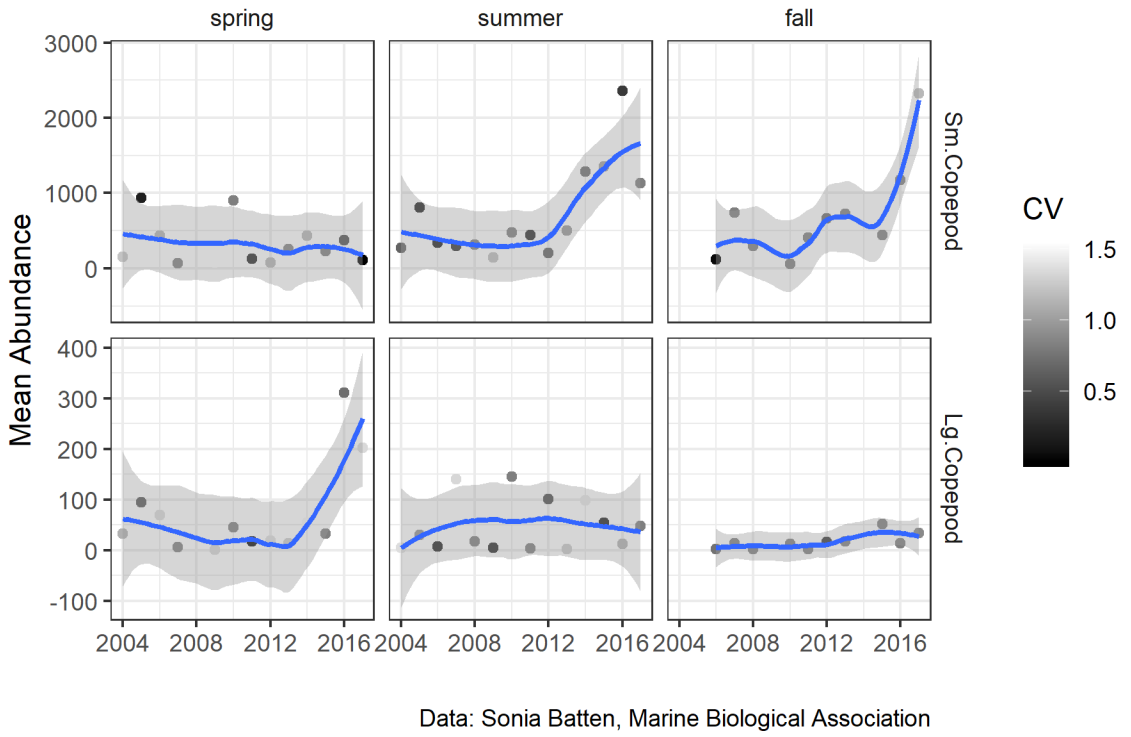

Figure 3-15. Mean abundance of small and large copepods by season (spring = March-May, summer = June-August, fall = September-November) from continuous plankton recorder samples collected on the northern Gulf of Alaska shelf. A loess smoother identifies the general trend (blue line) and standard error (grey polygon) over time. Coefficients of variation (CV) in abundance among months for each season and year are indicated by the color of points, with darker shades indicating lower CVs.

Within the bays of PWS there was a shift in the copepod community, as well as variability in copepod abundance during the PMH. An influx of warm water copepods began in fall 2013 (Figure 3-16). The largest positive anomalies of warm water copepods occurred for every month zooplankton were sampled during 2016, mirroring the sustained positive sea surface temperature anomalies observed in PWS throughout that year. Negative anomalies of large lipid-rich cold-water copepods coincided with the critical grazing period for planktivorous predators particularly during spring of 2014, but positive anomalies occurred in spring 2015 and persisted throughout spring 2016. The spring of 2018 began a return to pre-PMH zooplankton community conditions with strongly positive cold-water copepod anomalies, all zooplankton, and a negative warm water copepod anomaly not seen since before the marine heatwave.

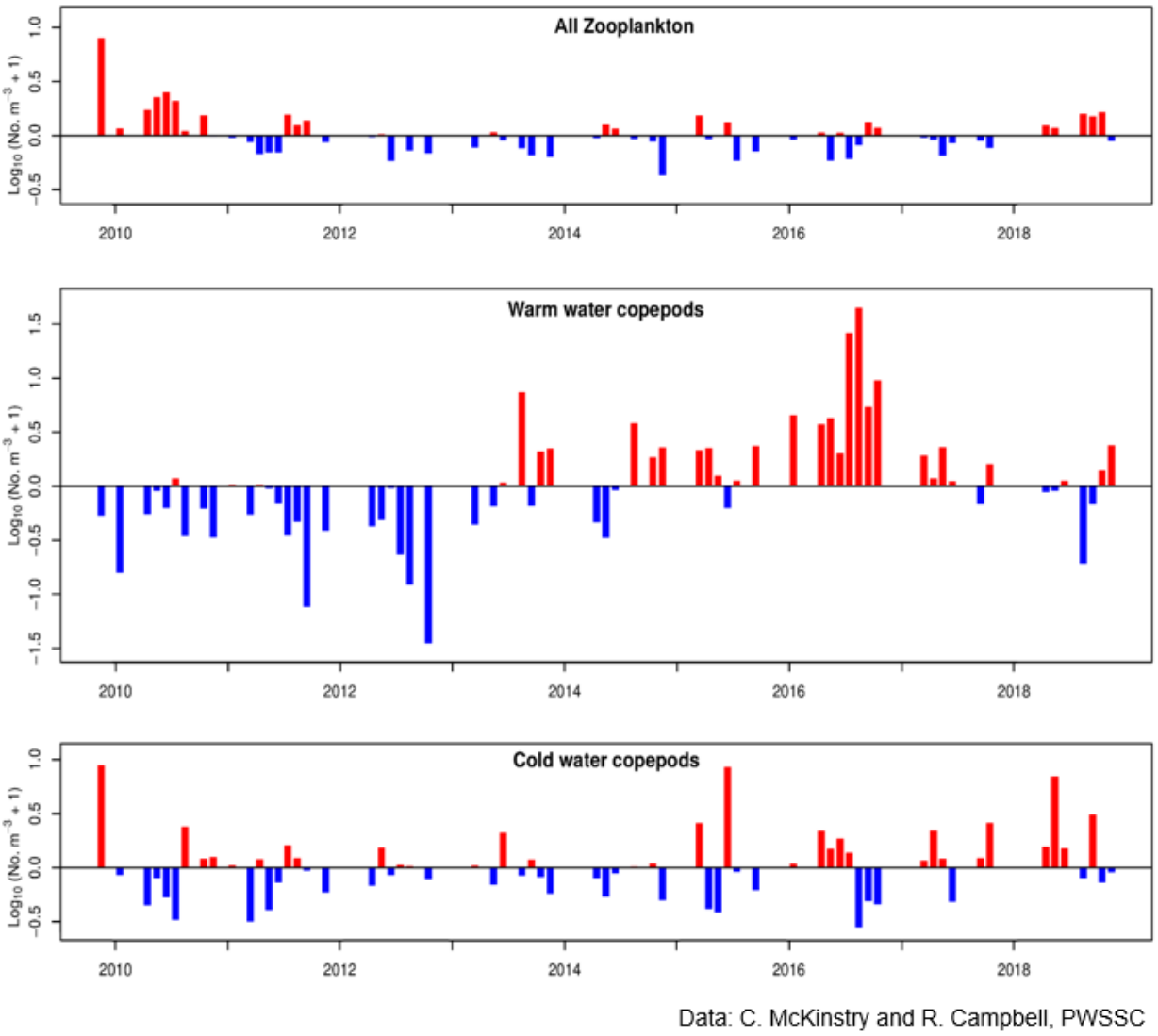

Figure 3-16. Prince William Sound monthly zooplankton abundance anomalies for 2009-2018. Three categories are presented, the entire community, warm water copepods, and cold-water copepods. Red bars indicate positive anomalies and blue bars indicate negative anomalies. All data were $log_{10}(n+1)$ transformed to stabilize variance, hence an anomaly of ±1 indicates an order of magnitude change.

Marine predators

Marine predators in the northern GOA showed evidence of shifts in distribution, reduced encounter rates, and reduced reproduction.

Unusually high densities of murres (2-3 standard deviations above normal) were found within PWS waters during fall 2014 and late fall of 2015, within nearshore areas of Katmai during

summer 2015 and late winter 2016, as well as for the Inner Shelf along the Seward Line during spring and fall 2015, just prior to the die-off (Figure 3-17).

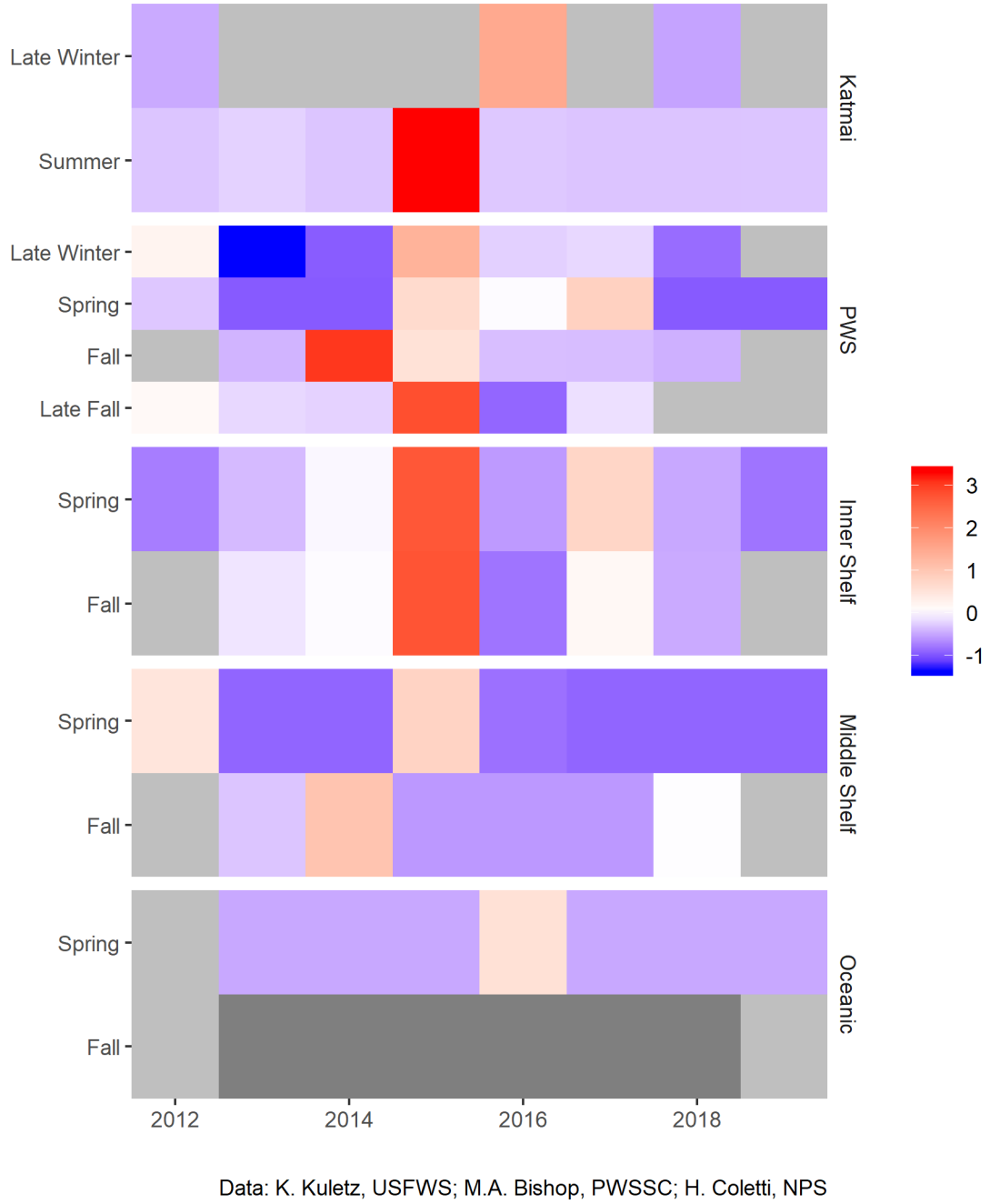

Figure 3-17. Standardized murre density (color, standardized to a mean of 0 and standard deviation of 1 for data collected in 2006-2019) by year, season, and region (Prince William Sound [PWS]). Light grey indicates no data, and dark grey indicates zero density in every survey.

PWS humpback whale encounter rates increased on fall surveys through 2014 and declined by 2017 when surveys were next conducted (Figure 3-18). A crude index of birth rate, weighted by encounter rate, declined significantly over time ($R^2 = 0.50$, $p = 0.03$, Figure 3-18). For fall 2019 encounter rates increased slightly but had not returned to pre-PMH levels. Between fall 2014 and fall 2017/2018 acoustic macrozooplankton index in humpback foraging habitat declined (Figure 3-13), which, along with historically low herring biomass in PWS (Figure 3-6) may largely explain the dramatic reduction in humpback whale encounter rates in the region.

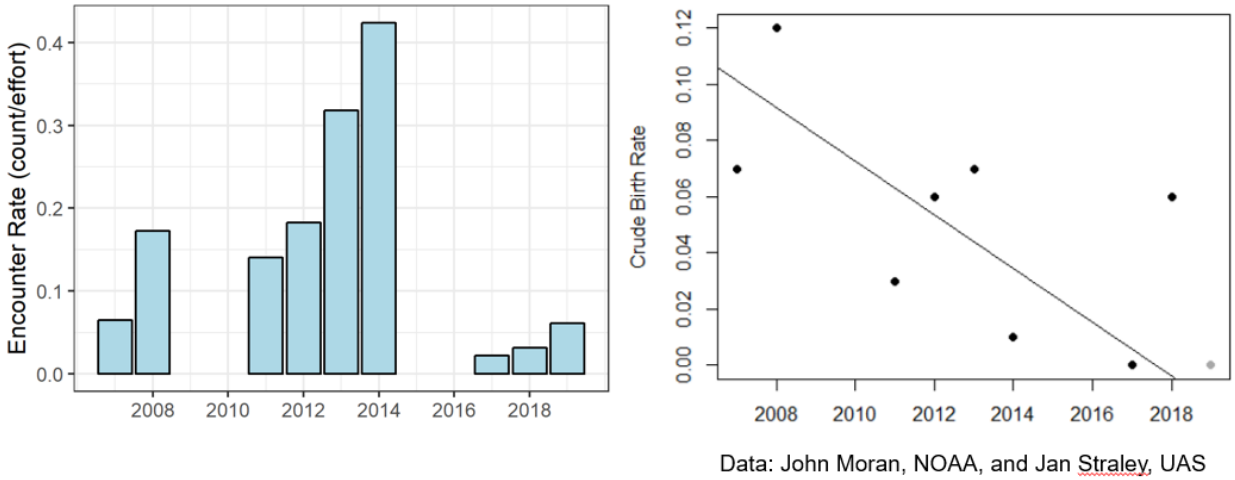

Figure 3-18. Humpback whale encounter rates (left) and crude index of birth rate (right) during fall surveys in Prince William Sound. The regression between crude index of birth rate by year (solid line) was weighted by the encounter rate ($R^2 = 0.50$, $p = 0.03$). The grey circle for 2019 is provisional.

Discussion

The multi-year PMH was coincident with changes to the middle trophic levels that led to simultaneously low availability and low nutritional quality in three key species of forage fish, which had apparent consequences for higher trophic level predators. This may have occurred for different reasons as these forage fish species have different life histories that can promote staggered year class strength and population trajectories. Capelin declined abruptly at the onset of the PMH, and spawning herring indices also declined abruptly between 2014-2015, whereas sand lance were apparently experiencing declining trends prior to the PMH.

The prolonged nature of the PMH produced poor condition for all the key prey species examined. Species-specific thermal optima are not well known, but because capelin is a more northern species associated with cooler ocean temperatures it is likely they contracted their distribution under warming conditions in the GOA or shifted locally to deeper, cooler waters (Rose 2005, Arimitsu et al. 2008, McGowan et al. 2018). Capelin size, body condition, and availability were negatively associated with warming temperatures (Sydeman et al. 2017, Thompson et al. 2019). In contrast, sand lance and herring have broader, more southerly distributions, and may be more tolerant of warmer temperatures. For example, sand lance were

positively associated with warmer conditions in the GOA during several decades prior to the PMH (Abookire and Piatt 2005, Sydeman et al. 2017, Thompson et al. 2019), but demonstrated a strong negative response in growth and whole body energy content in PWS during the PMH (von Biela et al. 2019b). Similarly, age-0 herring were related to higher diatom abundance and warmer temperatures in PWS, although the relationship broke down under extreme temperatures (Batten et al. 2016). The negative response in growth and energy content of sand lance and herring during the PMH suggests the temperature optima of these species may have been exceeded, which has been demonstrated in other species (Laurel et al. 2016).

TRUNCATION OF AGE AND SIZE STRUCTURE IN FORAGE FISH

Truncation of the older, larger size classes in capelin and sand lance, both species with relatively short life spans, could have been due to top-down pressures during the PMH. Changes in the demographic structure of fishes is a well-documented consequence of size-selective removal processes such as exploitation due to predation, disease, or fishing (Perry et al. 2010, Ohlberger et al. 2014). Such size truncation reduces the buffering capacity of the population to environmental variability leading to poor recruitment and survival (Perry et al. 2010, Planque et al. 2010). It can also alter spawning dynamics. For example, smaller, younger individuals should produce fewer eggs, since fecundity is strongly related to size (Gjøsæter 1998), and spawning by younger populations may occur over a reduced duration and spatial extent (Perry et al. 2010).

Top down pressures on forage species during the PMH are hypothesized to have resulted from increased metabolic needs of large predatory fish over multiple years of warm conditions (Piatt et al. in press, Barbeaux et al. 2018). A 2 ºC increase in temperature would have increased the daily rations of GOA pollock, Pacific cod, and arrowtooth flounder (*Astheresthes stomias*) by 70%, 34%, and 65%, respectively (Holsman and Aydin 2015). The prolonged nature of the PMH, spanning multiple winters, along with the increased consumption needs by ectothermic predatory fish could have provided a mechanism for large-scale top-down control of the middle trophic level.

Disease has also been identified as a top-down stressor limiting the PWS herring population. The primary pathogens are Viral Hemorrhagic Septicemia virus, with infection rates increasing when schools occur in dense aggregations such as during periods of spawning or predator-corralling, and *Ichthyophonus*, which tends to be more prevalent with increasing host size and age (Hershberger et al. 2010, 2016). No relationship between warming temperatures and disease prevalence has been established, but disease is thought to be an underlying stressor that may be a factor in the failure of the PWS herring population recovery.

DECREASED QUALITY OF FORAGE FISH

Lower quality of forage fish, manifested through lower growth and/or energy content, are suggestive of bottom up pressures that may have included poor quality zooplankton prey and/or thermal stress. In 2016, age-1 sand lance in PWS were 89% lower in total energy than in previous cool years. Similarly, herring showed signs of lower body condition, including lower weight at age (adults) and total energy (juveniles). A zooplankton community shift to one dominated by (less nutritious) small copepods both on the GOA shelf (Figure 3-15, Batten et al. 2018) and in the bays of PWS (Figure 3-16) could help explain negative growth anomalies and

lower condition of forage fish (Heintz et al. 2013); however, it's likely that large-scale depletions in forage fish are the more important driver of predator responses observed during the PMH.

Lower biomass and diversity of euphausiids oppose copepod trends

Euphausiid biomass decreased in the region after 2014 (Figures 3-12 and 3-13). Lower euphausiid biomass was driven by the loss of *T. inermis* and *T. longipes*. Based on Global Ocean Ecosystem Dynamics/Seward Line data, Pinchuk et al. (2008) found *T. inermis* abundance was positively associated with a cool regime in 1999-2002, perhaps because the species has a relatively high mass-specific metabolic rate and thus spends significantly more energy on metabolism during warmer winters. Following a warm winter, *T. inermis* would have less energy reserves in spring for spawning.

While euphausiids declined in biomass during the PMH, large-bodied spring copepod biomass generally increased on the shelf and in bays of PWS (Figures 3-14, 3-15, and 3-16), primarily due to faster development of stages in spring. Although warmer temperatures would have also shortened the generation times of the smaller taxa that dominated during the summer, the increased abundances were driven largely by contributions from smaller genera within both size classes that would have effectively lowered mean body size of the community (Batten et al. 2018, Kimmel and Duffy-Anderson 2020). While this community change may have influenced the poor nutritional quality of forage fish species, there was no evidence of abrupt declines in copepods on the GOA shelf or in coastal waters. This suggests that food availability was not a primary factor in the collapse of the forage fish populations during this time.

Changes in distribution, mass mortality, reduced breeding success, and malnutrition in predators

The influx of murres into PWS and the Inner Shelf of the northern GOA observed in 2014 and 2015 (Figure 3-17) preceded a massive die-off of common murres in winter 2015-2016. More than 62,000 dead or dying murres were recovered from Alaska to southern California, impacting an estimated 0.5-1.2 million birds (Piatt et al. 2020). This die-off was centered in the GOA, and the highest densities of carcasses were observed in PWS. Carcasses recovered throughout the range were emaciated, had little to no body fat, and most had empty stomachs, suggesting that starvation was the ultimate cause of mortality.

Additionally, harmful algal bloom neurotoxins (saxitoxin) were detected in about 1/3 of the die-off carcasses tested (n = 44, Van Hemert et al. 2020). Although the majority of samples had saxitoxin levels that were too low to quantify, a small number of die-off murres had detectable concentrations (up to 10.8 µ/100g) of saxitoxin in their livers. Similar rates of detection also were found in apparently healthy birds the next summer, although background levels of saxitoxin-producing algae were also high in summer 2016 (Vandersea et al. 2018). Importantly, detrimental levels of saxitoxin in seabirds are still unknown. Thus, in addition to reduced prey availability and prey quality as a primary factor, harmful algal blooms may have provided an additional stressor during the 2015-2016 murre die-off. Still, the large-scale inshore movement of murres prior to dying of starvation suggests that they were unable to obtain sufficient energy foraging offshore and were presumably seeking better foraging conditions in coastal waters.

Data that show decreasing humpback whale encounter rates and reduced number of calves in PWS (Figure 3-18) mirror observations in southeast Alaska (Neilson and Gabriele 2019). After more than 30 years of increasing abundance of humpback whales in Glacier Bay National Park and adjacent waters, numbers declined by more than 50% between 2013 and 2018. Annual monitoring efforts by Glacier Bay National Park also documented a decrease in calf production and apparent survival, in addition to an increase in observations of "skinny" whales. Additionally, an unusual mortality event of primarily fin and humpback whales in 2015-2016 (Savage 2017) may have been related to the collapse of forage fish and macrozooplankton in the northern GOA.

Conclusion

The opposing direction of changes at lower (copepods) and higher (murres and whales) trophic levels provides evidence for a large-scale reduction in energy transfer through the middle trophic level (forage fish and euphausiids). The declines in the availability and quality of forage fish and euphausiids were likely a primary driver of the mass mortalities, changes in distribution, reproductive failure, and malnutrition observed in piscivorous marine predators that depend on the pelagic food chain during the PMH. It appears that both bottom up and top down mechanisms played a role in the reduced quality and synchronous forage fish collapse during the prolonged marine heatwave. For example, we documented declines in growth and energy content of key forage fish that reflected classic bottom up regulation. At the same time, forage fish populations experienced age and size truncation typical of size-selective removals indicative of top-down regulation.

PMH conditions are associated with climate change and are increasing in frequency and duration globally. The PMH in 2014-2016 caused a large-scale perturbation in the marine food web that was manifested through a simultaneous reduction in the availability and quality of key forage taxa including fish and krill. Coincident increases in small and large copepod abundance, as well as massive die-offs and reproductive failures in top marine predators suggest that reduced transfer of energy through the middle trophic level was a key factor underlying the ecosystem disruption. For sand lance, declines apparently began before the PMH, but capelin and spawning herring declined abruptly when waters warmed. Shifts in age-structure, lower total energy, and changes in growth of forage fishes also occurred in the northern GOA during the PMH. Diversity of life history strategies in key middle trophic level species typically promotes resilience in marine food webs (Rooney et al. 2006, Sheaves 2009), however, this mechanism for creating stability in marine food webs apparently failed during the prolonged PMH.

Although the monitoring footprint of GWA is focused in the northern GOA, negative effects of the PMH were apparent in conspicuous marine predators throughout the GOA, which suggest the aggregate findings of the program are representative of the larger GOA marine ecosystem. This information may provide important context in understanding the response of large marine ecosystems to current and future events. For example, the Bering Sea and larger Arctic region have also undergone recent severe heat wave conditions, along with unusual mortality in predators. Continued efforts by the GWA long-term monitoring program are thus vital to understanding the effects of future perturbations and ecosystem-based management of the Alaska's productive marine ecosystems.

ACKNOWLEDGEMENTS

We thank the scientific and program management team of the GWA long-term monitoring program for their expertise and resources in support of this work. We thank the many field crews that contributed to decades of data collection efforts. Data from the GWA, including U.S. Geological Survey data releases (Arimitsu et al. 2017, von Biela et al. 2019a) and the Herring Research and Monitoring program are available at the Alaska Ocean Observing System Gulf of Alaska Data Portal at the following link: https://portal.aoos.org/gulf-of-alaska#search?type_group=all&tag|tag=evos-gulf-watch-projects&page=1. The research described in this publication was supported by the *Exxon Valdez* Oil Spill Trustee Council, U.S. Geological Survey Alaska Science Center, National Oceanic and Atmospheric Administration Alaska Fisheries Science Center, Marine Biological Association, PWS Science Center, National Park Service, Pole Star Ecological Research, Institute for Seabird Research and Conservation, University of Alaska Fairbanks, U.S. Fish and Wildlife Service, University of Washington, University of Alaska Southeast, National Science Foundation and Alaska Ocean Observing System. The findings and conclusions presented by the authors do not necessarily reflect the views or position of the *Exxon Valdez* Oil Spill Trustee Council. This paper has been peer reviewed and approved for publication consistent with U.S. Geological Survey Fundamental Science Practices (https://pubs.usgs.gov/circ/1367/). Any use of trade, firm, or product names is for descriptive purposes only and does not imply endorsement by the U.S. Government.

REFERENCES

Abookire, A.A., and J.F. Piatt. 2005. Oceanographic conditions structure forage fishes into lipid-rich and lipid-poor communities in lower Cook Inlet, Alaska, USA. Marine Ecology Progress Series 287:229-240.

Arimitsu, M.L., J.F. Piatt, B. Heflin, V.R. von Biela, and S.K. Schoen. 2018. Monitoring long-term changes in forage fish distribution, abundance, and body condition. *Exxon Valdez* Oil Spill Restoration Project Final Report (Restoration Project 16120114-O). *Exxon Valdez* Oil Spill Trustee Council. Anchorage, AK.

Arimitsu, M.L., J F. Piatt, and B.M. Heflin. 2017. Pelagic forage fish distribution, abundance, and body condition: U.S. Geological Survey data release, https://doi.org/10.5066/F74J0C9Z.

Arimitsu, M.L., J.F. Piatt, M.A. Litzow, A.A. Abookire, M.D. Romano, and M.D. Robards. 2008. Distribution and spawning dynamics of capelin (*Mallotus villosus*) in Glacier Bay, Alaska: a cold water refugium. Fisheries Oceanography 17:137-146.

Baker, M.R., M.E. Matta, M. Beaulieu, N. Paris, S. Huber, O.J. Graham, T. Pham, N.B. Sisson, C.P. Heller, and A. Witt. 2018. Intra-seasonal and inter-annual patterns in the demographics of sand lance and response to environmental drivers in the North Pacific. Marine Ecology Progress Series 617–618:221-244.

Baker, T.T., J.A. Wilcock, and B.W. McCracken. 1991. Stock assessment and management of Pacific herring in Prince William Sound, 1990. Alaska Department of Fish and Game, Division of Commercial Fisheries. Technical Fisheries Data Report No. 91-22. Juneau,

Alaska.

Barbeaux, S., K. Aydin, B. Fissel, K. Holsman, W. Palsson, K. Shotwell, Q. Yang, and S. Zador. 2018. Assessment of the Pacific cod stock in the Gulf of Alaska. North Pacific Fisheries Management Council. North Pacific Fishery Management Council Gulf of Alaska 2017 Stock Assessment and Fishery Evaluation Report. 605 W 4th Ave, Suite 306, Anchorage AK 99501.

Batten, S.D., S. Moffitt, W.S. Pegau, and R.W. Campbell. 2016. Plankton indices explain interannual variability in Prince William Sound herring first year growth. Fisheries Oceanography 25:420-432.

Batten, S.D., D.E. Raitsos, S. Danielson, R. Hopcroft, K. Coyle, and A. Mcquatters-Gollop. 2018. Interannual variability in lower trophic levels on the Alaskan Shelf. Deep-Sea Research Part II 147:79-86.

Batten, S.D., and A.W. Walne. 2011. Variability in northwards extension of warm water copepods in the NE Pacific. Journal of Plankton Research 33:1643-1653.

Bond, N.A., M.F. Cronin, H. Freeland, and N. Mantua. 2015. Causes and impacts of the 2014 warm anomaly in the NE Pacific. Geophysical Research Letters 42:3414-3420.

Brodeur, R.D., T.D. Auth, and A.J. Phillips. 2019a. Major shifts in pelagic micronekton and macrozooplankton community structure in an upwelling ecosystem related to an unprecedented marine heatwave. Frontiers in Marine Science 6:212 https://doi.org/10.3389/fmars.2019.00212.

Brodeur, R.D., M.E. Hunsicker, A. Hann, and T.W. Miller. 2019b. Effects of warming ocean conditions on feeding ecology of small pelagic fishes in a coastal upwelling ecosystem: a shift to gelatinous food sources. Marine Ecology Progress Series 617-618:149-163 https://doi.org/10.3354/meps12497

Brown, E.D. 2002. Life history, distribution, and size structure of Pacific capelin in Prince William Sound and the northern Gulf of Alaska. ICES Journal of Marine Science 59:983-996.

Childers, A.R., T.E. Whitledge, and D.A. Stockwell. 2005. Seasonal and interannual variability in the distribution of nutrients and chlorophyll a across the Gulf of Alaska shelf: 1998–2000. Deep Sea Research Part II 52:193-216.

Coletti, H.A., and K.A. Kloecker. 2017. Gulf Watch Alaska Nearshore Component: Marine Bird and Mammal Survey Data from Katmai National Park and Preserve and Kenai Fjords National Park, 2012-2016: U.S. Geological Survey Alaska Science Center, https://doi.org/10.5066/F7416V6H.

De Robertis, A., D.R. McKelvey, and P.H. Ressler. 2010. Development and application of an empirical multifrequency method for backscatter classification. Canadian Journal of Fisheries and Aquatic Sciences 67:1459-1474.

De Robertis, A., and O.A. Ormseth. 2018. Inshore acoustic surveys in the eastern and central Gulf of Alaska. Deep-Sea Research Part II: Topical Studies in Oceanography 65:255-267 doi.org/10.1016/j.dsr2.2018.05.001.

Demer, D.A., L. Berger, M. Bernasconi, E. Bethke, K.M. Boswell, D. Chu, R. Domokos, A. Dunford, S. Fassler, S. Gauthier, L.T. Hufnagle, J.M. Jech, N. Bouffant, A. Lebourges-Dhaussy, X. Lurton, G.J. Macaulay, Y. Perrot, T. Ryan, A.C. Parnell, S. Stienessen, T. Weber, and N. Williamson. 2015. Calibration of acoustic instruments. ICES Cooperative Research Report. Volume 326.

Di Lorenzo, E., and N. Mantua. 2016. Multi-year persistence of the 2014/15 North Pacific marine heatwave. Nature Climate Change 6:1-7.

Doyle, M.J., S.L. Strom, K.O. Coyle, A.J. Hermann, C. Ladd, A.C. Matarese, S.K. Shotwell, and R.R. Hopcroft. 2019. Early life history phenology among Gulf of Alaska fish species: Strategies, synchronies, and sensitivities. Deep-Sea Research Part II: Topical Studies in Oceanography 165:41-73.

Fisher, J.L., W.T. Peterson, and R.R. Rykaczewski. 2015. The impact of El Niño events on the pelagic food chain in the northern California Current. Global Change Biology 21:4401-4414.

Foote, K.G., H.P. Knudsen, G. Vestnes, D. MacLennan, and E. Simmonds. 1987. Calibration of acoustic instruments for fish density estimation: A practical guide. Copenhagen, Denmark. ICES Cooperative Research Report No. 144 69.

Gjøsæter, H. 1998. The population biology and exploitation of capelin (Mallotus villosus) in the Barents Sea. Sarsia 83:453-496.

Gorman, K.B., T.C. Kline, M.E. Roberts, F.F. Sewall, R.A. Heintz, and W.S. Pegau. 2018. Spatial and temporal variation in winter condition of juvenile Pacific herring (*Clupea pallasii*) in Prince William Sound, Alaska : Oceanographic exchange with the Gulf of Alaska. Deep-Sea Research Part II 147:116-126.

Hatch, S.A. 2013. Kittiwake diets and chick production signal a 2008 regime shift in the Northeast Pacific. Marine Ecology Progress Series 477:271-284.

Heintz, R.A., E.C. Siddon, E.V. Farley, and J.M. Napp. 2013. Correlation between recruitment and fall condition of age-0 pollock (*Theragra chalcogramma*) from the eastern Bering Sea under varying climate conditions. Deep-Sea Research Part II: Topical Studies in Oceanography 94:150-156.

Hershberger, P., J. Gregg, C. Grady, R. Collins, and J. Winton. 2010. Kinetics of viral shedding provide insights into the epidemiology of viral hemorrhagic septicemia in Pacific herring. Marine Ecology Progress Series 400:187-193.

Hershberger, P.K., J.L. Gregg, L.M. Hart, S. Moffitt, R. Brenner, K. Stick, E. Coonradt, E.O. Otis, J.J. Vollenweider, K.A. Garver, J. Lovy, and T.R. Meyers. 2016. The parasite *Ichthyophonus* sp. in Pacific herring from the coastal NE Pacific. Journal of Fish Diseases 39:395-410.

Hobday, A.J., E.C.J. Oliver, A. Sen Gupta, J.A. Benthuysen, M.T. Burrows, M.G. Donat, N.J. Holbrook, P.J. Moore, M.S. Thomsen, T. Wernberg, and S.A. Smale. 2018. Categorizing and naming heatwaves. Oceanography 31:162-173.

Holsman, K.K., and K. Aydin. 2015. Comparative methods for evaluating climate change impacts on the foraging ecology of Alaskan groundfish. Marine Ecology Progress Series 521:217-235.

Hooff, R.C., and W.T. Peterson. 2006. Copepod biodiversity as an indicator of changes in ocean and climate conditions of the northern California current ecosystem. Limnology and Oceanography 51:2607-2620.

Joh, Y., and E. Di Lorenzo. 2017. Increasing Coupling Between NPGO and PDO Leads to Prolonged Marine Heatwaves in the Northeast Pacific. Geophysical Research Letters 44:11,663-11,671.

Kimmel, D.G., and J.T. Duffy-Anderson. 2020. Zooplankton abundance trends and patterns in Skelikof Strait, western Gulf of Alaska, USA, 1990-2017. Journal Of Plankton Research 42:334-354 https://doi.org/10.1093/plankt/fbaa019.

Kondoh, M. 2003. Foraging adaptation and the relationship between food-web complexity and stability. Science 299:1388-1391.

Kuletz, K.J., E.A. Labunski, and S.G. Speckman. 2008. Abundance, distribution, and decadal trends of Kittlitz' s and marbled murrelets and other marine species in Kachemak Bay, Alaska. Final Report (Project No. 14) by U.S. Fish and Wildlife Service for Alaska Department of Fish and Game, State Nongame Wildlife Management.

Laurel, B.J., M. Spencer, P. Iseri, and L.A. Copeman. 2016. Temperature-dependent growth and behavior of juvenile Arctic cod (*Boreogadus saida*) and co-occurring North Pacific gadids. Polar Biology 39:1127-1135.

MacDonald, P.D. M., and T.J. Pitcher. 1979. Age-Groups from Size-Frequency Data: A Versatile and Efficient Method of Analyzing Distribution Mixtures. Journal of the Fisheries Research Board of Canada 36:987-1001.

McGowan, D.W., E.D. Goldstein, M.L. Arimitsu, A.L. Deary, O. Ormseth, A. De Robertis, J.K. Horne, L.A. Rogers, T. Matthew, K.O. Coyle, K. Holderied, J.F. Piatt, W.T. Stockhausen, and S. Zador. 2020. Spatial and temporal dynamics of Pacific capelin *Mallotus catervarius* in the Gulf of Alaska : implications for ecosystem-based fisheries management. Marine Ecology Progress Series 637:117-140.

McGowan, D.W., J.K. Horne, J.T. Thorson, and M. Zimmermann. 2018. Influence of environmental factors on capelin distributions in the Gulf of Alaska. Deep Sea Research Part II: Topical Studies in Oceanography 165:238-254 https://doi.org/10.1016/j.dsr2.2017.11.018.

McKinstry, C.A.E., and R.W. Campbell. 2018. Seasonal variation of zooplankton abundance and community structure in Prince Willaim Sound, Alaska, 2009-2016. Deep-Sea Research Part II 147:69-78.

Moffitt, S.D. 2017. Retrospective longitudinal growth history from scales of Pacific herring collected in Prince William Sound. Exxon Valdez Long-Term Herring Research and Monitoring Program Final Report (Project 13120111-N).

Mueter, F.J., and B. Norcross. 1997. Spatial and temporal patterns in the demersal fish community on the shelf and upper slope regions of the Gulf of Alaska. Fishery Bulletin 559-581.

Muradian, M.L., T.A. Branch, S.D. Moffitt, and P.-J.F. Hulson. 2017. Bayesian stock assessment of Pacific herring in Prince William Sound, Alaska. Plos One 12:e0172153.

Neilson, J.L., and C.M. Gabriele. 2019. Glacier Bay & Icy Strait Humpback Whale Population Monitoring: 2018 Update. Gustavus, Alaska.

Ohlberger, J., S.J. Thackeray, I.J. Winfield, S.C. Maberly, and L.A. Vøllestad. 2014. When phenology matters: Age - size truncation alters population response to trophic mismatch. Proceedings of the Royal Society B: Biological Sciences 281.

Ormseth, O.A. 2012. Preliminary assessment of forage species in the Gulf of Alaska: Introduction to the new forage species reports and their relation to the ecosystem considerations chapter. North Pacific Fishery Management Council Gulf of Alaska Appendix 2:759-804.

Ostrand, W.D., T.A. Gotthardt, S. Howlin, and M.D. Robards. 2005. Habitat Selection Models for Pacific Sand Lance (A*mmodytes hexapterus*) in Prince William Sound, Alaska. J.W. Orr, editor. Northwestern Naturalist 86:131-143.

Perry, R.I., P. Cury, K. Brander, S. Jennings, C. Möllmann, and B. Planque. 2010. Sensitivity of marine systems to climate and fishing: Concepts, issues and management responses. Journal of Marine Systems 79:427-435.

Piatt, J.F., J.K. Parrish, H.M. Renner, S.K. Schoen, T.T. Jones, M.L. Arimitsu, K.J. Kuletz, B. Bodenstein, M. García-Reyes, R.S. Duerr, R.M. Corcoran, R. Kaler, G.J. McChesney, R.T. Golightly, H.A. Coletti, R.M. Suryan, H.K. Burgess, J. Lindsey, K. Lindquist, P.M. Warzybok, J. Jahncke, J. Roletto, W.J. Sydeman, J. Jahnke, J. Roletto, and W.J. Sydeman. 2020. Extreme mortality and reproductive failure of common murres resulting from the northeast Pacific marine heatwave of 2014-2016. PLoS ONE 15:e0226087.

Pinchuk, A.I., K.O. Coyle, and R. Hopcroft. 2008. Climate-related variability in abundance and reproduction of euphausiids in the northern Gulf of Alaska in 1998–2003. Progress In Oceanography 77:203-216.

Planque, B., J.M. Fromentin, P. Cury, K.F. Drinkwater, S. Jennings, R.I. Perry, and S. Kifani. 2010. How does fishing alter marine populations and ecosystems sensitivity to climate? Journal of Marine Systems 79:403-417.

R Core Team. 2018. A Language and Environment for Statistical Computing. R Foundation for Statistical Computing. Vienna, Austria. https://www.R-project.org/. R Foundation for Statistical Computing, Vienna.

Robards, M.D., J.F. Piatt, and G.A. Rose. 1999. Maturation, fecundity, and intertidal spawning of Pacific sand lance in the northern Gulf of Alaska. Journal of Fish Biology 54:1050-1068.

Rooney, N., K. McCann, G. Gellner, and J.C. Moore. 2006. Structural asymmetry and the stability of diverse food webs. Nature 442:265-269.

Rose, G.A. 2005. Capelin (*Mallotus villosus*) distribution and climate: a sea "canary" for marine ecosystem change. ICES Journal of Marine Science 62:1524-1530.

Savage, K. 2017. Alaska and British Columbia Large Whale Unusual Mortality Event Summary Report. 2017. NOAA-NMFS, https://repository.library.noaa.gov/view/noaa/17715.

Schoen, S.K., J.F. Piatt, M.L. Arimitsu, B.M. Heflin, E.N. Madison, G.S. Drew, M. Renner, N.A. Rojek, D.C. Douglas, and A.R. DeGange. 2018. Avian predator buffers against variability in marine habitats with flexible foraging behavior. Marine Biology 165:47.

Sheaves, M. 2009. Consequences of ecological connectivity: The coastal ecosystem mosaic. Marine Ecology Progress Series 391:107-115.

Smale, D.A., T. Wernberg, E.C.J. Oliver, M. Thomsen, B.P. Harvey, S.C. Straub, M.T. Burrows, L.V. Alexander, J.A. Benthuysen, M.G. Donat, M. Feng, A.J. Hobday, N.J. Holbrook, S.E. Perkins-Kirkpatrick, H.A. Scannell, A. Sen Gupta, B.L. Payne, and P.J. Moore. 2019. Marine heatwaves threaten global biodiversity and the provision of ecosystem services. Nature Climate Change 9:306-312.

Sousa, L., K.O. Coyle, R.P. Barry, T.J. Weingartner, and R.R. Hopcroft. 2016. Climate-related variability in abundance of mesozooplankton in the northern Gulf of Alaska 1998–2009. Deep-Sea Research Part II: Topical Studies in Oceanography 132:122-135.

Stabeno, P.J., S. Bell, W. Cheng, S. Danielson, N.B. Kachel, and C.W. Mordy. 2016. Long-term observations of Alaska Coastal Current in the northern Gulf of Alaska. Deep Sea Research Part II: Topical Studies in Oceanography 132:24-40.

Stocking, J., M.A. Bishop, and A. Arab. 2018. Spatio-temporal distributions of piscivorous birds in a subarctic sound during the nonbreeding season. Deep-Sea Research Part II 147:138-147.

Sydeman, W.J., J.F. Piatt, S.A. Thompson, M. García-Reyes, S.A. Hatch, M.L. Arimitsu, L. Slater, J.C. Williams, N.A. Rojek, S.G. Zador, and H.M. Renner. 2017. Puffins reveal contrasting relationships between forage fish and ocean climate in the N. Pacific. Fisheries Oceanography 26:379-395.

Thayer, J.A., D.F. Bertram, S.A. Hatch, M.J. Hipfner, L. Slater, W.J. Sydeman, and Y. Watanuki. 2008. Forage fish of the Pacific Rim as revealed by diet of a piscivorous seabird: synchrony and relationships with sea surface temperature. Canadian Journal of Fisheries and Aquatic Sciences 65:1610-1622.

Thompson, S.A., M. García-Reyes, W.J. Sydeman, M.L. Arimitsu, S.A. Hatch, and J.F. Piatt. 2019. Effects of ocean climate on the length and condition of forage fish in the Gulf of Alaska. Fisheries Oceanography 28:658-671.

Vandersea, M.W., S.R. Kibler, P.A. Tester, K. Holderied, D.E. Hondolero, K. Powell, S. Baird, A. Doroff, D. Dugan, and R.W. Litaker. 2018. Environmental factors influencing the distribution and abundance of *Alexandrium catenella* in Kachemak bay and lower Cook Inlet, Alaska. Harmful Algae 77:81-92.

Van Hemert, C., S.K. Schoen, R.W. Litaker, M.M. Smith, M.L. Arimitsu, J.F. Piatt, W.C. Holland, D.R. Hardison, and J.M. Pearce. 2020. Algal toxins in Alaskan seabirds:

Evaluating the role of saxitoxin and domoic acid in a large-scale die-o ff of Common Murres. Harmful Algae 92:101730.

von Biela, V.R., M.L. Arimitsu, J.F. Piatt, B.M. Heflin, S.K. Schoen, J.L. Trowbridge, and C.M. Clawson. 2019a. Pacific sand lance energy density, length, and age, Prince William Sound, Alaska 2012-2016: U.S. Geological Survey data release, https://doi.org/10.5066/P96N5PVE.

von Biela, V.R., M.L. Arimitsu, J.F. Piatt, B. Heflin, S.K. Schoen, J.L. Trowbridge, and C.M. Clawson. 2019b. Extreme reduction in nutritional value of a key forage fish during the pacific marine heatwave of 2014-2016. Marine Ecology Progress Series 613:171-182.

Waite, J.N., and F.J. Mueter. 2013. Spatial and temporal variability of chlorophyll- a concentrations in the coastal Gulf of Alaska , 1998 – 2011 , using cloud-free reconstructions of SeaWiFS and MODIS-Aqua data. Progress in Oceanography 116:179-192. Elsevier Ltd.

Walsh, J.E., R.L. Thoman, U.S. Bhatt, P.A. Bieniek, B. Brettschneider, M. Brubaker, S. Danielson, R. Lader, F. Fetterer, K. Holderied, K. Iken, A. Mahoney, M. McCammon, and J. Partain. 2018. The High Latitude Marine Heat Wave of 2016 and Its Impacts on Alaska. Bulletin of the American Meteorological Society 99:S39-S43.

Weingartner, T.J., S.L. Danielson, and T.C. Royer. 2005. Freshwater variability and predictability in the Alaska Coastal Current. Deep Sea Research Part II: 52:169-191.

This page intentionally left blank.

CHAPTER 4 ECOSYSTEM RESPONSE TO A PROLONGED MARINE HEATWAVE IN THE GULF OF ALASKA

Robert M. Suryan[1], Mayumi Arimitsu[2], Heather Coletti[3], Russell R. Hopcroft[4], Mandy R. Lindeberg[1], Sonia Batten[5], Mary Anne Bishop[6], Rich Brenner[7], Rob Campbell[6], Dan Cushing[8], Seth Danielson[4], Dan Esler[9], Tom Gelatt[10], Scott Hatch[11], Stormy Haught[12], Kris Holderied[13], Katrin Iken[4], David Irons[14], David Kimmel[10], Brenda Konar[4], Kathy J. Kuletz[14], Ben Laurel[15], John M. Maniscalco[16], Craig Matkin[17], Caitlin McKinstry[6], Daniel Monson[9], John Moran[1], Dan Olsen[17], Scott Pegau[6], John Piatt[9], Lauren Rogers[10], Anne Schaefer[6], Jan Straley[18], Katherine Sweeney[10], Marysia Szymkowiak[1], Benjamin Weitzman[13], James Bodkin[9], and Stephani Zador[10]

[1]NOAA Alaska Fisheries Science Center, Juneau, Alaska rob.suryan@noaa.gov
[2]U.S. Geological Survey Alaska Science Center, Juneau, Alaska
[3]National Park Service, Fairbanks, Alaska
[4]University of Alaska Fairbanks, Fairbanks, Alaska
[5]Marine Biological Association, Nanaimo, BC, Canada
[6]Prince William Sound Science Center, Cordova, Alaska
[7]Alaska Department of Fish and Game, Juneau, Alaska
[8]Pole Star Ecological Research LLC, Anchorage, Alaska
[9]U.S. Geological Survey Alaska Science Center, Anchorage, Alaska
[10]NOAA Alaska Fisheries Science Center, Seattle, Washington
[11]Institute for Seabird Research and Conservation, Anchorage, Alaska
[12]Alaska Department of Fish and Game, Cordova, Alaska
[13]NOAA National Ocean Service, Homer, Alaska
[14]U.S. Fish and Wildlife Service, Anchorage, Alaska
[15]NOAA Alaska Fisheries Science Center, Newport, Oregon
[16]Alaska SeaLife Center, Seward, Alaska
[17]North Gulf Oceanic Society, Homer, Alaska
[18]University of Alaska Southeast, Sitka, Alaska

Abstract

The northeast Pacific marine heatwave (PMH) that began during the winter of 2013-14 and persisted for two years was the longest lasting heatwave globally over the past decade. By 2017, some physical metrics of the PMH began to dissipate throughout the Gulf of Alaska; however, the hiatus was short-lived and another heatwave re-intensified in fall-2018. Our analysis of 113 time series of biological metrics from the northern Gulf of Alaska demonstrates the degree to which this event coincided with abrupt changes in abundance and performance metrics of diverse taxa from lower to upper trophic levels and nearshore intertidal to offshore oceanic domains. The common trend among our time series from dynamic factor analysis indicated an abrupt change across metrics during the PMH with little recovery in the years following. Approximately half of the time series examined showed a significant response during the heatwave. The direction of response among time series, however, varied greatly by taxa. Whereas some metrics trended back toward long-term mean values during the heatwave hiatus, others did not. Taxa ranging from lower trophic level consumers to upper trophic level predators remained far from pre-PMH

values through the hiatus and up to at least 4 years after the onset of the PMH. Furthermore, our suite of Gulf of Alaska biological metrics showed distinct community-level groupings relative to at least a decade prior to the PMH. Since the beginning of the PMH, the Gulf of Alaska has experienced five of the ten warmest summers over the past 119 years. Given this multi-year warming coupled with anticipated increases in marine heatwaves under current climate projections, it remains uncertain when or if the Gulf of Alaska ecosystem will return to a pre-PMH state.

INTRODUCTION

Understanding how marine ecosystems respond to cyclical vs. linear environment change, or their additive effects, is a key challenge in marine ecology and resource management. Marine biological regime shifts (Overland et al. 2008) of various magnitudes have been documented globally (Chavez et al. 2003, Beaugrand et al. 2015). The Gulf of Alaska (GOA) has undergone one well defined and sustained ecosystem regime shift (Anderson and Piatt 1999, Hare and Mantua 2000), and several others that were less evident and did not persist (Batten and Welch 2004, Litzow 2006, Hatch 2013). Regime shifts in large marine ecosystems such as the GOA are often associated with basin scale climate variables (Beaugrand et al. 2015) such as the Pacific Decadal Oscillation (PDO; Mantua et al. 1997), El Niño Southern Oscillation (ENSO; Cane and Zebiak 1985), or North Pacific Gyre Oscillation (NPGO; Di Lorenzo et al. 2008). The strength or direction of these climate-biology relationships, however, can vary through time (Bond et al. 2003, Litzow et al. 2018).

It is reasonable to think that as a physical climate indicator, such as the PDO, returns back to a previous state, the ecosystem might respond by also switching to a previous state, but this is not always the case (Hare and Mantua 2000). Examples of such expectations come from the northeast Pacific (Peterson and Schwing 2003, Hatch 2013) where key indicators began trending back toward a previous state, but ultimately were not sustained (Litzow and Mueter 2014). These unexpected occurrences are in part a result of time varying climate-biology relationships (Litzow et al. 2019, Puerta et al. 2019). Given recent trends in global climate patterns (IPCC 2019), it is becoming more likely that current and future transitions may not shift back to prior regimes, but instead may produce novel ecosystem states.

A key driver in the occurrence of contemporary novel climate states are marine heatwaves. Marine heatwaves are becoming more frequent and of greater intensity worldwide (Oliver et al. 2018). Since 2012, there has been an increase from 30% to nearly 60% of global oceans experiencing severe heatwaves and the breadth of their impact is evidenced by a two order of magnitude increase in scientific publications on marine heatwaves during the past decade (Hobday et al. 2018). There has also been an increase in documentation of disturbance to marine ecosystems, biodiversity, and ecosystem services associated with marine heatwaves (Smale et al. 2019).

The northeast Pacific marine heatwave (PMH) that peaked in 2015 was particularly notable in lasting two years (Di Lorenzo and Mantua 2016), it was the only marine heatwave lasting through all four seasons, and 2-10 times longer than any other heatwave recorded globally in the past decade (Hobday et al. 2018). In mid-2016, the PMH began to dissipate, based on sea surface

temperature data (National Oceanic and Atmospheric Administration Optimum Interpolation V2) used by Hobday et al. (2018). Whereas *in situ* sea surface temperatures in some areas of the GOA did trend back toward pre-PMH conditions (Figure 4-1), water column and bottom temperature anomalies remained strongly positive (Figure 4-1; Jackson et al. 2018). The hiatus in the surface expression of the PMH, however, was short-lived and the warming re-intensified in late-2018 into fall 2019 (Figure 4-1; Cornwall 2019).

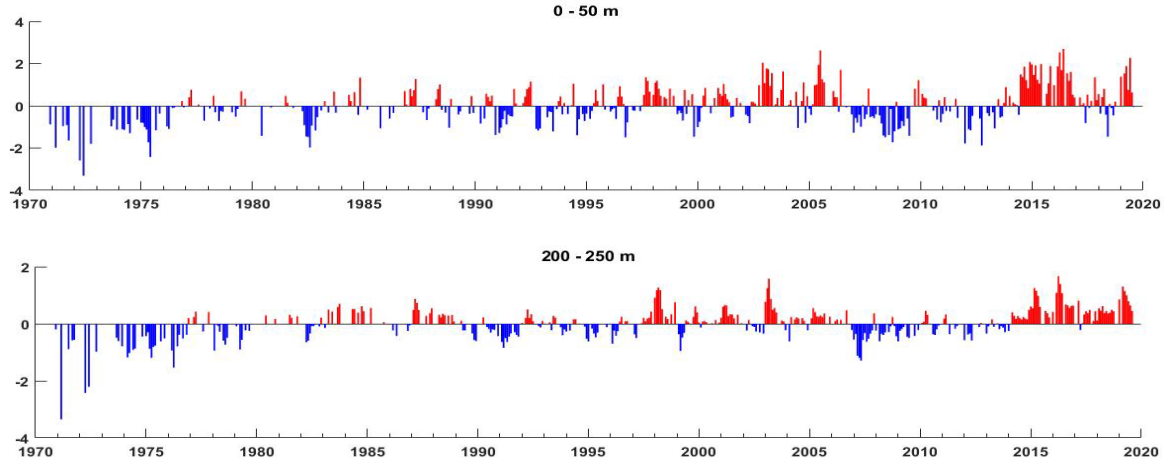

Figure 4-1. Anomalies (°C) of upper (0-50m) and lower (200-250 m) water column temperatures at the GAK1 oceanographic station in the Gulf of Alaska (for location, see Figure 4-2). The multi-year heatwave that began in 2014 was the most persistent in the 48-year time series and it extended throughout the water column of the continental shelf.

Initial biological responses, both positive and negative, to the 2014-2016 PMH were diverse, occurring throughout the North Pacific and including species range shifts (Sutherland et al. 2018), changes in lower trophic level community composition (Batten et al. 2018, Brodeur et al. 2019), predator mortality events (Jones et al. 2018, Harvell et al. 2019), and effects on commercial industries (Wade et al. 2019). Effects of the PMH were felt throughout Alaska (Walsh et al. 2018) and one of the largest marine bird mortality events occurred in the northern GOA (Piatt et al. 2020), a region of intensive, long-term marine studies.

We used more than 100 time series of annual, biological metrics including abundance (e.g., biomass) to performance (e.g., reproductive success) from the northern GOA representing trophic levels from zooplankton to commercial fisheries and including marine habitats from intertidal to oceanic to assess how the northern GOA ecosystem responded to a contemporary marine heatwave that was unparalleled in magnitude during the post-industrial age in terms of intensity and duration. We assessed: (1) how the biological community responded as a whole, (2) which taxa exhibited negative, positive, or neutral responses, and (3) whether taxa showed signs of recovery 4 years after the onset and 3 years after the peak intensity of the PMH.

METHODS

Biological time series (n=113) within our northern GOA study area (Figure 4-2) were obtained from several long-term research and monitoring programs in the region (Tables 4-1 and A1). A

single time series represented an annual measurement or mean value spanning at least 7 years from a single location or region. Although many time series were neither randomly selected nor consistent in spatial extent, they broadly represented examples of how lower to upper trophic level ecosystem components responded during the PMH in the northern GOA. Furthermore, only spatially replicated metrics (e.g., zooplankton, intertidal organisms, marine birds and mammals) were used to address potential spatial variability in response in the eastern versus western study area (Figure 4-2).

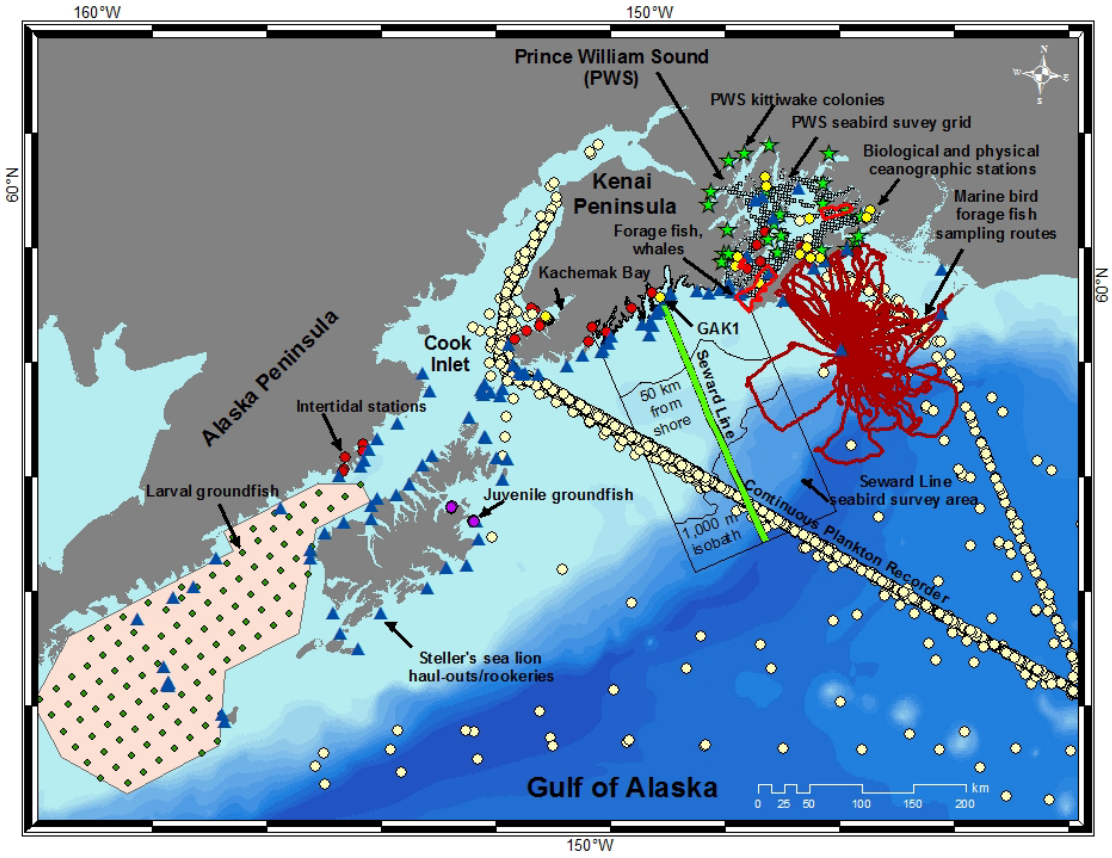

Figure 4-2. Sampling locations in the northern Gulf of Alaska. The division for references to eastern and western study area is the continuous plankton recorder transect into Cook Inlet. The black contours within the Seward Line marine bird survey area differentiate inner continental shelf (shore to 50 km from shore), middle shelf (50 km from shore to shelf-slope break, defined using 1,000 m isobath) and oceanic (seaward of the 1,000 m isobath) domains (Sousa et al. 2016). The 1,000 m isobath is also used to distinguish shelf vs. oceanic zooplankton samples from the continuous plankton recorder. Marine bird (black-legged kittiwake, rhinoceros auklet) foraging routes provided by Shannon Whelan, McGill University.

Time series varied in length from 6 to 49 years between 1971 and 2018 (Table A1). Different time series were used depending on the period of interest. For our primary analyses to assess GOA ecosystem response to the 2014-2016 PMH, we used all 113 time series from a 9-year

period (2010-2018), providing the most years pre-PMH while minimizing missing years in time series (n=8-9 years [82% of time series], n=5-7 years [18% of time series]). Missing values during the 2010-2018 period were due to either more recent start of a time series or alternate year sampling; however, all time series were initiated by 2012 and included years post 2012-2016 PMH. Most time series were collected by Gulf Watch Alaska, a long-term ecosystem monitoring program to assess environmental variability affecting recovery of injured resources following the *Exxon Valdez* oil spill in 1989. Additional analyses were conducted on a reduced number of time series that spanned longer time periods, 19-49 years, to assess biological trends during the 2014-2016 PMH relative to events of prior decades. Below we describe analytical approaches and general sample collection methods, see Table A1 for duration and frequency of sampling for each time series.

Table 4-1. Numbers and types of biological time series (n = 113 total) used to assess response to a marine heatwave in the Gulf of Alaska. Sources of time series include 74 from the Exxon Valdez *Oil Spill Trustee Council's Gulf Watch Alaska, 23 from National Oceanic and Atmospheric Administration Alaska Fisheries Science Center, 10 from Alaska Department of Fish and Game, 2 from the U.S. Fish and Wildlife Service, 2 from the Alaska SeaLife Center, and 2 from the* Exxon Valdez *Oil Spill Trustee Council's Herring Research and Monitoring program. See Table A1 for more details on time series metrics.*

Ecosystem Component	# of time series	Type
Zooplankton	14	abundance (n=10), size (n=4)
Intertidal	12	abundance
Forage fish	8	abundance (n=6), condition index (n=2)
Groundfish	16	early life stages (n=8), adult (n=8)
Marine birds	37	abundance (n=35), productivity (n=2)
Marine mammals	16	cetacean (n=3), pinniped (n=10), sea otter (n=3)
Commercial harvest (salmon)	10	quantity

DATA TREATMENT AND STATISTICAL ANALYSES

Annual arithmetic means were generated for all time series from seasonal or monthly means if multiple sampling events occurred throughout the year or from individual samples if sampling occurred during a single sampling period lasting shorter than a month. Metrics with skewed distributions of values varying by generally more than one order of magnitude were log transformed ($\log_{10}(x+1)$) prior to calculating annual (geometric) means and annual means were back transformed prior to analysis. Statistically significant periodic (e.g., seasonal) or secular (e.g., linear) trends in annual time series were removed to reduce potentially confounding patterns that could mask a PMH response. In these few cases, residual values were used in the final analyses. Data were processed using Matlab R2017b (The MathWorks, Natick, MA) and R v3.1.6 (R Core Team 2018)

We used dynamic factor analysis to identify the number and shape of trends that best describe common patterns in all time series (Zuur et al. 2003a). Dynamic factor analyses were conducted in R using the multivariate autoregressive state-space modeling package (Holmes et al. 2018a). We fit three model variance structures and three trends to the full set of 113 time series over a 9-year period that encompassed the PMH. Model variance structures that we tested included (1) same variance and covariance (R matrix specified as equalvarcov), (2) same variance and no covariance (diagonal and equal), and (3) different variance and no covariance (diagonal and unequal). We restricted the analysis to identifying a maximum of three trends to meet our objective of identifying potential common responses to the PMH, including a single response (positive or negative), multiple responses (e.g., change, then return to pre-PMH), and neutral or change not associated with the timing of PMH. We applied a z-score standardization to all time series prior to analysis and followed routine methods of fitting models outlined in Holmes et al. (2018b). A time series was considered associated with the common trend if factor loadings were > 0.20 (absolute value; Zuur et al. 2003b)

Whereas dynamic factor analysis identifies common trends sequentially across years, community analysis identifies which individual years, regardless of numeric sequence, are most similar or dissimilar in their 113 biological metrics. We conducted two community analyses, hierarchical cluster analysis and non-metric multidimensional scaling ordination (nMDS) using PRIMER v7 (PRIMER-e ltd, Quest Research Limited). The broad diversity in units and range of values in our 113 metrics warranted the use of normalized data (similar z-score noted above) and a resemblance matrix based on Euclidean distance, rather than the more typical square root transformation and Bray-Curtis similarity index when analyzing biological data with a common unit of measure (Clarke et al. 2014, Clarke and Gorley 2015). Stress for nMDS analysis was considered acceptable if < 0.20. We used a similarity profile routine in cluster analysis (999 permutations, $\alpha = 0.05$) and analysis of similarities in nMDS to test for significant differences among groups (Clarke et al. 2008, Clarke and Gorley 2015).

SAMPLE COLLECTION AND PROCESSING

Zooplankton and icthyoplankton

Zooplankton samples were collected using several sampling platforms. Continuous plankton recorders towed by commercial ships transiting through the study area to ports in Alaska and Asia collected samples throughout continental shelf and oceanic waters of the GOA (Figure 4-2; for more details see Batten et al. 2018). Research vessel-based net sampling was used to collect zooplankton samples in Prince William Sound (PWS) and Kachemak Bay. Samples were collected during spring through fall by using a 0.6 m bongo net (202 μm mesh) to a depth of 50 m or near bottom, whichever was shallowest (see McKinstry and Campbell 2018 for detailed methods). Metrics for zooplankton used in our analysis included overall zooplankton abundance, copepod community size index (Richardson et al. 2006), and the abundance of warm and cool water associated copepods, with warm species distinguished as *Calanus pacificus*, *Clausocalanus* spp., *Corycaeus anglicus*, *Ctenocalanus* spp., *Mesocalanus tenuicornis*, and *Paracalanus parvus*, and cool species as *Calanus marshallae*, *Pseudocalanus* spp., *Arcatia longiremis*, *Oithona similis*, *Neocalanus cristatus*, *N. flemingeri*, *N. plumchrus*, and *Eucalanus bungii* (Fisher et al. 2015).

Larval fishes were collected during oblique tows to a depth of 100 m or 10 m from the bottom by using 0.6 m bongo net (505 µm mesh) aboard research vessels in the western portion of our study area (Figure 4-2; see Matarese et al. 2003 and Laurel and Rogers 2020 for detailed methods). We included the larval abundance of four numerically dominant groundfish species (walleye pollock , *Gadus chalcogrammus*, Pacific cod, *Gadus macrocephalus*, northern rock sole, *Lepidopsetta polyxystra*, and southern rock sole, *L. bilineata*) and one forage fish species (Pacific sand lance, *Ammodytes personatus*) in our analysis.

Intertidal organisms

Rocky intertidal sampling was conducted at 21 sites in four regions across the northern GOA and included PWS, Kenai Peninsula (Kenai Fjords National Park), Kachemak Bay, and the Alaska Peninsula (Katmai National Park and Preserve). We selected a subsample of metrics to represent a primary producer (*Fucus distichus*), predators (sea stars, *Dermasterias imbricata*, *Evasterias troschelii*, *Pisaster ochraceus*, and *Pycnopodia helianthoides*), and prey (Pacific blue mussel, *Mytilus trossulus*) based on results from previous studies. See Weitzman et al. (Chapter 2, this report), Bodkin et al. (2018), and Konar et al. (2019) for detailed methods and analysis of rocky and mussel bed intertidal community changes during the PMH. We used percent cover of *Fucus* (# m^{-2} quadrat), counts of sea stars along a 50 m x 4 m transect (# 200 m^{-2}) at rocky intertidal sites, and density of large (>20 mm) mussels (# m^{-2} quadrat) at mussel bed sites. To standardize metrics among regions, *Fucus* was converted to normalized anomalies of percent cover, whereas sea stars and mussels were raw counts.

Forage fishes

We included juveniles and adults of three forage fishes (Pacific sand lance, Pacific capelin, *Mallotus catervarius*, and Pacific herring, *Clupea pallasii*) that, when available, support high productivity and abundance of marine bird and mammal predators within our northern GOA study area (Suryan and Irons 2001, Litzow et al. 2002, Harding et al. 2007, Hatch 2013, Moran et al. 2018). The relative availability of sand lance and capelin to predators was assessed by the biomass in diets of black-legged kittiwakes (*Rissa tridactyla*), a surface feeder, and rhinoceros auklets (*Cerorhinca monocerata*), a diving forager, that sample forage fishes from the nearshore to the offshore in our eastern study area (Figure 4-2; see Table A2 for results from subsequent analyses of marine bird diets in the western study area). Diet samples were collected during May – September from kittiwakes and auklets nesting on Middleton Island (Arimitsu et al. Chapter 3, this report).

We also included sand lance whole body energy content. Sand lance were collected by using purse seine, beach seine, herring jig, cast net, dip net, and gill net and whole-body energy determined using bomb calorimetry (see von Biela et al. 2019 for detailed methods). Samples were collected from PWS during July when annual body condition and lipid accumulation were highest (Robards et al. 1999) and would, therefore, potentially be most sensitive to change between PMH and non-PMH years.

We used cumulative annual miles days of milt from spawning adults in spring to represent herring abundance in PWS (Muradian et al. 2017) and scale growth from during the third year as an annual herring performance/condition index (Batten et al. 2016, Moffitt 2017).

Groundfish

In addition to larval groundfish abundance described above, we also included metrics for five species of juvenile and adult groundfish. The abundance of juvenile (age-0) walleye pollock, Pacific cod, and saffron cod (*Eleginus gracilis*) was estimated from 16 beach seine sites in two bays on eastern Kodiak Island (Figure 4-2). Trends in juvenile Pacific cod at these sites exhibit inter-annual variability that was consistent with sampling of larvae and future age-3 recruits sampled elsewhere in the GOA (Laurel and Rogers 2020). We determined juvenile (age-0) sablefish growth from samples from our eastern study area brought back to Middleton Island by nesting rhinoceros auklets. The annual growth index represents changes in size of juvenile sablefish from June to August of each year. We used stock assessment model output for estimates of walleye pollock age-1 recruit biomass and female spawning stock biomass (Dorn et al. 2018), Pacific cod age-1 recruit biomass and female spawning stock biomass (Barbeaux et al. 2018), and arrowtooth flounder age-1 recruit and age-1+ biomass (Spies and Palsson 2018).

Marine birds

Marine bird colony metrics that we included were abundance of breeding pairs of black-legged kittiwakes at 44 colony sites from throughout PWS (Figure 4-2) and reproductive success (chicks fledged pair^{-1}) of kittiwakes at these sites and Middleton Island. Annual estimates of kittiwake nesting abundance were summed for all colonies in PWS and annual reproductive success was first calculated for each colony as a whole, then averaged among colonies in PWS and among nest sites at the Middleton Island colony (for more details see Suryan and Irons 2001, Hatch 2013).

Marine bird abundance at sea was determined by using strip transect surveys from aboard small vessels (< 8 m) conducting alongshore transects adjacent to the Alaska Peninsula and Kenai Peninsula intertidal study sites described above, from transects within PWS, and aboard large vessels (> 36 m) along the Seward Line between oceanographic sampling stations and transits within the region depicted in Figure 4-2. Survey strip widths were 200 m on small vessels (two observers, 100 m each side of vessel) and 300 m on large vessels (one observer, 300 m one side of vessel). We included time series of summer marine bird abundance for five species from alongshore transects adjacent to the intertidal sites: black oystercatcher (*Haematopus bachmani*), *Brachyramphus* murrelets (marbled murrelet, *B. marmoratus*, and Kittlitz's murrelet, *B. brevirostris*), common murre (*Uria aalge*), pigeon guillemot (*Cepphus columba*), and harlequin duck (*Histrionicus histrionicus*). We included two time series each for fall (November and December) and winter (February and March) abundance of common murres and *Brachyramphus* murrelets in PWS. For Seward Line bird surveys in the GOA, we included time series from six species, in three oceanographic domains (inner continental shelf, middle shelf, and oceanic; see Figure 4-2 for boundaries), and two seasons, spring (May) and fall (September). Not all possible species-season-domain combinations were included; instead, we selected the season-domain combinations for when the selected species were most abundant. We selected the species that best represented the different domains and their primary foraging guilds, which included common murre (shelf associated diving piscivore), black-legged kittiwake (shelf associated surface feeding piscivore), sooty shearwater (*Ardenna grisea*; oceanic and outer shelf associated diving planktivore/omnivore), black-footed albatross (*Phoebastria albatrus*; outer shelf-oceanic

associated surface feeding piscivore), northern fulmar (*Fulmarus glacialis*; outer shelf-oceanic associated surface feeding omnivore), and fork-tailed storm-petrel (*Oceanodroma furcata*; outer shelf-oceanic associated surface feeding planktivore).

All data were summarized to the same density metric of # km^{-2}. For more details on specific methods see Coletti et al. (2018) and Bodkin (2011) for alongshore transects adjacent to intertidal sampling sites, Stocking et al. (2018) for PWS surveys, and Kuletz and Labunski (2017) for Seward Line surveys.

Marine mammals

Sea otter (*Enhydra lutris*) energy recovery rate during foraging was obtained at three of the four intertidal sampling regions, Alaska Peninsula, Kenai Peninsula, and PWS. Annual energy recovery rate for each region was obtained from direct observations of foraging bouts of individual otters during summer daylight hours and are a product of foraging dive length, interval between dives, proportion of dives where food was obtained and energy density of prey and reported as kcal min^{-1} (for more detailed methods see Coletti et al. 2016).

Pinniped abundance time series were generated by using multiple methods. Alongshore, vessel-based surveys for Steller sea lions (*Eumetopias jubatus*) and harbor seals (*Phoca vitulina*) were conducted during small vessel strip transect surveys described above for birds adjacent to intertidal sampling sites on the Alaska Peninsula and Kenai Peninsula. Densities were calculated as # km^{-2} from strip transect surveys (Coletti et al. 2018). Annual abundance of Steller sea lion pups and older age classes (hereafter "non-pups") were also obtained from Chiswell Island, a single index site off the Kenai Peninsula in the eastern half of our study area. Remote cameras placed on this rookery were used to count pups and non-pups throughout the breeding season (Maniscalco et al. 2014). A third, population-wide metric of Steller sea lion abundance was generated from aerial surveys of all haul-out sites and rookeries (including Chiswell Island) throughout our study area (Figure 4-2). Direct counts were conducted via observers in fixed-wing aircraft during summer. A custom-built model (agTrend) was used to estimate total population size based on raw counts from aerial surveys and accounting for missed survey sites due to events such as inclement weather (for more detailed methods see Sweeney et al. 2017).

Surveys of humpback whale (*Megaptera novaeanglaie*) in PWS were conducted during fall when whales are targeting prey populations, especially herring, prior to their southbound migration to low latitude breeding and calving grounds. Observers aboard vessels count and individually identify whales based on fluke photographic identification to generate an encounter rate metric of number of unique whales per day (for more detailed methods see Straley et al. 2018).

Time series of metrics for killer whales (*Orcinus orca*) included encounter rate, and number of animals per encounter. We used data from vessel-based surveys conducted during September and October in Montague Straight and lower Knight Island Passage, the western region and entrance to PWS (for more detailed methods see Olsen et al. 2018).

Commercial salmon harvest

We used salmon harvest metrics from two regions in our study area, Kodiak Island in the western portion of our study area and PWS-Copper River in the eastern portion. The metric used in our analysis was weight (lbs) of commercial harvest of wild and hatchery-reared Chinook (*Oncorhynchus tshawytscha*), coho (*O. kisutch*), sockeye (*O. nerka)*, pink (*O. gorbuscha)* and chum salmon (*O. keta)*. Harvest metrics were compiled by the Alaska Department of Fish and Game (ADFG 2018).

RESULTS

DYNAMIC FACTOR ANALYSIS

Of the nine models evaluated, the model with the lowest AICc included equal variance and covariance structure and one common trend (Table 4-2). The common trend line shows a steep decline starting in 2014 coincident with the PMH and continuing through 2017 with a slight increase in 2018, but remaining well below pre-PMH levels (Figure 4-3).

Table 4-2. Model results from dynamic factor analysis of 113 biological time series spanning 2010-2018 and encompassing the 2014-2016 northeast Pacific marine heatwave. The top five ranking models are shown based on ΔAICc. A total of nine models were run that included three different variance structures for the R matrix and three possible trends for each variance structure.

R	# of trends	logLik	K	ΔAICc
same variance and covariance	1	-1097.97	115	0.0
same variance, no covariance	1	-1100.94	114	3.3
same variance and covariance	2	-974.578	227	94.0
same variance, no covariance	2	-979.929	226	101.1
different variance, no covariance	1	-1054	226	249.3

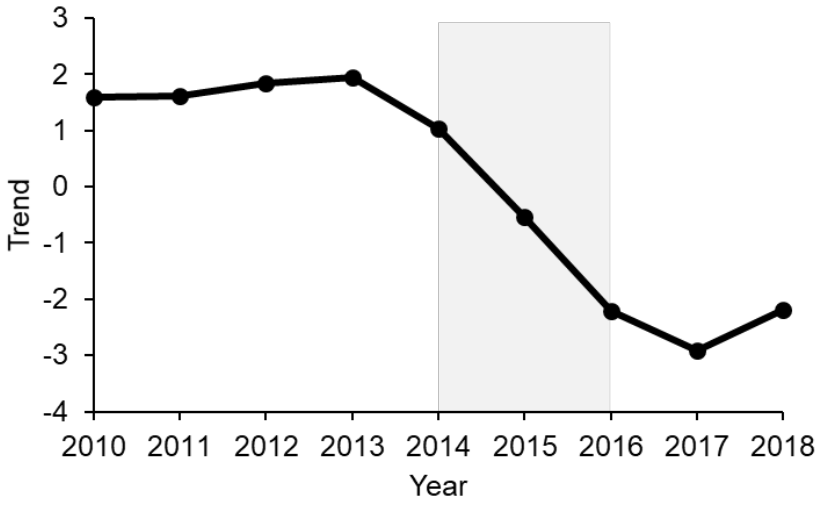

Figure 4-3. The common trend from the best model fit (lowest AICc; Table 4-2) identified from dynamic factor analysis of 113 biological time series including abundance (e.g., biomass) and performance (e.g., reproductive success) metrics. Grey shading represents the 2014-2016 northeast Pacific marine heatwave.

Approximately half of the time series (n = 64, 57%) had factor loadings indicating a strong negative or positive relationship to the trend line ($\geq$ 0.20, absolute value), whereas the other half (n = 49, 43%) of time series had marginal or weak factor loadings (< 0.20, absolute value) and were identified as a "neutral" response (Tables 4-3 and A1). The direction of response among time series, however, varied greatly by taxa. Taxa with a majority of negative responses were intertidal organisms (58%), forage fish (50%), marine bird metrics for breeding colonies (100%), and marine mammals (50%; Table 4-3). Zooplankton metrics primarily (93%) had positive (e.g., warm water associated species) or neutral (e.g., cool water associated species and copepod size) response and groundfish responses were evenly distributed among negative (31%), positive (31%), and neutral (38%). Marine bird abundance at-sea and salmon harvest metrics primarily exhibited neutral responses (65% and 70%, respectively; Table 4-3).

Table 4-3. Summary of trends based on factor loadings from dynamic factor analysis by taxa and metric of 113 biological time series. Time series are described as having a positive, negative, or neutral response coincident with the 2014-2016 Pacific marine heatwave. Each time series was identified as having a negative, positive, or neutral trend when factor loadings were ≥ 0.20, ≤ -0.20, or > -0.20 and < 0.20, respectively. The signs of factor loadings are opposite of time series trend because factor loadings describe how a given time series relates to the common trend, which was a negative during the Pacific marine heatwave (Figure 4-3). See Table A1 for factor loadings of individual time series.

Taxa and metric	Negative n (%)	Positive n (%)	Neutral n (%)
Zooplankton	1 (7%)	8 (57%)	5 (36%)
cool		1	3
warm		4	
all		2	
size	1	1	2
Intertidal	7 (58%)	3 (25%)	2 (17%)
algae	4		
invertebrates	3	3	2
Forage fish	4 (50%)	3 (38%)	1 (13%)
abundance	3	3	
performance/condition	1		1
Groundfish	5 (31%)	5 (31%)	6 (38%)
early life stage	3	3	5
adult	2	2	1
Marine birds	9 (24%)	6 (16%)	22 (59%)
colony	3		
at-sea	6	6	22
Marine mammals	8 (50%)	2 (13%)	6 (38%)
otters	1		2
pinnipeds	4	2	4
whales	3		
Commercial salmon harvest	2 (20%)	1 (10%)	7 (70%)
Chinook	1		1
coho		1	1
sockeye	1		1
pink			2
chum			2
Grand Total	**36**	**28**	**49**

Taxa with primarily negative responses

The negative trends in abundance of intertidal taxa were remarkably consistent among sampling areas throughout the northern GOA. Algal (*Fucus*) cover declined precipitously with some variability in timing in all areas (Figure 4-4). Similarly, the abundance of sea stars, key intertidal

predators, declined precipitously after the onset of the PMH in all areas except Kachemak Bay. In contrast, the abundance of mussels, a main sea star prey item, increased in most areas (Figure 4-4, Table A1).

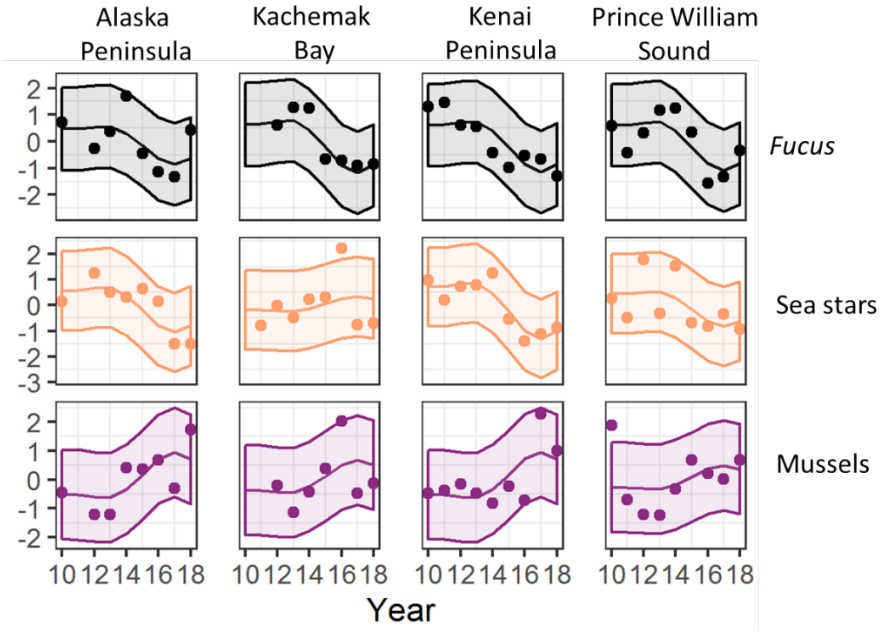

Figure 4-4. Mainly negative trends in algal and sea star (upper and middle panels) and mainly positive trends in mussel abundance (lower panel) at four regions across the northern Gulf of Alaska. Points are annual values, middle solid line is model fit to data, and shaded area is 95% confidence interval of model fit. Values are z-score standardizations so the y-axes are unitless.

Trends in the abundance of two forage fish species, capelin in the GOA and herring in PWS, decreased markedly and remained at consistently low values after the onset of the PMH (Figure 4-5). The decline in capelin was evident in diets of both surface feeding and diving birds. The abundance of sand lance larvae and juveniles showed an opposite trend of marked increase during the PMH. Performance metrics, however, of both age-3 herring growth and age-1 sand lance whole body energy decreased during the PMH (Figure 4-5).

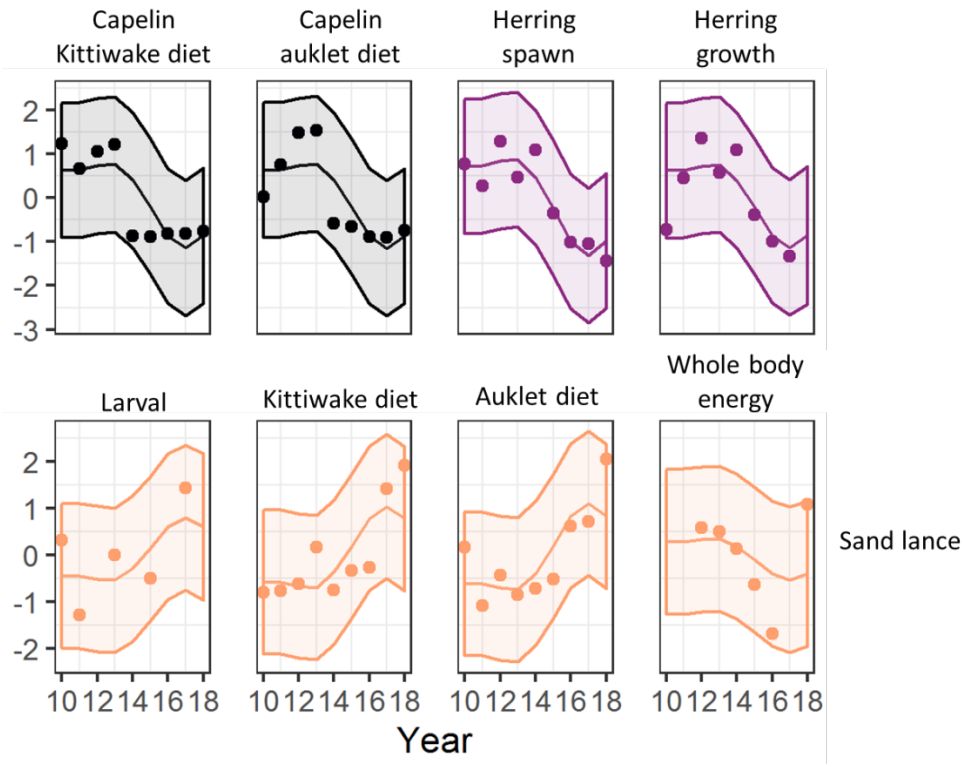

Figure 4-5. Negative trends in abundance of juvenile capelin from surface feeding (kittiwake) and diving (auklet) marine bird diets in the eastern portion of the northern Gulf of Alaska and herring abundance and growth in Prince William Sound (PWS; upper panel). Positive trends in abundance of larval and juvenile Pacific sand lance from western and eastern study areas, respectively, and negative trend in whole body energy content of sand lance in PWS (lower panel). Points are annual values, middle solid line is model fit to data, and shaded area is 95% confidence interval of model fit. Values are z-score standardizations so the y-axes are unitless.

Marine bird colony metrics and mammal abundance trends were primarily negative during the PMH. The abundance of kittiwake nests in PWS and breeding success in PWS and Middleton Island all declined, along with Steller sea lion pup counts on rookeries from throughout our northern GOA study area (Figure 4-6). Parallel declines also occurred for combined adult, sub-adult, and juvenile sea lions ("non-pups") in the eastern portion of our study area, but not the western (Figure 4-8). Interestingly, black-legged kittiwake breeding success and the abundance of sand lance and capelin to marine birds also did not decline in the west, like they did in the east. Although, the abundance and reproductive success of common murres (no data from west) did show a strong negative response, consistent with kittiwakes in the west (Table A2). Humpback and killer whale abundance (indexed by encounter rate) and killer whale group size in the PWS region also declined after the onset of the PMH (Figure 4-6).

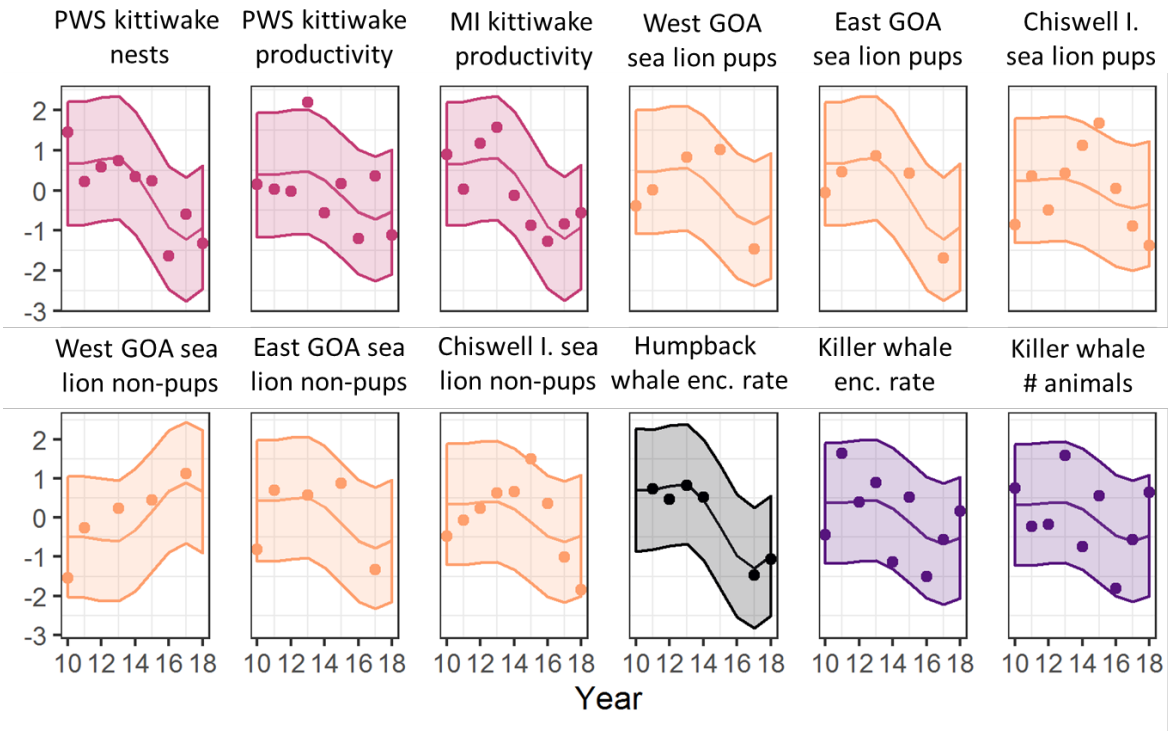

Figure 4-6. Negative trends in the abundance of kittiwake nests in Prince William Sound (PWS), kittiwake reproductive success in PWS and Middleton Island (MI), and Steller sea lion pup counts on rookeries throughout the northern Gulf of Alaska (GOA; upper panel). Negative trends (with one exception) in abundance of Steller sea lion non-pups at haul-out sites and rookeries from throughout the northern GOA and humpback and killer whale abundance indices in and adjacent to PWS (lower panel). Points are annual values, middle solid line is model fit to data, and shaded area is 95% confidence interval of model fit. Values are z-score standardizations so the y-axes are unitless.

Taxa with primarily positive responses

Zooplankton abundance trends were primarily positive or neutral during the PMH, in contrast to the generally negative trends in intertidal organisms, forage fishes, breeding birds, and mammals. Warm water associated zooplankton species increased markedly during the 2014-2016 marine heatwave, with the increase most distinct in continental shelf waters and in Kachemak Bay and PWS, and less so in oceanic waters (Figure 4-7). There was some variation in the timing of increase among domains; however, most anomalies stayed positive even as the upper water column cooled in 2017 and finally returned to pre-heatwave conditions in 2018. Surprisingly, the abundance of cool water associated zooplankton did not show a consistent declining trend regardless of domain, but instead generally no trend or a temporary increase (Figure 4-7).

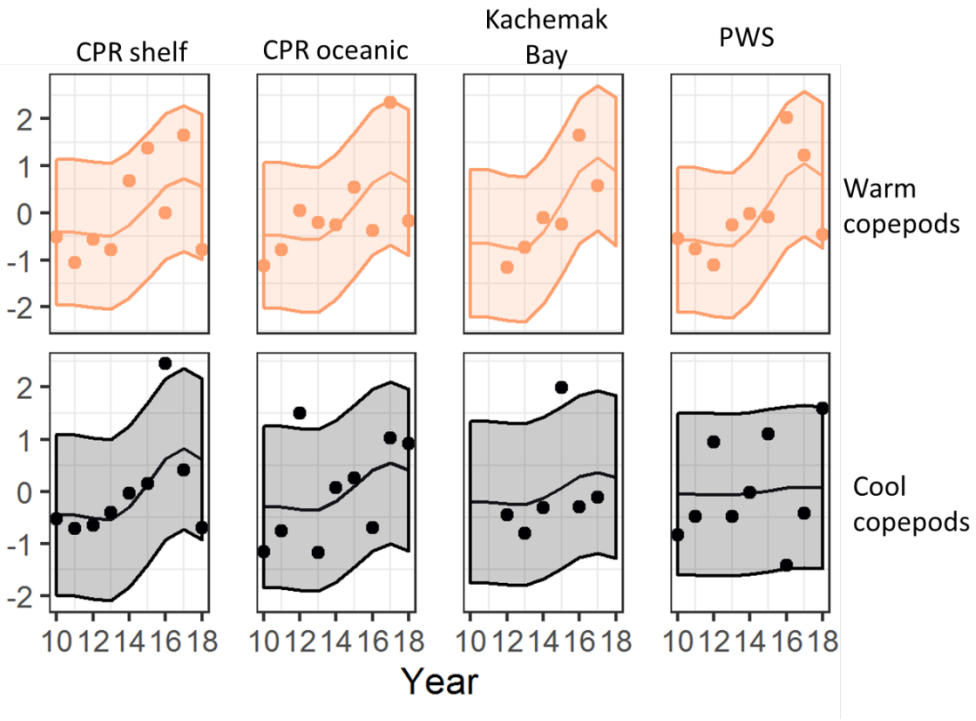

Figure 4-7. Standardized abundance of warm water (upper panel) and cool water (lower panel) associated copepod species from continuous plankton recorder (CPR) over oceanic and shelf waters and inside waters of Kachemak Bay and Prince William Sound (PWS). Points are annual values, middle solid line is model fit to data, and shaded area is 95% confidence interval of model fit. Values are z-score standardizations so the y-axes are unitless.

Taxa with primarily mixed or neutral responses

Taxa that exhibited mixed or neutral trends during the PMH included salmon, groundfish, and bird abundance at-sea. Chinook catch for Kodiak and sockeye catch for the PWS and Copper River area were the only two salmon harvest indices that had a negative trend coincident with the PMH. Trends in groundfish model output were also negative for Pacific cod female spawning stock biomass and arrowtooth flounder (Figure 4-8). In contrast, trends were positive during or post-PMH for coho salmon catch and juvenile walleye pollock around Kodiak, and juvenile sablefish growth in our eastern GOA study area and sablefish age-2+ biomass throughout the GOA (Figure 4-8).

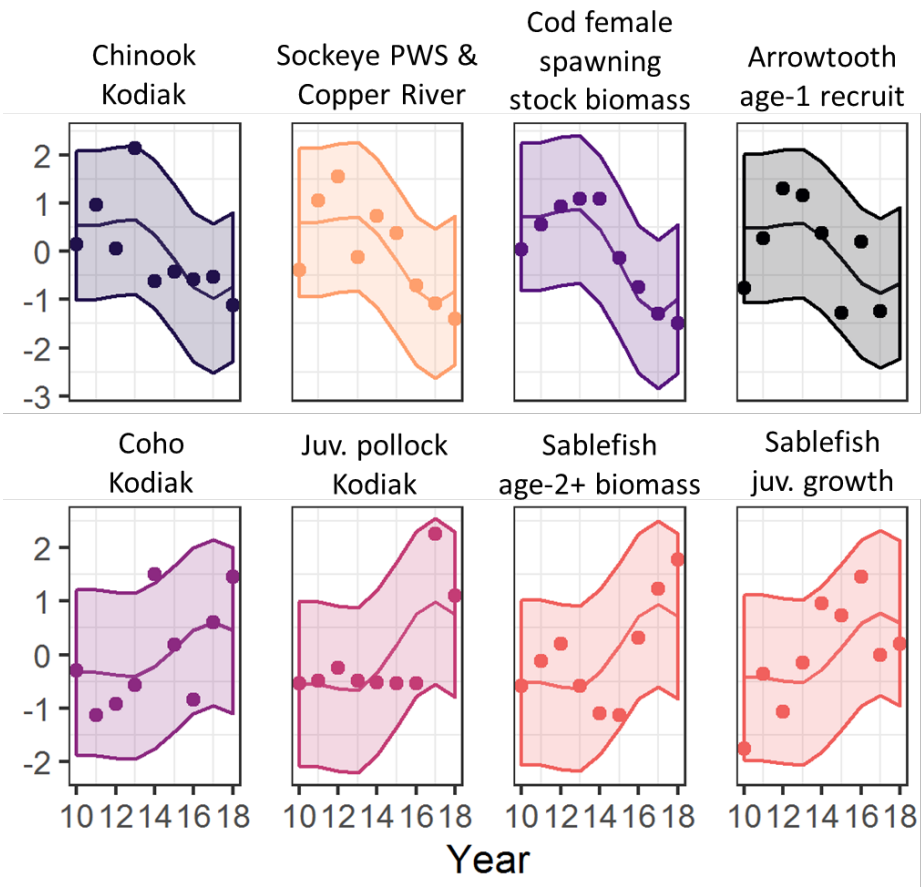

Figure 4-8. Contrasting negative (upper panel) and positive (lower panel) trends in various salmon and groundfish metrics during and after the 2014-2016 Pacific marine heatwave. Points are annual values, middle solid line is model fit to data, and shaded area is 95% confidence interval of model fit. Values are z-score standardizations so the y-axes are unitless.

Marine bird abundance at sea showed more short-term, annual variation, such as an influx of common murres and northern fulmars into PWS or the middle and inner shelf during the PMH (Figure 4-9). There was also an influx of fork-tailed storm-petrels into the inner shelf and away from the oceanic domain; however, the shift in storm-petrel distribution persisted for multiple years (Figure 4-9).

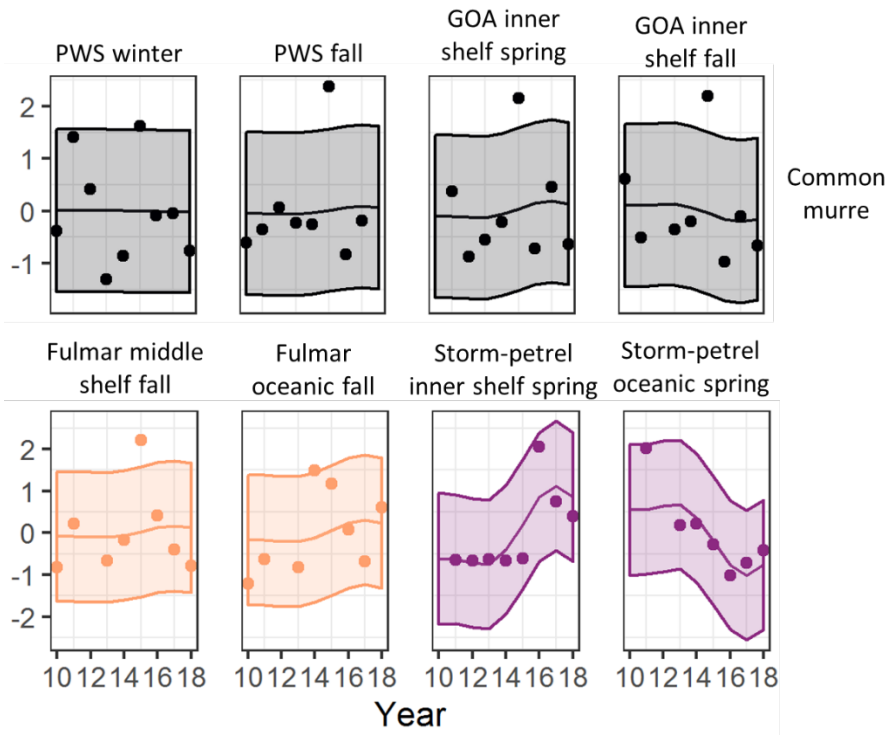

Figure 4-9. Marine bird abundance at sea exhibited primarily short-term, annual changes in Prince William Sound (PWS) and the Gulf of Alaska (GOA), including inshore shifts in distribution for common murres (primarily piscivores, upper panel) and northern fulmars (omnivores, lower panel). Only fork-tailed storm-petrels (primarily zooplanktivore) showed a persistent change in distribution (lower panel). Points are annual values, middle solid line is model fit to data, and shaded area is 95% confidence interval of model fit. Values are z-score standardizations so the y-axes are unitless.

Community Analysis

Annual patterns in the combined community composition of our 113 time series of the GOA ecosystem showed distinct groupings of before and after the onset of the PMH in both the cluster and nMDS analyses. Whereas years were more tightly clustered before the PMH (2010-2013), a period of relatively cold ocean temperatures (Figure 4-1), there was greater distance among years after the onset of the PMH (2015-2018). Cluster analysis differentiated the 9-year period before, during and after the PMH into three significantly different groups (similarity profiles, $p < 0.05$), 2010-2014, 2015, and 2016-2018 (Figure 4-10). A similar before-after PMH pattern was observed in the nMDS analysis, except that only two significantly different groups ($R = 0.815$ with all possible permutations) were identified, 2010-2015 and 2016-2018 (Figure 4-10).

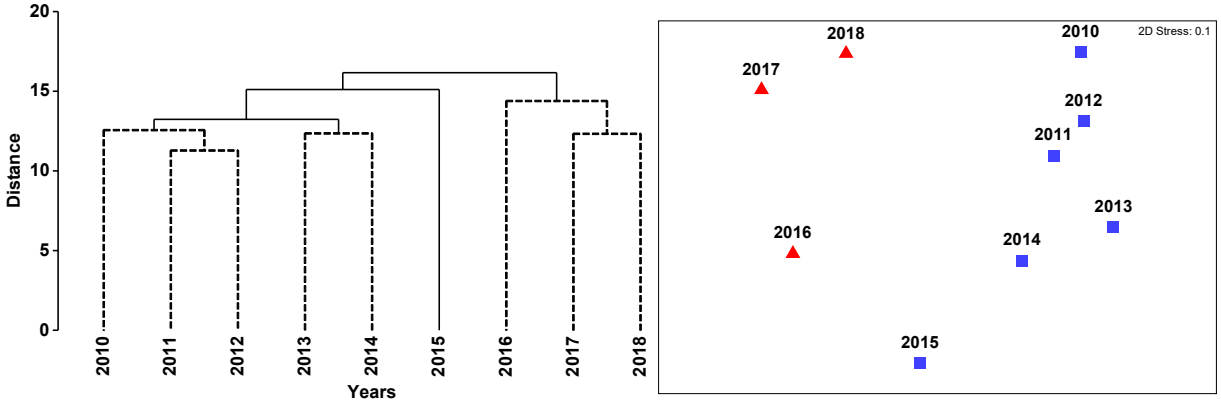

Figure 4-10. Cluster and community (nMDS) analyses of all biological time series combined prior to and during (strongest from 2014-2016) a multi-year marine heatwave in the Gulf of Alaska. In the cluster analysis (left) solid lines indicate significantly (similarity profile routine) different year groupings. In the nMDS (right) the different colors represent significantly (analysis of similarities) different year groupings.

Additional analyses confirmed that these results were not affected by missing values (0-20% of time series had missing values in any one year from 2010-2018) or in using a reduced length of time series. Rerunning the analyses with a reduced data set of 93 time series with no missing values during 2013-2018 (some time series initiated before 2012, were not sampled in 2012) resulted in only one less year grouping in the cluster analysis, but no difference in results with respect to before and after the PMH.

LONGER TIME SERIES PERSPECTIVE

Our time series that extend for decades prior to the PMH demonstrate that biological response in the northern GOA to this recent event was indeed anomalous. For example, we repeated our cluster analysis on a reduced number (n = 93) of our biological time series that spanned a 19-year period prior to, during, and after the 2014-2016 PMH. These longer time series confirm that 2016-2018, in particular, are distinct from the previous 16 years (Figure A1). Other examples include the abundance of warm water associated zooplankton, which had also increased during some previous warm periods in the GOA (e.g., 2003-2007), but not all (e.g., 1998 [prior to zooplankton time series shown], 2001, 2010), and not in magnitude or duration that was observed during the PMH (Figure 4-11). Likewise, for more than two decades the abundance of Pacific herring, humpback whales, and nesting black-legged kittiwakes varied between periods of warm and cold, but all exhibited a precipitous decline and remained low after the onset of the PMH (Figure 4-11). This was similarly true with the availability of sand lance and capelin to both surface feeding and diving birds foraging from Middleton Island, with the decline notably consistent among all metrics and persistent after the onset of the PMH (Figure 4-11), and unlike previous years of warm and cool periods. Reduction in the availability of capelin in the eastern GOA negatively affects the reproductive success of black-legged kittiwakes at Middleton Island, even at times when sand lance are available as alternative prey (Figure 4-11). Sablefish was one of the species showing a positive response after the onset of the

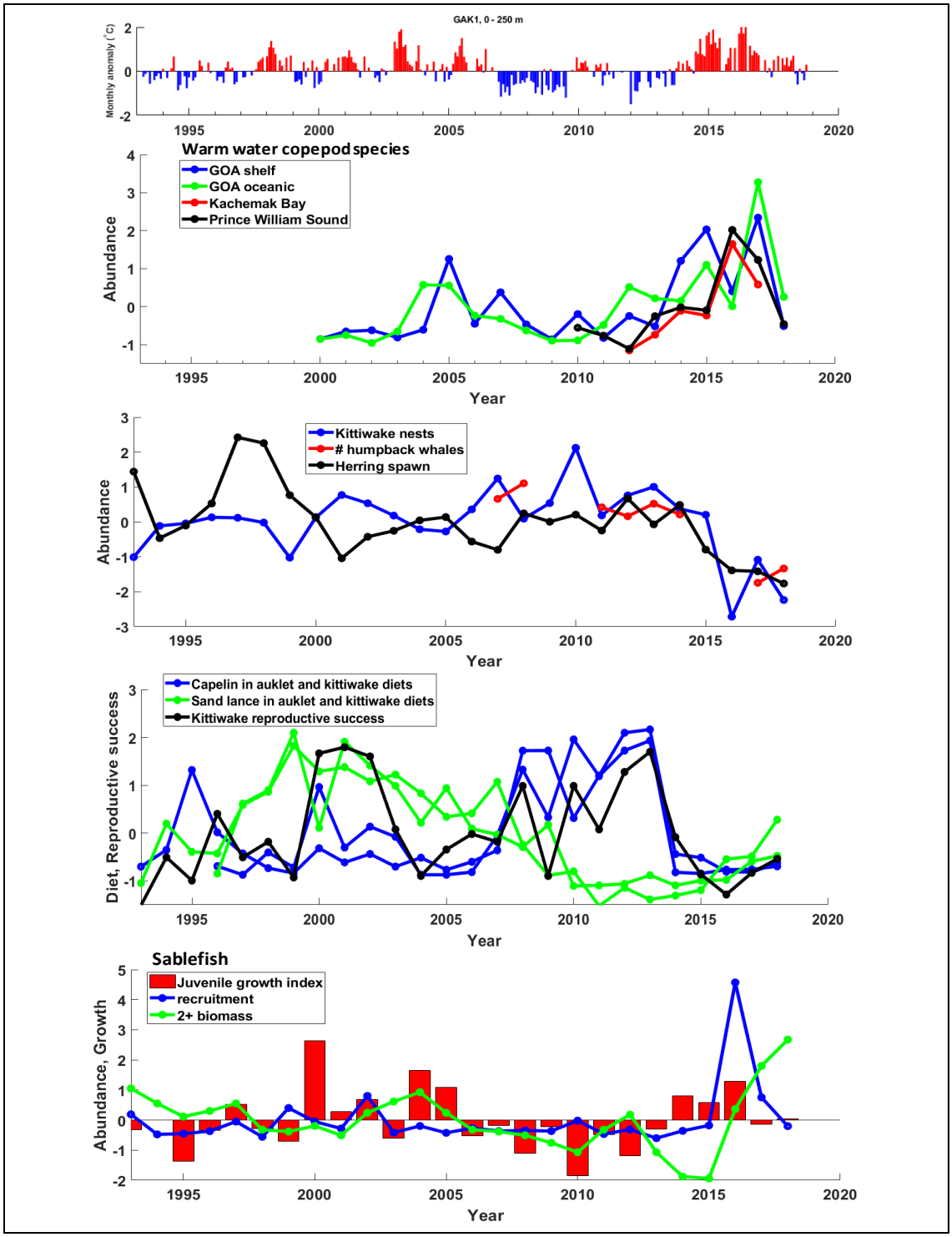

Figure 4-11. Long-term trends in water column temperature at the GAK1 station (top), the abundance of warm water associated copepod species in the Gulf of Alaska (GOA; 2nd from top), herring and herring dependent predators in Prince William Sound (3rd from top), capelin and sand lance availability to marine birds and reproductive success of kittiwakes foraging from Middleton Island (2nd from bottom), and sablefish abundance of recruits, age-2 biomass (Hanselman et al. 2018), and juvenile growth (bottom). Values are z-score standardizations so the y-axes are unitless.

PMH with increased juvenile growth, a strong recruitment class, and an increasing trend in modelled adult population abundance (Figure 4-11).

Discussion

We demonstrate the varied responses to a major ecosystem perturbation from organisms throughout the ecosystem. The common trend from dynamic factor analysis identified from the 113 biological time series was an abrupt change during the PMH and more than half of our time series showed either a significant positive or negative response. Collectively, this led to a novel biological community pattern in the GOA that was distinct from at least 4 to 14 years prior to the PMH. Whereas some metrics began trending back toward pre-PMH, this new community pattern has remained for 4 years post onset of the PMH. The PMH was particularly strong in not only the spatial extent, duration, and magnitude of warming (Hobday et al. 2018, Freeland and Ross 2019), but also in the depth of warming and the diversity of habitats affected, ranging from offshore oceanic to intertidal waters in glacial fjords (Danielson et al. Chapter 1, this report). Furthermore, while water temperatures in some areas trended back toward pre-heatwave levels in years following the 2014-2016 PMH, others did not or only intermittently with warm water anomalies persisting for 5 years after the beginning of the PMH, especially in the lower water column of the continental shelf (Figure 4-1; Danielson et al. Chapter 1, this report). Therefore, various life stages of many organisms were still experiencing anomalously warm conditions that likely explain the lag in returning to pre-heatwave values for the GOA community as a whole.

Biological community response during the PMH

Some patterns of response during the PMH emerge across taxa and food webs of various biological communities. For example, rocky intertidal communities across the northern GOA experienced abrupt declines in macroalgal cover with a subsequent increase in the abundance of filter feeding organisms such as barnacles and mussels (Figure 4-4; Weitzman et al. Chapter 2, this report). At the same time, one group of predatory intertidal invertebrates declined while another increased. Declines in sea stars (Figure 4-4), a major predator of mussels, was caused by wasting disease that is sometimes associated with warming events and other stressors (Harvell et al. 2019, Konar et al. 2019). The increase in mussels (Figure 4-4) was likely due to the release of predation pressure from decreased star abundance. The abundance of an avian predator of mussels, black oystercatchers, strongly increased along with mussels (Table A1). The abundance of piscivorous marine birds, pigeon guillemots and *Brachyramphus* murrelets, that were counted during the same surveys as the oystercatchers declined; however this was more likely due to changes in the pelagic food web, emphasizing that the PMH likely effected taxa differently depending on which food web and what trophic level a given taxon occupied.

Three main forage fishes of pelagic communities in the GOA (capelin, herring, and sand lance) showed declines in abundance or condition during the PMH, and two species, capelin and herring, remained at low abundance levels through 2018 (Figure 4-5; Arimitsu et al. Chapter 3, this report). The decline in size and total energy content of sand lance (von Biela et al. 2019) was particularly striking given that the occurrence of this species increased beginning in 2016 (Figure 4-5) and during other prior warm events in the GOA (Sydeman et al. 2017). While conditions in 2016 were presumably favorable for age-0 sand lance, the lower energy content

and size/age truncation observed in sand lance in that year suggest this key forage fish also experienced overall negative impacts during the PMH. The abundance of these three forage fishes varied over the previous two decades, however, the PMH was the only time that all three were similarly reduced over a prolonged, multi-year period. The systemic decline in forage fishes, including reduced size and condition, suggests bottom-up, nutritional limitation, likely related to generally small, lipid poor and warm water associated zooplankton prey (Arimitsu et al. Chapter 3, this report). However, there also is evidence for top-down regulation of forage fish populations during the PMH (see below). Large-scale reductions in these and other forage species in the northern GOA appeared to restrict energy transfer to upper trophic level species (Arimitsu et al. Chapter 3, this report), leading to the large-scale mortality events (Piatt et al. 2020, Savage 2019) and declines in the abundance and breeding success of forage fish dependent salmon, groundfish, birds and mammals (Figures 4-6 and 4-8).

Evidence points to potential top-down, as well as bottom-up mechanisms causing mid-trophic level forage reductions during the PMH (Barbeaux et al. 2018, Piatt et al. 2020). For example, contrary to expectations, cold water zooplankton species that typically decline in abundance during warm water periods (Fisher et al. 2015, Batten et al. 2018, McKinstry and Campbell 2018) showed a weak negative or neutral to positive response (Figure 4-7). The increase in zooplankton biomass overall, however, was dominated by smaller, warm water species, which likely hindered energy acquisition of zooplanktivores. The overall high biomass of warm and cold copepod species during the PMH could also suggest possible reduced grazing pressure by forage fishes and other zooplanktivores due to greater consumption of those species by ectothermic predators with increased energetic demands during warm water conditions (Piatt et al. 2020). Overall, more than half of our 113 time series showed a significant, multi-year response during the PMH and intertidal to pelagic community metrics showed how prior disparate trends coalesced during the PMH. These results signify the magnitude of the effect of the PMH and suggest the GOA ecosystem had passed a tipping point that could no longer be buffered by the functional redundancy supporting resiliency in this system (Blake et al. 2019).

HUMAN DIMENSION

Changes in the GOA ecosystem during the PMH that affected groundfish and salmon stocks subsequently affected commercial fisheries and local communities. Like all marine predators, fishermen are constantly adapting to changes in the abundance and distribution of their target species (Watson and Haynie 2018, Beaudreau et al. 2019). While the abundance of some commercial species, such as sablefish, exhibited a positive response during the PMH (Figure 4-11; Hanselman et al. 2018), other species that have a lower thermal tolerance, such as cod (Laurel et al. 2016), showed strongly negative effects (Figure 4-5; Barbeaux et al. 2018). Changes in groundfish abundance were accompanied by changes in distribution (Yang et al. 2019) that can collectively affect overall fishery revenue (Fissel et al. 2019). Resilience exists in fisheries and local economies through adjustments in the supply chain (e.g., price, timing of product delivery) so that commercial markets can adapt to heatwaves (Pershing et al. 2018). Uncertainty associated with repeated fishery closures and damage to natural attractions (e.g., whale watching), however, not surprisingly creates stress for fishing and tourist dependent communities (Curnock et al. 2019, Scyphers et al. 2019).

SIGNALS OF RECOVERY?

It is difficult to assess the potential duration of lasting effects of the PMH on the GOA ecosystem. Examples from the 2011 Western Australian marine heatwave indicate that after 7 years, only parts of the ecosystem are showing significant signs of recovery (Caputi et al. 2019), whereas Chandrapavan et al. (2019) reported partial recovery of a crab stock only 18 months after a marine heatwave in Australia, with the recovery linked to the return of mean summer water temperatures to below 24°C. Key factors in that system that positively influenced the recovery rate for individual species included the following: (1) species sensitive to temperature or at their thermal limit of their range, (2) spatial overlap between species distribution and the extent of the warming event, (3) the stage of the life cycle that was affected, (4) life-cycle duration and maturation time of the species affected, and the (5) management intervention (Caputi et al. 2019). It was likely that similar factors were at play during the PMH and will partly explain varying lags in responses among the many metrics that we are monitoring in the GOA.

Indications of return to pre-PMH levels by 2018 for time series with significant heatwave responses were strongest in metrics where a shorter-term response might be expected based on generation time of the metrics, such as zooplankton species composition (Figure 4-7), sand lance energy content (Figure 4-5), and juvenile sablefish growth (Figure 4-8). Although, even rocky intertidal macroalgal (*Fucus*) cover (Figure 4-4) and whale encounter rates (Figure 4-6) showed some, albeit relatively minor progress toward pre-PMH levels. Through 2018, nonetheless, the GOA community still appears distinct from pre-PMH years (Figure 4-11). While additional prey and predator metrics were showing some indication of trending back toward pre-PMH levels in 2019, such as capelin (Arimitsu et al. Chapter 3, this report), the re-intensification of the heatwave through fall 2018 and summer 2019 (Cornwall 2019, Danielson et al. Chapter 1, this report), suggests caution when interpreting observations during the hiatus.

FUTURE GULF OF ALASKA

Recent warming events that began with the PMH are affecting most of Alaska, including the GOA, Bering Sea, and Arctic Ocean, with recent years among the most anomalous on record (Walsh et al. 2018). Annual sea surface temperatures in the GOA and Bering Sea showed that half or more of the warmest 10 years over the past 119 years occurred after the onset of the PMH in 2014 (i.e., all years hence, with the exception of 2017 in the GOA; University of Alaska Fairbanks, Alaska Center for Climate Assessment and Policy). The sustained warm water anomalies over winter that were characteristic of the PMH was of particular concern for the GOA subarctic ecosystem. Cool winter temperatures can be important to slow larval growth and use of lipid reserves for species ranging from forage fish (Sewall et al. 2019) to predatory flatfish (Doyle et al. 2019). While some species such as sand lance (Figures 4-5 and 4-11) and juvenile walleye pollock (Figure 4-8) might respond favorably to warm periods in the GOA, thresholds exist where positive relationships between winter water temperature and recruitment deteriorate for some forage fish species (Toresen et al. 2019). Recent lack of sea ice over a single winter in the Bering Sea resulted northern zooplankton and fish communities becoming more similar to southern Bering Sea communities (Duffy-Anderson et al. 2019).

Extreme climate events such as the PMH are an emerging driver of marine ecosystem dynamics with potentially greater long-term impacts than slower warming that leads to gradual

reorganization and possible evolution and adaptation (Babcock et al. 2019). Models are successful in forecasting some physical aspects of events (not addressed in this report) such as the PMH (Jacox et al. 2019); however, we are still searching for mechanisms to forecast biological change in these complex ecosystems (Francis et al. 1998, Karp et al. 2019, Rogers and Dougherty 2019). Long-term monitoring efforts – coupled with targeted process studies - are critically important and contribute disproportionately to this effort (Hughes et al. 2017) and informed management decisions are compromised without dedicated long-term monitoring programs (Lonhart et al. 2019). Effective communication of knowledge regarding observed and projected change is also important to not only maintain support for long-term monitoring programs (Vander Naald et al. 2019), but also when evaluating trade-offs associated with climate change adaptation and effective management of marine resources during a period of rapid climate change (Hollowed et al. 2019).

ACKNOWLEDGEMENTS

This project was made possible by the Gulf Watch Alaska (GWA) long-term ecosystem monitoring program with financial support by the *Exxon Valdez* Oil Spill Trustee Council (EVOSTC). We thank the countless number of people whose efforts made collection, processing, archiving, and distribution of these valuable time series possible and the many government agencies, universities, and organizations that supported them. We thank the science review panels of GWA and the EVOSTC, and the EVOSTC science director, S. Wang, for valuable input on this study and the GWA program overall. We thank D. Aderhold and K. Hoffman of the GWA management team for their valiant efforts on program logistics and reporting. The research described in this paper was supported, in part, by the EVOSTC. However, the findings and conclusions presented by the authors are their own and do not necessarily reflect the views or position of the Trustee Council. Any use of trade, firm, or product names is for descriptive purposes only and does not imply endorsement by the U.S. Government.

REFERENCES

ADFG. 2018. Alaska Department of Fish and Game Statewide electronic fish ticket database 1985 to present. 1st edition. Alaska Department of Fish and Game, Division of Commercial Fisheries. (Accessed October 2019).

Anderson, P.J., and J.F. Piatt. 1999. Community reorganization in the Gulf of Alaska following ocean climate regime shift. Marine Ecology Progress Series 189:117-123.

Arimitsu, M.L., J.F. Piatt, R.M. Suryan, S. Batten, M.A. Bishop, R. Campbell, H. Coletti, D. Cushing, K. Gorman, S.A. Hatch, S. Haught, D. McGowan, J. Moran, S. Pegau, A. Schaefer, S. Schoen, J. Straley, and V. von Biela. Chapter 3, this report. Synchronous collapse of forage species disrupts trophic transfer during a prolonged marine heatwave. *In* The Pacific Marine Heatwave: monitoring during a major perturbation in the Gulf of Alaska. Gulf Watch Alaska Long-Term Monitoring Program (#19120114) Science Synthesis Report to the *Exxon Valdez* Oil Spill Trustee Council.

Babcock, R.C., R.H. Bustamante, E.A. Fulton, D.J. Fulton, M.D.E. Haywood, A.J. Hobday, R. Kenyon, R.J. Matear, E.E. Plagányi, A.J. Richardson, and M.A. Vanderklift. 2019.

Severe continental-scale impacts of climate change are happening now: extreme climate events impact marine habitat forming communities along 45% of Australia's coast. Frontiers in Marine Science 6.

Barbeaux, S., K. Aydin, B. Fissel, K.K. Holsman, B. Laurel, W.A. Palsson, K. Shotwell, Q. Yang, and S. Zador. 2018. Assessment of the Pacific cod stock in the Gulf of Alaska. National Marine Fisheries Service, Alaska Fisheries Science Center, Seattle, Washington, USA.

Batten, S.D., S. Moffitt, W.S. Pegau, and R. Campbell. 2016. Plankton indices explain interannual variability in Prince William Sound herring first year growth. Fisheries Oceanography 25:420-432.

Batten, S.D., D.E. Raitsos, S. Danielson, R. Hopcroft, K. Coyle, and A. McQuatters-Gollop. 2018. Interannual variability in lower trophic levels on the Alaskan Shelf. Deep Sea Research Part II: Topical Studies in Oceanography 147:58-68.

Batten, S.D., and D.W. Welch. 2004. Changes in oceanic zooplankton populations in the north-east Pacific associated with the possible climatic regime shift of 1998/1999. Deep-Sea Research Part II 51:863-873.

Beaudreau, A.H., E.J. Ward, R.E. Brenner, A.O. Shelton, J.T. Watson, J.C. Womack, S.C. Anderson, A.C. Haynie, K.N. Marshall, and B.C. Williams. 2019. Thirty years of change and the future of Alaskan fisheries: Shifts in fishing participation and diversification in response to environmental, regulatory and economic pressures. Fish and Fisheries 20:601-619.

Beaugrand, G., A. Conversi, S. Chiba, M. Edwards, S. Fonda-Umani, C. Greene, N. Mantua, S. A. Otto, P. C. Reid, M. M. Stachura, L. Stemmann, and H. Sugisaki. 2015. Synchronous marine pelagic regime shifts in the Northern Hemisphere. Philosophical Transactions of the Royal Society B-Biological Sciences 370:20130272.

Blake, R.E., C.L. Ward, M.E. Hunsicker, A.O. Shelton, and A.B. Hollowed. 2019. Spatial community structure of groundfish is conserved across the Gulf of Alaska. Marine Ecology Progress Series 626:145-160.

Bodkin, J. 2011. SOP for conducting marine bird and mammal surveys - Version 4.1: Southwest Alaska Inventory and Monitoring Network. Natural Resource Report NPS/SWAN/NRR— 2011/392. National Park Service, Fort Collins, Colorado, USA.

Bodkin, J.L., H.A. Coletti, B.E. Ballachey, D.H. Monson, D. Esler, and T.A. Dean. 2018. Variation in abundance of Pacific Blue Mussel (*Mytilus trossulus*) in the Northern Gulf of Alaska, 2006–2015. Deep Sea Research Part II: Topical Studies in Oceanography 147:87-97.

Bond, N.A., J.E. Overland, M. Spillane, and P. Stabeno. 2003. Recent shifts in the state of the North Pacific. Geophysical Research Letters 30:1-3.

Brodeur, R.D., T.D. Auth, and A.J. Phillips. 2019. Major shifts in pelagic micronekton and macrozooplankton community structure in an upwelling ecosystem related to an unprecedented marine heatwave. Frontiers in Marine Science 6.

Cane, M.A., and S.E. Zebiak. 1985. A Theory for El-Nino and the Southern Oscillation. Science 228:1085-1087.

Caputi, N., M.I. Kangas, A. Chandrapavan, A. Hart, M. Feng, M. Marin, and S. de Lestang. 2019. Factors affecting the recovery of invertebrate stocks from the 2011 Western Australian extreme marine heatwave. Frontiers in Marine Science 6.

Chandrapavan, A., N. Caputi, and M.I. Kangas. 2019. The decline and recovery of a crab population from an extreme marine heatwave and a changing climate. Frontiers in Marine Science 6.

Chavez, F.P., J. Ryan, S.E. Lluch-Cota, and M. Niquen. 2003. From anchovies to sardines and back: Multidecadal change in the Pacific Ocean. Science 299:217-221.

Clarke, K.R., and R.N. Gorley. 2015. Getting started with PRIMER v7. PRIMER-E ltd Plymouth, UK.

Clarke, K.R., R.N. Gorley, P.J. Somerfield, and R.M. Warwick. 2014. Change in marine communities: an approach to statistical analysis and interpretation. PRIMER-E ltd Plymouth, UK.

Clarke, K.R., P.J. Somerfield, and R.N. Gorley. 2008. Testing of null hypotheses in exploratory community analyses: similarity profiles and biota-environment linkage. Journal of Experimental Marine Biology and Ecology 366:56-69.

Coletti, H., D. Esler, B. Ballachey, J. Bodkin, G. Esslinger, K. Kloecker, D. Monson, B. Robinson, B. Weitzman, T. Dean, and M. Lindeberg. 2018. Gulf Watch Alaska: Nearshore benthic systems in the Gulf of Alaska. Long-Term Monitoring Program (Gulf Watch Alaska) Final Report (*Exxon Valdez* Oil Spill Trustee Council Project 16120114-R), *Exxon Valdez* Oil Spill Trustee Council, Anchorage, Alaska.

Coletti, H.A., J.L. Bodkin, D.H. Monson, B.E. Ballachey, and T.A. Dean. 2016. Detecting and inferring cause of change in an Alaska nearshore marine ecosystem. Ecosphere 7:e01489.

Cornwall, W. 2019. A new 'Blob' menaces Pacific ecosystems. Science 365:1233-1233.

Curnock, M.I., N.A. Marshall, L. Thiault, S. F. Heron, J. Hoey, G. Williams, B. Taylor, P.L. Pert, and J. Goldberg. 2019. Shifts in tourists' sentiments and climate risk perceptions following mass coral bleaching of the Great Barrier Reef. Nature Climate Change 9:535-541.

Danielson, S.L., T.D. Hennon, D.H. Monson, R.M. Suryan, R. Campbell, S.J. Baird, K. Holderied, and T.J. Weingartner. Chapter 1, this report. A study of marine temperature variations in the northern Gulf of Alaska across years of marine heatwaves and cold spells. *In* The Pacific Marine Heatwave: monitoring during a major perturbation in the Gulf of Alaska. Gulf Watch Alaska Long-Term Monitoring Program (#19120114) Science Synthesis Report to the *Exxon Valdez* Oil Spill Trustee Council.

Di Lorenzo, E., and N. Mantua. 2016. Multi-year persistence of the 2014/15 North Pacific marine heatwave. Nature Clim. Change 6:1042-1047.

Di Lorenzo, E., N. Schneider, K.M. Cobb, P.J.S. Franks, K. Chhak, A.J. Miller, J.C. McWilliams, S.J. Bograd, H. Arango, E. Curchitser, T.M. Powell, and P. Riviere. 2008. North Pacific Gyre Oscillation links ocean climate and ecosystem change. Geophysical Research Letters 35:6.

Dorn, M., K. Aydin, B. Fissel, W.A. Palsson, K. Spalinger, S. Stienessen, K. Williams, and S. Zador. 2018. Assessment of the walleye pollock stock in the Gulf of Alaska. National Marine Fisheries Service, Alaska Fisheries Science Center, Seattle, Washington, USA.

Doyle, M.J., S.L. Strom, K.O. Coyle, A.J. Hermann, C. Ladd, A.C. Matarese, S.K. Shotwell, and R.R. Hopcroft. 2019. Early life history phenology among Gulf of Alaska fish species: Strategies, synchronies, and sensitivities. Deep Sea Research Part II: Topical Studies in Oceanography 165:41-73.

Duffy-Anderson, J.T., P. Stabeno, A.G. Andrews III, K. Cieciel, A. Deary, E. Farley, C. Fugate, C. Harpold, R. Heintz, D. Kimmel, K. Kuletz, J. Lamb, M. Paquin, S. Porter, L. Rogers, A. Spear, and E. Yasumiishi. 2019. Responses of the Northern Bering Sea and Southeastern Bering Sea Pelagic Ecosystems Following Record-Breaking Low Winter Sea Ice. Geophysical Research Letters 46:9833–9842.

Fisher, J.L., W.T. Peterson, and R.R. Rykaczewski. 2015. The impact of El Niño events on the pelagic food chain in the northern California Current. Global Change Biology 21:4401-4414.

Fissel, B., M. Dalton, B. Garber-Yonts, A. C. Haynie, S. Kasperski, J. Lee, D. Lew, A. Lavoie, C. Seung, K. Sparks, M. Szymkowiak, and S. Wise. 2019. Stock assessment and fishery evaluation report for the groundfish fisheries of the Gulf Of Alaska and Bering Sea/Aleutian Islands area: Economic status of the groundfish fisheries off Alaska, 2017. National Marine Fisheries Service, Alaska Fisheries Science Center, Seattle, Washington, USA.

Francis, R.C., S.R. Hare, A.B. Hollowed, and W.S. Wooster. 1998. Effects of interdecadal climate variability on the oceanic ecosystems of the NE Pacific. Fisheries Oceanography 7:1-21.

Freeland, H., and T. Ross. 2019. 'The Blob' - or, how unusual were ocean temperatures in the Northeast Pacific during 2014-2018? Deep Sea Research Part I: Oceanographic Research Papers 150:103061.

Hanselman, D.H., C.J. Rodveller, K.H. Fenske, S.K. Shotwell, K.B. Echave, P.W. Malecha, and C.R. Lunsford. 2018. Assessment of the Sablefish stock in Alaska. National Marine Fisheries Service, Alaska Fisheries Science Center, Seattle, Washington, USA.

Harding, A.M.A., J.F. Piatt, J.A. Schmutz, M.T. Shultz, T.I. Van Pelt, A.B. Kettle, and S.G. Speckman. 2007. Prey density and the behavioral flexibility of a marine predator: The common murre (*Uria aalge*). Ecology 88:2024-2033.

Hare, S.R., and N.J. Mantua. 2000. Empirical evidence for North Pacific regime shifts in 1977 and 1989. Progress in Oceanography 47:103-145.

Harvell, C.D., D. Montecino-Latorre, J.M. Caldwell, J.M. Burt, K. Bosley, A. Keller, S.F. Heron, A.K. Salomon, L. Lee, O. Pontier, C. Pattengill-Semmens, and J.K. Gaydos. 2019. Disease epidemic and a marine heat wave are associated with the continental-scale collapse of a pivotal predator (*Pycnopodia helianthoides*). Science Advances 5:eaau7042.

Hatch, S.A. 2013. Kittiwake diets and chick production signal a 2008 regime shift in the Northeast Pacific. Marine Ecology Progress Series 477:271-284.

Hobday, A., E. Oliver, A. Sen Gupta, J. Benthuysen, M. Burrows, M. Donat, N. Holbrook, P. Moore, M. Thomsen, T. Wernberg, and D. Smale. 2018. Categorizing and Naming Marine Heatwaves. Oceanography 31:162-173.

Hollowed, A.B., M. Barange, V. Garçon, S.-i. Ito, J.S. Link, S. Aricò, H. Batchelder, R. Brown, R. Griffis, and W. Wawrzynski. 2019. Recent advances in understanding the effects of climate change on the world's oceans. ICES Journal of Marine Science 76:1215–1220.

Holmes, E., E. Ward, M. Scheuerell, and L. Wills. 2018a. MARSS: Multivariate Autoregressive State-Space Modeling. Northwest Fisheries Science Center, NOAA, Seattle, WA, USA.

Holmes, E.E., E.J. Ward, and M.D. Scheuerell. 2018b. Analysis of multivariate time-series using the MARSS package, v3.10.10. Northwest Fisheries Science Center, NOAA, Seattle, WA, USA.

Hughes, B.B., R. Beas-Luna, A.K. Barner, K. Brewitt, D.R. Brumbaugh, E.B. Cerny-Chipman, S.L. Close, K.E. Coblentz, K.L. de Nesnera, S.T. Drobnitch, J.D. Figurski, B. Focht, M. Friedman, J. Freiwald, K.K. Heady, W.N. Heady, A. Hettinger, A. Johnson, K.A. Karr, B. Mahoney, M.M. Moritsch, A.-M.K. Osterback, J. Reimer, J. Robinson, T. Rohrer, J.M. Rose, M. Sabal, L.M. Segui, C. Shen, J. Sullivan, R. Zuercher, P.T. Raimondi, B.A. Menge, K. Grorud-Colvert, M. Novak, and M.H. Carr. 2017. Long-Term Studies Contribute Disproportionately to Ecology and Policy. BioScience 67:271-281.

IPCC. 2019. Summary for policymakers. In: IPCC special report on the ocean and cryosphere in a changing climate [H.- O. Pörtner, D.C. Roberts, V. Masson-Delmotte, P. Zhai, M. Tignor, E. Poloczanska, K. Mintenbeck, M. Nicolai, A. Okem, J. Petzold, B. Rama, N. Weyer (eds.)]. Accessed on 11/5/2019.

Jackson, J.M., G.C. Johnson, H.V. Dosser, and T. Ross. 2018. Warming From Recent Marine Heatwave Lingers in Deep British Columbia Fjord. Geophysical Research Letters 45:9757-9764.

Jacox, M., D. Tommasi, M.A. Alexander, G. Hervieux, and C. Stock. 2019. Predicting the evolution of the 2014-16 California Current System marine heatwave from an ensemble of coupled global climate forecasts. Frontiers in Marine Science 6.

Jones, T., J.K. Parrish, W.T. Peterson, E.P. Bjorkstedt, N.A. Bond, L.T. Ballance, V. Bowes, J.M. Hipfner, H.K. Burgess, J.E. Dolliver, K. Lindquist, J. Lindsey, H.M. Nevins, R.R. Robertson, J. Roletto, L. Wilson, T. Joyce, and J. Harvey. 2018. Massive mortality of a planktivorous seabird in response to a marine heatwave. Geophysical Research Letters 45:3193-3202.

Karp, M.A., J.O. Peterson, P.D. Lynch, R.B. Griffis, C.F. Adams, W.S. Arnold, L.A.K. Barnett, Y. deReynier, J. DiCosimo, K.H. Fenske, S.K. Gaichas, A. Hollowed, K. Holsman, M. Karnauskas, D. Kobayashi, A. Leising, J.P. Manderson, M. McClure, W.E. Morrison, E. Schnettler, A. Thompson, J.T. Thorson, J.F. Walter, III, A.J. Yau, R.D. Methot, and J.S. Link. 2019. Accounting for shifting distributions and changing productivity in the development of scientific advice for fishery management. ICES Journal of Marine Science 76:1305-1315.

Konar, B., T.J. Mitchell, K. Iken, H. Coletti, T. Dean, D. Esler, M. Lindeberg, B. Pister, and B. Weitzman. 2019. Wasting disease and static environmental variables drive sea star assemblages in the Northern Gulf of Alaska. Journal of Experimental Marine Biology and Ecology 520:151209.

Kuletz, K.J., and E.A. Labunski. 2017. Seabird Distribution and Abundance in the Offshore Environment, Final Report. US Dept. of the Interior, Bureau of Ocean Energy Management, Alaska OCS Region. OCS Study BOEM 2017-004. Anchorage, Alaska, USA.

Laurel, B.J., and L.A. Rogers. 2020. Loss of spawning habitat and prerecruits of Pacific cod during a Gulf of Alaska heatwave. Canadian Journal of Fisheries and Aquatic Sciences 77:644-650.

Laurel, B.J., M. Spencer, P. Iseri, and L.A. Copeman. 2016. Temperature-dependent growth and behavior of juvenile Arctic cod (*Boreogadus saida*) and co-occurring North Pacific gadids. Polar Biology 39:1127-1135.

Litzow, M.A. 2006. Climate regime shifts and community reorganization in the Gulf of Alaska: how do recent shifts compare with 1976/1977? ICES Journal of Marine Science 63:1386-1396.

Litzow, M.A., L. Ciannelli, C.J. Cunningham, B. Johnson, and P. Puerta. 2019. Nonstationary effects of ocean temperature on Pacific salmon productivity. Canadian Journal of Fisheries and Aquatic Sciences 76:1923-1928.

Litzow, M.A., L. Ciannelli, P. Puerta, J.J. Wettstein, R.R. Rykaczewski, and M. Opiekun. 2018. Non-stationary climate–salmon relationships in the Gulf of Alaska. Proceedings of the Royal Society B: Biological Sciences 285:20181855.

Litzow, M.A., and F.J. Mueter. 2014. Assessing the ecological importance of climate regime shifts: An approach from the North Pacific Ocean. Progress in Oceanography 120:110-119.

Litzow, M.I., J.I. Piatt, A.I. Prichard, and D.I. Roby. 2002. Response of pigeon guillemots to variable abundance of high-lipid and low-lipid prey. Oecologia 132:286-295.

Lonhart, S.I., R. Jeppesen, R. Beas-Luna, J.A. Crooks, and J. Lorda. 2019. Shifts in the distribution and abundance of coastal marine species along the eastern Pacific Ocean during marine heatwaves from 2013 to 2018. Marine Biodiversity Records 12:13.

Maniscalco, J.M., A.M. Springer, P. Parker, and M.D. Adkison. 2014. A Longitudinal Study of Steller Sea Lion Natality Rates in the Gulf of Alaska with Comparisons to Census Data. PLoS ONE 9:e111523.

Mantua, N J., S.R. Hare, Y. Zhang, J.M. Wallace, and R.C. Francis. 1997. A Pacific interdecadal climate oscillation with impacts on salmon production. Bulletin of the American Meteorological Society 78:1069-1080.

Matarese, A.C., Blood, D.M., S. J. Picquelle, and J.L. Benson. 2003. Atlas of abundance and distribution patterns of ichthyoplankton from the northeast Pacific Ocean and Bering Sea ecosystems based on research conducted by the Alaska Fisheries Science Center (1972-1996). NOAA Professional Paper NMFS 1.

McKinstry, C.A.E., and R.W. Campbell. 2018. Seasonal variation of zooplankton abundance and community structure in Prince William Sound, Alaska, 2009–2016. Deep Sea Research Part II: Topical Studies in Oceanography 147:69-78.

Moffitt, S.D. 2017. Retrospective longitudinal growth history from scales of Pacific herring collected in Prince William Sound. *Exxon Valdez* Long-Term Herring Research and Monitoring Program Final Report (Project 13120111-N), *Exxon Valdez* Oil Spill Trustee Council. Anchorage, AK.

Moran, J.R., R.A. Heintz, J.M. Straley, and J.J. Vollenweider. 2018. Regional variation in the intensity of humpback whale predation on Pacific herring in the Gulf of Alaska. Deep Sea Research Part II: Topical Studies in Oceanography 147:187-195.

Muradian, M.L., T.A. Branch, S.D. Moffitt, and P.-J.F. Hulson. 2017. Bayesian stock assessment of Pacific herring in Prince William Sound, Alaska. PLoS ONE 12:e0172153.

Oliver, E.C. J., M.G. Donat, M.T. Burrows, P.J. Moore, D.A. Smale, L.V. Alexander, J.A. Benthuysen, M. Feng, A. Sen Gupta, A. J. Hobday, N. J. Holbrook, S. E. Perkins-Kirkpatrick, H. A. Scannell, S. C. Straub, and T. Wernberg. 2018. Longer and more frequent marine heatwaves over the past century. Nature Communications 9:1324.

Olsen, D.W., C.O. Matkin, R.D. Andrews, and S. Atkinson. 2018. Seasonal and pod-specific differences in core use areas by resident killer whales in the Northern Gulf of Alaska. Deep Sea Research Part II: Topical Studies in Oceanography 147:196-202.

Overland, J., S. Rodionov, S. Minobe, and N. Bond. 2008. North Pacific regime shifts: Definitions, issues and recent transitions. Progress in Oceanography 77:92-102.

Pershing, A.J., K E. Mills, A.M. Dayton, B.S. Franklin, and B.T. Kennedy. 2018. Evidence for adaptation from the 2016 marine heatwave in the Northwest Atlantic Ocean. Oceanography 31:152-161.

Peterson, W.T., and F.B. Schwing. 2003. A new climate regime in northeast Pacific ecosystems. Geophysical Research Letters 30:1896.

Piatt, J.F., J.K. Parrish, H.M. Renner, S. Schoen, T. Jones, K. Kuletz, B. Bodenstein, M. Arimitsu, M. García-Reyes, R. Duerr, R. Corcoran, R. Kaler, G. McChesney, R. Golightly, H. Coletti, R.M. Suryan, H. Burgess, J. Lindsey, K. Lindquist, P. Warzybok, J. Jahncke, J. Roletto, and W. Sydeman. 2020. Mass mortality and chronic reproductive

failure of common murres during and after the 2014-2016 northeast Pacific marine heatwave. PLoS ONE 15(1):e0226087.

Puerta, P., L. Ciannelli, R. Rykaczewski, M. Opiekun, and M.A. Litzow. 2019. Do Gulf of Alaska fish and crustacean populations show synchronous non-stationary responses to climate? Progress in Oceanography 175:161-170.

R Core Team. 2018. R: A language and environment for statistical computing. R Foundation for Statistical Computing. Vienna, Austria. https://www.R-project.org/.

Richardson, A.J., A.W. Walne, A.W.G. John, T.D. Jonas, J.A. Lindley, D.W. Sims, D. Stevens, and M. Witt. 2006. Using continuous plankton recorder data. Progress in Oceanography 68:27-74.

Robards, M.D., J.A. Anthony, G.A. Rose, and J.F. Piatt. 1999. Changes in proximate composition and somatic energy content for Pacific sand lance (Ammodytes hexapterus) from Kachemak Bay, Alaska relative to maturity and season. Journal of Experimental Marine Biology and Ecology 242:245-258.

Rogers, L.A., and A.B. Dougherty. 2019. Effects of climate and demography on reproductive phenology of a harvested marine fish population. Global Change Biology 25:708– 720.

Savage, K. 2019. 2018 Alaska Region marine mammal stranding summary. Protected Resources Division, National Marine Fisheries Service, Alaska Region, Juneau, Alaska 99802.

Scyphers, S.B., J.S. Picou, and J.H. Grabowski. 2019. Chronic social disruption following a systemic fishery failure. Proceedings of the National Academy of Sciences 116:22912-22914.

Sewall, F., B. Norcross, J. Vollenweider, and R. Heintz. 2019. Growth, energy storage, and feeding patterns reveal winter mortality risks for juvenile Pacific herring in Prince William Sound, Alaska, USA. Marine Ecology Progress Series 623:195-208.

Smale, D.A., T. Wernberg, E.C.J. Oliver, M. Thomsen, B.P. Harvey, S.C. Straub, M.T. Burrows, L.V. Alexander, J.A. Benthuysen, M.G. Donat, M. Feng, A.J. Hobday, N.J. Holbrook, S.E. Perkins-Kirkpatrick, H.A. Scannell, A. Sen Gupta, B.L. Payne, and P.J. Moore. 2019. Marine heatwaves threaten global biodiversity and the provision of ecosystem services. Nature Climate Change 9:306–312.

Sousa, L., K.O. Coyle, R.P. Barry, T.J. Weingartner, and R.R. Hopcroft. 2016. Climate-related variability in abundance of mesozooplankton in the northern Gulf of Alaska 1998–2009. Deep Sea Research Part II: Topical Studies in Oceanography 132:122-135.

Spies, I., and W.A. Palsson. 2018. Assessment of the arrowtooth flounder stock in the Gulf of Alaska. National Marine Fisheries Service, Alaska Fisheries Science Center, Seattle, Washington, USA.

Stocking, J., M.A. Bishop, and A. Arab. 2018. Spatio-temporal distributions of piscivorous birds in a subarctic sound during the nonbreeding season. Deep Sea Research Part II: Topical Studies in Oceanography 147:138-147.

Straley, J.M., J.R. Moran, K.M. Boswell, J.J. Vollenweider, R.A. Heintz, T.J. Quinn Ii, B.H. Witteveen, and S.D. Rice. 2018. Seasonal presence and potential influence of humpback whales on wintering Pacific herring populations in the Gulf of Alaska. Deep Sea Research Part II: Topical Studies in Oceanography 147:173-186.

Suryan, R.M., and D.B. Irons. 2001. Colony and population dynamics of black-legged kittiwakes in a heterogeneous environment. Auk 118:636-649.

Sutherland, K.R., H.L. Sorensen, O.N. Blondheim, R.D. Brodeur, and A.W.E. Galloway. 2018. Range expansion of tropical pyrosomes in the northeast Pacific Ocean. Ecology 99:2397-2399.

Sweeney, K., L.W. Fritz, R. Towell, and T. Gelatt. 2017. Results of Steller Sea Lion Surveys in Alaska, June-July 2017. National Marine Fisheries Service, Alaska Fisheries Science Center, Seattle, Washington, USA.

Sydeman, W.J., J.F. Piatt, S.A. Thompson, M. García-Reyes, S.A. Hatch, M.L. Arimitsu, L. Slater, J.C. Williams, N.A. Rojek, S.G. Zador, and H.M. Renner. 2017. Puffins reveal contrasting relationships between forage fish and ocean climate in the North Pacific. Fisheries Oceanography 26:379-395.

Toresen, R., H.R. Skjoldal, F. Vikebø, and M.B. Martinussen. 2019. Sudden change in long-term ocean climate fluctuations corresponds with ecosystem alterations and reduced recruitment in Norwegian spring-spawning herring (*Clupea harengus*, Clupeidae). Fish and Fisheries 20:686-696.

Vander Naald, B.P., C.J. Sergeant, and A.H. Beaudreau. 2019. Public perception and valuation of long-term ecological monitoring. Ecosphere 10:e02875.

von Biela, V.R., M.L. Arimitsu, J.F. Piatt, B. Heflin, S.K. T.J.L. Schoen, and C.M. Clawson. 2019. Extreme reduction in nutritional value of a key forage fish during the Pacific marine heatwave of 2014-2016. Marine Ecology Progress Series 613:171-182.

Wade, N.M., T.D. Clark, B.T. Maynard, S. Atherton, R.J. Wilkinson, R.P. Smullen, and R.S. Taylor. 2019. Effects of an unprecedented summer heatwave on the growth performance, flesh colour and plasma biochemistry of marine cage-farmed Atlantic salmon (*Salmo salar*). Journal of Thermal Biology 80:64-74.

Walsh, J.E., R.L. Thoman, U.S. Bhatt, P.A. Bieniek, B. Brettschneider, M. Brubaker, S. Danielson, R. Lader, F. Fetterer, K. Holderied, K. Iken, A. Mahoney, M. McCammon, and J. Partain. 2018. The high latitude marine heat wave of 2016 and its impacts on Alaska. Bulletin of the American Meteorological Society 99:S39-S43.

Watson, J.T., and A.C. Haynie. 2018. Paths to resilience: Alaska pollock fleet uses multiple fishing strategies to buffer against environmental change in the Bering Sea. Canadian Journal of Fisheries and Aquatic Sciences In press.

Weitzman, B., B. Konar, K. Iken, H. Coletti, D. Monson, R. Suryan, T. Dean, D. Hondolero, and M. Lindeberg. Chapter 2, this report. Changes in rocky intertidal community structure during a marine heatwave in the northern Gulf of Alaska. *In* The Pacific Marine Heatwave: monitoring during a major perturbation in the Gulf of Alaska. Gulf Watch

Alaska Long-Term Monitoring Program (#19120114) Science Synthesis Report to the *Exxon Valdez* Oil Spill Trustee Council.

Yang, Q., E.D. Cokelet, P.J. Stabeno, L. Li, A.B. Hollowed, W.A. Palsson, N.A. Bond, and S.J. Barbeaux. 2019. How "The Blob" affected groundfish distributions in the Gulf of Alaska. Fisheries Oceanography 28:434-453.

Zuur, A.F., R.J. Fryer, I.T. Jolliffe, R. Dekker, and J.J. Beukema. 2003a. Estimating common trends in multivariate time series using dynamic factor analysis. Environmetrics 14:665-685.

Zuur, A.F., I.D. Tuck, and N. Bailey. 2003b. Dynamic factor analysis to estimate common trends in fisheries time series. Canadian Journal of Fisheries and Aquatic Sciences 60:542-552.

APPENDIX

Table A1. Biological time series (n=113) used to assess ecosystem response to a multi-year marine heatwave in the Gulf of Alaska. Time series include taxonomic group, sampling method, geographic domain where sampled, derived metric, time series start year, end year, and number of years (n; most, but not all are sample annually), factor loadings from dynamic factor analysis, and data source. Note that a positive factor loading indicates the time series relates positively to the common trend and given that the common trend is a negative response during the PMH (Figure 4-3), a positive factor loading refers to a negative response during the PMH and vice versa. We use a factor loading of 0.20 (absolute value) as the cutoff for whether or not a time series significantly relates to the common trend. Data sources were from Gulf Watch Alaska (GWA), Herring Research and Monitoring program (HRM), National Oceanic and Atmospheric Administration, Alaska Fisheries Science Center (AFSC), Alaska Department of Fish and Game (ADFG), U.S. Fish and Wildlife Service (USFWS), and Alaska SeaLife Center (ASLC).

	Taxa	Method	Domain	Metric	Start year	End year	n (years)	Factor loadings	Data source
1	Zooplankton	Continuous plankton recorder	Shelf	Copepod Size Index	2000	2018	19	-0.149	GWA
2	Zooplankton	Continuous plankton recorder	Oceanic	Copepod Size Index	2000	2018	19	0.281	GWA
3	Zooplankton	Continuous plankton recorder	Shelf	Warm water zooplankton abundance	2000	2018	19	-0.251	GWA
4	Zooplankton	Continuous plankton recorder	Oceanic	Warm water zooplankton abundance	2000	2018	19	-0.294	GWA
5	Zooplankton	Continuous plankton recorder	Shelf	Cool water zooplankton abundance	2000	2018	19	-0.280	GWA
6	Zooplankton	Continuous plankton recorder	Oceanic	Cool water zooplankton abundance	2000	2018	19	-0.187	GWA
7	Zooplankton	Plankton net	Kachemak Bay	Copepod Size Index	2012	2017	6	-0.084	GWA
8	Zooplankton	Plankton net	Kachemak Bay	All zooplankton abundance	2012	2017	6	-0.229	GWA
9	Zooplankton	Plankton net	Kachemak Bay	Warm water zooplankton abundance	2012	2017	6	-0.401	GWA

	Taxa	Method	Domain	Metric	Start year	End year	n (years)	Factor loadings	Data source
10	Zooplankton	Plankton net	Kachemak Bay	Cool water zooplankton abundance	2012	2017	6	-0.127	GWA
11	Zooplankton	Plankton net	Prince William Sound	Copepod Size Index	2010	2018	9	-0.343	GWA
12	Zooplankton	Plankton net	Prince William Sound	All zooplankton abundance	2010	2018	9	-0.403	GWA
13	Zooplankton	Plankton net	Prince William Sound	Warm water zooplankton abundance	2010	2018	9	-0.358	GWA
14	Zooplankton	Plankton net	Prince William Sound	Cool water zooplankton abundance	2010	2018	9	-0.032	GWA
15	Intertidal organism	Quadrat	Prince William Sound	Pacific blue mussel density	2010	2018	9	-0.167	GWA
16	Intertidal organism	Transect	Prince William Sound	Sea star density	2010	2018	9	0.279	GWA
17	Intertidal organism	Quadrat	Prince William Sound	*Fucus* percent cover	2007	2018	10	0.377	GWA
18	Intertidal organism	Quadrat	Kenai Peninsula	Pacific blue mussel density	2008	2018	11	-0.323	GWA
19	Intertidal organism	Transect	Kenai Peninsula	Sea star density	2008	2018	11	0.449	GWA
20	Intertidal organism	Quadrat	Kenai Peninsula	*Fucus* percent cover	2008	2018	11	0.388	GWA
21	Intertidal organism	Quadrat	Kachemak Bay	Pacific blue mussel density	2012	2018	7	-0.231	GWA
22	Intertidal organism	Transect	Kachemak Bay	Sea star density	2009	2018	9	-0.117	GWA
23	Intertidal organism	Quadrat	Kachemak Bay	*Fucus* percent cover	2012	2018	7	0.404	GWA

	Taxa	Method	Domain	Metric	Start year	End year	n (years)	Factor loadings	Data source
24	Intertidal organism	Quadrat	Alaska Peninsula	Pacific blue mussel density	2008	2018	10	-0.322	GWA
25	Intertidal organism	Transect	Alaska Peninsula	Sea star density	2006	2018	11	0.361	GWA
26	Intertidal organism	Quadrat	Alaska Peninsula	*Fucus* percent cover	2006	2018	12	0.292	GWA
27	Forage Fish	Aerial survey	Prince William Sound	Pacific herring miles of spawn	1974	2018	45	0.450	HRM
28	Forage Fish	Scale growth increment	Prince William Sound	Pacific herring growth to age-4	1979	2017	39	0.389	HRM
29	Groundfish	Plankton net	Kodiak region	Walleye pollock larvae density	1981	2017	32	0.185	AFSC
30	Groundfish	Plankton net	Kodiak region	Pacific cod larvae density	1981	2017	32	0.213	AFSC
31	Forage Fish	Plankton net	Kodiak region	Sand lance larvae density	1981	2017	32	-0.275	AFSC
32	Groundfish	Plankton net	Kodiak region	Northern rock sole larvae density	1981	2017	32	0.102	AFSC
33	Groundfish	Plankton net	Kodiak region	Southern rock sole larvae density	1981	2017	32	-0.214	AFSC
34	Forage Fish	Marine bird diet	Middleton Island region	Sand lance percent biomass from black-legged kittiwake diet	1978	2019	26	-0.357	AFSC
35	Forage Fish	Marine bird diet	Middleton Island region	Capelin percent biomass from black-legged kittiwake diet	1978	2019	26	0.393	AFSC
36	Forage Fish	Marine bird diet	Middleton Island region	Sand lance percent biomass from rhinoceros auklet diet	1978	2019	30	-0.379	AFSC

	Taxa	Method	Domain	Metric	Start year	End year	n (years)	Factor loadings	Data source
37	Forage Fish	Marine bird diet	Middleton Island region	Capelin percent biomass from rhinoceros auklet diet	1978	2019	30	0.396	GWA
38	Forage Fish	nets (seine, dip, gill, cast), hook and line	Prince William Sound	Sand lance whole body energy content	2012	2018	6	0.180	GWA
39	Groundfish	Marine bird diet	Middleton Island region	Sablefish juvenile growth index, increase in of fish from June to August	1990	2019	27	-0.267	GWA
40	Groundfish	Stock assessment model	Alaska	Sablefish recruitment biomass	1977	2018	42	-0.278	AFSC
41	Groundfish	Stock assessment model	Gulf of Alaska	Sable age 2+ biomass	1977	2018	42	-0.325	AFSC
42	Groundfish	Beach seine	Kodiak Island	Walleye pollock age-0 abundance	2006	2018	13	-0.341	AFSC
43	Groundfish	Beach seine	Kodiak Island	Pacific cod age-0 abundance	2006	2018	13	-0.036	AFSC
44	Groundfish	Beach seine	Kodiak Island	Saffron cod age-0 abundance	2006	2018	13	-0.177	AFSC
45	Groundfish	Stock assessment model	Gulf of Alaska	Walleye pollock female spawning stock biomass	1977	2018	42	0.128	AFSC
46	Groundfish	Stock assessment model	Gulf of Alaska	Walley pollock age-1 recruit biomass	1977	2018	42	0.174	AFSC
47	Groundfish	Stock assessment model	Gulf of Alaska	Pacific cod age-1 recruit biomass	1977	2018	42	0.240	AFSC
48	Groundfish	Stock assessment model	Gulf of Alaska	Pacific cod female spawning stock biomass	1977	2018	42	0.449	AFSC
49	Groundfish	Stock assessment model	Gulf of Alaska	Arrowtooth flounder age-1+ biomass	1971	2017	47	0.435	AFSC

	Taxa	Method	Domain	Metric	Start year	End year	n (years)	Factor loadings	Data source
50	Groundfish	Stock assessment model	Gulf of Alaska	Arrowtooth flounder age-1+ recruit biomass	1971	2017	47	0.299	AFSC
51	Marine bird productivity	Vessel-based survey	Prince William Sound	Black-legged kittiwake breeding success	1985	2018	34	0.243	USFWS
52	Marine bird abundance colony	Vessel-based survey	Prince William Sound	Black-legged kittiwake nest abundance	1985	2018	34	0.419	USFWS
53	Marine bird productivity	Vessel-based survey	Middleton Island	Black-legged kittiwake breeding success	1978	2018	39	0.413	GWA
54	Marine bird abundance at-sea	Vessel-based survey	Prince William Sound	Common murre density November-December	2007	2017	11	-0.031	GWA
55	Marine bird abundance at-sea	Vessel-based survey	Prince William Sound	Common murre density February-March	2008	2018	11	0.004	GWA
56	Marine bird abundance at-sea	Vessel-based survey	Prince William Sound	*Brachyramphus* murrelet density November-December	2007	2017	11	0.065	GWA
57	Marine bird abundance at-sea	Vessel-based survey	Prince William Sound	*Brachyramphus* murrelet density February-March	2008	2018	11	-0.333	GWA
58	Marine bird abundance at-sea	Vessel-based survey	Seward Line - inner shelf	Common murre abundance May	2007	2019	12	-0.065	GWA
59	Marine bird abundance at-sea	Vessel-based survey	Seward Line - inner shelf	Common murre abundance September	2006	2019	13	0.070	GWA
60	Marine bird abundance at-sea	Vessel-based survey	Seward Line - inner shelf	Black-legged kittwake abundance May	2007	2019	12	-0.181	GWA
61	Marine bird abundance at-sea	Vessel-based survey	Seward Line - inner shelf	Black-legged kittwake abundance September	2006	2019	13	0.207	GWA
62	Marine bird abundance at-sea	Vessel-based survey	Seward Line - inner shelf	Sooty shearwater abundance May	2007	2019	12	0.089	GWA

	Taxa	Method	Domain	Metric	Start year	End year	n (years)	Factor loadings	Data source
63	Marine bird abundance at-sea	Vessel-based survey	Seward Line - oceanic	Sooty shearwater abundance May	2007	2019	10	-0.140	GWA
64	Marine bird abundance at-sea	Vessel-based survey	Seward Line - inner shelf	Sooty shearwater abundance September	2006	2019	13	0.180	GWA
65	Marine bird abundance at-sea	Vessel-based survey	Seward Line - oceanic	Sooty shearwater abundance September	2006	2019	13	0.119	GWA
66	Marine bird abundance at-sea	Vessel-based survey	Seward Line - middle shelf	Black-footed albatross abundance - May	2007	2019	12	-0.079	GWA
67	Marine bird abundance at-sea	Vessel-based survey	Seward Line - oceanic	Black-footed albatross abundance - May	2007	2019	10	0.152	GWA
68	Marine bird abundance at-sea	Vessel-based survey	Seward Line - middle shelf	Black-footed albatross abundance - September	2006	2019	13	0.110	GWA
69	Marine bird abundance at-sea	Vessel-based survey	Seward Line - oceanic	Black-footed albatross abundance - September	2006	2019	13	0.068	GWA
70	Marine bird abundance at-sea	Vessel-based survey	Seward Line - middle shelf	Northern fulmar abundance - May	2007	2019	12	-0.201	GWA
71	Marine bird abundance at-sea	Vessel-based survey	Seward Line - oceanic	Northern fulmar abundance - May	2007	2019	10	-0.107	GWA
72	Marine bird abundance at-sea	Vessel-based survey	Seward Line - middle shelf	Northern fulmar abundance - September	2006	2019	13	-0.056	GWA
73	Marine bird abundance at-sea	Vessel-based survey	Seward Line - oceanic	Northern fulmar abundance - September	2006	2019	13	-0.107	GWA
74	Marine bird abundance at-sea	Vessel-based survey	Seward Line - inner shelf	Fork-tailed storm petrel abundance - May	2007	2019	12	-0.385	GWA
75	Marine bird abundance at-sea	Vessel-based survey	Seward Line - oceanic	Fork-tailed storm petrel abundance - May	2007	2019	10	0.347	GWA
76	Marine bird abundance at-sea	Vessel-based survey	Seward Line - inner shelf	Fork-tailed storm petrel abundance - September	2006	2019	13	-0.185	GWA

	Taxa	Method	Domain	Metric	Start year	End year	n (years)	Factor loadings	Data source
77	Marine bird abundance at-sea	Vessel-based survey	Seward Line - oceanic	Fork-tailed storm petrel abundance - September	2006	2019	13	0.016	GWA
78	Marine bird abundance shoreline	Vessel-based survey	Alaska Peninsula	Black oystercatcher abundance - summer	2006	2018	12	-0.366	GWA
79	Marine bird abundance at-sea	Vessel-based survey	Alaska Peninsula	*Brachyramphus* murrelet abundance - summer	2006	2018	12	0.263	GWA
80	Marine bird abundance at-sea	Vessel-based survey	Alaska Peninsula	Common murre abundance - summer	2006	2018	12	-0.030	GWA
81	Marine bird abundance at-sea	Vessel-based survey	Alaska Peninsula	Harlequin duck abundance - summer	2006	2018	12	0.135	GWA
82	Marine bird abundance at-sea	Vessel-based survey	Alaska Peninsula	Pigeon guillemot abundance - summer	2006	2018	12	0.238	GWA
83	Marine bird abundance at-sea	Vessel-based survey	Kenai Peninsula	Black oystercatcher abundance - summer	2007	2018	12	-0.485	GWA
84	Marine bird abundance at-sea	Vessel-based survey	Kenai Peninsula	*Brachyramphus* murrelet abundance - summer	2007	2018	12	0.218	GWA
85	Marine bird abundance at-sea	Vessel-based survey	Kenai Peninsula	Common murre abundance - summer	2007	2018	12	-0.260	GWA
86	Marine bird abundance at-sea	Vessel-based survey	Kenai Peninsula	Harlequin duck abundance - summer	2007	2018	12	0.069	GWA
87	Marine bird abundance at-sea	Vessel-based survey	Kenai Peninsula	Pigeon guillemot abundance - summer	2007	2018	12	0.311	GWA
88	Pinniped abundance	Vessel-based survey	Alaska Peninsula	Harbor seal abundance on haul outs and rookeries	2006	2018	12	-0.341	GWA
89	Pinniped abundance	Vessel-based survey	Kenai Peninsula	Harbor seal abundance on haul outs and rookeries	2007	2018	12	0.190	GWA

	Taxa	Method	Domain	Metric	Start year	End year	n (years)	Factor loadings	Data source
90	Pinniped abundance	Vessel-based survey	Alaska Peninsula	Steller sea lion abundance on haul outs and rookeries	2006	2018	12	0.160	GWA
91	Pinniped abundance	Vessel-based survey	Kenai Peninsula	Steller sea lion abundance on haul outs and rookeries	2007	2018	12	-0.156	GWA
92	Otter foraging	Shore-based observation	Kenai Peninsula	Sea otter foraging (energy recovery rate)	2007	2018	12	0.054	GWA
93	Otter foraging	Shore-based observation	Alaska Peninsula	Sea otter foraging (energy recovery rate)	2006	2018	12	0.261	GWA
94	Otter foraging	Shore-based observation	Prince William Sound	Sea otter foraging (energy recovery rate)	2000	2017	13	-0.065	GWA
95	Pinniped abundance	Aerial survey	Western GOA	Steller sea lion non-pup abundance on haul outs and rookeries	2000	2017	13	-0.305	AFSC
96	Pinniped abundance	Aerial survey	Western GOA	Steller sea lion pup abundance on haul outs and rookeries	2000	2017	13	0.286	AFSC
97	Pinniped abundance	Aerial survey	Eastern GOA	Steller sea lion non-pup abundance on haul outs and rookeries	2000	2017	12	0.268	AFSC
98	Pinniped abundance	Aerial survey	Eastern GOA	Steller sea lion pup abundance on haul outs and rookeries	2005	2019	15	0.415	AFSC
99	Pinniped abundance	Island - based remote camera observation	Chiswell Island	Steller sea lion age-1+ abundance on Chiswell Island	2005	2019	15	0.211	ASLC
100	Pinniped abundance	Island - based remote camera observation	Chiswell Island	Steller sea lion pup abundance on Chiswell Island	2003	2018	13	0.151	ASLC

	Taxa	Method	Domain	Metric	Start year	End year	n (years)	Factor loadings	Data source
101	Whale abundance	Vessel-based survey	Prince William Sound	Humpack whale individuals encountered per day of surveying	2007	2018	8	0.441	GWA
102	Whale abundance	Vessel-based survey	Prince William Sound	Killer whale individual per day encounter rate	2005	2019	15	0.232	GWA
103	Whale abundance	Vessel-based survey	Prince William Sound	Killer whale encounter rate	2005	2019	15	0.207	GWA
104	Salmon commercial harvest	Commercial fishing vessels	Prince William Sound and Copper River	Chinook salmon, pounds harvested	1971	2019	49	0.014	ADFG
105	Salmon commercial harvest	Commercial fishing vessels	Prince William Sound and Copper River	Coho salmon pounds harvested	1971	2019	49	-0.169	ADFG
106	Salmon commercial harvest	Commercial fishing vessels	Prince William Sound and Copper River	Sockeye salmon pounds harvested	1971	2019	49	0.371	ADFG
107	Salmon commercial harvest	Commercial fishing vessels	Prince William Sound and Copper River	Pink salmon pounds harvested	1971	2019	49	0.117	ADFG
108	Salmon commercial harvest	Commercial fishing vessels	Prince William Sound and Copper River	Chum salmon pounds harvested	1971	2019	49	-0.169	ADFG
109	Salmon commercial harvest	Commercial fishing vessels	Kodiak	Chinook salmon, pounds harvested	1971	2019	49	0.336	ADFG
110	Salmon commercial harvest	Commercial fishing vessels	Kodiak	Coho salmon pounds harvested	1971	2019	49	-0.206	ADFG

	Taxa	Method	Domain	Metric	Start year	End year	n (years)	Factor loadings	Data source
111	Salmon commercial harvest	Commercial fishing vessels	Kodiak	Sockeye salmon pounds harvested	1971	2019	49	0.118	ADFG
112	Salmon commercial harvest	Commercial fishing vessels	Kodiak	Pink salmon pounds harvested	1971	2019	49	0.011	ADFG
113	Salmon commercial harvest	Commercial fishing vessels	Kodiak	Chum salmon pounds harvested	1971	2019	49	-0.132	ADFG

Table A2. Results from additional biological time series of marine birds at Chowiet Island (Semidi Islands) and East Amatuli (Barren Islands) in the western study. These time series were included in the final version of this chapter that was submitted for publication. This is a subset of the output from a new model run on a 187 time series to highlight the additional marine bird colony-based metrics. A few key differences compared to the eastern study area included in this report were that black-legged kittiwake breeding success and the abundance of sand lance and capelin to marine birds did not have negative responses in the west, like they did in the east. However, the abundance and reproductive success of common murres (no data from west) did show a strong negative response, consistent with kittiwakes in the west. Time series include taxonomic group, sampling method, geographic domain where sampled, derived metric, time series start year, end year, and number of years (n; most, but not all are sampled annually), and factor loadings from dynamic factor analysis. Note that a positive factor loading indicates the time series relates positively to the common trend and given that the common trend is a negative response during the Pacific marine heatwave (Figure 4-3), a positive factor loading refers to a negative response during the Pacific marine heatwave and vice versa. We use a factor loading of 0.20 (absolute value) as the cutoff for whether or not a time series significantly relates to the common trend.

Taxa	Method	Domain	Metric	Start year	End year	n (years)	Factor Loadings
Forage Fish	Marine bird diet	Chowiet	Sand lance biomass from rhinoceros auklet diet	1998	2019	16	0.131
Forage Fish	Marine bird diet	Chowiet	Capelin percent biomass from rhinoceros auklet diet	1998	2019	16	0.006
Forage Fish	Marine bird diet	Chowiet	Hexagrammid percent biomass in glaucous-winged gull diets	1998	2019	14	-0.255
Invertebrate prey	Marine bird diet	Chowiet	Mytilus percent biomass in glaucous-winged gull diets	2004	2019	15	-0.239
Invertebrate prey	Marine bird diet	Chowiet	Chiton percent biomass in glaucous-winged gull diets	2004	2019	15	0.152
Forage Fish	Marine bird diet	Chowiet	Fish percent volume in glaucous-winged gull diets	2004	2019	15	-0.120
Avian prey	Marine bird diet	Chowiet	Birds percent volume in glaucous-winged gull diets	2004	2019	15	0.157
Marine bird	Land-based survey	Chowiet	Common Murre breeding success	1979	2019	25	-0.153
Marine bird	Land-based survey	Chowiet	Common Murre abundance	1989	2019	22	0.322

Taxa	Method	Domain	Metric	Start year	End year	n (years)	Factor Loadings
Marine bird	Land-based survey	Chowiet	Parakeet auklet breeding success	1998	2019	16	-0.037
Marine bird	Land-based survey	Chowiet	Rhinoceros auklet breeding success	2012	2019	7	0.022
Marine bird	Land-based survey	Chowiet	Tufted puffin breeding success	2005	2019	14	-0.074
Marine bird	Land-based survey	Chowiet	Black-legged kittiwake breeding success	1979	2019	24	-0.179
Marine bird	Land-based survey	Chowiet	Black-legged kittiwake abundance	1977	2019	28	0.075
Marine bird	Land-based survey	Chowiet	Glaucous-winged gull breeding success	1998	2019	12	-0.203
Marine bird	Land-based survey	Chowiet	Pelagic cormorant breeding success	2010	2019	8	0.053
Marine bird	Land-based survey	E. Amatuli	Common Murre breeding success	1993	2018	21	0.294
Marine bird	Land-based survey	E. Amatuli	Common Murre abundance	1993	2018	23	0.403
Marine bird	Land-based survey	E. Amatuli	Black-legged kittiwake breeding success	1993	2019	24	0.114
Marine bird	Land-based survey	E. Amatuli	Fork tailed storm petrel breeding success	1998	2019	20	0.170

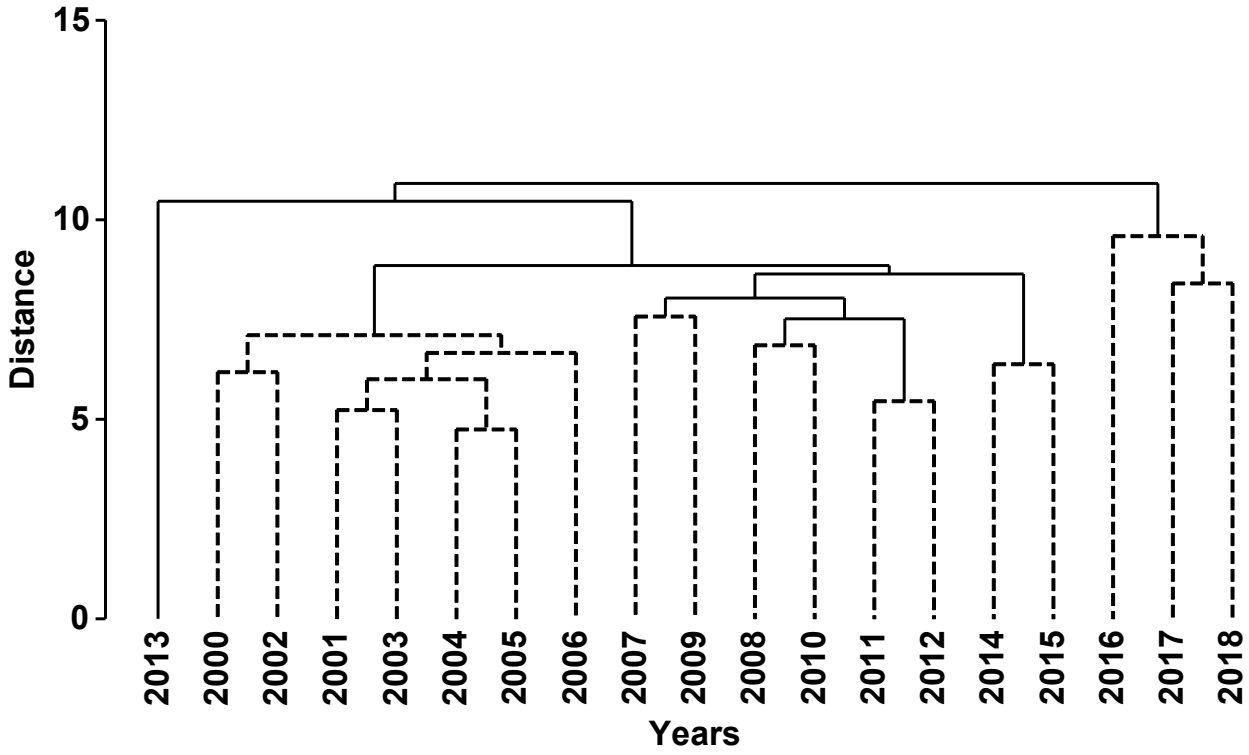

Figure A1. Cluster analyses of biological time series over a 19-year period prior to, during, and after the 2014-2016 marine heatwave in the Gulf of Alaska. Solid lines indicate significantly different year groupings. In this analysis we used fewer time series (n=93) that extended over a longer time period to provide further support for results from our core analysis of more time series (n=113), but over a short time period (2010-2018). These longer time series confirm that years following the 2013 onset of the Pacific marine heatwave do indeed stand out from the others.